

Development of Functional Improved and Environmentally Friendly Synthetic Musks with Reduced Human Health Risks using In Silico Methods

By

© Xixi Li, BEng, MEng

A Thesis submitted to the School of Graduate Studies
in partial fulfilment of the requirements for the degree of

Doctor of Philosophy

Faculty of Engineering & Applied Science

Memorial University of Newfoundland

May, 2022

St. John's, Newfoundland and Labrador
Canada

Abstract

Synthetic musks (SMs) as alternatives to natural musk have been widely used in personal care products (PCPs), such as fragrances, shampoos, soaps, and household items. These SMs are used in increasingly large quantities and are widely detected in natural waters, soil, air, as well as sludge and effluent from the wastewater treatment plants worldwide, including the Arctic region. Some SMs like galaxolide (HHCB) have been recognized as emerging contaminants with potential human health concerns due to their ubiquitous existence, high lipophilicity, and long persistence in the environment. However, the studies on environmental properties, transformation processes, and toxicity of SMs are still very limited, and there is a strong desire for the design of functional approved and environmentally friendly SMs. This study thus focuses on the investigation and evaluation of the environmental and functional properties of SMs, their transformation and toxicity, as well as the design of new SM derivatives based on molecular modelling. It includes the following objectives: 1) conducting a comprehensive literature review to summarize SM classification, synthetic routes, analysis and occurrence, fate and toxicity in the environment, as well as the associated risk and toxicity assessment and pollution mitigation; and 2) evaluating the toxicity of SMs and their transformation by-products; and 3) designing functionally improved and environmentally friendly HHCB derivatives; and 4) evaluating and controlling spontaneous abortion risk in pregnant women caused by inhalation and ingestion of SMs; and 5) assessing the human health risks of SMs from dermal exposure, investigating the bioaccumulation mechanism of SMs on humans and developing the risk control strategies. The study would lead to a better understanding of SM environmental behaviors and health risks and provide the theoretical basis for designing functionally improved and environmentally friendly alternatives of other PCPs.

Acknowledgments

I would like to express my sincere gratitude to my supervisor, Dr. Baiyu (Helen) Zhang. I am especially indebted for her guidance, motivation, inspiration, and patience in both my Ph.D. research and my life. I could not imagine having a better supervisor and mentor like her. I also greatly appreciate my co-supervisors, Dr. Bing Chen and Dr. Tahir Husain, for their great supports and invaluable advice. Dr. Chen always supported me with his innovative suggestions, insightful enlightenment, and great opportunities. Dr. Husain has inspired me with his valuable feedback, patience, and an optimistic attitude. They consistently provided invaluable advice and encouragement whenever I ran into any problem about my research or life. I could not achieve the goals of my thesis without their help.

I gratefully acknowledge the Natural Sciences and Engineering Research Council of Canada (NSERC) and the Canadian Foundation of Innovation (CFI) for their funding support to my research. Special thanks also go to Memorial University, which provided me with a magnificent research environment and financial support.

Finally, I would like to give my special thanks to Lidan Tao for her assistance with materials and advice. My further gratitude is given to my colleagues Dr. Zhiwen Zhu, Dr. Weiyun Lin, Dr. Wenwen Gu, Dr. Fuqiang Fan, Yuanyuan Zhao, Minghao Li, Wei He, Xinyi Chen, Jiawen Yang, Qing Li, Meijin Du, Dr. Xing Song, Dr. Bo Liu, Dr. Hongjing Wu, Xudong Ye, Qiao Kang, Fei Wu, Min Yang, Yiqi Cao, Guihua Dong, and their members, for their friendship and assistance.

“This dissertation is dedicated to my parents, who I am grateful for being their daughter every single day of my life.”

Table of Contents

Abstract	I
Acknowledgements	II
Table of Contents	IV
List of Tables	VIII
List of Figures	X
List of Abbreviations	XI
CHAPTER 1 INTRODUCTION	1
1.1 Background	2
1.2 Statement of Problems	3
1.3 Objectives	5
1.4 Thesis Organization	6
CHAPTER 2 LITERATURE REVIEW	9
2.1 Introduction.....	10
2.2 Classification and Classic Synthetic Routes of SMs	12
2.2.1 Classification of SMs	12
2.2.2 Synthetic status of SMs.....	19
2.3 Occurrence of SMs in Environmental Samples	23
2.3.1 Water samples	23
2.3.2 Solid samples	26
2.3.3 Air samples.....	28
2.4 Fate and Toxicity of SMs in the Environment.....	32
2.4.1 Migration of SMs	32
2.4.2 Bioaccumulation of SMs.....	33
2.4.3 Toxicological effects of SMs	36
2.5 Analysis of SMs in Environmental Samples	46
2.5.1 Sample pre-treatment	46
2.5.2 Sample analysis	55
2.6 Risk Assessment and Control of SM Pollution	56
2.6.1 Environmental risk assessment	56
2.6.2 Pollution control.....	59
2.6.3 Environmentally friendly alternatives to SMs	61
2.7 Summary	70

CHAPTER 3 3D-QSAR AIDED TOXICITY ASSESSMENT OF SMS AND THEIR TRANSFORMATION BY-PRODUCTS	71
3.1 Introduction.....	72
3.2 Materials and Methods.....	77
3.2.1 3D-QSAR model construction for SM biological toxicity (LC_{50}) prediction.....	77
3.2.2 3D -QSAR aided LC_{50} assessment of SMs and the transformation by-products	79
3.3. Results and Discussion	82
3.3.1 Performance evaluation of the constructed CoMSIA based 3D-QSAR model ..	82
3.3.2 SMs by-products identified from chlorination experiments	85
3.3.3 Toxicity prediction of the SM and SMs by-products using the constructed 3D-QSAR model	91
3.4 Summary	97
Appendices.....	98
CHAPTER 4 FUNCTIONAL MODIFICATION OF HHCB: STRATEGY FOR OBTAINING ENVIRONMENTALLY FRIENDLY DERIVATIVES	105
4.1 Introduction.....	106
4.2 Materials and Methods.....	110
4.2.1 Molecular design for obtaining functionally improved and environmentally friendly HHCB derivatives	110
4.2.2 Evaluation of behaviors of a selected representative HHCB derivative	115
4.3 Results and Discussion	118
4.3.1 Evaluation of the constructed 3D-QSAR models for predicting HHCB functional and environmental properties	118
4.3.2 Determination of HHCB molecular substituted sites and groups based on contour maps of 3D-QSAR model	121
4.3.3 HHCB derivatives with improved functional and environmental properties....	123
4.3.4 Human health risk assessment of HHCB derivatives using toxicokinetic analysis and molecular docking	128
4.3.5 Environmental behavior evaluation of the selected representative HHCB derivative and its transformation by-products.....	134
4.3.6 Evaluation of the HHCB derivative and other PCP additives interactions and the related human health risk assessment	145
4.3.7 Potential applications of HHCB derivatives	152
4.4 Summary	153

Appendices.....	155
CHAPTER 5 INHALATION AND INGESTION OF SMS IN PREGNANT WOMEN: IN SILICO SPONTANEOUS ABORTION RISK EVALUATION AND CONTROL	163
5.1 Introduction.....	164
5.2 Methodology.....	167
5.2.1 Establishment of relationships between SMs and their abortion risk to pregnant women.....	167
5.2.2 Reduction of spontaneous abortion risk by supplementary diet plans assisted with L ₁₂ Taguchi experiment design.....	169
5.2.3 Reduction of spontaneous abortion risk by designing SM derivatives through 3D-QSAR modelling.....	169
5.2.4 Reduction of spontaneous abortion risk by integration of supplementary diet plans and molecular modification.....	173
5.3 Results and Discussion	173
5.3.1 Establishment of relationships between SMs and their abortion risk to pregnant women.....	173
5.3.2 Reduction of spontaneous abortion risk by supplementary diet plans.....	176
5.3.3 Reduction of spontaneous abortion risk by designing SM derivatives through 3D-QSAR modelling.....	180
5.3.4 Reduction of spontaneous abortion risk by integration of supplementary diet plans and molecular modification.....	192
5.4 Summary.....	193
Appendices.....	195
CHAPTER 6 DERMAL EXPORSURE TO SYNTHETIC MUSKS: HUMAN HEALTH RISK ASSESSMENT, MECHANISM, AND CONTROL STRATEGY. .	210
6.1 Introduction.....	211
6.2 Materials and Methods.....	215
6.2.1 Human health risk assessment of functional SMs using molecular docking and molecular dynamic simulations.....	215
6.2.2 Exploration of SM bioaccumulation mechanism through 2D-QSAR modelling	218
6.2.3 Control of SM human health risk.....	222
6.3 Results and Discussion	224

6.3.1 Human health risk assessment of SMs.....	224
6.3.2 SM bioaccumulation mechanism	224
6.3.3 Control of SM human health risk.....	231
Summary.....	238
Appendices.....	239
CHAPTER 7 CONCLUSIONS AND RECOMMENDATIONS.....	263
7.1 Conclusions.....	264
7.2 Research Contributions.....	267
7.3 Recommendations for Further Work	269
REFERENCES	270

List of Tables

Table 2-1 Five kinds of nitro musks compounds.....	15
Table 2-2 Six kinds of polycyclic musks compounds	16
Table 2-3 Five kinds of macrocyclic musks compounds.....	17
Table 2-4 Three kinds of alicyclic musks compounds.....	18
Table 2-5 The level of synthetic musks in different media.....	30
Table 2-6 Summarize the parameters of environmental impact assessment indicators for 76 kinds of polycyclic musks	40
Table 2-7 A summary of the SMILES coding of partial polycyclic musks.....	44
Table 2-8 Analysis of synthetic musks in water samples	47
Table 2-9 Analysis of synthetic musks in sediments and sludge.....	51
Table 2-10 Analysis of synthetic musks in air samples	53
Table 2-11 Analysis of synthetic musks in biological samples	54
Table 2-12 Differences of molecular structures in emerging contaminants	63
Table 3-1 Characteristics of six synthetic musk (SM) precursors.....	81
Table 3-2 Statistical parameters of the CoMSIA model.....	83
Table 3-3 SM by-products generated using different treatment methods.....	86
Table 3-4 Selected by-products with the same common skeleton of Musk #28 from chlorination experiment.....	89
Table 3-5 The predicted LC_{50} values of SM by-products obtained from the constructed CoMSIA model.....	94
Table 4-1 Statistical parameters of the established 3D-QSAR models	119
Table 4-2 Predicted values of half-life for SMs' derivatives using CoMFA model	124
Table 4-3 Functional and environmental properties of SMs' derivatives.....	127
Table 4-4 Toxicokinetic prediction and assessment of HHCB before and after modification using TOPKAT Extensible module	130
Table 4-5 The environmental properties of Derivative 7 by-products under different treatment methods	133
Table 4-6 Toxicokinetic prediction and assessment of HHCB and Derivative 7's transformation products using TOPKAT Extensible module	139
Table 4-7 The binding energy of HHCB-4ZRY and Derivative 7-4ZRY with additives present.....	148
Table 4-8 Calculation of binding energy and signal to noise ratio (SNR) of the HHCB-4ZRY	

and Derivative 7-4ZRY complexes	149
Table 5-1 The LibDock scores and binding energies of 74 complexes (SMs to the AChE enzyme).	175
Table 5-2 Statistical parameters for performance evaluation of the constructed 3D-QSAR models.....	181
Table 6-1 The definition of 32 SM descriptors.....	221
Table 6-2 The obtained 2D-QSAR formulas of SMs-4ZRY and SMs-OR5AN1.....	226
Table 6-3 The predicted environmental properties of PHAN derivatives using 3D-QSAR models.....	234
Table 6-4 The total energy of body wash components atomic units (a.u.).....	237

List of Figures

Figure 1-1 Schematic diagram of the thesis structure	8
Figure 2-1 Synthetic routes of 6 kinds of synthetic musks	22
Figure 2-2 Historical process of the representative synthetic musk invention.....	64
Figure 2-3 Theoretical design schemes for environmentally friendly synthetic musk substitutes	69
Figure 3-1 The transport, fate and impact of SMs and their by-products	76
Figure 3-2 The structure of Musk #28 and the alignment of common molecular skeleton	78
Figure 3-3 The observed versus predicted LC_{50} values based on the CoMSIA model	84
Figure 4-1 Plot of observed vs predicted values using the CoMFA model	120
Figure 4-2 The (a) molecular structure of (4S, 7R)-HHCB, contour maps of (b) HHCB (electrostatic field) and (c) HHCB (steric field).....	122
Figure 4-3 The photodegradation (A), biotransformation (B), chlorination (C) and metabolic pathways in algal cells (D) pathways of HHCB and Derivative 7. ΔE is in kJ/mol.	137
Figure 4-4 Binding energy of HHCB-4ZRY and Derivative 7-4ZRY complexes from a Taguchi experimental design.....	151
Figure 5-1 The structure and the alignment of the common molecular skeleton of template molecules SM-25, SM-43 and MK.....	171
Figure 5-2 LibDock scores of SMs with progesterone and estrogen under supplementary diet plans based on L12 Taguchi experimental design.	177
Figure 5-3 (i) The contour maps of HHCB; (ii) the contour maps of MK	184
Figure 5-4 The substituted sites of HHCB (a) and MK (b).	185
Figure 5-5 The predicted values of change rates of LibDock scores (SM-C, SM-P, and SM- E), functional and environmental properties of (a) HHCB derivatives and (b) MK derivatives.....	187
Figure 5-6 Verification of the binding mechanism of HHCB and its derivatives with progesterone.....	191
Figure 6-1 The Ramachandran Plot of human olfactory protein (OR5AN1).....	217
Figure 6-2 The influence degree on the bioaccumulation and olfactory sensitivity of SMs	229

List of Abbreviations

2D-QSAR	Two-dimensional quantitative structure-activity relationship
3D-QSAR	Three-dimensional quantitative structure-activity relationship
ADBI	Celestolide
AHTN	Tonalide
BCF	Bioconcentration factor
CoMFA	Comparative molecular field analysis
CoMSIA	Comparative molecular similarity indices analysis
DFT	Density functional theory
HHCb	Galaxolide
LC_{50}	lethal concentration 50%
MD	Molecular dynamics simulation
MK	Musk ketone
MX	Musk xylene
PCP	Personal care products
PHAN	Phantolide
SM	Synthetic musk
TRASE	Traseolide
WWTP	Wastewater treatment plant
DW	Dry weight
LW	Lipid weight
VP	Vapor pressure
EC_{50}	Half maximal effective concentration
Ref.	Reference

CHAPTER 1
INTRODUCTION

1.1 Background

Synthetic musks (SMs), known as a class of synthetic fragrance additives, are widely used in a number of personal care and household products (e.g., skin care lotions, fabric softeners, perfumes, shampoos, and detergents, etc.) (Reiner et al., 2007b). Polycyclic musks dominate the SMs market with a market share of over 61% (Nakata et al., 2007). As one of the most widely used polycyclic musks, galaxolide (HHCB) is known as a high production-volume chemical whose production reached 1427 metric tons in 2000 in Europe (European Union Risk Assessment Report, 2008). The production of tonalide (AHTN) were as high as 5000 tons in worldwide in 2004 (Tumová et al., 2019). Recent data showed that HHCB and AHTN were produced or imported between 1000 and 10 000 tons per year in the European Union (Aminot et al., 2021). The SMs have been frequently detected in natural waters, soil, air as well as sludge and effluent from the wastewater treatment plants (Zhang et al., 2020a; Hong et al., 2021; Jo et al., 2021; Košnář et al., 2021). Studies have shown that, SMs used in the personal care products were released to and detected in different wastewater treatment plants worldwide such as Czech Republic, Dalian (China), Thailand, and Northern Italy (Košnář et al., 2021; Tasselli et al., 2021; Ren et al., 2020; Juksu et al., 2020). HHCB and tonalide (AHTN) have been detected with the highest concentration of 3039 ng/L and 1486 ng/L, respectively in the wastewater treatment plants from China (Tasselli and Guzzella 2020).

After disinfection of SMs in the wastewater treatment plants, SM byproducts (e.g., HHCB-lactone) have also been frequently detected in the effluent (Horii et al., 2007; Tasselli et al., 2021). The residual SMs will then enter the surface water and may continue be biodegraded and photodegraded into by-products in the environment. Although the concentrations are low in the environmental systems, bioaccumulation of these SMs leads to potential risk to the environment and humans. SMs have been proved with toxicity to

organisms. The toxicity experiments of SMs were constructed by Wollenberger et al. (2003) and found that SMs strongly inhibit the larval development of the *Acartia tonsa* (a kind of marine copepod). Carlsson and Norrgren (2004) indicated that SMs have adverse impacts on zebra fish. The toxicity of common SMs has been investigated, but the toxicity studies on their by-products are extremely limited.

Besides the biotoxicity of SMs to organisms, they have also been found to have adverse impacts on human bodies. SMs have also been detected in human skin keratin, blood and breast milk (Hutter et al., 2010; Gao et al., 2016; Yin et al., 2016; Zhang et al., 2017a) through inhalation, dermal, and oral uptake (Lu et al., 2011b; Nakata et al., 2015). SMs can be accumulated in human bodies at a remarkably high concentration in human fat (28–189 $\mu\text{g}/\text{kg}$ for HHCB, 8–33 $\mu\text{g}/\text{kg}$ for AHTN), human blood (average 0.77 $\mu\text{g}/\text{L}$ for HHCB and 0.27 $\mu\text{g}/\text{L}$ for AHTN), and breast milk (16–108 $\mu\text{g}/\text{kg}$ HHCB, 11–58 $\mu\text{g}/\text{kg}$ AHTN) (Lange et al., 2015). Li et al. (2013) demonstrated that HHCB inhibited the production of progesterone and cortisol. As the natural hormone in the human body, progesterone and estrogen prevent abortion risks to pregnant women. As the inhibition of HHCB and AHTN on human progesterone and estrogen activities, it is necessary to conduct an in-depth investigation on the evaluation and reduction of the spontaneous abortion risk. Overall, SMs alternatives with lower environmental and human health impacts should be designed.

1.2 Statement of Problems

Most of the SMs contained in personal care products enter the wastewater treatment plants (WWTPs) and eventually reach the surface water together with their by-products. However, even after disinfection, the incompletely treated SMs and their transformation by-products (vary depending on the disinfection methods) still exist in the effluent. For example, Horii et al. (2007) detected HHCB, AHTN, and HHCB-lactone (a recognized disinfection by-product of HHCB) in the effluents of a WWTP in Kentucky, the United States, and their

concentrations were 44, 130, and 229 ng/L, respectively. The residual SMs will then enter the surface water and may continue to be biodegraded and photodegraded into by-products in the environment. Although the toxicity of common SMs has been investigated, toxicity studies on their by-products are extremely limited. Besides, these toxicity analyses of SMs are based on experiments requiring special equipment, manpower, materials, and costs. Therefore, a reliable and cost-effective approach is desired to test the toxicity of SMs and their transformation by-products.

After SMs enter the environment, they can then come into the food chain and gradually accumulate in organisms and had a medium-range transport (detected in the Arctic) (Xie et al., 2007; Peng et al., 2018; Peng et al., 2019; Ding et al., 2020; Ehiguese et al., 2021). HHCBs in liver tissues of seals, sea lions, Atlantic sharpnose shark, river otter, mink, common merganser, lesser scaup, greater scaup, and mallard and even the human body has been documented (Kannan et al., 2005). Recent studies highlighted the ecological risk of HHCB residues in the environment. It could significantly decrease the algal growth rate (Ding et al. 2020), bring oxidative stress to zebra mussels and lead to genetic damage (Parolini et al., 2015), as well as decrease the growth, survival, and reproduction of youth gastropod (*Potamopyrgus antipodarum*) (Pedersen et al., 2009). Besides the algae and arctic organisms, HHCB could also pose potential risks to humans. Li et al. (2013) demonstrated that HHCB inhibited the production of progesterone and cortisol. The large consumption of HHCB and their ecological toxicity call for the systematic development of environmentally friendly HHCB alternatives with desired properties and functions, lower ecological toxicities (e.g., bio-toxicity, bio-accumulation ability, and mobility in this study), smaller human health risks and less environmental footprint.

Additionally, SMs have been frequently detected in human blood and breast milk in recent years. In Vienna, Austria, Hutter et al. (2010) determined the exposure levels of 11

SMs in human blood and found that the detection rates of HHCB and MX in human blood were 89% and 62%, at concentrations as high as 6900 ng/L and 190 ng/L, respectively. SMs in the atmosphere can enter the blood system through breathing or skin interaction, thereby causing potential harm to human health (Gao et al., 2016). Thirteen kinds of SMs were identified in 1237 human breast milk collected from 12 provinces in China (Yin et al., 2016). Among these breast milk samples, the average detected concentration of HHCB was as high as 18.03 ng/g. Hu et al. (2010) concluded that SMs may be transferred from pregnant women to their children. SMs widely present in the environment, so it is inevitable that they could enter the human's body through inhalation and ingestion (Sousa et al., 2020). Therefore, it is important to study the potential risks brought from SMs to human beings, especially groups that need special attention, such as pregnant women. Moreover, the studies on the mechanism of how SMs lead to toxicity to human beings need to be further investigated.

1.3 Objectives

The proposed research aims at the development of molecular modelling (e.g., 3D-QSAR, molecular docking, and molecular dynamics analysis) based methodologies to design functionally improved and environmentally friendly SM alternatives, as well as to evaluate their properties, toxicity and environmental risks. It entails five main research tasks:

- (1) To conduct a comprehensive literature review to summarize SM classification, synthetic routes, analysis and occurrence, fate and toxicity in the environment, as well as the associated risk and toxicity assessment and pollution mitigation;
- (2) To construct a 3D-QSAR model by using known biological toxicity (LC_{50}) and molecular structures of SMs, predicting the biological toxicity of the SMs transformation by-products;
- (3) To develop a systematic molecular design, screening and performance evaluation approach for generating functionally improved and environmentally friendly HHCB

derivatives;

- (4) To evaluate and control abortion risk of SMs to pregnant women through conducting 3D-QSAR model-based risk prediction and SM molecular modification, as well as establishing supplementary diet plans; and
- (5) To provide an in-depth investigation of human health risks assessment, mechanism, and risk control of SMs through dermal exposure by using in silico methods.

1.4 Thesis Organization

The thesis is written in manuscript format, and the title of the manuscripts are used as chapter titles (where applicable). The outline of the thesis is summarized as follows:

Chapter 2 provides a brief overview of the classification, transport fate, environmental impacts and risks, and pollution control of synthetic musks. The challenges and relevant concerning of SMs were also highlighted in the published manuscript.

Chapter 3 is the first study on the biological toxicity of synthetic musk (SM) transformation by-products predicted by the 3D-QSAR model. This area remains unexplored due to the rare identification of broad SM by-products and the lack of effective toxicity evaluation and management tools. This study tackled six commonly used SMs (i.e., galaxolide (HHCB), tonalide (AHTN), phantolide (PHAN), traseolide (TRASE), celestolide (ADBI) and musk ketone (MK)). Fifty-eight SM by-products of biodegradation, photodegradation, advanced oxidation (UV and ozone aided), and chlorination were identified by literature review and lab experiment. A 3D-QSAR model was first proposed to predict the toxicity of these by-products based on lethal concentration (LC_{50}) of mysid for SMs structures. The research outputs led to valuable reference data and useful guidance for understanding the fate of SMs and improving treatment strategies for mitigation of these emerging contaminants.

Chapter 4 provides theoretically comprehensive methodologies for creating and

screening environmentally friendly synthetic musks (SMs), evaluating their environmental properties, and managing the associated human health risks. This study helps to better understand SMs' environmental behaviors and facilitates their treatment after usage.

Chapter 5 provides the theoretical circumvention strategy to reduce the abortion risk of SMs to pregnant women by designing the supplementary diet plan and environmentally friendly SMs derivatives. The assessment and control of abortion risks of SMs to the human body were also conducted in this study, which has been never tackled before. This study provides the theoretical circumvention strategy for inhibiting the interaction between SMs with progesterone and estrogen, helps to provide scientific support for designing new pharmaceutical and personal care products.

Chapter 6 presents the mechanisms of SMs affect the bioaccumulation ability in human skin keratin and odor sensitivity. SM derivatives with lower environmental and human health impacts but improved odor sensitivity to human beings were designed. It also included an in-depth investigation of the bioaccumulation mechanisms of SM at a molecular level, and risk control approaches were constructed accordingly.

Chapter 7 presents a summary, conclusions, and recommendations for future work.

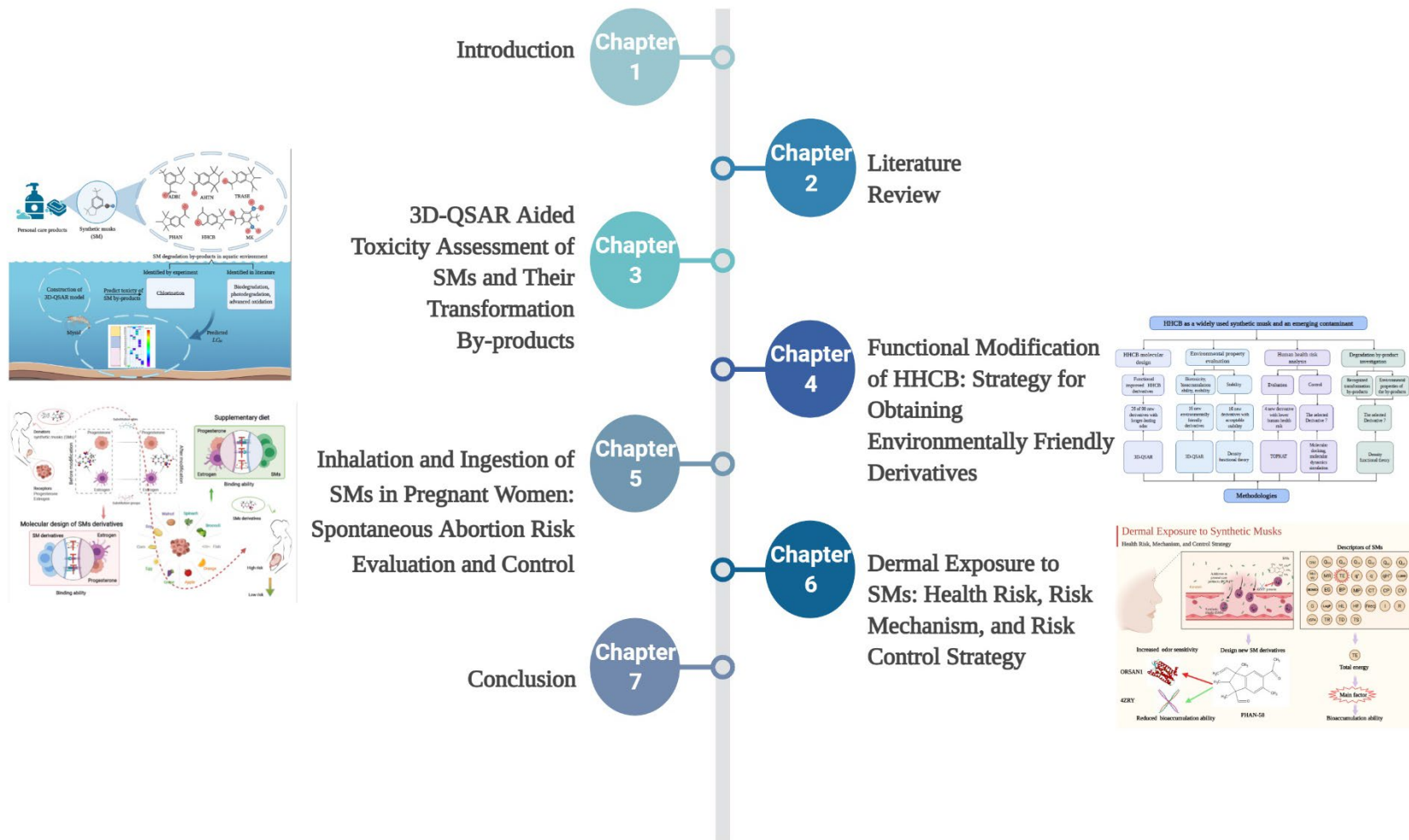


Figure 1-1 Schematic diagram of the thesis structure

CHAPTER 2

LITERATURE REVIEW

This chapter has been published in *Advances in Marine Biology* (2018): 81, 213-280. I carried out most literature reviews, including conceptualization, data collection, and writing - review & editing. I prepared the first draft of the manuscript and subsequently revised the manuscript based on the co-authors' feedback as well as the comments received from the peer-review process.

Li, X., Chu, Z., Yang, J., Li, M., Du, M., Zhao, X., Zhu, Z., Li, Y. (2018). Synthetic musks: a class of commercial fragrance additives in personal care products (PCPs) causing concern as emerging contaminants. *Advances in Marine Biology*, 81, 213-280.

DOI: 10.1016/bs.amb.2018.09.008

2.1 Introduction

Synthetic musks (SMs), known as a class of synthetic fragrance additives, are widely used in a number of personal care and household products (e.g., skin care lotions, fabric softeners, perfumes, shampoos, and detergents, etc.) (Reiner et al., 2007b). As economic substitutes to their natural counterparts, SMs can be classified into four main groups, namely nitro, polycyclic, macrocyclic, and alicyclic musks (Homem et al., 2015a). The production of SMs worldwide amounted to 6,000 tons per year at the end of 1999 (Tanabe, 2005). Among them, Polycyclic musks and nitro musks took a leading role in the market at a production volume of 61% and 35%, respectively (Nakata et al., 2007). Owing to the long persistence, potential carcinogenicity and endocrine-disrupting activity, SMs are recognized as one of the major emerging pollutants in personal care products (PCPs) (Gao et al., 2016; Homem et al., 2015a; Johnson and Sumpter, 2001). The release of SMs into the environment thus has been very much in the foreground recently.

Considered as the major source of SMs to the environment, the sewage sludges and effluents of the waste water treatment plant (WWTP) facilities were identified with relatively high concentrations (mg/L range) of SMs (Nakata et al., 2007). The semi-volatile and pseudo-persistent (chemicals that are continuously injected into the environment even with short half-lives) SMs could easily find their way into the aquatic and soil environment through the sewage and wastewater system (Brausch and Rand, 2011). The occurrences of SMs have been reported in many environmental media, including surface water (Buerge et al., 2003; Peck et al., 2004), sewage (Llompart et al., 2003; Clara et al., 2011), sludge (DiFrancesco et al., 2004; Sun et al., 2014), sediment (Sapozhnikova et al., 2010), soil (Yang et al., 2006), air (Fontal et al., 2016). The worldwide identification of SMs along the Pacific to the Atlantic East Coast, in the Mediterranean and Adriatic Seas (Montesdeoca-Esponda et al., 2018), as well as within the Antarctic and Arctic regions (Xie et al., 2007), suggests their widespread distribution.

Accompanied by the migration of the highly lipophilic natured SMs in the environment,

their accumulation in the lipid-rich samples and tissues of aquatic organisms (e.g., trout (Chou and Dietrich, 1999), mussels (Nakata et al., 2012), crustaceans (Nakata et al., 2007), and marine mammals (Reiner et al., 2007)), and humans (e.g., breast milk (Lee et al., 2015) and blood (Yin et al., 2016)) have been reported. High concentrations of musk ketone (4-tert-butyl-2,6-dimethyl-3,5-dinitroacetophenone), a widely used nitro musk, were detected in clams and mussels from Canadian coastal waters, at concentrations ranging from 2200 to 17 700 ng/g on a lipid wt. basis (Nakata et al., 2007). Similarly, the most commonly used polycyclic musks galaxolide (1,3,4,6,7,8-hexahydro-4,6,6,7,8,8-hexamethylcyclopenta[g]-2-benzopyrane-HHCB) and tonalide (7-acetyl-1,1,3,4,4,6-hexamethyltetrahydronaphthalene-AHTN) could be accumulated at a remarkably high concentration in human fat (28-189 µg/kg for HHCB, 8–33 µg/kg for AHTN), human blood (average 0.77 µg/L for HHCB and 0.27 µg/L for AHTN), and breast milk (16-108 µg/kg HHCB, 11-58 µg/kg AHTN) (Lange et al., 2015). The bioaccumulation of SMs has been frequently associated with various negative effects, including short- and long-term toxicity and endocrine-disrupting effects (Maekawa et al., 1990; Emig et al., 1996; Yamauchi et al., 2008).

To facilitate the environment impact evaluation and assessment of SMs, several analytical methods have been developed for the identification and quantification of SMs in various environmental samples. At present, detection methods are mostly based on the gas chromatography (GC) coupled to mass spectrometry (MS) or tandem quadrupoles (MS-MS), given their inherent physicochemical properties (Kallenborn et al., 1999; Cavalheiro et al., 2013; Godayol et al., 2015a). The electron ionization (EI) mode is selected to achieve the desired accuracy and sensitivity of the target compound (Zeng et al., 2005). The introduction of MS/MS could further improve the removal of coeluting peak interference, and thus enhance the sensitivity of target components at trace levels (Groz et al., 2014). The application of other detectors such as the electron capture detector (ECD), the flame ionization detector (FID), and the nitrogen phosphorus detector (NPD) was also reported (Aguirre et al., 2014).

Based on our reviews, the increasing discharge of SMs into the environment leads to surface and groundwater contamination, causing adverse effects on industrial and agricultural use and in the ecosystem (Postigo and Barceló, 2015; Vimalkumar et al., 2021). Biodegradation, photochemical degradation and ozonation are considered effective approaches to eliminate SMs in the water and wastewater. Moreover, the modification and/or synthesis of musk derivatives with low toxicity and high biodegradability could be promising, too.

With the environmental concern of SMs increasingly in the public eye, a number of studies have been published on the related research topic. However, no attempt has been made to provide a comprehensive summary and in-depth investigation on the occurrence, transportation, toxicity, as well as the analysis and treatment of SMs in the environment. The aim of this work, therefore, is to summarize the up-to-date SMs studies; describe the occurrences of SMs in the environmental samples; discuss their fate and toxicity (i.e., physiological toxicity and genotoxicity), compare their analysis methods; and in the end, evaluate the risk assessment of SMs and the traditional and advanced treatment process. Through this research effort, the understanding of SMs in the environment could be advanced, and the development of pollution mitigation strategies could be fostered.

2.2 Classification and Classic Synthetic Routes of SMs

2.2.1 Classification of SMs

Natural musk is a class of dry aromatic substances secreted from the sub-umbilical sac gland of mature male musk deer (Wu et al., 2014). An increasing musk demand in recent years, however, has outstripped its supply (Chan et al., 2004; Wang et al., 2014). In order to meet the demand and to promote the conservation of musk deer, artificial musks have been synthesized, serving as the substitutes for natural musks widely used in PCPs (such as shampoos, lotions, softeners, face creams, air fresheners, and washing powders) and fragrance additives (Reiner and Kannan, 2006; Salvador and Chisvert, 2007; Kang et al.,

2010; Ramírez et al., 2011). They can be divided into four categories: polycyclic musks, nitro musks, macrocyclic musks, and alicyclic musks (Homem et al., 2015b).

2.2.1.1 Nitro musks

Nitro musks are the first synthesized group among SMs. Consisting of a series of alkyl-substituted nitrobenzene compounds that are completely different from the chemical structure of natural musks, nitro musks have a typical musk fragrance. The nitro musks mainly include five types: musk xylene (MX), musk ketone (MK), musk tibetene (1-tert-butyl-3,4,5-trimethyl-2,6-dinitrobenzene, MT), musk ambrette (1-tert-butyl-3,4,5-trimethyl-2,6-dinitrobenzene, MA) and musk moskene (1,1,3,3,5-pentamethyl-4,6-dinitro-2H-indene, MM).

As firstly and widely used substitutes for natural musks, nitro musks can easily infiltrate into human cells and exert a strong bioaccumulation effect. Due to the discovery of the photosensitivity and neurotoxicity of the musk ambrette and the carcinogenicity of the MX, the European Commission decided to ban MX under REACH (Registration, Evaluation, Authorization and Restriction of Chemicals) (European Commission, 2011). The use of nitro musks thus was decreased at a rate of about 5% per year, whose market share was gradually replaced by polycyclic musks (European Commission, 2011). The basic chemical information of the five nitro musks groups and their applications are listed in Table 2-1.

2.2.1.2 Polycyclic musks

Polycyclic musks, as the name suggests, are musks with more than one ring in the molecular structure without any substituted nitro groups. Again, these chemical groups show a quite different structure from natural musks. The common polycyclic musks are: musk phantolid (1,1,2,3,3,6-Hexamethyl-5-Acetyl-indanyl, AHMI), HHCB, AHTN, cashmeran (1,1,2,3,3-pentamethyl-1,2,3,5,6,7-hexahydro-4h-inden-4-one, DPMI), celestolide (4-Acetyl-6-tert-butyl-1,1-dimethylindan, ADBI), traseolide (1,1,2,6-Tetramethyl-3-isopropyl-5-acetylindan, ATII). Polycyclic musks are now the primary groups of SMs used in PCPs (Roosens et al., 2007; Arbulu et al., 2011; Homem et al., 2015a; Nakata et al., 2015), with

AHTN and HHCB particularly frequently used in PCPs worldwide (Reiner and Kannan, 2011; Wu et al., 2012). Table 2-2 shows the information and applications of the six main polycyclic musks.

2.2.1.3 Macrocyclic musks

Macrocyclic musks compounds contain a circular macromolecular structure that does not contain nitro groups. Their structures are similar to that of natural musks, such as lactone, cyclic diester, and cyclic ketone containing 13-19 carbons. Macrocyclic musks are difficult to synthesize, and the availability of the commercial raw materials are limited, namely muscone (3-Methylcyclopentadecanone), ethylene glycol brassylate cyclic diester (Musk T), cyclopentadecanonum, and pentadecanolide.

Compared with the nitro musks and polycyclic musks, macrocyclic musks have more intense odor, requiring smaller quantities to acquire the same performances with other SMs. Meanwhile, macrocyclic musks are less sensitive to light and more stable under alkaline conditions, which promote the value of this group in the flavor and fragrance industries. Contributing to the complicated processing requirements and relatively high production costs, macrocyclic musks only share a small portion of the market, almost exclusively used in perfumes (Vallecillos et al., 2012a; Homem, 2015b). We can find the structural formula and applications of the five main macrocyclic musks in Table 2-3.

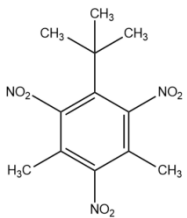
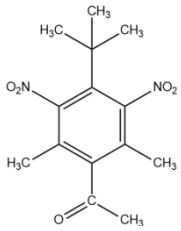
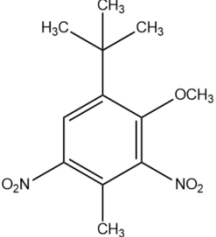
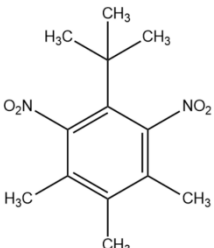
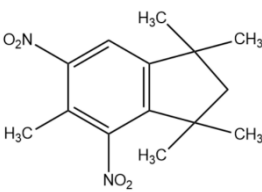
2.2.1.4 Alicyclic musks

This alicyclic musks, also known as linear musks, is a relatively new category of the SMs family. Unlike previous musks (i.e., NMs, polycyclic musks and macrocyclic musks), the molecular structure of alicyclic musks is composed of alkyl esters. Alicyclic musks are a novel SMs group that have hardly ever come into the focus of any research to date, and their use in PCPs has been very limited reported (Arbulu et al., 2011; Zhang et al., 2018a). The essential information of the three main alicyclic musks is listed in Table 2-4.

Non-toxic or low-toxic alicyclic musks can be very stable and have an easy-to-disperse aroma once formulated; this group of SMs thus has attracted increasing attention and is

expected to have a broad application in industries (Homem et al., 2015a; Rainieri et al., 2016; Homem et al., 2017; Castro et al., 2018).

Table 2-1 Five kinds of nitro musks compounds

Name	Molecular formula	Structural formula	Application
Musk xylene (MX)	$C_{12}H_{15}N_3O_6$		Cosmetics and soap flavors. Banned.
Musk ketone (MK)	$C_{14}H_{18}N_2O_5$		Modulation cosmetics and soap essence.
Musk ambrette (MA)	$C_{12}H_{16}N_2O_5$		Stopped production.
Musk tibetene (MT)	$C_{13}H_{18}N_2O_4$		Critical raw materials of fine perfumes. Banned.
Musk moskene (MM)	$C_{14}H_{18}N_2O_4$		Stopped production.

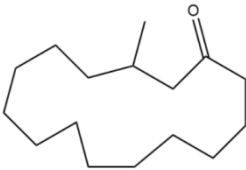
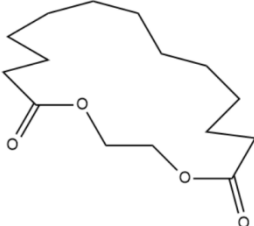
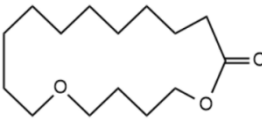
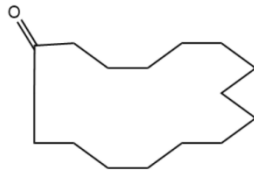
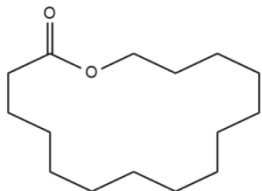
Information derived from Ahmed et al., (2018); European Commission (2011); European Parliament (2009).

Table 2-2 Six kinds of polycyclic musks compounds

Name	Molecular formula	Structural formula	Application
HHCB	C ₁₈ H ₂₆ O		It can treat myocardial infarction and has a reputation as a “king of musk”.
AHTN	C ₁₈ H ₂₆ O		High-end cosmetics, detergents and fabric softeners.
AHMI	C ₁₇ H ₂₆ O		Stopped production.
ADBI	C ₁₇ H ₂₄ O		Cosmetics and soap essences.
ATII	C ₁₈ H ₂₆ O		Fabric, personal care and high-grade fragrance formulations.
DPMI	C ₁₄ H ₂₂ O		Advanced perfumes and cosmetics.

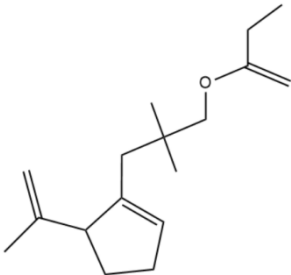
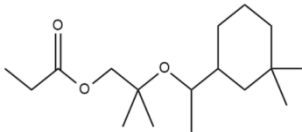
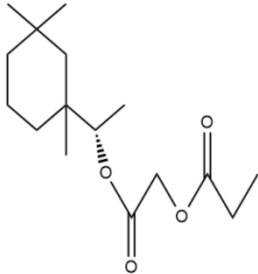
Information derived from Kevekordes et al., 1997; Draisci et al., 1998; Arpinpont et al., 2016.

Table 2-3 Five kinds of macrocyclic musks compounds

Name	Molecular formula	Structural formula	Application
Muscone	$C_{16}H_{30}O$		High-grade cosmetic essences, medicine.
Musk T	$C_{15}H_{26}O_4$		Blending fragrance for colognes, cosmetics, shampoos, detergents, etc.; perfume compound for soap.
Musk M	$C_{15}H_{28}O_3$		Cosmetic fragrance perfume compound for soap.
Cyclopentadecanone	$C_{15}H_{28}O$		Cosmetic essences, even food and medicine industries.
Pentadecanolide	$C_{15}H_{28}O_2$		High-grade cosmetic essences, co-aromatic action.

Information derived from Zhou, 2016 (in Chinese).

Table 2-4 Three kinds of alicyclic musks compounds

Name	Molecular formula	Structural formula	Application
Cyclomusk	$C_{17}H_{28}O_2$		It is very stable and easy to emit fragrance, and it is very common to use it in combination with macrocyclic musks, especially in “white musk fragrance”.
Helvetolide	$C_{17}H_{32}O_3$		It performs particularly well in a variety of liquid end products (such as alcohol solutions, shampoos, and shower gels) and lotions. It is one of the rare “top note” musk.
Romandolide	$C_{15}H_{26}O_4$		Most similar to HHCB.

Information derived from Arpinpont et al., 2016.

2.2.2 Synthetic status of SMs

2.2.2.1 Synthetic status of Musk Ketone

Musk ketone is one of the key aroma components of natural musks. Research efforts have been centered on the synthesis of musk ketones during the past years. The left-lateral isomer of musk ketone has a much stronger musk aroma than the right-lateral one. Thus, the synthesis of the left-lateral musk ketone isomer is extensively studied.

A recent patent (Tanabe et al., 2005) disclosed a left-lateral ketone isomer synthesis. Chiral citronellic acid derivatives and undecylenic acid esters were used as raw materials and Claisen condensation, decarboxylation, cyclization, and hydrogenation were involved during the synthesis. This reaction route was short, the total yield could reach 72%, and the use of the expensive 9-nonyl Grignard reagent was avoided. Compared with the synthesis route of Janis et al. (2001), the raw material costs were further reduced, and progress has been achieved towards the industrialization of left-lateral isomer ketone. This synthetic route is shown in Figure 2-1 (a). Ye et al. (2011) generated a Michael reaction that was also used to generate left-lateral ketone *isomer* (Yang et al., 2010). Cycloketene and disulfone methane were used as the raw material and the ketone was synthesized through carbonyl protection, selective removal of disulfone, and then decarboxylation protection. This reaction route, as shown in Figure 2-1 (b), easily operated and lowly cost, has been developed for industrial application.

An environmental and health concern on the SMs products led to the development of the new alicyclic musks. A continuous musk synthesis development opens up the possibilities of advancing the synthesis routes, generating low-toxic and cost-effective SMs products. As environmentally-friendly alternatives to nitro musks (e.g., MKs) and polycyclic musks, the synthesis of alicyclic musks has attracted increasing attention. The synthetic routes for representative alicyclic musks are discussed as follows.

2.2.2.2 Synthetic status of Helvetolide

Helvetolide is an artificial, commercial product synthesized and registered by Firmenich. It has a strong musk aroma, accompanied by fruity notes. According to the patent literature disclosed by Firmenich (Wolfgang and Karl-Heinrich, 1992), the ketal was formed using 3,3-dimethylcyclohexyl methyl ketone and 2-methyl propylene glycol with Lewis acid as a catalyst. Then, DIBAH (Diisobutylaluminium hydride) was used to catalyze the ring-opening to produce compound I, which was then reacted with propionyl chloride under the catalysis of pyridine to form an ester, that is, the Helvetolide, with a total yield of 21.2%. The specific synthesis route is shown in Figure 2-1 (c).

2.2.2.3 Synthetic status of Romandolide

Romandolide is a successful alicyclic musk introduced by Firmenich as a successor to the Helvetolide and has also achieved excellent results for the deployment of fragrance. According to the published Firmenich patent document (Williams, 2000), the synthetic process for Romandolide initially required synthesis of (1S, 1'R)-1- [(3', 3'-dimethyl-1'-cyclohexyl)] ethanol from (+)- β -dihydromyrcene (Ansari, 1973). This was then reacted with compound II to form an ester (i.e., Romandolide). The specific synthesis route is shown in Figure 2-1 (d).

2.2.2.4 Synthetic status of Serenolide

Serenolide [2- [1'- (3'', 3''-dimethylcyclohexyl) ethoxy]-2-methyl-propyl] cyclopropane has a strong musky aroma, accompanied by mild woody and licorice-like notes. It can be used in daily cosmetic formulations, and the ratio used in flavors can reach 12.5%. The company GIV used a compound I discovered by Firmenich to synthesize a series of alicyclic musks, including Serenolide.

The patent literature (Philip and Riccardo, 2008) published by GIV showed that the synthesis route of Serenolide was as follows. 3,3-dimethylcyclohexylethanol and 3-methylbutylene oxide was reacted under the catalysis of ethyl aluminum chloride to form

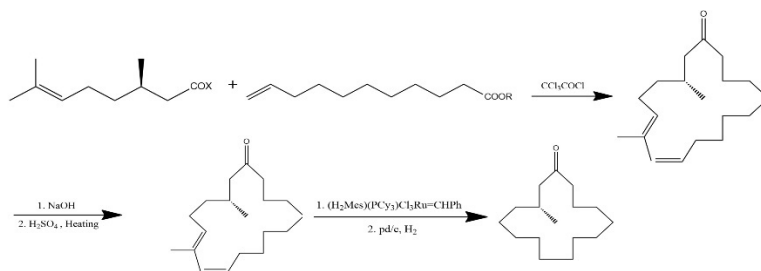
Compound I, which was then reacted with cyclopropanecarboxylic acid to produce Serenolide. The yield of the first synthesis step for Compound I was 38%, while that for the synthesis of Compound A was 75%. The total yield of the process was 28.5%, which showed that GIV Corporation had made a breakthrough in the synthesis of Compound I. The specific synthesis route is shown in Figure 2-1 (e).

2.2.2.5 Synthetic status of Sylkolide

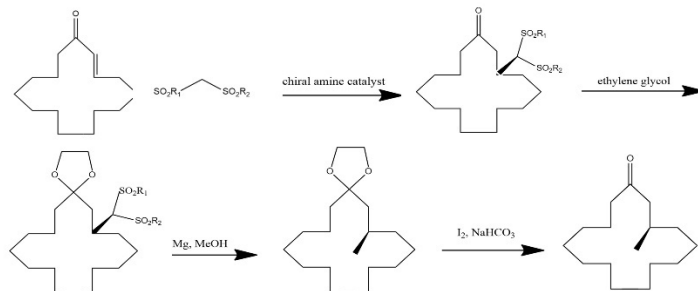
Sylkolide [2'-(3", 5"-Dimethylhexa-3"-ene-2"-yloxy)-2'-methylpropyl cyclopropanecarboxylate] has musky, powdery notes with a slight scent of green grass. Due to its unique properties, it is particularly suitable for fruity-flowery scents and Cashmere wood essences.

According to the published patent document by GIV (Kraft and Mueller, 2011), the synthesis route for Sylkolide involves reduction of 3(E)-3, 5-dimethyl-3-hexen-2-one with lithium aluminum hydrogen to give 3(E)-3, 5-dimethyl-3-hexen-2-ol. This is then reacted with 3-methylbutylene oxide under the catalysis of tin tetrachloride to form 3'(E)-2-(3',5'-dimethyl-3'-hexene-2-yloxy)-2-Methyl propanol, and then finally, Steglich esterification with cyclopropyl carbamate produces Sylkolide. This patent does not disclose the yield of this compound and the synthetic route is shown in Figure 2-1 (f).

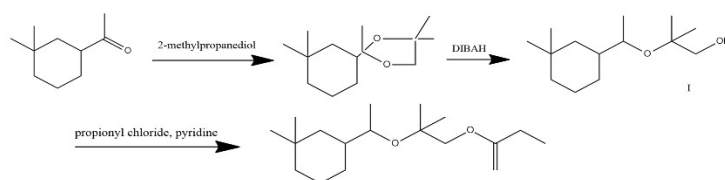
Musks spices are of great significance in both the pharmaceutical and perfume industries. In traditional Chinese medicine (TCM), a large number of prescriptions used musks, and some expensive TCM formulae required a lot of SMs. Currently, however, the production capacity for left-lateral isomer ketone is still very small and expensive. If the synthetic route for left-lateral isomer ketone can be further developed and perfected to achieve industrial-scale production, it will certainly enrich the perfumer's raw materials library, and can also be widely applied in the deployment of daily use chemical essences – and so this area has been the subject of much attention from organic synthesis researchers for a considerable period.



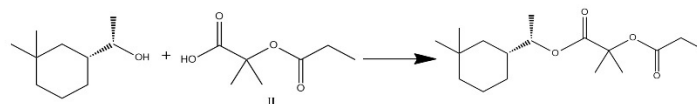
(a) Synthetic route of left-lateral musk ketone. Tanabe, et al., 2007.



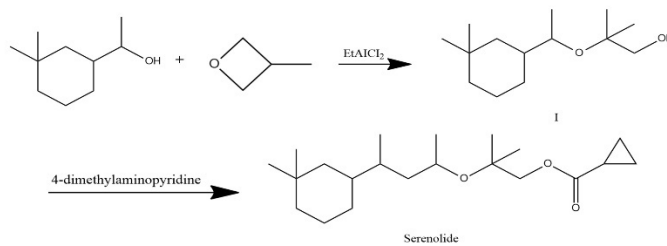
(b) Synthetic route of left-lateral musk ketone with simpler conditions. Ye and Sun, 2011.



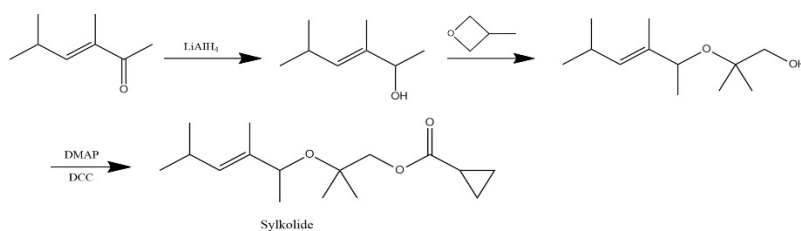
(c) Synthetic route of Helvetolide. Wolfgang and Karl-Heinrich, 1992.



(d) Synthetic route of Romandolide. Williams, 2000.



(e) Synthetic route of Serenolide. Philip and Riccardo, 2008.



(f) Synthetic route of Sylkolide. Kraft and Mueller, 2011.

Figure 2-1 Synthetic routes of 6 kinds of synthetic musks

2.3 Occurrence of SMs in Environmental Samples

As a class of relatively non-polar industrial additives, SMs have strong lipophilicity, low degradability, and great bioaccumulation (Lu et al., 2011a). The extensive usage of SMs has led to their ubiquitous distribution in the environment. To date, the occurrences of SMs have been reported in environmental samples such as those from surface water, sewage, sludge, sediment, soil, air, marine biota, human milk and blood (Hu et al., 2010; Sun et al., 2014; Cunha et al., 2015; Fontal et al., 2016; Montesdeoca-Esponda et al., 2018). In addition, SMs have been measured in a number of different regions, including the United States, Canada, Germany, Switzerland, and China (Schwartz et al., 2000; Peck et al., 2004; Andresen et al., 2007; Yin et al., 2012; Huang et al., 2016), as well as from the Arctic (Xie et al., 2007).

2.3.1 Water samples

2.3.1.1 Surface water

Researchers have reviewed the concentration and distribution of SMs in surface water (lakes, rivers and oceans) since the 1990s (Rimkus et al., 1999; Bester et al., 2009; Vallecillos et al., 2015a). The occurrence of SMs in North America (such as the United States and Canada) has been widely recorded. Peck et al. (2004) monitored water from Lake Michigan in the USA in 2001 and evaluated the average water concentration of AHTN was 4.7 ng/L, which was higher than that of HHCB (1.0 ng/L). Andresen et al. (2007) carried out comparative analyses of water samples from Lake Ontario in Canada and the German Bight in 2005. Their study showed that the concentration of HHCB in water samples of Lake Ontario ranged from 2-7 ng/L and the concentration of AHTN ranged from 0.2-0.8 ng/L, while the concentration of HHCB from German Bight ranged from 0.5-5.5 ng/L, and the concentration of AHTN ranged from 0.2-1.4 ng/L, revealing that overall the water samples of Lake Ontario had a higher concentration of HHCB and a lower concentration of AHTN than those from German Bight.

High concentration levels of polycyclic musks have been detected in water samples in Europe, especially in western European countries, largely due to the habitual use of polycyclic musks in PCPs, and the usage habits. Sumner et al. (2010) analyzed surface water samples near the Tamar Valley in Cornwall and Devon, England in 2007. The detected HHCB and AHTN concentrations ranged from 6-28 ng/L and 3-10 ng/L, respectively. Schwartz et al. (2000) sampled the Ruhr, Elbe, and Rhine rivers in North Rhine-Westphalia, Germany, and the results showed that the concentrations of HHCB were 370 ng/L, 120 ng/L, and 70 ng/L, respectively. Quednow et al. (2010) sampled 25 sites in the Schwarzbach, Modau, Winkelbach, and Weschnitz rivers in southern Frankfurt, Germany, and found that HHCB concentrations ranged from 5-678 ng/L, with an average of 141 ng/L; AHTN concentrations ranged from 3-299 ng/L, and the average value was 46 ng/L. This study also showed that the concentrations of HHCB and AHTN changed seasonally and that generally, concentrations were lower in summer than in winter.

Buerge et al. (2003) analyzed water samples from lakes, rivers, and streams in central Switzerland, and found that HHCB concentration in the lakes ranged from 2-47 ng/L, and that AHTN concentration in the lakes ranged from 1-18 ng/L. In this study, HHCB concentration in the rivers ranged from 5-564 ng/L, and AHTN concentration ranged from 2.3-186 ng/L, so the concentration of HHCB was found to be higher than that of AHTN in the lakes and rivers.

Analysis of the concentrations of polycyclic musks in water environments worldwide revealed that they were higher in water samples in Europe than in the United States and Canada, and that in most regions, the concentration of HHCB was higher than that of AHTN (Inseok et al., 2010).

Some studies have been conducted to assess the occurrence of SMs in marine and coastal seawater (Sumner et al., 2010; Vecchiato et al., 2016). Sumner et al. (2010) studied the

occurrence of SMs fragrances in an estuarine and coastal environment. High concentrations of HHCB and AHTN (987-2098 ng/L and 55-159 ng/L, respectively) as well as lower concentrations of ADBI (4–13 ng/L), AHMI (6–9 ng/L), MX (4–7 ng/L) and MK (18–30 ng/L) were identified in the sewage treatment plants effluents discharging into the Tamar and Plym Estuaries (UK), and the other musks were generally not detected in the estuarine and coastal waters. SMs in sewage was found to be emitted into the surface seawater through the Venice Lagoon (Vecchiato et al., 2016). SMs (i.e., HHCB and AHTN) were detected in the coastal surface seawater of Terra Nova Bay in the Ross Sea, Antarctica, where emissions from the nearby research station, as well as a contribution from atmospheric transport, were hypothesized (Vecchiato et al., 2017). A total concentration 112 ng/L of SMs was also investigated in the surface seawater of the Sicily Channel, Central Mediterranean in offshore and coastal areas (Vecchiato et al., 2018a). Recently, the occurrence of SMs has been reported in the seawater and snow of Ny-Ålesund, Svalbard (Vecchiato et al., 2018b), with the concentrations of SMs up to 72 ng/L in the surface snow near the settlement.

2.3.1.2 Sewage

Approximately 77% of SMs gain access to the sewerage system and reach WWTPs (Reiner et al., 2007a). Numbers of publications have reported the concentrations of SMs in the sewage (Llompart et al., 2003; Horii et al., 2007; Reiner et al., 2007b; Clara et al., 2011; Vallecillos et al., 2014a). The residue of SMs in WWTP effluent will contaminate both freshwater and marine environment (Horii et al., 2007; Clara et al., 2011). A study of the distribution of polycyclic musk fragrance in WWTP effluents in the United States reported that AHTN levels in effluents ranged from < 0.05 ng/L to 0.44 ng/L, with a mean value and standard deviation of 0.18 ± 0.11 ng/L (Sun et al., 2014). HHCB levels in sewage were relatively higher, ranging from 0.45 to 4.79 ng/L, with a mean value and standard deviation of 1.86 ± 1.01 ng/L. Clara et al. (2011) investigated the occurrence of DPMI, ATII, HHCB,

and AHTN in sewage during wastewater treatment. They found that AHTN and HHCB were the commonest SMs, with influent concentrations of 0.41-1.8 ng/L and 0.9-13 ng/L, respectively. DPMI was also detected, although in notably lower concentrations.

2.3.2 Solid samples

2.3.2.1 Sludge

Sludge is considered to be an appropriate matrix for investigating the concentration and distribution of SMs from WWTPs. Sun et al. (2014) monitored the concentrations of AHTN and HHCB in sludges collected from 40 WWTPs in the USA. The AHTN concentrations in sludge ranged from 0.65-15.0 mg·kg⁻¹ DW (dry weight), and HHCB sludge concentrations were between 4.1 and 91 mg·kg⁻¹. The results showed that the level of HHCB was 10 times higher than AHTN in the effluent, and averaged 9.4 times in the sludge, indicating that HHCB emissions far exceeded that of AHTN. Similarly, Di Francesco et al. (2004) suggested the concentrations of AHTN in the sludge ranged from 8-51 mg·kg⁻¹, HHCB levels from 22-86 mg·kg⁻¹. Osemwengie (2006) reported AHTN and HHCB levels in the sludge ranging from 8.7-17.1 and 31.8-76.7 mg·kg⁻¹, respectively. The average concentrations of AHTN and HHCB in sludge collected from a WWTP in Kentucky were 3.1 and 9.5 mg·kg⁻¹, respectively (Horii et al., 2007). Reiner et al. (2007b) reported AHTN and HHCB concentrations of 2.73 ± 1.09 and 26.6 ± 14.0 mg·kg⁻¹, respectively, in sludge from a New York WWTP. All above studies showed that HHCB level was generally greater than AHTN.

2.3.2.2 Sediments

Settling at the bottom of the water body (i.e., lakes and rivers), sediments could serve as an environmental sink for SMs. Peck et al. (2006b) studied sediments from Lake Ontario, Canada and Lake Erie in the United States in 2003. The concentration of HHCB in Lake Erie was 3.2 ng/g, while the HHCB in Lake Ontario had a higher concentration of 16 ng/g DW, and the AHTN concentration was 0.96 ng/g DW. Sapozhnikova et al. (2010) analyzed

sediments from three rivers entering Chesapeake Bay, USA, the Magothy, Corsica, and Rhodi rivers. The Magothy River was found to have the highest SMs contamination, whose sediment contains 9.2 ng/g DW HHCB, and 8 ng/g DW AHTN. In the Rhodi River, HHCB concentration was 2.3 ng/g DW and AHTN concentration was 0.15 ng/g DW. The lowest sediment contamination was reported in the Corsica River, with reported HHCB and AHTN concentrations of 1.6 ng/g DW and 0.14 ng/g DW, respectively. Heberer (2002) carried out studies of polycyclic musks in river sediments from Berlin, Germany, and found that the average concentrations of HHCB, AHTN, ADBI, and ATII were 0.40 $\mu\text{g}\cdot\text{g}^{-1}$, 0.46 $\mu\text{g}\cdot\text{g}^{-1}$, 0.01 $\mu\text{g}\cdot\text{g}^{-1}$, and 0.04 $\mu\text{g}\cdot\text{g}^{-1}$, respectively, indicating that AHTN showed a higher concentration in sediment samples. Similarly, the enrichment of polycyclic musks in the sediments of the Lippe River in Germany was also detected (Kronimus et al., 2004). The occurrences of SMs are also reported in Asian areas. Hu et al. (2011a) detected the accumulation of SMs in the water and sediment of the Haihe River, and claimed that the results might reveal the increase of organic contaminant in the river's sediments over the years. Studies have shown a statistically significant correlation between SMs (HHCB and AHTN) and Total Organic Content.

Recently, research efforts attempted to assess the occurrence of SMs in marine and coastal sediments (Subedi et al., 2014; Lee et al., 2014; Huang et al., 2016). Lee et al. (2014) determined the concentrations of SMs in the coastal environments of Korea. Owing to the dilutive effect of tidal movement in the estuary mouth coastal sediments showed a lower detection frequency of SMs (16 out of 25 sampling sites) and concentration levels (ND to 4.4 ng/g DW) compared with freshwater sediments. Homem et al. (2017) assessed the seasonal variation of SMs in beach sands in Oporto coastal area. Among 45 collected coastal sediment samples, the concentrations of SMs ranged from 0.01 to 27 ng/g DW, and the AHTN (93%) and HHCB (76%) were the most commonly detected compounds. Higher

concentrations of SMs were detected in the summer season (total average concentration of 9.21 ng/g DW).

2.3.2.3 Soils

The occurrence of SMs in soils appears to be site and climate-specific. SMs contamination was detected in the Yangtze River Delta (China) farmland. HHCB and AHTN were reported in soil samples, at concentrations of 5.28 ng/g DW, and 3.18 ng/g DW (Zhang et al., 2011). Farmland irrigation water came from the nearby riverine environment, so it was speculated that the SMs entered the soils via contaminated irrigation water. Another study was carried out on agricultural soils of Peterborough, Canada. HHCB and AHTN were detected at the average levels of 1.00 ng/g and 1.30 ng/g, respectively (Yang et al., 2006). In addition, SMs contents in the farmland soil of the Yangtze River Delta were lower than that of sediment from the Suzhou River and sewage from treatment plants in Hangzhou City, China. It indicated that the adsorption capacity and accumulation of SMs in soil were less than those for sediments and sludge (Liu et al., 2014).

2.3.3 Air samples

Xie et al. (2007) reported a median level of HHCB and AHTN in the air of the North Sea and rural northern Germany. A higher concentration of HHCB (28 pg·m⁻³ in the North Sea and 71 pg·m⁻³ in northern Germany) were discovered in both regions than that of AHTN (18 pg·m⁻³ in the North Sea and 21 pg·m⁻³ in northern Germany). Additionally, air samples were taken from Kieller, Norway, had the HHCB concentrations of 0.14 ± 0.06 ng·m⁻³ and the AHTN concentrations of 0.052 ± 0.020 ng·m⁻³ (Kallenborn et al., 1999). In North America, HHCB and AHTN were determined in urban and rural air of Iowa and the Great Lakes with concentrations ranging 0.036 - 0.80 ng·m⁻³ for HHCB and 0.032 - 0.33 ng·m⁻³ for AHTN (Peck and Hornbuckle, 2004). The concentrations of HHCB and AHTN determined at the GKSS Research Centre and over the North Sea appeared consistent with

those determined in Kjeller, Norway (Kallenborn et al., 1999), and in rural areas in North America (Peck and Hornbuckle, 2006).

SMs have also been detected in the air of the Polar Regions (Xie et al., 2007; Vallecillos et al., 2015a). Xie et al. (2007) measured HHCB and AHTN in the atmosphere and brine in the Arctic and the North Sea. The medial levels of gaseous phase HHCB and AHTN were 4 and 18 $\text{pg}\cdot\text{m}^{-3}$ in the Arctic, as well as 28 and 18 $\text{pg}\cdot\text{m}^{-3}$ in the North Sea, and HHCB was found to be quickly removed by atmospheric degradation, while AHTN was relatively persistent in the atmosphere. In the Arctic, deposition fluxes dominated the air-sea gas exchange of HHCB and AHTN, suggesting atmospheric inputs were the main source of HHCB and AHTN in the Polar Regions (Xie et al., 2007).

The concentrations of SMs in different media are shown in Table 2-5, and the ratio of the accumulation to the lowest background value (Relative concentration) was calculated using suitable data from the literature. The reports above on the concentrations and distributions of SMs showed that most researchers investigated SMs in just one or two types of environmental samples, such as surface waters (Buerge et al., 2003), sewage sludge (Zeng et al., 2005), sediments (Lou et al., 2016), air (Fontal et al., 2016). Some reports involved a comparative analysis of SMs concentrations in samples from similar environments in different areas; however, a comparison of SMs concentrations from many different environmental samples would help the comprehensive analysis of SMs distribution. In addition, there are few studies or mechanism analyses on the migration and transformation of SMs in various environmental media. The stereoisomerism of SMs needs to be properly

Table 2-5 The level of synthetic musks in different media

Categories	Location	Environment or biota	Sample collection	Concentration	Relative concentration (%)	Reference
HHCB	Atlantic Ocean	Spinner dolphins	Collected from animals stranded in Florida coastal waters	183 ng/g (LW) ^a	23.7	Kannan et al., (2005)
HHCB	Atlantic Ocean	Bottle-nose dolphins		12-76 ng/g (LW) ^a	0.62-9.27	
HHCB	Atlantic Ocean	Dwarf sperm whale		7.4 ng/g (LW) ^a	N/A	
HHCB	Pacific Ocean	Mussels	Collected from Asia-Pacific coastal waters	1300 ng/g (LW) ^a	N/A	Nakata et al., (2012)
AHTN	Pacific Ocean	Mussels		230 ng/g (LW) ^a		
HHCB	Atlantic Ocean	Blue mussels	collected from 1991 to 2005 from New Bedford Harbor	836 ng/g (LW) ^a	1.39-176.88	Subedi et al., (2014)
AHTN	Atlantic Ocean	Blue mussels		376 ng/g (LW) ^a	0.07-79	
ΣSM	Oporto coastal area	dune plants	Collected from 15 beaches in the Matosinhos and Vila Nova de Gaia municipalities in March 2016.	4.7-350 ng/g (DW) ^b	N/A	Ribeiro et al., (2017)
HHCB	Puhe estuary	Mussels	Collected from Ebro Delta, Po estuary and Tagus estuary	34.52 ng/g (DW) ^c	N/A	Cunha et al., (2015)
HHCB	Ebro delta	Calms	Collected from Ebro Delta	33.10 ng/g (DW) ^c	N/A	
HHCB	Italy rivers	Freshwater fish	Collected in northern Italy from rivers Piave, Po, Livenza, Ticino, Adige, Torrent Gadera and Lake Sompunt;	4-47 ng/g (LW) ^b	N/A	Draisci et al., (1998)
AHTN	Italy rivers	Freshwater fish	River Garigliano located in southern Italy	4-105 ng/g (LW) ^b	N/A	
AHMI	Italy rivers	Freshwater fish		4-5 ng/g (LW) ^b	N/A	
HHCB	Haihe river (China)	surface water	A total of 23 surface water samples and 13 sediment samples from 23 sites along the Haihe River, Dagu Drainage River, and Chentaizi	3.5-32 ng/L ^b	N/A	Hu et al., (2011a)
AHTN	Haihe river	surface water		2.3-26.7 ng/L ^b	N/A	
ΣSM	Haihe river (China)	surface water		5.9-120.6 ng/L ^b	N/A	
HHCB	Haihe river (China)	Sediment		1.5-32 ng/g (DW) ^b	N/A	
AHTN	Haihe river (China)	Sediment		2-21.9 ng/g (DW) ^b	N/A	
ΣSM	Haihe river (China)	Sediment		1.7-58.8 ng/g (DW) ^b	N/A	
HHCB	Haihe river (China)	Fish	Drainage River were collected from	2.9-5.3 ng/g (DW) ^b	-0.84-0.93	
AHTN	Haihe river (China)	Fish		3-6.8 ng/g (DW) ^b	-0.69-0.5	
ΣSM	Haihe river (China)	Fish	December 29 to 30	6-18.6 ng/g (DW) ^b	-0.68-2.53	

			2008. Fish samples were collected from the Haihe River and Chentaizi Drainage River.				
HHCb	Lippe river (Germany)	Sediment	Collected from Lippe river (Germany) taken between August 1999 and March 200	0.5-20 ng/g (DW) ^b	N/A	Kronimus et al., (2004)	
AHTN	Lippe river (Germany)	Sediment		23-90 ng/g (DW) ^b	N/A		
HHCb	New York (US)	Human adipose fat samples	Collected from a hospital in New York City during 2003–2004	12-798 ng/g (LW) ^b	N/A	Kannan et al., (2005)	
AHTN	New York (US)	Human adipose fat samples		5-134 ng/g (LW) ^b	N/A		
HHCb	Austria	Female plasma	Collected from 58 women older than 50	6900 ng/L (maximum) ^c	N/A	Hutter et al., (2010)	
AHTN	Austria	Female plasma		190 ng/L (maximum) ^c	N/A		
HHCb	China	Breast milk	Collected in 2006 and 2007 from 100 volunteer women living in Shang-hai, Wuxi and Shaoxing.	63 ng/g (LW) ^a	N/A	Zhang et al., (2011)	
AHTN	China	Breast milk		5 ng/g (LW) ^a	N/A		
MX	China	Breast milk		17 ng/g (LW) ^a	N/A		
MK	China	Breast milk		4 ng/g (LW) ^a	N/A		
HHCb	Shang hai (China)	Breast milk	46 breast milk samples were collected from Luwan District of Shanghai, China in October 2006, October 2008, and August 2010.	17.7 ng/g (LW) ^a	N/A	Zhou et al., (2012)	
HHCb	Sichuan (China)	Breast milk	110 milk samples was collected from May to June in 2009.	16.5 ng/g (LW) ^a	N/A	Yin et al., (2012)	
HHCb-lactone	Sichuan (China)	Breast milk			11.5 ng/g (LW) ^a		N/A
AHTN	Sichuan (China)	Breast milk			7.85 ng/g (LW) ^a		N/A
ΣSM	Korean	Adipose tissues	43 adipose tissue samples in female collected from May 2007 and May 2008	38-253 ng/g (LW) ^b	N/A	Moon et al., (2012)	
ΣSM	Korean	Breast milk	208 samples collected from 87 lactating women	286 ng/g (LW) ^a	N/A	Lee et al., (2015)	

* Relative concentration means that the ratio of the accumulation of a substance to the lowest background value in the same environment.

^a Mean concentration ; ^b concentration range; ^c Highest concentration

taken into consideration in the content analysis of SMs in environmental samples. These issues, taken together, indicate that the pervasiveness and pollution threshold concentrations of SMs remain difficult issues that need further study, with the view to eventually develop management laws and regulations.

2.4 Fate and Toxicity of SMs in the Environment

2.4.1 Migration of SMs

To date, there have been few studies aim at the migration of SMs; and therefore, in-depth investigations in this area are desired. Kallenborn et al. (1999) tested the concentration of SMs in Norwegian air, and the results showed that the main SMs detected by the sampling was HHCB, followed by AHTN. The concentration of nitro musks in the sample was relatively low, accounting for approximately 3-12% of the total amount of SMs detected. The low concentration of nitro musks could be explained by the decreasing use of nitro musk compounds in European cosmetics at the time, though the possibility of their partial photodegradation in the atmosphere could be another contributor.

Through evaluating the concentrations of SMs in the atmosphere and water of the Lower Great Lakes, Canada, Mcdonough et al. (2016) tried to establish the relationship between SMs distribution and their volatilization in the environment. Taking the city population center as the source of these compounds near the Great Lakes, the mobilities of the polycyclic musk compounds in air and water were assessed using passive polyethylene sampler (PE) equipment, the volatility of SMs from water into the atmosphere could therefore be determined. The results indicated that AHTN volatility was detected in surface waters near Toronto and on the banks of Lake Ontario. It was concluded that polycyclic musk compounds flowed from the population center, as a source, into the water body, and then accompanied the volatilization of water into the atmosphere. The possibility of SMs

migration by an aerial route is thus suggested. The study by Villa et al. (2014) supported this hypothesis through the investigation of a medium distance atmospheric migration of polycyclic musk compounds in a glacial flow area of the Fogni Glacier (Alps in Northern Italy). Fresh snowfall and water samples were analyzed for the presence of AHTN and HHCB. Both musks were detected in the samples, supporting the statement of SMs transport via the medium distance atmosphere. By hindcasting the trajectories of the local air mass, the researchers were able to show that the local air masses had previously flowed through a densely populated area in northern Italy.

Studies have shown that the use of treated wastewater to irrigate agricultural crops may introduce artificial musks into surface waters through agricultural runoff (Pedersen et al., 2005; Ternes et al., 2007). Though their concentrations were lower than published aquatic toxicology data, the potential for more subtle effects on aquatic organisms could not be excluded (Pedersen et al., 2005).

The studies by Ternes et al. (2007) reported that SMs might be adsorbed or transformed through the soil layer, because the lipophilic properties of SMs make it cannot migrate in the soil-aquifer. There still needs some studies to clearly demonstrate the possibility of SMs to migrate in soil, whether the artificial musks in the soil can evaporate from the soil and enter the atmosphere.

2.4.2 Bioaccumulation of SMs

2.4.2.1 In marine aquatic organisms

Many researchers have examined the levels of SMs in aquatic organisms such as mollusks, crustaceans, fish, and mammals. In analyzing fish and shellfish, HHCB and AHTN have been the SMs of most concern, and nitro musks have also been included in the pollutants targeted by researchers (Cunha et al., 2015).

Montesdeoca-Esponda et al. (2018) compared SMs levels in marine organisms across

different regions. In their study, a significant HHCB concentration difference was noticed, between between organisms in Asian coastal areas and the ones in other parts of the world, particularly the Atlantic East Coast and the Mediterranean Sea. HHCB concentrations in shellfish from the Adriatic coast in Italy were similar to those of coastal areas in Massachusetts and California. AHTN concentration was more consistent in marine organisms from different regions, though a large difference of AHTN concentrations between the Mediterranean coast of Spain and the South China Sea were perceived Kannan et al. (2005) studied aquatic organisms found in the United States. The highest HHCB concentration, 183 ng/g lipid weights, was detected in adult male spinner dolphins on the coast of Florida. Others, such as the bottle-nose dolphins, showed HHCB concentrations ranging from 12-76 ng/g lipid concentration. The lowest concentration, 7.4 ng/g lipid weights, was found in dwarf sperm whales. Nakata et al. (2012) analyzed the accumulation of SMs from the entire Asia-Pacific coastal region. The frequency of HHCB detected in the samples was 81% and the frequency of AHTN was 60%, indicating that the production and use of HHCB had resulted in its bioaccumulation in Asia Pacific waters. Ribeiro et al. (2017) studied different samples collected along the coast of Porto, and showed that in all analyzed samples, HHCB has the highest concentration and detection frequency among tested SMs and then followed by MK.

2.4.2.2 In riverine aquatic organisms

Draisici et al. (1998) studied the accumulation of SMs in freshwater fish in Italian rivers and lakes, and found that AHTN and HHCB were the most discovered SMs, with AHMI presents in very small concentrations in a few samples, and no ADBI detected. The study found that SMs residue levels in the sampled fish were positively correlated with fish lipid content. Hu et al. (2011a) studied the accumulation of SMs in the Haihe River, China, and the results showed that the biota-sediment accumulation factor (BSAF) (for AHTN and

HHCB) in common carp, silver carp, and crucian carp were 2.5 and 4.0, 1.5 and 1.9, and 2.0 and 2.4, respectively. The value of BSAFs equals the concentrations of chemicals in an organism divided by the concentrations of the same chemicals in sediments (Tracey and Hansen, 1996). A value of 1.7 has been regarded as the global average BSAF in risk assessment (National Research Council, 2001). A majority of the BSAF values of the organisms in rivers were higher than 1.7, indicating that bioaccumulation of SMs was occurring in the river. Cunha et al. (2015) found higher levels of HHCB in mussels from the mouth of the Puhe River than those from the Ebro Delta. Mussels sampled from the Tagus Estuary and the Ebro Delta, had low values of HHCB and AHTN, and a high correlation was observed between HHCB and AHTN concentrations in the same samples. In addition, some studies have reported differences in HHCB concentrations detected in different aquatic organisms. The HHCB concentration in Danish salmon was 52.6 µg/kg fresh weight (Duedahl-Olesen et al., 2005), and the HHCB concentration in fish from a Swiss lake was 42 - 230 µg/kg lipid weights (Schmid et al., 2007). Its concentration was 89 - 102 µg/kg in shellfish (Picot-Groz et al., 2014) and 16 - 367 µg/kg DW in sea food from Tarragona, Spain (Trabalón et al., 2015).

2.4.2.3 In the human body

SMs have been detected many times in human biological samples such as human breast milk and blood. The SMs uptake and accumulation have been widely reported in Asian countries. Zhang et al. (2011) investigated the occurrence of SMs in breast milk in three cities (Shanghai, Wuxi, and Shaoxing) of the Yangtze River Delta. This research indicated that the concentrations of SMs were relatively low compared with that from other regions (i.e., Germany, Denmark, USA, and South Korea), and the hierarchy of the four SMs concentrations was HHCB>MX>AHTN≈MK. The average values of HHCB, AHTN, MX and MK in the samples were 63, 5, 17, and 4 ng/g lipid weights, respectively. Hu et al. (2010)

studied the SMs in the blood of 204 subjects in China and found that the median levels of HHCB and AHTN were 0.85 ng/g and 0.53 ng/g, respectively, which showed that the HHCB level was relatively higher than AHTN level. Kang et al. (2010) tested the SMs levels in Korean women of childbearing age. They observed that the median concentration of SMs (HHCB+AHTN+HHCB-lactone) in breast milk was 199 ng/g lipid weights, lower than that in serum (915 ng/g). A little correlation between SMs concentration and biological samples (e.g., umbilical cord serum, maternal serum, and breast milk, etc.) was found. SMs were identified in the blood of young Austrians, at a median HHCB concentration of 580 ng/L, in female blood (Hutter et al., 2005). and found that. SMs have also been reported in western countries too. Kannan et al. (2005) studied human tissues and nearby aquatic organisms found in the United States. Levels of AHTN and HHCB enriched in body fat sampled in New York were 12-798 ng/g and 5-134 ng/g, respectively, with a significant positive correlation detected between the concentrations of the two. Hutter et al. (2010) studied the concentrations of 11 musk products in the blood of Austrian women aged over 50, and the results showed that the accumulation concentration for polycyclic musks was higher than that for nitro musks. The percentages of HHCB, MX, MK, and AHTN in plasma samples were 89%, 63%, 43%, and 23%, respectively. The rising concentration of HHCB detected in human plasma is suggested to be associated with its increased production and use.

2.4.3 Toxicological effects of SMs

2.4.3.1 Physiological toxicity effects

There have been many studies on the toxic effects of SMs accumulated in organisms. Ford et al. (1990) exposed rats to SMs for 90 days and found that SMs produced neurotoxicity and testicular atrophy. Carlsson et al. (2000) found that MK adversely affected the reproduction and survival of zebrafish; the length and weight of female zebrafish decreased, and the mortality of their embryos increased. Wollenberger et al. (2003) studied

the effects of one kind of nitro musk compound and three kinds of polycyclic musk compounds on marine crustaceans, and found that SMs compounds can strongly inhibit the larval growth and development of the marine copepod *Acartia tonsa* at low concentrations.

SMs can induce the production of toxic enzymes. Maekawa et al. (1990) studied the toxic effects of MX on liver enzymes. The results showed that after 80 weeks of exposure to liver cells, based on a dietary level of 0.15%, malignant hepatic cell tumors increased significantly. Mersch-Sundermann et al. (1996) reported that MX and MK were powerful inducers of hepatotoxic enzymes in rats, and found that SMs compounds have a synergistic effect with toxic enzymes. Data from Luckenbach et al. (2004) showed that SMs were effective inhibitors of multixenobiotic resistance (MXR) transport proteases in marine mussels. SMs can facilitate the accumulation of other toxic substances in cells by inhibiting the function of the MXR transport proteases. Składanowski et al. (2005) conducted in vitro experiments with rats and found that SMs can inhibit the activity of AMP deaminase, which is involved in the major purine nucleotide interconversion and degradation pathways in rats. Inhibition of AMP deaminase can cause disturbances in the cellular ATP pool, including the physiological effects on muscles. Schnell et al. (2009) found that polycyclic musk compounds had the potential to interfere with steroid synthesis and metabolic activity. Nitro musks mainly interfere with the sulfation of estradiol, and with the catalytic reaction of the CYP1A enzyme, while HHCB and AHTN can strongly inhibit the catalytic activity of CYP3A, CYP17 and CYP19 enzymes.

SMs are endocrine disruptors. Yamauchi et al. (2008) showed that polycyclic musk compounds and nitro musk compounds could reduce estrogen receptor expression levels, while Schreurs et al. (2002) researched the effects of AHTN and HHCB on estrogen receptors and found that the weak estrogen effect was observed at 10 μM for the SMs and the anti-estrogen effect was observed at 0.1 μM . Li et al. (2013) assessed the effects of AHTN

and HHCB on seven types of steroid hormones and steroid synthesis pathways, and their results showed that high levels of AHTN could affect the sensitivity of H295R cells to ACTH, and that HHCB and AHTN inhibited progesterone and cortisol production, mainly by affecting the use of 3 β HSD2 and CYP21 enzymes in the H295R cell line. Taylor et al. (2014) found that the concentration of nitro musk compounds in blood was negatively correlated with the concentration of luteinizing hormone – with findings that were supported by animal models and laboratory studies, indicating that nitro musks were a group of weak estrogen, and that nitro musk compounds may increase the genotoxicity of other chemicals.

2.4.3.2 Genotoxicity effects

SMs may have a mutagenic effect on biological genes. Emig et al. (1996) studied the genotoxicity of five nitro musks through the Salmonella microsome toxicity test and the SOS chromosomal aberration test. Their results showed that mutagenicity and genotoxicity were not found in MX, MK, MM or MT. However, MA showed mutagenicity by metabolic activation of rat liver mitochondrial supernatant (S9), indicating that the mutagenicity of different nitro musks varied. Kevekordes et al. (1997) conducted a micronucleus test of Hep G2 in human lymphocytes and human hepatoma cell lines using polycyclic musk compounds, and found no genotoxicity in polycyclic musk compounds such as HHCB, AHTN, ADBI, or AHMI. The study by Mersch-Sundermann et al. (2001) showed that MK played a key role in inducing the activation of benzo(a)pyrene, amplifying the genotoxic effects of benzo(a)pyrene in human Hep G2 cells. The study also showed that human exposure to MK may increase their susceptibility to health hazards associated with benzo(a)pyrene and other polycyclic aromatic hydrocarbons.

Zhang et al. (2017b) studied the long-term carcinogenicity of musk xylose by using normal human hepatocytes. The researchers found that MX induced proliferation of normal human hepatic cells in the human liver TGF- β signaling pathway, which in turn reduced the

inhibitory effect of the TGF- β pathway on C-myc oncogene, showing that the indefinite cell proliferation may cause of liver tumors.

Finally, 76 kinds of polycyclic musks (Liu et al., 2004) were reviewed. Their structures were determined. The SMILES (Simplified Molecular Input Line Entry System) codes (Table 2-7) were introduced and integrated with various environmental impact indicators collected from the EPI database (Table 2-6), for use as an environmental assessment reference. Missing data for environmental indicators highlights areas where additional research is needed.

In summary, SMs compounds could directly or indirectly volatilize into the atmosphere and/or migrate to other regions. The migratory effects of synthetic compounds such as macrocyclic musk compounds and lipid musk compounds should be included in the associated research. In addition to the transportation and fate of SMs within short- and medium- distances, research efforts need to be extended to their long-distance transportation potential, where secondary contamination might occur.

Furthermore, more information on the exposure of SMs in the environment, and their potential toxicological impact on the ecosystems (e.g., body loadings and related toxic and mutagenic effects) are desired.

Table 2-6 Summarize the parameters of environmental impact assessment indicators for 76 kinds of polycyclic musks

No.	logK _{ow}	VP (Pa)	Henry law constant (atm-m ³ /mole)		logK _{aw}	logK _{oa}	logK _{oc}	logBCF	logBAF	EC ₅₀	Biotransformation Half-lives (hr)				LC ₅₀ (mg/L)		
			Bond Est	Group Est							Bond Est	Green Algae	Air	Water	Soil	Sediment	Fish
1	5.854	0.0195	3.18E-005	7.73E-006	-2.886	8.74	4.3587	2.94	3.29	0.182	16.9	1440	2880	13000	0.069	0.056	0.005
2	5.93	0.0195	3.18E-005	7.05E-006	-2.886	8.816	4.401	2.993	3.094	0.162	34.5	1440	2880	13000	0.06	0.049	0.004
3	6.42	0.0247	4.22E-005	9.96E-006	-2.763	9.183	4.672	3.317	4.64	0.078	15.7	1440	2880	13000	0.023	0.019	0.0011
4	6.35	0.0252	4.22E-005	1.09E-005	-2.245	7.945	4.274	2.843	4.058	0.088	14.5	1440	2880	13000	0.027	0.023	0.00134
5	4.75	0.000949	2.10E-004	N/A	-2.066	N/A	6.816	N/A	3.487	1.335	2.801	2.401	13.6	900	1800	8100	0.862
6	6.26	0.0683	1.32E-004	7.56E-007	-2.268	8.168	4.098	3.56	3.261	0.101	6.79	1440	2880	13000	0.032	0.027	0.0017
7	6.33	0.00852	1.32E-004	N/A	-2.268	N/A	8.598	N/A	4.336	0.023	3.846	3.494	6.66	1440	2880	13000	0.027
8	6.97	0.00306	4.66E-005	N/A	-2.72	N/A	9.69	N/A	4.976	0.007	3.678	3.394	26.1	1440	2880	13000	0.008
9	5.55	0.00472	1.86E-005	N/A	-3.119	N/A	8.669	N/A	4.191	0.108	2.743	3.218	23	1440	2880	13000	0.137
10	7.18	0.00212	3.28E-004	N/A	-1.873	N/A	9.053	N/A	5.289	0.005	4.038	4.468	23.9	1440	2880	13000	0.005
11	6.28	0.00526	2.24E-004	4.06E-005	-2.038	8.318	4.791	3.814	4.77	0.091	37.4	1440	2880	13000	0.028	0.024	0.00148
12	5.87	0.0019	9.99E-006	2.13E-005	-3.389	9.259	4.62	3.543	3.955	0.186	8.37	1440	2880	13000	0.07	0.057	0.005
13	6.37	0.000824	1.33E-005	-3.265	9.635	4.897	3.867	4.492	8.46	N/A	1440	2880	13000	0.027	0.023	0.00133	0.09
14	7.21	0.00035	6.23E-006	-3.594	10.804	5.08	4.022	3.037	9.38	N/A	1440	2880	13000	0.006	0.017	N/A	0.047
15	6.26	0.000333	5.71E-006	-3.632	9.892	4.325	3.576	3.297	2.66	N/A	1440	2880	13000	0.083	0.016	N/A	0.064
16	6.04	0.00321	2.58E-006	-3.977	10.017	4.093	3.655	4.354	3.66	N/A	1440	2880	13000	0.113	0.024	N/A	0.093
17	6.31	0.00911	4.22E-005	-2.763	9.073	4.611	3.245	3.258	13.2	N/A	1440	2880	13000	0.029	0.024	0.00148	0.093
18	6.44	0.0116	4.81E-005	-2.706	9.146	4.258	3.915	3.85	8.17	N/A	1440	2880	13000	0.066	0.012	N/A	0.049
19	7.18	0.00212	3.28E-005	-1.873	9.053	5.289	4.038	4.468	23.9	N/A	1440	2880	13000	0.005	0.005	1.44E-004	0.024

20	5.64	0.000581	7.93E-005	-5.489	11.129	4.011	2.806	3.603	11.4	0.176	1440	2880	13000	0.192	0.05	N/A	0.176
21	4.3	0.00204	1.58E-004	N/A	-2.19	N/A	6.49	N/A	3.238	1.501	2.502	2.066	9.66	900	1800	8100	N/A
22	4.75	0.000935	2.1E-004	N/A	-2.066	N/A	6.816	N/A	3.487	0.862	2.801	2.401	10.9	900	1800	8100	N/A
23	4.89	0.111	2.17E-005	4.25E-006	-3.052	N/A	7.942	N/A	3.826	0.452	2.308	2.942	40.3	900	1800	8100	N/A
24	4.89	0.111	2.17E-005	4.25E-006	-3.052	7.942	3.826	2.308	2.942	0.752	40.3	900	1800	8100	0.452	0.335	0.061
25	5.44	0.0383	2.40E-005	4.55E-006	-3.008	8.448	4.13	2.669	2.935	0.335	18.2	1440	2880	13000	0.155	0.121	0.014
26	6.4	0.00727	3.51E-005	8.29E-006	-2.843	9.243	4.661	3.305	3.335	0.081	25.6	1440	2880	13000	0.024	0.02	0.00115
27	5.98	0.0138	2.65E-005	4.88E-006	-2.965	8.945	4.428	3.03	2.891	0.148	28.8	1440	2880	8100	0.053	0.044	0.003
28	5.97	0.0131	3.18E-005	1.04E-005	-2.886	8.856	4.423	3.018	2.84	0.153	23	900	1800	8100	0.055	0.045	0.004
29	5.47	0.0338	2.40E-005	7.39E-006	-3.008	8.478	4.146	2.694	2.704	0.315	26.8	900	1800	8100	0.144	0.112	0.013
30	6.53	0.0148	9.58E-005	7.92E-005	-2.407	8.937	4.733	3.391	4.357	0.066	35.3	1440	2880	13000	0.018	0.016	8.14E-004
31	5.96	0.0239	4.36E-005	-2.749	8.709	3.992	3.602	3.516	10.6	N/A	1440	2880	13000	0.111	0.025	N/A	0.093
32	5.89	0.0317	4.36E-005	-2.749	8.639	3.954	3.554	3.701	10.6	N/A	1440	2880	13000	0.121	0.028	N/A	0.103
33	5.47	0.0629	3.28E-005	-2.873	8.343	3.721	3.278	3.194	11.2	N/A	1440	2880	13000	0.188	0.054	N/A	0.18
34	5.96	0.0266	4.36E-005	-2.749	8.709	3.992	3.602	3.464	10.2	N/A	1440	2880	13000	0.111	0.025	N/A	0.093
35	6.42	0.00777	4.22E-005	-2.763	9.183	4.672	3.317	3.42	30	N/A	1440	2880	13000	0.023	0.019	0.0011	0.078
36	6.42	0.00777	4.22E-005	-2.763	9.183	4.672	3.317	3.42	30	N/A	1440	2880	13000	0.023	0.019	0.0011	0.078
37	6.35	0.00784	4.22E-005	-2.763	9.113	4.633	3.268	3.709	15.7	N/A	1440	2880	13000	0.027	0.023	0.00134	0.088
38	6.84	0.00578	5.61E-005	-2.639	9.479	4.904	3.592	3.797	26.1	N/A	1440	2880	13000	0.01	0.009	0.000369	0.043
39	5.79	0.0176	1.69E-004	-2.161	7.951	4.52	3.49	3.207	64.4	N/A	1440	2880	13000	0.073	0.059	0.005	0.187
40	5.06	0.0629	1.88E-005	-3.131	8.191	3.92	2.418	2.499	30.3	N/A	900	1800	8100	0.32	0.241	0.038	0.576
41	5.47	0.0317	2.40E-005	7.39E-006	-3.008	8.478	4.146	2.694	2.704	0.315	28	900	1800	8100	0.144	0.112	0.013
42	6.42	0.00777	4.22E-005	9.96E-006	-2.763	9.183	4.672	3.317	3.42	0.078	29.9	1440	2880	13000	0.023	0.019	0.0011

43	5.44	0.0383	2.40E-005	4.55E-006	-3.008	8.448	4.13	2.669	2.935	0.335	18.2	1440	2880	13000	0.155	0.121	0.014
44	5.4	0.0314	2.40E-005	8.10E-006	-3.008	8.408	4.108	2.645	2.85	0.354	15.5	900	1800	8100	0.167	0.13	0.016
45	5.4	0.0314	2.40E-005	8.10E-006	-3.008	8.408	4.108	2.645	2.85	0.354	14.7	900	1800	8100	0.167	0.13	0.016
46	5.93	0.0192	3.18E-005	7.05E-006	-2.886	8.816	4.401	2.993	3.094	0.162	34.5	1440	2880	13000	0.06	0.049	0.004
47	5.93	0.0192	3.18E-006	7.05E-007	-2.886	8.816	4.401	2.993	3.094	0.162	18	1440	2880	13000	0.06	0.049	0.004
48	5.93	0.014	3.18E-005	6.43E-006	-2.886	N/A	8.816	N/A	4.401	0.06	2.993	4.092	16	1440	2880	13000	N/A
49	5.47	0.109	2.40E-005	6.74E-006	-3.008	N/A	8.478	N/A	4.146	0.144	2.694	3.213	14.1	900	1800	8100	N/A
50	5.38	0.161	2.88E-005	6.00E-006	-2.929	N/A	8.309	N/A	4.097	0.174	2.632	3.834	30.9	1440	2880	13000	N/A
51	6.84	0.00429	5.61E-005	-2.639	9.479	4.904	3.592	5.293	15.1	N/A	1440	2880	13000	0.01	0.009	3.69E-004	0.043
52	7.29	0.00226	7.45E-005	-2.513	9.806	5.153	3.397	5.999	17.8	N/A	1440	2880	13000	0.004	0.004	1.12E-004	0.022
53	5.06	0.0442	1.81E-005	-3.131	8.191	3.92	2.418	3.031	14	N/A	900	1800	8100	0.32	0.241	0.038	0.576
54	5.55	0.0169	2.4E-005	-3.008	8.558	4.191	2.742	3.207	13.7	N/A	900	1800	8100	0.123	0.097	0.011	0.28
55	5.55	0.0227	2.4E-005	-3.008	8.558	4.191	2.742	3.207	14.6	N/A	900	1800	8100	0.123	0.097	0.011	0.28
56	5.47	0.0224	2.4E-005	-3.008	8.478	4.146	2.964	3.322	14.1	N/A	900	1800	8100	0.144	0.112	0.013	0.315
57	6.42	0.00573	4.22E-005	-2.763	9.183	4.672	3.317	4.706	15	N/A	1440	1800	13000	0.023	0.019	0.0011	0.078
58	6.35	0.0252	4.22E-005	-2.245	7.945	4.274	2.843	4.058	14.5	N/A	1440	1800	13000	0.027	0.023	0.00134	0.088
59	5.96	0.0225	4.36E-005	-2.749	8.709	3.992	3.602	4.602	10.3	N/A	1440	1800	13000	0.111	0.025	N/A	0.093
60	6.46	0.00904	5.78E-005	-2.627	9.087	4.269	3.926	5.169	9.99	N/A	1440	1800	13000	0.065	0.011	N/A	0.048
61	3.88	0.0037	1.19E-004	-2.313	6.193	3.006	2.226	1.841	15.8	N/A	900	1800	8100	2.482	4.22	1.312	1.334
62	3.88	0.0037	1.19E-004	-2.313	6.193	3.006	2.226	1.841	9.84	N/A	900	1800	8100	2.482	4.22	1.312	1.334
63	5.84	0.0225	9.95E-005	-2.391	8.231	4.065	3.522	3.108	7.49	N/A	1440	2880	13000	0.071	0.058	0.005	0.186
64	5.92	0.0161	9.95E-005	-2.391	8.311	4.109	3.571	3.056	7.32	N/A	1440	2880	13000	0.061	0.05	0.004	0.165
65	5.84	0.0225	9.95E-005	-2.391	8.231	4.065	3.522	3.051	7.01	N/A	1440	2880	13000	0.071	0.058	0.005	0.186

66	5.43	0.0444	7.50E-005	-2.513	7.943	3.838	3.247	2.804	8.56	N/A	1440	2880	13000	0.159	0.124	0.015	0.341
67	6.3	0.0121	1.32E-004	-2.268	8.568	4.319	3.821	3.748	7.74	N/A	1440	2880	13000	0.029	0.025	0.00154	0.095
68	5.43	0.0444	7.50E-005	-2.513	7.943	3.838	3.247	2.804	8.56	N/A	1440	2880	13000	0.159	0.124	0.015	0.341
69	6.83	0.00342	1.75E-004	1.09E-006	-2.145	8.95	4.574	4.17	8.03	N/A	1440	2880	13000	0.011	0.01	0.009	3.81E-004
70	6.79	0.00469	1.75E-004	-2.145	8.935	4.59	4.145	4.438	8.05	N/A	1440	2880	13000	0.011	0.01	4.22E-004	0.046
71	6.75	0.00462	1.75E-004	-2.145	8.895	4.568	4.122	4.333	6.68	N/A	1440	2880	13000	0.012	0.011	4.66E-004	0.049
72	6.33	0.00852	1.32E-004	-2.268	8.598	4.336	3.846	3.494	6.23	N/A	1440	2880	13000	0.027	0.023	0.00139	0.09
73	6.33	0.00852	1.32E-004	-2.268	8.598	4.336	3.846	3.494	6.23	N/A	1440	2880	13000	0.027	0.023	0.00139	0.09
74	6.71	0.0161	6.05E-004	-1.607	8.317	4.693	4.092	4.619	3.02	N/A	1440	2880	13000	0.012	0.01	4.73E-004	0.047
75	7.09	0.0121	8.03E-004	-1.484	8.574	4.903	4.082	5.469	3.17	N/A	1440	2880	13000	0.006	0.005	1.76E-004	0.027
76	6.36	0.00339	1.55E-005	-3.198	9.558	4.639	3.28	3.108	25.8	N/A	1440	2880	13000	0.025	0.022	0.00127	0.085

*76 kinds of polycyclic musks structure list Liu et al. 2004 (in Chinese). The author obtained SMILES codes by drawing a definite structure of 76 molecules, and used SMILES codes to assemble various environmental impact indicators from the EPI database (<https://www.epa.gov/tsca-screening-tools/epi-suitetm-estimation-program-interface>).

Table 2-7 A summary of the SMILES coding of partial polycyclic musks

No.	SMILES	No.	SMILES	No.	SMILES
1	<chem>CC(=O)C1=CC2C(C)(C)C(C)C(C)(C)C=2C=C1C</chem>	27	<chem>C(C)(=O)c1c2C(C)(C)CC(C)(C)c2cc(C)c1C</chem>	53	<chem>C(C)(=O)c1c(C)cc2c(C(C)(C)CCC2)c1</chem>
2	<chem>CC(=O)C1=C2C(=CC(=C1)C(C)(C)C(C)(C)CC2</chem>	28	<chem>C(C)(=O)c1c2c(C(C)(C)CC2)cc(C(C)CC)c1</chem>	54	<chem>C(C)(=O)c1c(CC)cc2c(C(C)(C)CCC2)c1</chem>
3	<chem>O=C(c(c(cc(c1C(CC2)(C)C)C2(C)C)CC)c1)C</chem>	29	<chem>C(C)(=O)c1c2c(C(C)(C)CC2)cc(C(C)C)c1</chem>	55	<chem>C(C)(=O)c1c(C(C)(C)C)cc2c(c1)CCCC2</chem>
4	<chem>O=C(c(c(cc(c1C(CC2C)(C)C)C2(C)C)C)c1)C</chem>	30	<chem>C(C)(=O)c1c(C)c(C(C)(C)CC)cc(C(C)(C)C)c1</chem>	56	<chem>C1(C)(C)c2c(C(C)CC1)cc(C(C)=O)c(C)c2</chem>
5	<chem>C1(C)(C)c2c(C(C)C)cc(C(C)C)cc2OC(=O)C1</chem>	31	<chem>C1(C)(C)c2c(C(C)(CC)C1)cc(C)c(C=O)c2</chem>	57	<chem>C1(C)(C)c2c(C(C)(CC)CC1)cc(C)c(C(C)=O)c2</chem>
6	<chem>O(CC(c(c1cc(c2C(C3C)(C)C)C3(C)C)c2)C)C1</chem>	32	<chem>C1(C)(C)c2c(C(C)(C)C1)cc(C)c(C=O)c2</chem>	58	<chem>C1(C)(C)c2c(C(C)(C)C(C)C1)cc(C(C)=O)c(C)c2</chem>
7	<chem>C1(C)(C)c2c(C(C)(C)CC1)cc1c(C(C)COC1)c2</chem>	33	<chem>C1(C)(C)c2c(C(C)(C)C1)cc(C)c(C=O)c2</chem>	59	<chem>C1(C)(C)c2c(C(C)(C)CC1)cc(C)c(C=O)c2</chem>
8	<chem>C(C)(C)(c1c(C)c2C(C)(C)CCc2c(C(C)=O)c1)CC</chem>	34	<chem>C1(C)(C)c2c(c(C=O)cc(C(C)(C)C)c2)CC1</chem>	60	<chem>C1(C)(C)c2c(C(C)(C)CC1)cc(CC)c(C=O)c2</chem>
9	<chem>C1(C)(C)c2c3c(C(C)(C)CC3CC1)cc(C(C)=O)c2</chem>	35	<chem>C(=O)(c1c2c(C(C)(C)CC2)cc(C(C)(C)C)c1)CC</chem>	61	<chem>c1(C(C)C)c(C(C)C)cc2c(c1)CCC(=O)O2</chem>
10	<chem>C1(C)(C)c2c(C(C)(C)C1)cc(C(C)C)c(C#N)c(C)c2</chem>	36	<chem>C(C)(C)(C)c1c2c(C(C)(C)CC2)cc(C(=O)CC)c1</chem>	62	<chem>c12c(c(C(C)C)cc(C(C)C)c1)OC(=O)CC2</chem>
11	<chem>C1(C)(C)c2c(C(C)(C)CC1)cc(C#N)c(CC)c2</chem>	37	<chem>C1(C)(C)c2c(C(C)(C)C1)cc(C(=O)CC)c(C)c2</chem>	63	<chem>C1(C)(C)c2c(C(C)(C)C1)cc1c(c2)CCOC1</chem>
12	<chem>C1(C)(C)c2c(C(C)(C)CC1)c(OC)c(C#N)c(C)c2</chem>	38	<chem>C1(C)(C)c2c(c(C(=O)C(C)C)cc(C(C)(C)C)c2)CC1</chem>	64	<chem>C1(C)(C)c2c(C(C)(C)CC1)cc1c(c2)CCOC1</chem>
13	<chem>C1(C)(C)c2c(C(C)(C)CC1)c(OC)c(C#N)c(CC)c2</chem>	39	<chem>C(#N)c1c2c(C(C)(C)CC2)cc(C(C)(C)C)c1</chem>	65	<chem>C1(C)(C)c2c(C(C)(C)C1)cc1c(C(C)COC1)c2</chem>
14	<chem>C1(C)(C)c2c(C(C)(C)C1)cc(C(C)C)c(O)c(C(C)C)c2</chem>	40	<chem>C(C)(=O)c1c2c(cc(C(C)(C)C)c1)CCCC2</chem>	66	<chem>C1(C)(C)c2c(C(C)(C)C1)cc1c(c2)CCOC1</chem>
15	<chem>C1(C)(C)c2c(C(C)(C)CC1)c(O)c(C=O)c(C)c2</chem>	41	<chem>C(C)(=O)c1c2c(C(C)CC2)cc(C(C)(C)C)c1</chem>	67	<chem>C1(C)(C)c2c(C(C)(C)C1)cc1C(C)(C)COCc1c2</chem>
16	<chem>C1(C)(C)c2c(C(C)(C)CC1)c(OC)c(C=O)c(C)c2</chem>	42	<chem>C(C)(=O)c1c2c(C(C)(CC)CC2)cc(C(C)(C)C)c1</chem>	68	<chem>C1(C)(C)c2c(cc3C(C)(C)CCc3c2)COC1</chem>
17	<chem>C1(C)(C)c2c(C(C)(C)C1)cc(C(C)=O)c(C)c2</chem>	43	<chem>C1(C)(C)c2c(C(C)(C)C1)cc(C(C)=O)c(C)c2</chem>	69	<chem>C1(C)(C)c2c(C(C)(C)CC(C)C1)cc1c(c2)CCOC1</chem>
18	<chem>C1(C)(C)c2c(C(C)(C)C1)c(C)c(C=O)c(C)c2</chem>	44	<chem>C1(C)(C)c2c(C(C)C1)cc(C(C)=O)c(C)c2</chem>	70	<chem>C1(C)(C)c2c(C(C)(C)CC1)cc1C(C)(C)COCc1c2</chem>
19	<chem>C1(C)(C)c2c(C(C)(C)C1)cc(C(C)C)c(C#N)c(C)c2</chem>	45	<chem>C1(C)(C)c2c(C(C)C1)cc(C)c(C(C)=O)c2</chem>	71	<chem>C1(C)(C)c2c(C(C)(C)C(C)C1)cc1c(c2)CCOC1</chem>
20	<chem>C1(C)(C)c2c(C(C)(C)CC1)c(C)c(C=O)c(C(C)=O)c2</chem>	46	<chem>C(C)(C)(C)c1c2c(C(C)(C)CC2)cc(C(C)=O)c1</chem>	72	<chem>C1(C)(C)c2c(C(C)(C)CC1)cc1c(c2)CC(C)OC1</chem>
21	<chem>c1(C(C)C)c2c(C(C)CC(=O)O2)cc(C(C)C)c1</chem>	47	<chem>C(C)(=O)c1c(C(C)(C)C)ccc2C(C)(C)CCc12</chem>	73	<chem>C1(C)(C)c2c(C(C)(C)CC1)cc1c(C(C)OCC1)c2</chem>

22	C(C)(C)(C)c1cc(C(C)C)c2c(C(C)CC(=O)O2)c1	48	C1(C)(C)c2c(C(C)(C)CC1)cc(C(C)=O)c(C)c2	74	C1(C)(C)c2c(C(C)(C)CC1)cc1c(c2)CCC01
23	C1(C)(C)c2c(C(C)(C)C1)cc(C(C)=O)cc2	49	C1(C)(C)c2c(C(C)CC1)cc(C(C)=O)c(C)c2	75	C1(C)(C)c2c(C(C)(C)C1)cc1C(C)(C)CCOc1c2
24	C(C)(=O)c1c2C(C)(C)CC(C)(C)c2ccc1	50	C1(C)(C)c2c(C(C)(C)CC1)cc(C(C)=O)cc2	76	C(C)(=O)c1c2c(C(C)(C)CC2)cc2C(C)(C)CCc12
25	C(C)(=O)c1c2C(C)(C)CC(C)(C)c2ccc1C	51	C1(C)(C)c2c(C(C)(C)CC1)cc(C(C)=O)c(C(C)C)c2		
26	C(C)(=O)c1c2C(C)(C)C(C)C(C)(C)c2cc(C)c1C	52	C1(C)(C)c2c(C(C)(C)CC1)cc(C(C)(C)C)c(C(C)=O) c2		

2.5 Analysis of SMs in Environmental Samples

The analytical methods of SMs include sample pretreatment (i.e., extraction, purification and concentration), and sample analysis (mainly chromatographic determination).

2.5.1 Sample pre-treatment

The pre-treatment methods for SMs relate to the sample matrixes and the analytical methods adopted. The occurrences and distributions of SMs in the various environment have been reported, including surface water, sewage, sludge, sediment, soil, air, marine biota, human milk and blood and other environmental media (Buerge et al., 2003; Yang et al., 2006; Kang et al., 2010; Sapozhnikova et al., 2010; Clara et al., 2011; Fontal et al., 2016; Montesdeoca-Esponda et al., 2018). The following sub-sections give a comprehensive summary of the determination, concentration, and distribution of SMs in various environments.

2.5.1.1 Water samples

Certain water environments have been reported to be seriously contaminated with SMs, so water samples detection has been essential (Rimkus et al., 1999). Water-based SMs researches have been associated with sewage and surface water (rivers, lakes, and sea water), as shown in Table 2-8. Sewage usually contains a large number of suspended particles that exhibit an SMs adsorption property, so sewage samples are usually separated by centrifuge and filtration into aqueous and solid phases, followed by subsequent extraction of the aqueous phase (Horii et al., 2007; Shek et al., 2008). Surface water contains relatively few solid particles or suspended sediment, so it can generally be directly extracted without filtering (Inseok et al., 2010) by applying one of the commonly used methods, such as liquid-liquid extraction (LLE), solid-phase extraction (SPE), solid-phase microextraction (SPME), or liquid-phase microextraction (LPME) (Bester et al., 2009; Vallecillos et al., 2015a).

Table 2-8 Analysis of synthetic musks in water samples

Samples	Compounds	Extraction	Purification	Detection	LODs (ng·L ⁻¹)	Ref.
Surface water	PCMs	LLE-n-hexane	None	GC-MS	5-20	Clara et al., 2011
Surface water domestic water	PCMs, NMs	SPE-C ₁₈	None	GC-MS	0.09-0.18	Lv et al., 2009
Surface water sewage	NMs	DLL-ME	None	GC-MS	4-33	López-Nogueroles et al., 2011
Surface water sewage	PCMs, NMs	LLE-methylene dichloride/n-hexane	None	GC-MS	0.5-2.9	Schnell et al., 2009
Sea water	PCMs	SDME	None	GC-MS	3.4-11	Wang et al., 2014
Sea water	PCMs, NMs	SPE-C ₁₈ , UAE-methylenedichloride/n-hexane	(Water phase) None, (Solid phase) florisil	GC-MS/MS	0.0032-0.0511 (Filtrate), 0.0006-0.0439 (Suspended solids)	Zhang et al., 2015b
Lake water	PCMs, NMs	SPE-XAD resin-acetone/n-hexane	Silicone	GC-MS	0.3-0.5	Peck et al., 2004
Domestic water	PCMs, MCMs	SPME	None	GC-MS	0.1-9.0	Garcia-Jares et al., 2002
Sewage	PCMs	SPME	None	GC-ECD	0.25-3.6	Polo et al., 2007
Sewage	PCMs	DLLME	None	GC-MS	0.1-1.5	Yang et al., 2012
Sewage	PCMs, NMs	HS-SDME	None	GC-MS/MS	10-30	Vallecillos et al., 2012a
Effluent wastewater	PCMs	SBSE	None	GC-MS	0.02-2.54	Gómez et al., 2011
Influent/effluent wastewater	PCMs, NMs, MCMs	On-line SPE	None	GC-MS	1-30	Vallecillos et al., 2014a
Influent/effluent wastewater	MCMs	MEPS C ₁₈ Ethyl acetate	None	GC-MS	5-10	Vallecillos et al., 2012b
Influent/effluent wastewater	MCMs	HS-SPME	None	GC-MS	0.75-5	Vallecillos et al., 2013b
Influent/effluent wastewater, River water	PCMs, NMs	SBSE	None	GC-MS	0.02-30	Ramírez et al., 2011

PCMs: polycyclic musks; NMs: nitro musks; MCMs: macrocyclic musks.

LLE is the most commonly used extraction method for water samples, as it avoids interference by solid particles in the water with extraction of the target compounds. SMs are less polar, so the commonly selected extraction solvents include n-hexane, cyclohexane, methylene chloride, toluene, petroleum ether, and various mixed solvents (Peck et al., 2004; Moldovan et al., 2009). SPE is a selective extraction method that has been rapidly used in recent years, and has the advantages of rapidity, efficiency, simplicity, low solvent consumption, and high selectivity. The solid phases that are used include C₁₈, C₈, Bio-beads SMs-2 columns, XAD-2 resin, XAD-4, XAD-8 and Absolut Nexus (Simonich et al., 2002; Buerge et al., 2003; Lv et al., 2009). At present, there is keen research for new, solid-phase adsorption material, with nano-materials based on graphene showing promise (Vallecillos et al., 2015a).

The advantages of SPME are simple operation, good reproducibility, a requirement for just a small sample, and that no extraction solvents are required. In addition, analysis techniques are relatively easy, involving GC or high-performance liquid chromatography (HPLC). The commonly used extraction head materials are Polydimethylsiloxane (PDMS), PDMS/Divinylbenzene (DVB), Carboxen-PDMS and Carboxen-DVB (Artolagaricano et al., 2003b; Bester et al., 2009). Sanchez-Prado et al. (2010) used SPME to extract nitro musks from water with the surface fiber of PDMS and the extraction mode of headspace extraction. Some research has been devoted to the development of new extraction materials, and amino-modified graphene extraction heads can detect five SMs types in the water. The performance of the extraction materials relates to interactions with the target compounds, including π - π stacking and hydrogen bond reactions. SPME is reported to have good thermal stability, excellent solvent resistance, long service life and recovery rates of 82.3% - 112% (Li et al., 2016).

The LPME process involves a combination of sampling, separation, purification, concentration, and sample injection. It is simple and quick, can detect many types of organic

solvents, and can be used directly with GC, HPLC, high performance capillary electrophoresis (HPCE), GC-MS, or capillary electrophoresis-mass spectrometry (CE-MS). It can, therefore, be used for the analysis of complex media, trace components, and components with special properties (Peck et al., 2004; Vallecillos et al., 2015a).

Dispersion liquid-liquid microextraction (DLLME) and single droplet microextraction (SDME) have also been successfully applied to the analysis of SMs in domestic sewage, influent/effluent wastewater, river water and sea water (López-Nogueroles et al., 2011; Homem et al., 2016).

2.5.1.2 Solid samples

The solid samples such as sludge and sediments strongly adsorb SMs, so they are commonly freeze-dried and extracted for analysis (Huang et al., 2016). The pre-treatments of SMs from sludge or sediments in several studies are shown in Table 2-9, and extraction methods have included soxhlet, ultrasound-assisted extraction (UAE), microwave-assisted extraction (MAE), and rapid solvent extraction (ASE) (Zeng et al., 2008; Hu et al., 2011c; Song et al., 2015).

Soxhlet is characterized by simple operation and wide application and is, therefore, the most commonly used method for the extraction of SMs from sludge or sediments. The extraction solvents are mainly cyclohexane, n-hexane, methylene chloride, acetone, or a mixture of these (Bester et al., 2009; Tian et al., 2011). However, this method consumes a large amount of reagents and needs a long extraction time.

UAE uses ultrasound to increase the penetrating power of the solvent, thereby accelerating the entry of target components into the solvent and facilitating their extraction (Montesdeoca-Esponda et al., 2013). MAE uses polar molecules to rapidly generate heat in the solvent and accelerate target compound extraction. UAE has the advantages of rapidity, high efficiency, and environmental friendliness, but it is not often reported in SMs extraction applications (Svoboda

et al., 2007).

ASE uses high temperature (50-200 °C) and pressure (6-20 MPa) to rapidly extract solid or semi-solid samples, and has the advantages of low solvent consumption, short extraction time, low matrix effects and high recovery, as well as good reproducibility. The solvents for ASE include acetonitrile, dichloromethane, n-hexane/acetic acid, and n-hexane/acetone, and the extraction time is generally 15-30 min.

Che et al. (2011) compared soxhlet extraction, UAE, and ASE to analyze the target compounds HHCB, AHTN, MX, and MK from sediments from Taihu Lake in China. The results showed that the ASE technique had the advantages of automation, high efficiency, time-saving and solvent-saving; the sample recovery rate was 86.0% - 104%, along with the detection limit of 0.03 - 0.05 ng/g.

Sludge and sediments contain large amounts of additional impurities, so the sample needs to be purified to reduce interference from the impurities with the analysis. Common purification methods include solid-phase extraction (C₁₈, alumina, silica gel and magnesium silicate), gel permeation chromatography (GPC), and silica/alumina composite columns, GPC/silica columns, and C₁₈ columns/silica gel column (Zhang et al., 2015a; Lou et al., 2016).

Table 2-9 Analysis of synthetic musks in sediments and sludge

Samples	Compounds	Extraction	Purification	Detection	LODs (ng·L ⁻¹)	Ref.
Sediment	PCMs, NMs	SE-methylene, dichloride /n-hexane	Silicone, Alumina column	GC-MS	0.20-0.28	Lou et al., 2016
Sediment	PCMs, NMs	UAE-methylene, dichloride /n-hexane	Magnesium, silicate column	GC-MS /MS	0.0022-0.042	Zhang et al., 2015a
Sediment	PCMs, NMs	ASE-n-hexane /acetone	Magnesium, silicate column	GC-MS	0.03-0.05	Che et al., 2011
Sediment	PCMs, NMs	SE- methylene dichloride	Silicone column	GC-MS	0.025-5.1	Peck et al., 2006b
Sludge	PCMs, NMs	PLE-Acetone/hexane	Silica gel column	GC-MS	3-10	Guo et al., 2010
Sludge	PCMs, NMs	HS-SPME	none	GC-MS	0.028-0.448	Llompart et al., 2003
Sludge	MCMs	HS-SPME	none	GC-MS	0.005-0.025	Vallecillos et al., 2013a
Sludge	PCMs, NMs, MCMs	HS-SBSE	none	GC-MS	5-30	Vallecillos et al., 2014b
Sludge	PCMs, NMs	PLE-ultrapure water/methanol	In-cell clean-up Florisil	GC-MS /MS	1-3	Vallecillos et al., 2012c

2.5.1.3 Air samples

SMs have semi-volatile properties that make them detectable in the air, where they exist in two forms: in a gaseous phase, and as a solid through adsorption on atmospheric particles, as noted in Table 2-10. For the gas phase, Peck et al. (2006a) used XAD-2 resin to collect air samples and applied soxhlet extraction with n-hexane/acetone mixed solvent. The samples were then purified with a foresail column, and finally, two SMs, HHCB and AHTN, were detected by GC-MS. For atmospheric particles, Fontal et al. (2016) used various collectors to sample different sized atmospheric particles, and then extracted them by soxhlet and rapid solvent extraction. After derivatization with trimethyl silane, HHCB was detected in atmospheric particulates by gas chromatography-electron impact ionization-mass spectrometry (GC-EI-MS).

2.5.1.4 Biological samples

Most biological samples are treated in a similar method to sludge and sediments (Zhang et al., 2015c; Ribeiro et al., 2017). Soxhlet extraction, ASE, MAE, and UAE can be used to extract SMs from biological samples, with LLE, SPE, SPME and cold extraction or other methods also used, as shown in Table 2-11. Solid support liquid-liquid extraction (SLE) is a liquid-liquid extraction process performed on specially treated diatomite, which increases the specific surface area available for liquid-liquid extraction and can significantly improve the extraction efficiency, simplify the process, and reduce reagent usage. SLE has been successfully applied to sample preparation for SMs in blood and urine, and has become another sample pre-treatment method for analyzing complex matrix samples (Dong et al., 2014).

As biological samples contain more fat and macromolecular compounds, they need to be purified in order to reduce and avoid the interference of matrix effects (Bester et al., 2009). The purification of biological samples is generally performed by GPC, followed by the use of a silica gel, silica gel/Al₂O₃ composite, or SPE column. Olesen et al. (2005) used a liquid-liquid extraction method to perform experiments on human breast milk, with the solvent of ethanol/diethyl ether/pentane in the ratio of 2:1:1. After extraction, the breast milk was purified by GPC (by use of a Bio-Beads S-X3 column) and SPE (by use of a Sep-Pak magnesium silicate column).

Table 2-10 Analysis of synthetic musks in air samples

Samples	Compounds	Sampling	Extraction	Purification	Detection	LODs (ng·L ⁻¹)	Ref.
Indoor air	PCMs, NMs	SPE-Tenax	HS- SPME	None	GC-MS	0.029-0.38	Regueiro et al., 2007
Indoor air	PCMs, NMs	SPE-Tenax	None	None	TD-GC-MS	0.03-2.1	Ramírez et al., 2010
Indoor air	PCMs, NMs	PUF	Sonication-Acetone/hexane	Florisil	GC-MS	N/A	Sofuoglu et al., 2010
Indoor air, cosmetic plant	PCMs	PUF	Soxhlet Dichloromethane	Silica-alumina	GC-MS	N/A	Chen et al., 2007
Indoor air	PCMs, NMs	PUF	PLE-Hexane/diethyl ester	None	GC-MS	N/A	Fromme et al., 2010
Indoor air	PCMs, NMs	TA sorbent	HS-SPME	None	GC-MS	N/A	Regueiro et al., 2009
Outdoor air	PCMs, NMs	TA tubes	Thermal desorption	None	GC-MS	N/A	Ramírez et al., 2011
Outdoor air	PCMs, NMs	XAD-2 resin	SE-n-hexane/acetone (1:1)	Florisil	GC-MS	0.00029-0.056	Peck et al., 2006b

N/A: Information not found in the literature.

Table 2-11 Analysis of synthetic musks in biological samples

Samples	Compounds	Extraction	Purification	Detection	LODs (ng·L ⁻¹)	Ref.
Blood	PCMs	LLE-n-pentane	SPE—Silicone	GC-MS	0.002-0.062	Hutter et al., 2005
Blood	PCMs	SLE	None	GC-MS /MS	0.098-3.37	Liu et al., 2015a
Breast milk	PCMs, NMs, MCMs	ASE-methylene, dichloride /n-hexane	GPC-Biobeads SX-3, magnesium silicate	GC-MS /MS	0.18-1.6	Yin et al., 2012
Breast milk	PCMs, NMs	LLE-ethanol /diethyl ether	GPC-Biobeads SX-3, SPE-Silicone	GC-MS	2-5	Reiner et al., 2007b
Breast milk	PCMs, NMs	LLE-ethanol /diethyl ether	GPC-Biobeads SX—3, Sep—Pak Florisil	GC-MS	0.23-52.6	Duedahl-Olesen et al., 2005
Fish	PCMs, NMs	UAE-methylene dichloride	GPC-Bio-beads, magnesium silicate	GC-MS /MS	0.0003-0.022	Zhang et al., 2015c
Fish	PCMs, NMs	ASE-methylene dichloride /ethyl acetate	SPE-Silicone, GPC	GC-MS /MS	1.6-38	Subedi et al., 2011
Fish	PCMs, NMs	Soxhlet	Hexane Aluminum oxide	GC-MS	0.2-1.3	Wan et al., 2006
Fish	PCMs, NMs	PLE	In-cell clean-up Florisil	GC-MS /MS	0.25-10	Vallecillos et al., 2015b

2.5.2 Sample analysis

At present, domestic and foreign detection methods for SMs have included GC, GC-MS and GC-MS/MS (Kallenborn et al., 1999; Cavalheiro et al., 2013; Godayol et al., 2015a, b). The commonly used detectors of GC mainly include ECD, FID, and NPD (Aguirre et al., 2014). Since nitro musks contain electronegative groups, ECD is very sensitive to the presence of nitro musks in samples, greatly improving the detection limit of the analytical method. Polo et al. (2007) used ECD and headspace solid-phase microextraction to analyze for MX, MK, MM, and MT in water samples. The results showed the recovery rate of samples was 92% - 108% and the detection limit of this method was 0.25 - 3.6 ng/L. GC-MS fully integrates the high separation characteristics of gas chromatography with the high discrimination ability of mass spectrometry, and is currently a widely used detection method in the analysis of SMs; most researchers used EI with ion flow stabilization, good reproducibility, and good selectivity (Zeng et al., 2005). GC-MS/MS also plays an important role in SMs analysis, has strong anti-interference abilities, and can provide enough structural information on compounds for qualitative analysis (Zhang et al., 2015a). Therefore, GC-MS/MS is suitable for the analysis of complex matrix samples such as sludge, sediments, and biological samples. Groz et al. (2014) used the GC-MS/MS detection method combined with the QuEChERS extraction method in the analysis of four SMs: HHCB, DPMI, ADBI and MK. The detection limit of this method was at a trace level (ng/g) and the average recovery rate of samples was 91% - 112%.

With the continuous introduction of SMs into the environment, as the main components of PCPs, accurate selection of the correct analytical methods is of importance for research into the environmental, ecological, and toxicological risks of SMs. In addition, as SMs are ubiquitous in environmental samples, including water, sludge, sediments, soils, air, and marine organisms,

and can be transmitted and amplified along the food chain, there will be differences in the matrix interference caused by SMs from different environmental areas. Applying suitable pre-treatment methods for different types of samples to reduce matrix interference is a continuing issue in the detection and analysis of SMs.

2.6 Risk Assessment and Control of SM Pollution

2.6.1 Environmental risk assessment

2.6.1.1 Exposure assessment

Although the high-concentrated SMs discharged into the river are largely diluted, they can still be detected in the marine environment, revealing that these SMs have widespread distribution and bioaccumulation potential (Rimkus, 1999). SMs are one of the main sources of PCPs. Researchers found that AHTN, HHCB, MK and MX are the dominant musks in these PCPs (Reiner and Kannan, 2006; Nakata et al., 2015). In consideration of the concentration of AHTN and HHCB, MK and MX in the PCPs, HHCB is the dominant component of musks (with the highest concentration) in human exposure (Roosens et al., 2007). HHCB existed in hair care products, body lotion and body washes with the concentration of $130 \mu\text{g}\cdot\text{g}^{-1}$, $140 \mu\text{g}\cdot\text{g}^{-1}$ and $190 \mu\text{g}\cdot\text{g}^{-1}$, respectively (Nakata et al., 2015). Reiner and Kannan (2006) pointed out that the determination of levels of HHCB and AHTN in PCPs is important to the assessment and characterization of potential sources of human and environmental exposures. After a series of experiments, they found that the highest concentration of HHCB and AHTN was taken into human's body through the cutaneous absorption or inhalation of shower gel, perfumes and skin creams. Lu et al. (2011a) reached a similar conclusion by confirming that shampoo is the largest contributor of musks exposure to women in China.

Due to the distribution and bioaccumulation potential, SMs have been detected in the

environment, including surface water, sewage, sludge, sediment, soil, air, marine biota, human milk and blood (Hu et al., 2010; Sun et al., 2014; Cunha et al., 2015; Fontal et al., 2016; Montesdeoca-Esponda et al., 2018). Together with the used PCPs, they entered into the marine environment through domestic wastewater discharge, and eventually interfered with marine water system (Lange et al., 2015). A number of studies that focused on the monitoring SMs in the WWTPs demonstrated that AHTN and HHCB showed the highest levels among these compounds (Yang and Metcalfe, 2006; Horii et al., 2007; Sumner et al., 2010; Wang et al., 2013; Federle et al., 2014; Sun et al., 2014; Godayol et al., 2015a, b). Specifically, the concentrations of HHCB and AHTN are 173.1 ± 43.4 ng/L and 41.6 ± 15.8 ng/L (WWTP), 52.6 μ g/kg and 32.0 ng/g DW (marine organisms), as well as 28 and 18 pg/L (Antarctic and Arctic regions) (Yang and Metcalfe, 2006; Xie et al., 2007; Montesdeoca-Esponda et al., 2018).

2.6.1.2 Impact assessment

Considering the extensive use of these PCPs, and their widespread distribution and bioaccumulation potential, SMs could pose an ecological risk (Balk and Ford, 1999). Plenty of studies have been conducted to investigate the risks brought by SMs. Gao et al. (2016) concluded that the acute (LC_{50}) and chronic toxicity values (ChV) of AHTN were obtained as 0.10 and 0.02 mg/L, respectively. Based on the toxicity criteria ($LC_{50} < 1.0$ mg/L acute toxicities and $ChV < 0.1$ mg/L chronic toxicities), AHTN is very toxic to fish, which indicates an increased risk to aquatic organisms. Lange et al. (2015) also reached the conclusion that HHCB and AHTN showed high bioaccumulation potential by measuring the musk concentrations in fish. Compared with two previous dominant chemicals, the MX and MK have been proved to have strong inducers of detoxifying liver enzymes by the detection of the induce detoxifying enzymes in the liver of rats (Mersch-Sundermann et al., 1996). However, the environmental impact of SMs remains to be controversial. Sun et al. (2014) employed the criteria of NOECs (no observed

effect concentrations) and PNEC (predicted no effect concentration) to reflect the chronic toxicity of AHTN and HHCB, and found that the detected effluent concentration of these two chemicals indicating a negligible risk to biological communities around WWTPs. Wang et al. (2013) conducted research on the regeneration of reclaimed wastewater from a park. The results indicated that AHTN and HHCB exhibit little acute toxicity with the concentration levels expected in soils. They also proved that although irrigation of reclaimed wastewater has led to the accumulation of AHTN and HHCB in receiving soils, their in-soil concentrations did not go up substantially to exceed the limits of detection. However, it may exceed the limits after a period of 243 years for AHTN and 666 years for HHCB if the reclaimed wastewater irrigation was continuously in use.

To better assess the risks of SMs in an ecological environment, BSAF is applied. Zhang et al. (2013) pointed out that BSAF is a useful parameter for understanding the distribution of SMs between sediments and organisms and can be used to estimate the bioaccumulation capacity of aquatic organisms. According to the partitioning theory between tissue lipid and sediment carbon, the standard BSAF value is 1.7 (Ozkoc et al., 2007; Hu et al., 2011a). BSAF values less than 1.7 can be explained by the partitioning theory between sediment and bivalve, while values greater than 1.7 require additional explanation to increase lipid uptake, such as biomagnification in addition to partitioning theory (Ozkoc et al., 2007). For example, the BSAFs of AHTN and HHCB were 2.5 and 4.0 for common carp, 1.5 and 1.9 for silver carp, and 1.6–2.4 and 1.6–2.6 for crucian carp, respectively, in which the larger values (over 1.7) suggested that amplification rate exists in the musks bioaccumulation of three fishes in the Haihe River (Hu et al., 2011a). Since 2007, more studies have started using BSAF to estimate the bioaccumulation capacity of an organism (Hu et al., 2011a; Zhang et al., 2013).

Furthermore, the high lipophilicity property of SMs leads to their accumulation in human

tissues. Polycyclic musks have been found in human milk and blood samples. Hutter et al. (2005) detected the concentration of four polycyclic musk compounds in the blood plasma samples and found that HHCB and AHTN accounted for the highest percentages, while cashmeran and celestolide were below the detection limit in all blood samples. HHCB and MX were detected in blood samples of women over 50 years old, with concentrations of 6900 and 190 ng/L, respectively. The authors also pointed out that the continual PCPs use, and the physiological aging-related changes might lead to higher cutaneous absorption of SMs and their accumulation in plasma (Hutter et al., 2010). Zhang et al. (2011) detected the concentrations of HHCB, AHTN, MX and MK in the breast milk of a 25-year-old mother in China, demonstrating that the highest concentration is 782 ng/g lipid weight of HHCB. They continuously compared the result to the ones reported from a number of other countries. Results found that US has the highest levels of AHTN, HHCB and MK, while the greatest MX concentration was detected in human milk in Germany (Reiner et al., 2007b; Raab et al., 2008). Therefore, the SMs bioaccumulation in human milk is more relevant to the usage frequency of PCPs than the age (Kannan et al., 2005; Reiner et al., 2007b; Kang et al., 2010; Zhang et al., 2015).

2.6.2 Pollution control

SMs have been considered as a class of contaminants that is difficult to biodegrade. The treatment of SMs typically includes biodegradation, photooxidation and ozonation. They have been extensively investigated in recent years.

2.6.2.1 Biodegradation

The biodegradability of SMs in natural environments was initially disputed. With recent, in-depth research, the biodegradation rate of SMs in natural water bodies was annually increasing, though further research about the degradation of SMs in water bodies is still required.

The $\log K_{oc}$ values of HHCB and AHTN were 3.8 ± 0.2 and $3.8 \pm 0.2 \text{ L}\cdot\text{kg}^{-1}$, respectively, through independent experiments with inactivated sludge (Artola-Garicano et al., 2003b). According to the definition of the $\log K_{oc}$ coefficient by McCall (1980), when the $\log K_{oc}$ coefficient of contaminants was greater than 3.69, they were difficult to remove from the soil. Seyfried et al. (2014) studied alicyclic musk Romandolide degradation in Organization for Economic Cooperation and Development (OECD) screening tests with activated sludge. The results showed that 60% of Romandolide can be degraded within 28 days. Besha et al. (2017) reported that the HHCB and AHTN treated after primary sludge and secondary sludge could be degraded to 64% and 53%, respectively.

The membrane bioreactor process has been widely used for the treatment of micro-contaminants, though, owing to the pore size, the removal efficiency of water-soluble SMs is less effective (Yang et al., 2017). The HHCB and AHTN degraded 36% after the treatment of membrane bioreactor, while it was degraded 60% by the treatment of activated sludge (Besha et al., 2017). Krzeminski et al. (2016) found that 60% of AHTN and HHCB were removed after the treatment of membrane bioreactor.

2.6.2.2 Photochemical degradation

Butte et al. (1999) studied photochemical degradation of nitro musks and found that all nitro musk compounds were photochemically degradable. Outdoor experiments with MT showed that they were also converted under natural sunlight. Canterino et al. (2008) found that photochemical degradation of nitro musks was a more prolonged process under light irradiation, and the half-life of direct degradation of photodegradation by-products in the summer was predicted to be 1 to 1.5 hours, rising to 6 to 10 hours in winter. With increased latitude and decreased temperature, photochemical degradation by-products lasted longer. Thus, the

opportunities for access to the food chain of aquatic organisms were increased. Similarly, Gao et al. (2016) studied photochemical degradation by-products of AHTN and found that both the bioaccumulation and toxicity of H-extracted products decreased. However, the aquatic toxicity of the OH extraction product increased at a lower temperature, and the bioaccumulation index of the by-product was 8 times that of AHTN.

2.6.2.3 Ozone oxidative degradation

Ozonation is a technique used for degrading SMs in oxidative wastewater treatment. Li et al. (2016) indicated that the removal efficiency of HHCB and celestolide can reach 99% and 96%, respectively, at a dosage of 1 mg O₃/mg DOC. The removal efficiency of several SMs during oxidative degradation such as Phantolide, traseolide and AHTN ranges from 60% to 70%. Ternes et al. (2003) reported that the use of ozone with a concentration of 5-15 mg/L would have a good oxidative degradation effect on HHCB and AHTN. Godayol et al. (2015a, b) indicated that MX and MK could not be degraded in the ozone oxidation reaction. Therefore, ozonation can only effectively degrade some SMs. Oxidative degradation of SMs was influenced by pH, ozone dosage and temperature. The authors found that the degradation efficiencies of HHCB follow the trend of O₃ > UV/O₃ > UV (Liu et al., 2012). To avoid toxic by-products and increase the removal rate, further studies should be investigated.

2.6.3 Environmentally friendly alternatives to SMs

2.6.3.1 Methodologies for generating the environmentally friendly SMs

The potential risks of PCPs to the environment and personal health have been widely identified (Balk and Ford, 1999). Synthetic, environmentally friendly products are urgently needed to replace these contaminants. Alternative compounds have been discovered to replace toxic contaminants. Table 2-12 illustrates the differences in molecular structures in these

compounds.

Penta- and Octa-BDEs have been gradually banned due to increasing environmental concerns. As an alternative, the production and use of Hexabromocyclododecane (HBCD), 1, 2-bis (2, 4, 6-dibromophenoxy) ethane (BTBPE), decabromodiphenylethane (DBDPE), and Dechlorane are suggested (Covaci et al., 2011). HBCD undergoes bromination of cis, trans, and trans-cyclododecatriene (Arsenault et al., 2007). Compared with PBDEs, the resulting parental structures of HBCD changed from biphenyl rings to cyclododecanes. The structure of BTBPE and DBDPE are similar, and the chain structure in the middle of two benzene rings is changed. Oxidized with hydrogen peroxide phenol and bromine were converted to 2,4,6-tribromophenol and 1,2-dichloroethane, respectively. These two products were further used to synthesize BTBPE through condensation reaction (Covaci et al., 2011). DBDPE was generated with dichloroethane and phenol by bromination as a brominating agent (Liu, 2002).

Thiram, a replacement of Mirex as Table 2-12 illustrated, was generated by ammonia through condensation and hydrogen peroxide oxidation (Adeppa et al., 2010). Levorotatory-muscone was selected as an alternative to the emerging pollutant musk ketone. The updated products, as abovementioned, not only fulfilled the function of their parent products, but also exerted less adverse impact on the environment (Liu, 2002). Their potential application in the modification of SMS, therefore could be investigated.

Table 2-12 Differences of molecular structures in emerging contaminants

Categories	Restricted chemicals	Emerging contaminants (Substitutions of the restricted chemicals)	Alternative structures
BFR	PBDEs	HBCD	Parent structure
		BTBPE	Chain structure
	PCBs	DBDPE	Chain structure
		SCCPs	Parent structure
Pesticide	Mirex	Thiram	Parent structure
		Bisultap	Parent structure
	Chlordane	chlorpyrifos	Parent structure
		Deltamethrin	Parent structure
PCP	Musk ketone	Levorotatory-muscone	Substituent
	Helvetolide	Romandolide	Substituent
		Serenolide	Substituent
	Bisphenol A	Bisphenol F	Substituent
		Bisphenol S	Parent structure

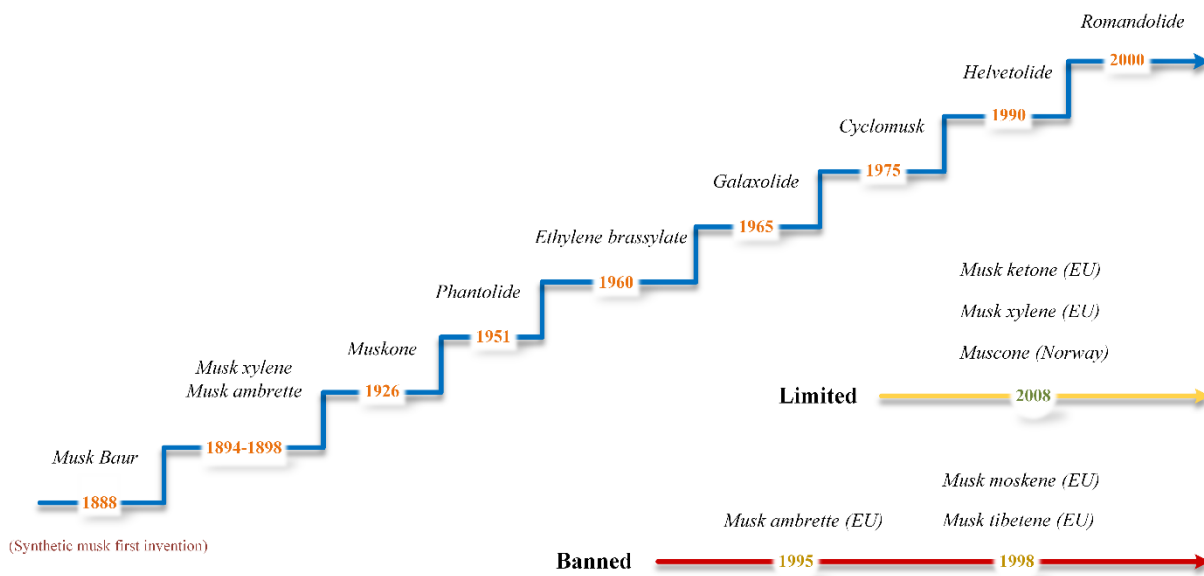


Figure 2-2 Historical process of the representative synthetic musk invention

With the invention of the first nitro musk in 1888, the history of SMs was started (Figure 2-2) (Che et al., 2011). The MX and musk ketone in nitro musks have been widely used. In addition, a variety of nitro musks such as musk ambrette and moskene have been developed. Because nitro musks tend to accumulate in the human body and produce toxicity (Liu and Duan, 1998), musk ambrette was banned by the European Union in 1995 because of its strong photosensitivity (Müller et al., 1996). In the 1998, moskene and musk tibetene were banned (Zhao and Schwack, 1999). Since 2008, both nitro musks of MK and MX have also been limited in use.

Judging from the structure of nitro musks, most nitro musks changed on the substituents. In the 1950s, with the invention of phantolide in the category of polycyclic musks, polycyclic musk gradually replaced the nitro musk, which was harmful to organisms. Polycyclic musks are used as a substitute for nitro musks. Polycyclic musks are no longer limited to changes in the substituents, but mainly change in the parent structure. In recent years there have also been reports of accumulation and endocrine disruption of organisms by polycyclic musks (Kannan et al., 2005; Yamauchi et al., 2008). The list of restricted uses of musk ketone has been included in Norway. The third-generation substitutes for macro musks are abandoning the benzene ring, which is a nitro-free cyclic macromolecular compound. At present, it has not been found that the macro musks have similar hazards to organisms as nitro musks and polycyclic musks. The fourth generation of alicyclic musks, with the appearance of cyclo musks in 1975 (Gautschi et al., 2001), is completely different in structure from the first three generations of SMs. Its molecular structure is composed of alkyl esters.

It can be seen that the current synthesis process of most POPs contaminant substitutes is mainly reflected in the renewal of raw materials and catalysts (Arsenault et al., 2007; Covaci et al., 2011). Substitutions for some contaminants change their parent structure compared to

previous contaminants. However, when SMs have a stable structure and better physicochemical properties, more alternatives are still substituted on the substituents. Substituting the substituent of the molecule with the same parent structure can ensure that the substitute molecule retains the excellent properties of the pre-modified molecule, and it may be easier to weaken the molecular pollution activity. With the increasing demand for alternatives, how to efficiently obtain the best artificial SMs substitute is one of the issues that need further study in the future.

2.6.3.2 Theoretical substitution for generating the environmentally friendly SMs

The method of theoretical substitution is increasingly important in molecular modification studies. Quantitative structure-activity relationship (QSAR) models are used to predict physical-chemical properties of chemicals, mathematically establish the quantitative chemical structure-activity relationship in order to provide effective information for chemical design and the follow-up environmental behavior prediction (Ma and Zhou, 2007). Both two-dimensional quantitative structure-activity relationship (2D-QSAR) and three-dimensional quantitative structure-activity relationship (3D-QSAR) have been reported in the related QSAR studies in the field. Some research uses the 2D-QSAR method to identify the substitute of target compound with less toxicity. 2D-QSAR was also used to explore the shed light on the mechanisms of structure medication on fluoroquinolones (Abdel-Aziz et al., 2011). Wang et al. (2018) employed 2D-QSAR method combined with fractional factorial methods to study the adsorption mechanism of pesticides in a contaminant system.

Compared with the 3D-QSAR method, the 2D-QSAR method has many quantum chemical descriptors. Therefore, the established model is difficult to accurately express the influence of the physical and chemical properties of the molecule on its environmental activity. Originally, 3D-QSAR model was used to design drugs by exploring the relationship between chemical structure and its physical-chemical properties (Verma et al., 2010). According to Martin (1999),

compounds with similar chemical and physical properties also have similar biological properties. Thus, the similarity principle of QSAR requires a series or structural class, which means that only the homolog molecules can be used to construct the model (Martin, 1999; Chen et al., 2016). 3D-QSAR can be used to predict the persistence, accumulation and toxicity of chemical compounds, such as pesticides (Koleva and Georgieva, 2013). It has been widely used to design environmentally friendly chemicals in recent years (Chen et al., 2016; Gu et al., 2020; Li et al., 2021b). Besides, 3D-QSAR method was further integrated with fractional factorial experimental methods to improve the structure prediction accuracy during modification of molecules. Then density functional theory (DFT) is used to evaluate the functional indicators of modified molecules. The influencing factors that affect the mobility of PCBs with 3D-QSAR and 2D-QSAR were studied by using fractional factorial design (Xu et al., 2016). Integrated QSAR-full factorial experiment design methodology was applied in the investigation of the significant pharmacophore features and the substituent effects in toxicity, concentration and migration of PBDEs (Jiang et al., 2016), the migration ability of PCNs, polychlorinated biphenyls and polychlorinated naphthalenes (Chen et al., 2016; Gu et al., 2017; Wang et al., 2017b). Other researchers have used the 3D-QSAR binding molecule docking method to study the effects of newly designed surrogate molecules and proteins after theoretical docking. This methodology has been used to generate surrogate molecules for pentachlorophenol with low bioconcentration and can be used as a pesticide (Wang et al., 2017a).

2.6.3.3 Theoretical substitution scheme for environmentally friendly SMs

The development of environmentally friendly SMs has drawn increasing attention from the public due to the excess use of these PCPs. Therefore, theoretical research on SMs should be further strengthened.

The parameters of SMs building parameters can be studied by 2D-QSAR, 3D-QSAR, 4D-

QSAR, and 5D-QSAR methods (Kuz'min et al., 2005; Oberdorf et al., 2010; Qiu et al., 2018). At the same time, the physical and chemical properties of artificial musks are analyzed. For areas that affect the environmental index parameters of SMs, other methods such as fractional factorial experiment design methods can be used to locate and study the influence of various factors on molecular substitutes. In order to assess whether the functional properties of alternatives remain the same or increase, density functional theory can be used for calculations. After researching the effect of substitutions and proteins on their binding, mechanisms such as molecular dynamics, quantum mechanics/molecular mechanics (QM-MM), and molecular docking techniques can be used to study the mechanism (Berendsen et al., 1984; Crespo et al., 2005; Wang et al., 2003). For the evaluation of human health risks of alternatives, physiologically based pharmacokinetic (PBPK) models or risk index methods can be used to evaluate the environmental risks of SMs (Price et al., 2003; Chang et al., 2014). The alternative theory of SMs is described in Figure 2-3.

Based on our review, significant amounts of toxic by-products can be produced as a result of SMs degradation. An increasing SMs discharge imposed the requirement on the treatment capacity and efficiency of WWTP. As an environmentally friendly alternative, the 3D-QSAR model can be used to study the relationship between molecular environmental parameters and the structure of SMs, in order to provide evidence for the alternatives of SMs. DFT theory can be used to calculate the functional index of SMs, whereas EPI database can be used to evaluate the environmental indicators of the substitutes. The effect of substitution molecules and protein binding could be investigated by molecular docking technology. The human health risk of SMs can be assessed with the hazard index method.

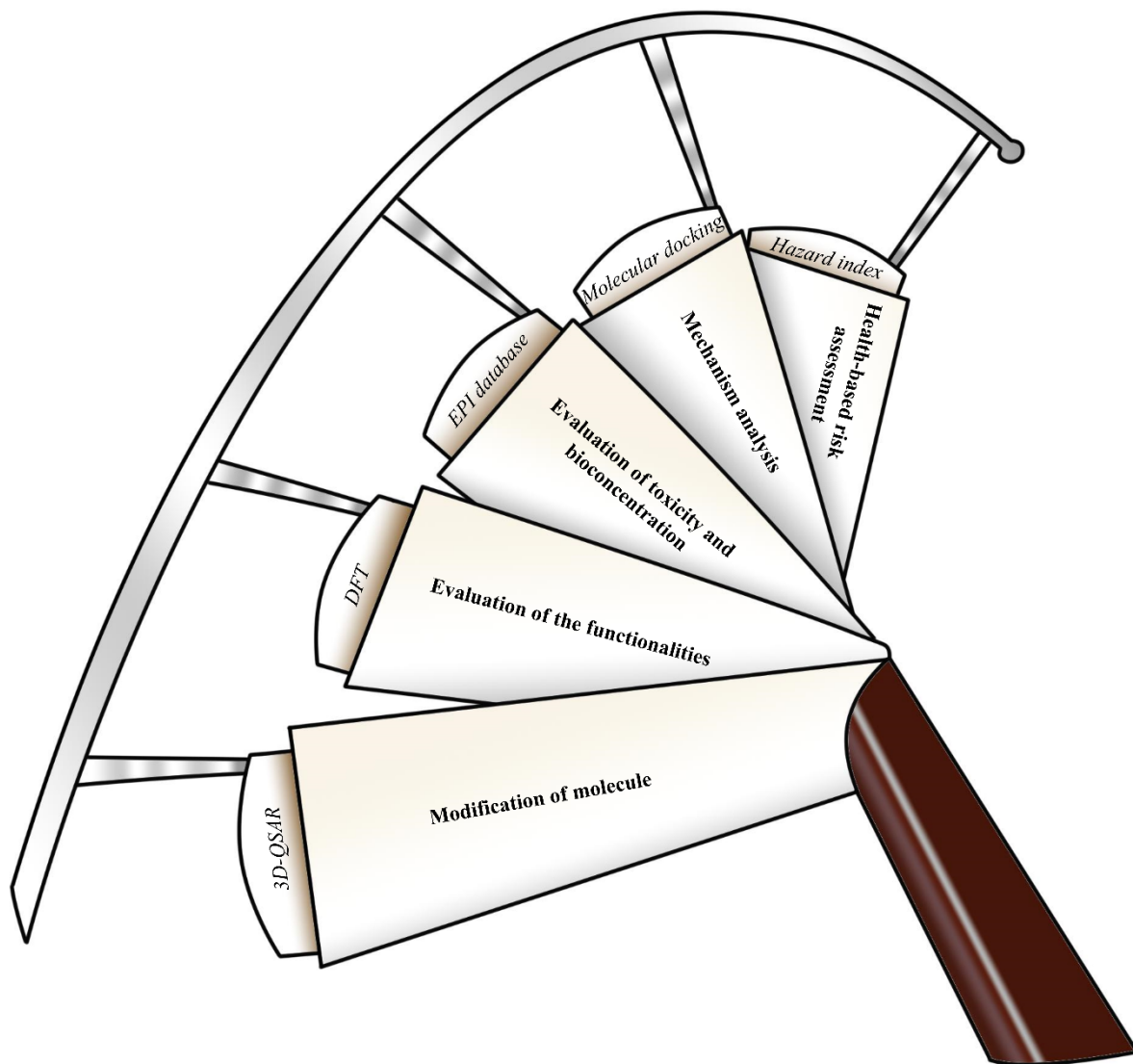


Figure 2-3 Theoretical design schemes for environmentally friendly synthetic musk substitutes

2.7 Summary

This chapter summarized a systematic elaboration of the classification, applications and typical synthetic routes of SMs. The occurrence and distributions of SMs in all types of environments, including surface water, sewage, sludge, sediment, soil, air, biological samples, marine biota and polar regions, as well as the determination methods, including pre-treatment and detection methods are also comprehensively reviewed. Furthermore, the bioaccumulation (in marine or river aquatic organisms and in humans) and toxicity (physiological toxicity and genotoxicity), as well as the related environmental risk assessment and pollution control are also summarized in this review. In the end, environmentally friendly strategies, modification and generation of low-toxic SMs, were put forward in this study. Those newly generated SMs products could help to reduce the environmental effects of PCPs, facilitating ongoing SMs use.

Despite the fact that great progress has been achieved in recent years, continuous research efforts are needed to fill the research gaps. The development of efficient pre-treatment methods is encouraged to minimize the matrix effect and enhance the analysis accuracy. Extra drilling on the occurrence and distribution of SMs would be beneficial, particularly to comparative analyses of SMs in various environments. An in-depth investigation should be pursued on the monitoring and evaluation of environmental behaviors of SMs (e.g., evaporation, natural biodegradation and photo-oxidation, their interaction with different contaminants and their migration among different media) to facilitate proper risk assessment and pollution control. In addition, the bioaccumulation of SMs in the organisms and their toxicological impact on the surrounding environment are required. An understanding of the pollution thresholds of SMs is of great importance, to facilitate the management and the promulgation of appropriate laws and regulations. Till now, SMs have not been included in routine monitoring programs. Some environmentally friendly alternatives, such as the theoretical substitution for low toxic SMs molecular modification and generation, could be applied.

CHAPTER 3

3D-QSAR AIDED TOXICITY ASSESSMENT OF SMS AND THEIR TRANSFORMATION BY-PRODUCTS

This chapter has been published in the *Environmental Science and Pollution Research* (2021): 1-13. I am the primary author of this paper, and am mainly responsible for the research initiation, data collection, model development, result analysis and generation of the manuscript. The co-author Guangzhu Li is mainly responsible for conducting the chlorination experiments, Bing Chen helps to conduct the data analysis and polish the manuscript, Weiyun Lin helps to edit the manuscript and Baiyu Zhang is the principal investigator of the manuscript involved research project/funds and is mainly responsible for supervising me throughout the research and finalizing the manuscript.

Li, X., Li, G., Chen, B., Lin, W., & Zhang, B. (2021). 3D-QSAR-aided toxicity assessment of synthetic musks and their transformation by-products. *Environmental Science and Pollution Research*, 1-13.

DOI: 10.1007/s11356-021-14672-1

3.1 Introduction

Musks are a group of aromatic organic ingredients originally derived from the glands of adult musk deer (Hu et al., 2018). Due to their high demands and high costs, synthetic musks (SMs) were invented as an economical substitute. These SMs were widely used in personal care products, including sanitizers, fragrances, cosmetics, and shampoos (Tseng and Tsai 2019). Commonly used SMs include polycyclic musks, such as tonalide (AHTN), galaxolide (HHCB), celestolide (ADBI) and phantolide (PHAN) and nitro musks, such as musk xylene (MX) and musk ketone (MK) (Homem et al., 2015b; Li et al., 2018). These SMs are used in increasingly large quantities. The annual usage of HHCB in the United States has increased by approximately one million pounds from 2000 to 2004 (USEPA 2014). According to the European Union risk assessment report (2008), the production of undiluted HHCB in 2000 is between 1000 and 5000 tons in Europe.

Most of the SMs contained in personal care products enter the wastewater treatment plants (WWTPs) and eventually reach the surface water together with their by-products. An estimated 77% of fragrance ingredients used in products became sewage in Europe (Wu et al., 2018). HHCB and AHTN have been detected in the influents of WWTPs in China (with the highest concentration of 3039 ng/L and 1486 ng/L, respectively) and in the Spain (with the highest concentration of 3400 and 1700 ng/L, respectively) (Tasselli and Guzzella 2020). After the secondary treatment (e.g., biodegradation), the wastewater enters the disinfection system (advanced UV/Chlorine/Ozone aided oxidation) in WWTPs. However, even after disinfection, the incompletely treated SMs and their transformation by-products (vary depending on the disinfection methods) still exist in the effluent. For example, Horii et al. (2007) detected HHCB, AHTN, and HHCB-lactone (a recognized disinfection by-product of HHCB) in the effluents of

a WWTP in Kentucky, the United States, and their concentrations were 44, 130, and 229 ng/L, respectively. The residual SMs will then enter the surface water and may continue to be biodegraded and photodegraded into by-products in the environment.

SMs, especially HHCB and AHTN, have been frequently found in surface water (Juksu et al., 2020; Krzeminski et al., 2017; Lange et al., 2015). HHCB (with the highest concentration of 547 ng/g) and AHTN (with the highest concentration of 439 ng/g) were detected in the Pearl River, China, where drinking water was extracted (Zeng et al., 2018). Although the concentrations are low in the environmental systems, bioaccumulation of these SMs leads to potential risk to the environment and humans. For example, HHCB and AHTN were detected in mussels collected from offshore of India, Cambodia, Japan, Korea, China, Indonesia, Philippines, Malaysia, and the Pacific Ocean. The highest concentrations were found in the mussel samples from Kohyongsong Bay, Korea (14,000 ng/g lipid weight) and San Francisco Bay, USA (2200 ng/g lipid weight), respectively (Nakata et al., 2012). Lang et al. (2015) reviewed that high concentrations of SMs were detected in human fat (8-33 ng/g of AHTN, 28-189 ng/g of HHCB), blood (average 0.27 µg/L of AHTN and 0.77 µg/L of HHCB) and breast milk (11–58 ng/g of AHTN, 16-108 ng/g of HHCB) in different studies. The transport, fate, and impact of SMs and their by-products are shown in Figure 3-1.

Existing studies investigated the toxicity of SMs. Wollenberger et al. (2003) conducted a 5-day subchronic toxicity test and reported that HHCB, AHTN, ADBI, and MK could strongly inhibit the larval development of the *Acartia tonsa* (a kind of marine copepod). The five-day- EC_{50} -values were 0.160 mg/L (ADBI), 0.026 mg/L (AHTN), 0.059 mg/L (HHCB), and 0.066 mg/L (MK), respectively, considered as “very toxic” to the *A. tonsa* larval. Fan et al. (2019) compared chronic species sensitivity distribution among HHCB, AHTN, and MK and reported that MK was more toxic to aquatic organisms than HHCB and AHTN. Although the toxicity of

common SMs has been investigated, toxicity studies on their by-products are extremely limited. Besides, these toxicity analyses of SMs are based on experiments requiring special equipment, manpower, materials, and costs. Therefore, a reliable and cost-effective approach is desired to test the toxicity of SMs and their by-products.

The three-dimensional quantitative structure-activity relationship (3D-QSAR) can be an alternative to the traditional experiments to test toxicity. 3D-QSAR is a computer-assisted method used to design new drugs (Winkler, 2018) by predicting the chemical and biological activities according to the internal energy changes of molecules and the energy changes of intermolecular interactions (Zhu et al., 2018). 3D-QSAR model has also been successfully applied in the toxicity assessment and prediction of environmental toxicants (Zhang et al., 2020). Wang et al. (2017a) studied the ecotoxic effects of pentachlorophenol by using a 3D-QSAR method associated with molecular docking; Zhang et al. (2020) investigated the genotoxicity of fluoroquinolones derivatives; Chen et al. (2016) predicted octanol-air partition coefficients (K_{oa}) of polychlorinated biphenyls, and Zhao et al. (2018a) established two 3D-QSAR models (comparative molecular field analysis (CoMFA) and comparative molecular similarity indices analysis (CoMSIA)) to predict the bioconcentration (BCF) values of polychlorinated naphthalene's congeners. Despite the existing literature, no studies were found on the toxicity assessment of SMs and their by-products using 3D-QSAR modelling.

The 3D-QSAR model for toxicity assessment contains two components: molecular structure and toxicity of the target SMs. The molecular structures of SMs and their toxicities can be obtained from existing studies and databases, and hence be used to build the model that explains the structure-toxicity relationship. The obtained 3D-QSAR model can further predict the toxicity of SM by-products (which remains largely unknown) using their molecular structures as model inputs. The SM by-products, and therefore their molecular structures, vary

depending on the wastewater treatment methods. This information (or model inputs) was collected from existing literature reporting the by-products generated from different treatment methods, including biodegradation, photodegradation, chlorine-incorporating ultraviolet treatment, advanced (UV and ozone aided) oxidation (Fang et al., 2008; Gatermann et al., 1998; Martin et al., 2007; Sanchez-Prado et al., 2004; Wang and Liu, 2019;), and disinfection with NaClO (Kuhlich et al., 2011). Among these, chlorination is widely used in WWTPs for disinfection during which SMs oxidation happens, but its associated by-product generation from ADBI, PHAN and MK has not been well studied.

Therefore, the objectives of the present study include: (1) building a 3D-QSAR model by using known biological toxicity (LC_{50}) and molecular structures of SMs; (2) summarizing molecular structures (as inputs for model prediction) of SM transformation by-products (i.e., AHTN, HHCB, MK, ADBI, PHAN, TRASE, and MK) from literature; (3) determining unknown by-products (as well as their molecular structures) of SMs (i.e., ADBI, PHAN and MK) based on chlorination experiment; and (4) predicting the biological toxicity of the above SMs transformation by-products using the constructed 3D-QSAR model. This study aims to provide an effective method to predict the toxicity of SMs by-products and evaluate the potential risk caused by the current treatment methods.

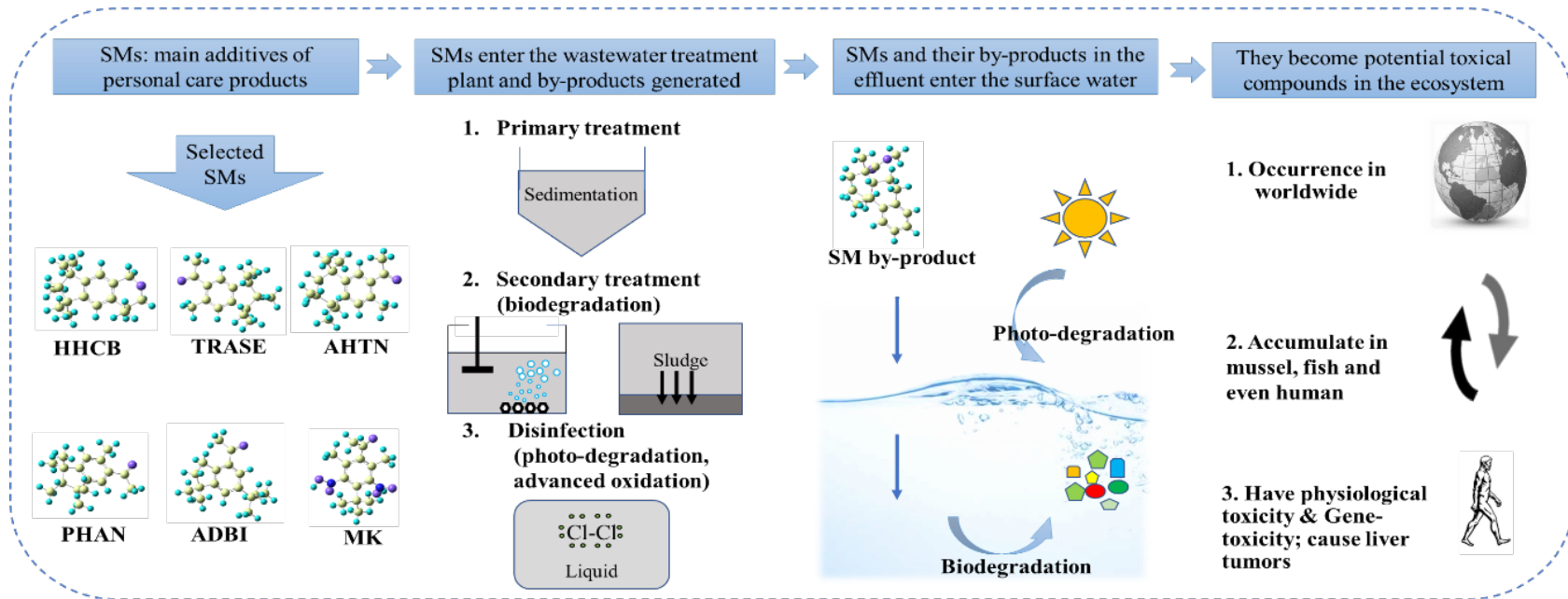


Figure 3-1 The transport, fate and impact of SMs and their by-products

3.2 Materials and Methods

3.2.1 3D-QSAR model construction for SM biological toxicity (LC_{50}) prediction

3.2.1.1 Data source

The 3D-QSAR model serves as a robust and cost-effective tool to predict the LC_{50} value (model output) based on the molecular structure (model input) of a certain SM/by-product and the structure- LC_{50} relationship in this study. A total of 33 SMs obtained from literature were selected as the database of model inputs, consisting of a training set (26 compounds) for 3D-QSAR model generation and a test set (7 compounds) for model validation (Table S3-1). LC_{50} stands for the lethal concentration of a chemical in water or air that kills 50% of the test living organisms during the observation period was chosen as the toxicity indicator. It indicates the behavior of organisms after being exposed to toxic compounds in the environmental systems. When the LC_{50} value decreases, the toxicity of the chemical increases. Obtaining accurate and reliable LC_{50} values has theoretical and practical significance (Kooijman 1987) for 3D-QSAR model construction. In this study, the 96hr- LC_{50} values of the 33 selected SMs in mysid were obtained using the prediction function in the Estimation Programs Interface (EPI) Suite™ of U.S. Environmental Protection Agency (USEPA).

3.2.1.2 Molecular structure optimization and alignment of the 3D-QSAR model

The 3D-QSAR model was constructed using the SYBYL-X2.0 software to establish the relationship between SMs' molecular structures and the associated LC_{50} values (Chen et al., 2016). The 33 SMs' molecular structures obtained from literature were drawn and optimized in SYBYL-X2.0. The optimization of SMs was performed using the Tripos force field and Gasteiger-Hückel charges (Reihaneh and Jahan, 2013). The Powell's method was used with a

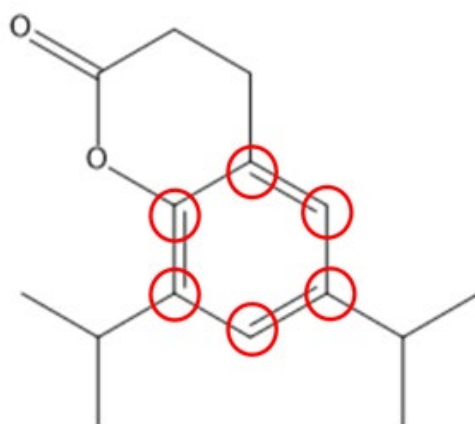


Figure 3-2 The structure of Musk #28 and the alignment of common molecular skeleton

maximum of 10,000 optimizations and an energy convergence gradient value of 0.005 kJ/mol, and all the rest parameters were set to default values (Wang et al., 2017a, b). SM molecules with a common molecular skeleton were labeled (shown in Figure 3-2). Musk #28, which had the highest LC_{50} value, was selected as the template to align the rest of the molecules (Liu et al., 2015b).

3.2.1.3. Evaluation parameters and validation of the constructed 3D-QSAR model

The CoMSIA module, which has the function of increasing hydrogen bond donor and acceptor, electrostatic, steric, and hydrophobic fields, was chosen in the QSAR model (Gu et al., 2019). The 26 log LC_{50} values of the selected SMs (training set) were introduced to the training table, and all the associated evaluating parameters of the model were calculated automatically by SYBYL-X2.0. Partial least-squares regression analysis was applied to establish the relationships between the structures and biotoxicity of the associated compounds. The leave-one-out method was used to cross-validate the training set and determine the values of q^2 and n . The non-cross-validation analysis was then conducted to obtain the r^2 , F , and the SEE values. The standard error of prediction (SEP) of the cross-validation of the input and predictive biotoxicity values of the 7 selected SMs (test set) and the external predictive set cross-checking coefficient (R^2_{pred}) were used as the parameters for indicating the ability for external prediction of the constructed CoMSIA model (Zhao and Li, 2018).

3.2.2 3D -QSAR aided LC_{50} assessment of SMs and the transformation by-products

3.2.2.1 Molecular structures of SM by-products obtained from literature and chlorination experiment

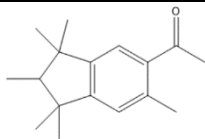
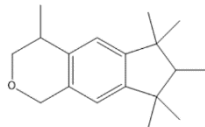
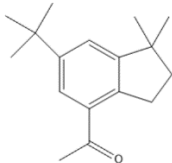
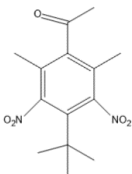
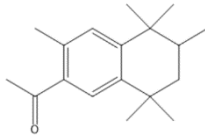
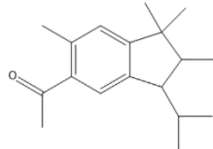
Literature was reviewed to obtain the molecular structures of SM by-products of AHTN,

HHCB, MK, ADBI, PHAN, and TRASE generated after different treatment processes, including biodegradation, photodegradation, and advanced/ozone-aided disinfection. Chlorination is another disinfection treatment method widely used in the WWTP, but its associated SM by-products are not well studied. Therefore, this study conducted a lab experiment simulating the chlorination disinfection process and investigated the by-product generation from three SMs (i.e., ADBI, PHAN and MK). The molecular structures of AHTN, HHCB, MK, ADBI, PHAN, and TRASE are shown in Table 3-1.

HPLC vials (1.5 mL) were used as disinfection basins. In each run, 300 μ L of one of the SMs (i.e., ADBI, PHAN and MK, respectively) solution in methanol (C=1 mg/mL) was mixed with 500 μ L sodium hypochlorite solution (100 mg/L). The volume of sodium hypochlorite solution was doubled in all runs (500 μ L instead of 250 μ L), comparing Kuhlich et al.'s method to enhance the oxidizability. Then 800 μ L of ethyl acetate was added, and the mixture was shaken for 10 minutes and left to stand for 72h. After separation of the water layer, the organic solvent was dried over anhydrous sodium sulfate and the residue was then reconstituted in dichloromethane for further gas chromatography/mass spectrometry (GC-MS) analysis to identify SMs and their by-products. In the chlorination experiment, ADBI, PHAN and MK (purchased from Macklin) and other chemicals used are all at the HPLC grade and the sodium hypochlorite solution is with the analytical-reagent grade.

GC-MS-QP2010 (Made by Shimadzu) equipped with a flame ionization detector (FID) in the electron impact mode (70 eV) and an InertCap-5 capillary column as carrier gas (helium) at 1 mL per minute was utilized. The column temperature was initially kept at 70 °C for 2 min, increased to 340 °C at a rate of 15 °C/min, and kept for 10 min. The injector and detector temperatures were set at 280 °C and 200 °C, respectively.

Table 3-1 Characteristics of six synthetic musk (SM) precursors

Synthetic musk	Abbreviation	CAS number	Molecular formula	Molecular structure
Phantolide	PHAN	15323-35-0	C ₁₇ H ₂₄ O	
Galaxolide	HHCB	1222-05-5	C ₁₈ H ₂₆ O	
Celestolide	ADBI	13171-00-1	C ₁₇ H ₂₄ O	
Musk ketone	MK	81-14-1	C ₁₄ H ₁₈ N ₂ O ₅	
Tonalide	AHTN	21145-77-7	C ₁₈ H ₂₆ O	
Traseolide	TRASE	68140-48-7	C ₁₈ H ₂₆ O	

Chlorination experiments were conducted through revising the method proposed by Kuhlich et al. (2011).

3.2.2.2 LC_{50} assessment of SMs and the transformation by-products

Among the SMs with known molecular structures, 33 SMs with LC_{50} prediction value were selected as the database to construct and validate the 3D-QSAR model. However, the LC_{50} prediction values of another 15 SMs (shown in Table S3-2) cannot be obtained from EPI database. Their LC_{50} values were thus predicted using the constructed CoMSIA model. These predicted values provide a supplement to the incomplete data source.

The transformation by-products of AHTN, HHCB, MK, ADBI, PHAN, and TRASE were obtained from literature and experiment. These transformation by-products have the same common molecular skeleton as the Musk #28. The biological toxicity of these SMs by-products was predicted using the constructed model to evaluate the potential risk caused by the current treatment options.

3.3. Results and Discussion

3.3.1 Performance evaluation of the constructed CoMSIA based 3D-QSAR model

Evaluation parameters of the constructed CoMSIA model are displayed in Table 3-2. The cross-validated q^2 is greater than 0.5, the non-cross-validated R^2 is greater than 0.9 and the standard errors of the estimate (SEE) is close to zero, indicating that the model met the basic requirements (Zhang et al., 2019). The non-cross-validated R^2 is greater than 0.8 and the standard errors of the estimate (SEE) are low (Zhao et al., 2018a). The standard error of prediction (SEP) of the cross-validation of the experimental and predictive values is 0.656 (lower value preferable), and the external predictive set cross-checking coefficient (R^2_{pred}) is greater than 0.6, indicating that the constructed CoMSIA model has a high ability for external prediction (Zhao and Li 2018).

Table 3-2 Statistical parameters of the CoMSIA model

Model	q^2	n	SEE	R^2	F	SEP	R^2_{pred}
CoMSIA	0.759	10	0.042	0.998	860.027	0.656	0.936

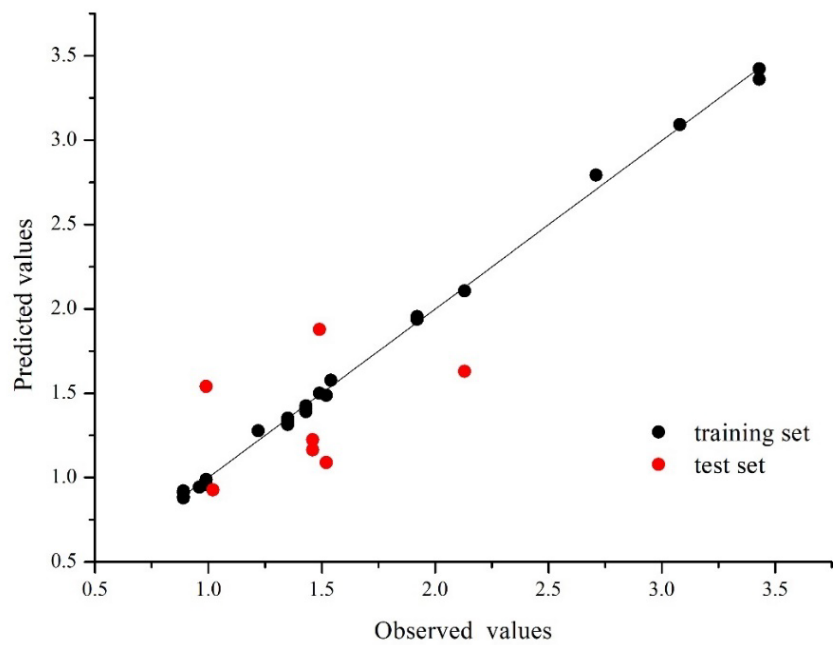


Figure 3-3 The observed versus predicted LC_{50} values based on the CoMSIA model

The observed and predicted values of LC_{50} (shown in Figure 3-3) in the training set and test set based on CoMSIA model revealed a good linear relationship with $n=33$, $p=0.001$, $r_0=0.532$, $r=0.9674 > r_0$. Results confirmed that the CoMSIA model has high predictive ability.

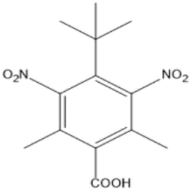
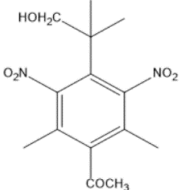
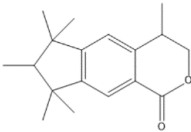
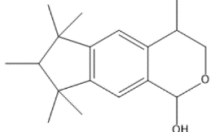
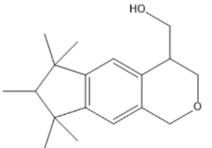
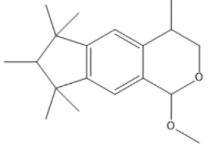
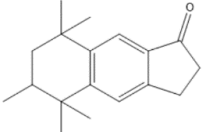
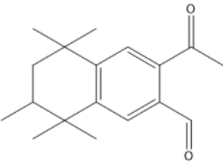
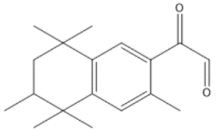
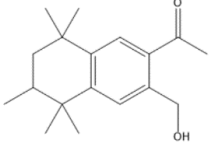
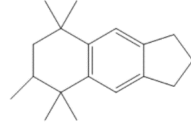
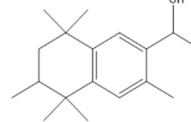
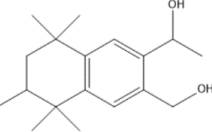
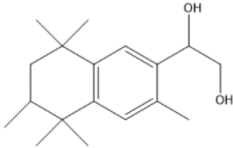
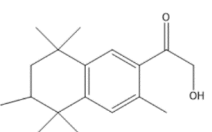
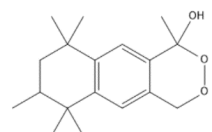
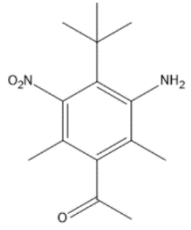
3.3.2 SMs by-products identified from chlorination experiments

A total of 48 by-products of AHTN, HHCB, MK, ADBI, PHAN, and TRASE were found from literature and their molecular structures were summarized in Table 3-3. All the molecules have the same common molecular skeleton of Musk #28, which can be used as prediction inputs of the CoMSIA model.

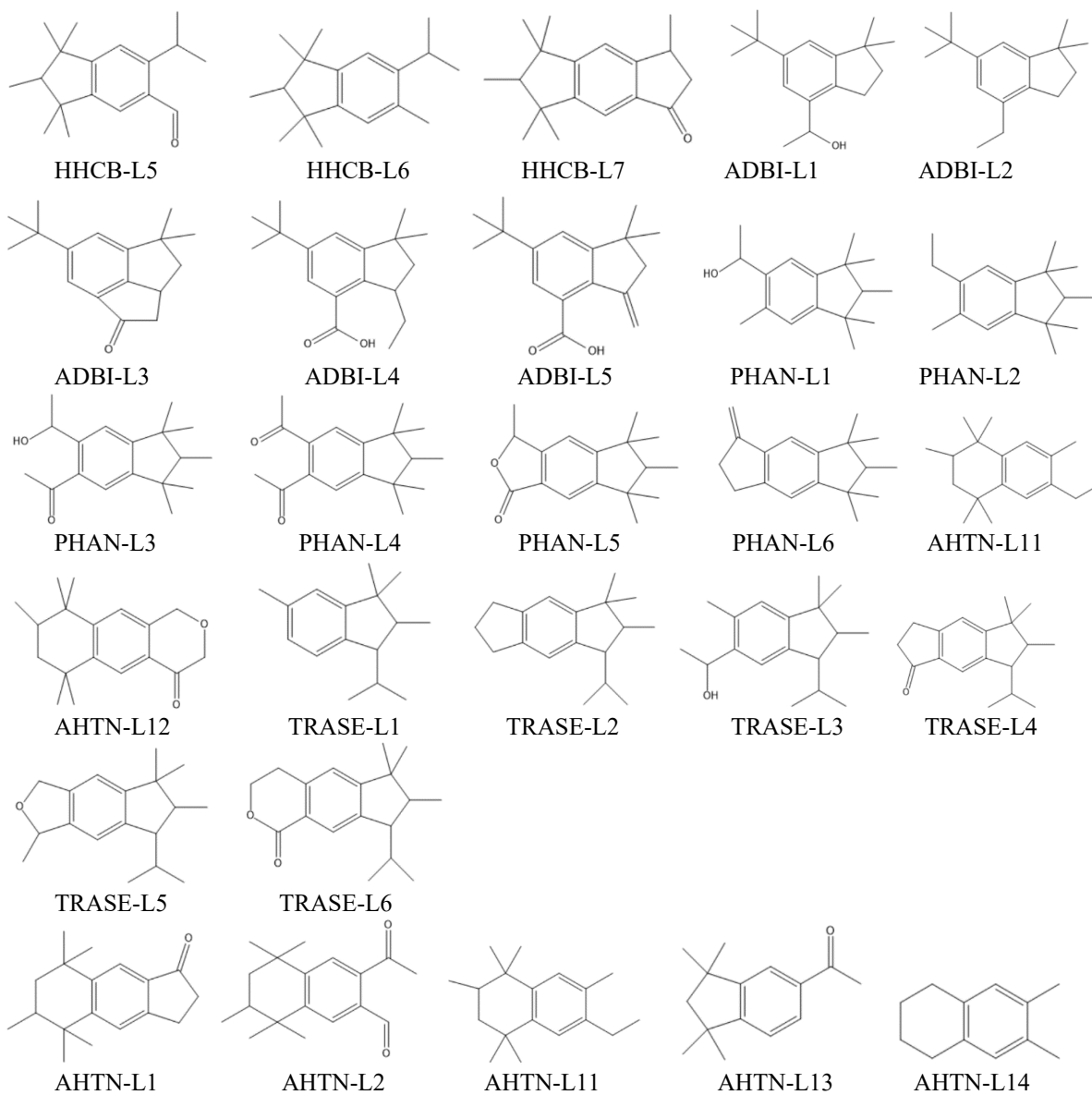
The by-products generation from three SM precursors (ADBI, PHAN and MK) after 72h contact with sodium hypochlorite were identified. A total of 5, 5, and 0 cyclic by-products of ADBI, PHAN, and MK were observed, respectively (summarized in Table 3-4). All these by-products with the same common molecular skeleton of Musk #28, which can be used in CoMSIA model.

According to the results, there are no cyclic MK by-products detected in the solution after 72h. With the existence of electron-withdrawing groups such as Nitro and Carbonyl groups in MK, the benzene ring was easy to be attacked by hydroxyl radical and subsequently opened loop and resulted in bond broken (Zhao et al., 2016). There are five cyclic by-products of PHAN that existed in the solution after 72h, namely PHAN-E1 to PHAN-E5. ADBI-E1 to ADBI-E5 are the by-products of ADBI. ADBI-E2, ADBI-E3 and ADBI-E5 are also named as diisobutyl phthalate, dibutyl phthalate and diethyl hexylphthalate, respectively. These phthalate esters are used as plasticizers and softeners in a wide variety of packing products (Gao et al., 2021). Chlorination is a complex process that can produce various by-products with diverse chemical structures. All the generated cyclic chlorination by-products have higher molecular weight and more complex structure than those of their precursors, indicating that these by-products may be harder to be degraded.

Table 3-3 SM by-products generated using different treatment methods

Treatment methods	Molecular structures of SM by-products					Reference	
Ozone oxidation						Fang et al., 2008	
	MK-L1	MK-L2					
Biotransformation							
	HHCB-L1	HHCB-L2	HHCB-L3	HHCB-L4	AHTN-L1		
						Martin et al., 2007; Gatermann et al., 1998	
	AHTN-L2	AHTN-L3	AHTN-L4	AHTN-L5	AHTN-L6		
							
	AHTN-L7	AHTN-L8	AHTN-L9	AHTN-L10	MK-L3		

Photodegradation

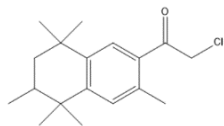


**UV-Chlorination
(drinking water)**

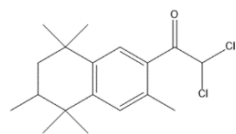
Sanchez-Prado et al., 2004

Wang and Liu, 2019

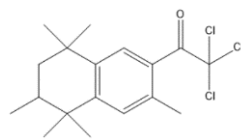
**Disinfection with
hypochlorite**



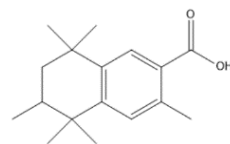
AHTN-L15



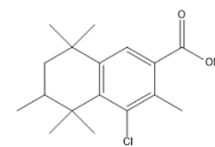
AHTN-L16



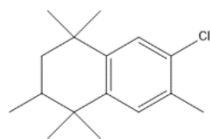
AHTN-L17



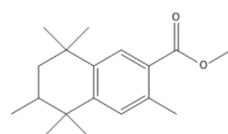
AHTN-L18



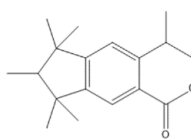
AHTN-L19



AHTN-L20



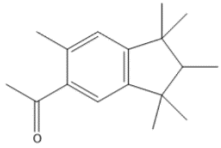
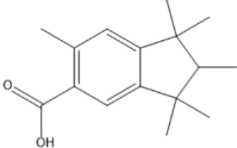
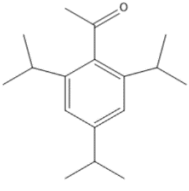
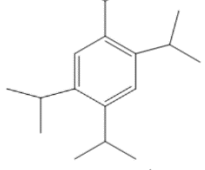
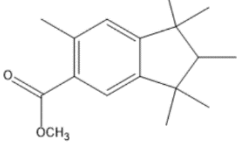
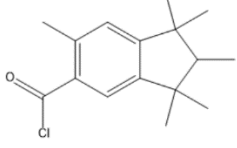
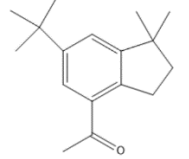
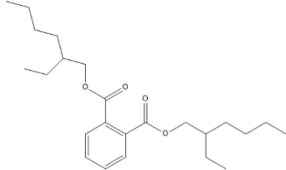
AHTN-L21

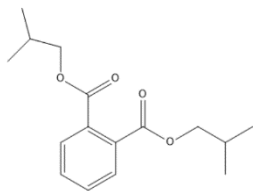
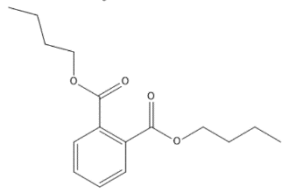
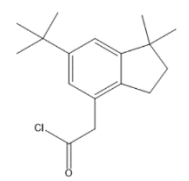
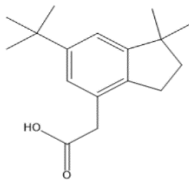


HHCb-L1

Kuhlich et al., 2011

Table 3-4 Selected by-products with the same common skeleton of Musk #28 from chlorination experiment

SMs and their by-products	Molecular formula	Molecular structure	Molecular weight (g/mol)
PHAN (precursor)	C ₁₇ H ₂₄ O		244
PHAN-E1	C ₁₆ H ₂₂ O ₂		246
PHAN-E2	C ₁₇ H ₂₆ O		246
PHAN-E3	C ₁₈ H ₃₀		246
PHAN-E4	C ₁₇ H ₂₄ O ₂		260
PHAN-E5	C ₁₆ H ₂₁ ClO		264
ADBI (precursor)	C ₁₇ H ₂₄ O		244
ADBI-E1	C ₂₄ H ₃₈ O ₄		390

ADBI-E2	$C_{16}H_{22}O_4$		278
ADBI-E3	$C_{16}H_{22}O_4$		278
ADBI-E4	$C_{17}H_{23}ClO$		278
ADBI-E5	$C_{17}H_{24}O_2$		260

3.3.3 Toxicity prediction of the SM and SMs by-products using the constructed 3D-QSAR model

3.3.3.1 Toxicity prediction of SMs using the constructed 3D-QSAR model

Among the SMs with known molecular structures, 33 SMs with LC_{50} prediction value were selected as the database, while the LC_{50} prediction value of 15 SMs among the rest SMs can not be obtained from EPI database. Thus, these 15 SMs (shown in Table S3-2) were selected, and their LC_{50} values were predicted using the CoMSIA model. These predicted values provide a supplement to the incomplete data source. Five of fifteen SMs have higher biotoxicity than HHCB ($LC_{50}=0.862\times 10^{-6}$ mmol/pT). Previous studies have proved that HHCB can be toxic to aquatic organisms. For example, Fan et al. (2019) showed that HHCB is highly toxic to aquatic organisms in China, especially the amphibious black spot frog. Chen et al. (2011) also found that in the acute lethal studies of HHCB on earthworm (*Eisenia fetida*), the 48h- LC_{50} value was 11.87 $\mu\text{g}/\text{cm}^2$. Eleven SMs have higher biotoxicity than that of PHAN ($LC_{50}=1.420$ mmol/pT), fourteen SMs have higher biotoxicity than that of TRASE ($LC_{50}=2.532$ mmol/pT). Therefore, the existence of these SMs has a potential risk to the environment and human health.

3.3.3.2 Toxicity prediction of SM by-products from literature and chlorination experiments

The LC_{50} values of SM by-products with the same common skeleton as Musk#28 can be predicted using the CoMSIA model, including 48 by-products of AHTN, HHCB, MK, ADBI, PHAN, and TRASE from literature and 10 by-products of PHAN and ADBI from chlorination experiments. There are no MK by-products sharing the same common skeleton of Musk#28, therefore the MK by-products cannot be predicted by the CoMSIA model. The predicted LC_{50} values of selected SMs and their by-products are shown in Table 3-5. The change rate of LC_{50}

values can be calculated as follows:

$$\text{Change rate of } LC_{50} (\%) = (LC_{50} \text{ value of SM by-products} - LC_{50} \text{ value of SM precursor}) / LC_{50} \text{ value of SM precursor} \quad (3-1)$$

Figure 3-4 reflects the LC_{50} values of SMs by-products generated using different treatment methods. Compared to MK, the biotoxicity of MK-L1 (ozonation) increased by 179.16%. MK-L2 and MK-L3 have decreased biotoxicity compared with MK. Rimkus et al. (1999) reported that MK-L3 (2-NH₂-MK) is the main by-product of MK found in a WWTP in Germany. TRASE (18 µg/kg) is one of the SMs detected in the milk fat of humans (Mersch-Sundermann et al., 1998). Five out of six TRASE by-products were predicted with 18.40%-57.39% higher biotoxicity than their precursors after photodegradation. In the literature, AHTN-L1~AHTN-L10 was generated from the biodegradation treatment. Among them, the biotoxicity of eight by-products was decreased compared to their precursors, with only two slightly increased by 8.02% (AHTN-L2) and 19.12% (AHTN-L3). AHTN-L1, AHTN-L2, AHTN-L11, AHTN-L13 and AHTN-L14 are the by-products of UV/chlorine oxidation (Wang and Liu 2019). Compared to AHTN, the increased biotoxicity of AHTN-L2 (increased 8.02%) predicted by 3D-QSAR model was also observed in this study. HHCb is another common polycyclic musk found in the sludges. Its by-products have higher biotoxicity after biodegradation (i.e., HHCb-L2, HHCb-L3, and HHCb-L4). Among these, two of these by-products' biotoxicity increased by over 40%. After photodegradation, the biotoxicity of HHCb by-products (HHCb-L5, HHCb-L6, and HHCb-L7) seems decreased, while the biotoxicity of AHTN-L12 increased by about 30%. Santiago-Morales et al. (2012) treated AHTN and HHCb using different photochemical methods and found the growth rate of algal decreased by 60% using UV method. It can be proved that the formation and accumulation of toxic by-products were generated during the treatment. The existence of HHCb and AHTN by-products in the water lead to adverse effect to the aquatic organisms (Santiago-Morales et al., 2012). To decrease the toxicity of these by-products, multiple methods can be combined. For example, researchers combined ozone and UV treatment methods and found the toxicity of treated HHCb decreased (Santiago-Morales et al.,

2012).

Among the ten SMs by-products detected from the chlorination experiment, four are more toxic than their precursors. After predicting the LC_{50} values of these ten by-products, diisobutyl phthalate (ADBI-E2) was found with increased toxicity of 5.77% than ADBI. Diisobutyl phthalate was also with the developmental toxicity for rats (Saillenfait et al., 2006) and could disrupt fetal testicular development due to the existence of testicular toxicants diethylhexyl phthalate and di-n-butyl phthalate (Borch et al., 2006). ADBI-E5, named diethylhexylphthalate is a colorless, organic carcinogen with a slight odor (Zhang et al., 2018b). It has also been proved that ADBI could strongly inhibit larval development in calanoid copepod *Acartia tonsa* (Wollenberger et al., 2003). Further treatment of ADBI is thus desired due to its risks to the environment. Most of PHAN's by-products are more toxic compared with PHAN, and the increased toxicity ranges from 26.27% to 48.17%. Although there are few studies about the toxicity of PHAN, the predicted results showed that three out of five PHAN by-products are more toxic to mysid, compared with ADBI. In addition, the biotoxicity of PHAN-E1 increased 48.17% and 16.74%, respectively, when comparing it with PHAN and ADBI. Results indicated that chlorination could pose potential environmental risks when pollutants such as SMs exist in sewage. AHTN-L15 to AHTN-L21 and HHCB-L1 are the by-products of AHTN and HHCB obtained from chlorination as well (Kuhlich et al., 2011). Among which, AHTN-L15, AHTN-L17, and AHTN-L21 are shown an increased biotoxicity of 3.52%, 41.65% and 29.56%, respectively. The predicted results indicated that the position of chloride in the structure of these by-products may affect their biotoxicity. When the chloride was added to the acetyl side chain of a structure (e.g., AHTN-L15 and AHTN-L17), the associated toxicity increased. HHCB-L1 is not only a by-product of HHCB after biodegradation, but also the by-product of HHCB after chlorination. Due to the high risk of HHCB by-products and their wide existence in the effluents (Lange et al., 2015; Vallecillos et al., 2017), further treatment can be considered after the chlorination disinfection.

Table 3-5 The predicted LC_{50} values of SM by-products obtained from the constructed CoMSIA model

Sources of information	SMs and by-products	Predicted values of LC_{50} ($\times 10^{-6}$ mmol/pT)	Change rate of LC_{50}^* (%)
Literature	ADBI (precursor)	0.884	
	ADBI-L1	1.187	34.28%
	ADBI-L2	1.394	57.69%
	ADBI-L3	1.097	24.10%
	ADBI-L4	0.879	-0.57%
	ADBI-L5	0.952	7.69%
	AHTN (precursor)	0.910	
	AHTN-L1	0.979	7.58%
	AHTN-L2	0.837	-8.02%
	AHTN-L3	0.736	-19.12%
	AHTN-L4	1.499	64.73%
	AHTN-L5	1.367	50.22%
	AHTN-L6	1.296	42.42%
	AHTN-L7	0.935	2.75%
	AHTN-L8	1.541	69.34%
	AHTN-L9	1.051	15.49%
	AHTN-L10	0.977	7.36%
	AHTN-L11	1.611	77.03%
	AHTN-L12	0.642	-29.45%
	AHTN-L13	1.104	21.32%
	AHTN-L14	2.726	199.56%
	AHTN-L15	0.878	-3.52%
	AHTN-L16	1.207	32.64%
	AHTN-L17	0.531	-41.65%
	AHTN-L18	1.246	36.92%
	AHTN-L19	1.199	31.76%
	AHTN-L20	1.581	73.74%
	AHTN-L21	0.641	-29.56%
	HHCB (precursor)	0.862	
	HHCB-L1	1.013	17.52%
	HHCB-L2	0.663	-23.09%
	HHCB-L3	0.485	-43.74%
	HHCB-L4	0.48	-44.32%
HHCB-L5	1.105	28.19%	
HHCB-L6	1.598	85.38%	

	HHCB-L7	0.993	15.20%
	PHAN (precursor)	1.420	
	PHAN-L1	1.197	-15.70%
	PHAN-L2	1.559	9.79%
	PHAN-L3	1.455	2.46%
	PHAN-L4	0.665	-53.17%
	PHAN-L5	0.599	-57.82%
	PHAN-L6	1.692	19.15%
	TRASE (precursor)	2.532	
	TRASE-L1	1.662	-34.36%
	TRASE-L2	2.066	-18.40%
	TRASE-L3	2.598	2.61%
	TRASE-L4	1.079	-57.39%
	TRASE-L5	1.675	-33.85%
	TRASE-L6	1.099	-56.60%
	MK (precursor)	-0.499	
	MK-L1	-1.393	-179.16%
	MK-L2	-0.338	32.26%
	MK-L3	1.108	322.04%
	ADBI (precursor)	0.884	
Chlorination experiments	ADBI-E1	1.384	56.56%
	ADBI-E2	0.833	-5.77%
	ADBI-E3	1.293	46.27%
	ADBI-E4	0.971	9.84%
	ADBI-E5	1.441	63.01%
	PHAN (precursor)	1.420	
	PHAN-E1	0.736	-48.17%
	PHAN-E2	0.853	-39.93%
	PHAN-E3	1.047	-26.27%
	PHAN-E4	2.008	41.41%
	PHAN-E5	2.432	71.27%

Note: * Refers to the percentage change rate of LC_{50} values of SM by-products compared with their precursors

SM-L#: by-products collected from literatures

SM-E#: by-products identified from chlorination experiments

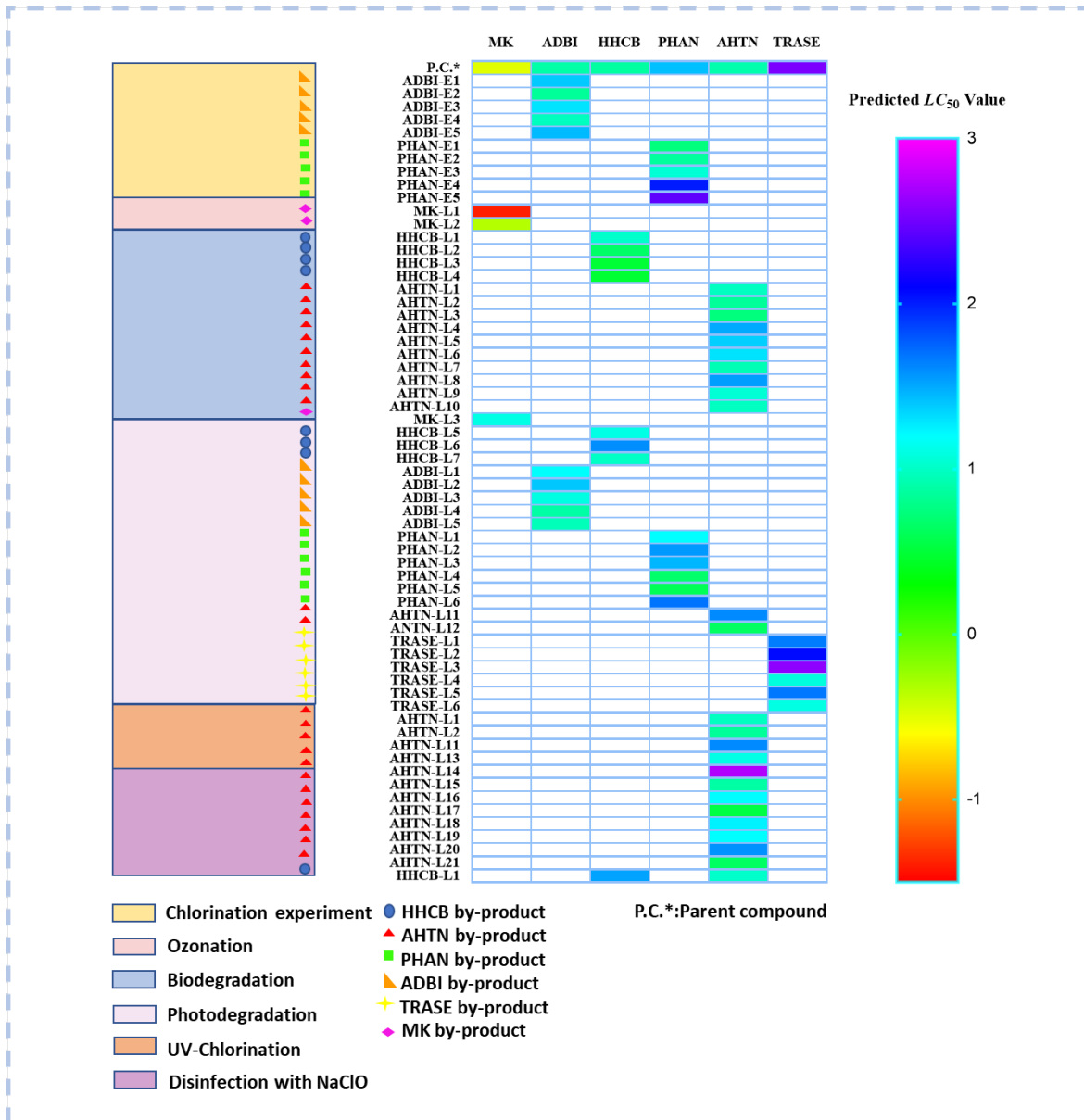


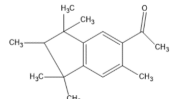
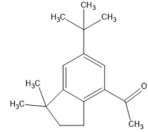
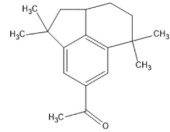
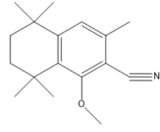
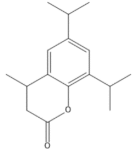
Figure 3-4 The LC_{50} values of SMs by-products generated using different treatment methods

3.4 Summary

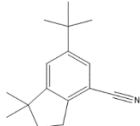
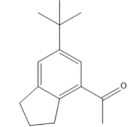
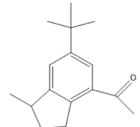
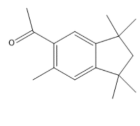
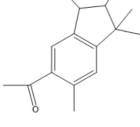
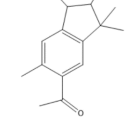
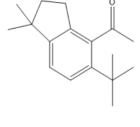
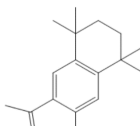
In this chapter, a 3D-QSAR model was developed to predict the biotoxicity of SM by-products. The molecular structures of SM (i.e., HHCB, AHTN, ADBI, PHAN, MK and TRASE) transformation by-products were collected from chlorination experiments and other treatment methods (from literature). Results showed that the chlorination process generated various SM by-products with more complex chemical structures than their precursors, and these by-products can be more difficult to degrade. Based on the model, 4 out of 10 SMs by-products from chlorination experiment have higher toxicity (up to 48.17%) than the associated SM precursors, and 19 out of 48 SMs by-products have higher toxicity (up to 179.16%) than their precursors after ozone oxidation, photodegradation, biodegradation and disinfection with NaClO. Results indicated that the potential environmental risk of these disinfection by-products should be further recognized. In addition, the model prediction of LC_{50} values of eight SMs supplements to the existing data. The research output provides theoretical support to design new SM molecules that are less harmful to the environment and human health.

Appendices

Table S3-1 Names, molecular formula, CAS number and molecular structure of synthetic musks (SMs) used in the database for the 3D-QSAR model construction

SMs	Name (cited from ChemSpider)	Molecular formula	Smiles	CAS number**	logLC ₅₀ (EPI predicted) (×10 ⁻⁶ mmol/pT)	Molecular structure
Musk #1	1-(1,1,2,3,3,6-Hexamethyl-2,3-dihydro-1H-inden-5-yl)ethanone (AHD1)	C ₁₇ H ₂₄ O	<chem>C1(C)(C)c2c(C(C)(C)C1C)cc(C(C)=O)c(C)c2</chem>	15323-35-0	0.99	
Musk #2	1-[1,1-Dimethyl-6-(2-methyl-2-propanyl)-2,3-dihydro-1H-inden-4-yl]ethanone (ADBI)	C ₁₇ H ₂₄ O	<chem>C(C)(=O)c1c2c(C(C)(C)CC2)cc(C(C)(C)C)c1</chem>	13171-00-1	0.89	
Musk #3	1-(2,2,6,6-tetramethyl-1,2,6,7,8,8a-hexahydroacenaphthylen-4-yl)ethanone	C ₁₈ H ₂₄ O	<chem>C1(C)(C)c2c3c(C(C)(C)CC3CC1)cc(C(C)=O)c2</chem>	/	1.35	
Musk #4	6-ethynyl-5-methoxy-1,1,4,4,7-pentamethyl-1,2,3,4-tetrahydronaphthalene	C ₁₇ H ₂₃ NO	<chem>C1(C)(C)c2c(C(C)(C)CC1)c(OC)c(C#N)c(C)c2</chem>	/	0.96	
Musk #5	6,8-diisopropyl-4-methylchroman-2-one	C ₁₆ H ₂₂ O ₂	<chem>c1(C(C)C)c2c(C(C)CC(=O)O2)cc(C(C)C)c1</chem>	/	3.08	

Musk #6	6-(tert-butyl)-8-isopropyl-4-methylchroman-2-one	C ₁₇ H ₂₄ O ₂	<chem>C(C)(C)(C)c1cc(C(C)C)c2c(C(C)CC(=O)O2)c1</chem>	/	2.71	
Musk #7*	1-(1,1,3,3-tetramethyl-2,3-dihydro-1H-inden-5-yl)ethanone	C ₁₅ H ₂₀ O	<chem>C1(C)(C)c2c(C(C)(C)C1)cc(C(C)=O)cc2</chem>	17610-14-9	2.13	
Musk #8	1-(1,1,3,3-tetramethyl-2,3-dihydro-1H-inden-5-yl)ethanone	C ₁₅ H ₂₀ O	<chem>C(C)(=O)c1c2C(C)(C)CC(C)(C)c2ccc1</chem>	/	2.13	
Musk #9*	1-(1,1,3,3,5-pentamethyl-2,3-dihydro-1H-inden-4-yl)ethanone	C ₁₆ H ₂₂ O	<chem>C(C)(=O)c1c2C(C)(C)CC(C)(C)c2ccc1C</chem>	/	1.46	
Musk #10	1-(1,1,3,3,5,6-hexamethyl-2,3-dihydro-1H-inden-4-yl)ethanone	C ₁₇ H ₂₄ O	<chem>C(C)(=O)c1c2C(C)(C)CC(C)(C)c2cc(C)c1C</chem>	/	0.76	
Musk #11	1-(6-(sec-butyl)-1,1-dimethyl-2,3-dihydro-1H-inden-4-yl)ethanone	C ₁₇ H ₂₄ O	<chem>C(C)(=O)c1c2c(C(C)(C)CC2)cc(C(C)CC)c1</chem>	/	0.89	
Musk #12	1-(6-isopropyl-1,1-dimethyl-2,3-dihydro-1H-inden-4-yl)ethanone	C ₁₆ H ₂₂ O	<chem>C(C)(=O)c1c2c(C(C)(C)CC2)cc(C(C)C)c1</chem>	/	1.43	
Musk #13	1-(3-Isopropyl-1,1,2,6-tetramethyl-2,3-dihydro-1H-inden-5-yl)ethanone (ATII)	C ₁₈ H ₂₆ O	<chem>C1(C)(C)c2c(C(C)(C)C1C)cc(C)c(CC(C)=O)c2</chem>	68140-48-7	1.22	

Musk #14*	6-(tert-butyl)-1,1-dimethyl-2,3-dihydro-1 <i>H</i> -inden-4-carbonitrile	C ₁₆ H ₂₁ N	<chem>C(#N)c1c2c(C(C)(C)CC2)cc(C(C)(C)C)c1</chem>	/	1.02	
Musk #15	1-(6-(tert-butyl)-2,3-dihydro-1 <i>H</i> -inden-4-yl)ethanone	C ₁₅ H ₂₀ O	<chem>C(C)(=O)c1c2c(cc(C(C)(C)C)c1)CCC2</chem>	/	1.92	
Musk #16	1-(6-(tert-butyl)-1-methyl-2,3-dihydro-1 <i>H</i> -inden-4-yl)ethanone	C ₁₆ H ₂₂ O	<chem>C(C)(=O)c1c2c(C(C)CC2)cc(C(C)(C)C)c1</chem>	/	1.43	
Musk #17*	1-(1,1,3,3,6-pentamethyl-2,3-dihydro-1 <i>H</i> -inden-5-yl)ethanone	C ₁₆ H ₂₂ O	<chem>C1(C)(C)c2c(C(C)(C)C1)cc(C(C)=O)c(C)c2</chem>	/	1.46	
Musk #18	1-(1,1,2,3,6-pentamethyl-2,3-dihydro-1 <i>H</i> -inden-5-yl)ethanone	C ₁₆ H ₂₂ O	<chem>C1(C)(C)c2c(C(C)C1C)cc(C(C)=O)c(C)c2</chem>	/	1.52	
Musk #19*	1-(1,2,3,3,6-pentamethyl-2,3-dihydro-1 <i>H</i> -inden-5-yl)ethanone	C ₁₆ H ₂₂ O	<chem>C1(C)(C)c2c(C(C)C1C)cc(C)c(C(C)=O)c2</chem>	/	1.52	
Musk #20	1-(5-(tert-butyl)-1,1-dimethyl-2,3-dihydro-1 <i>H</i> -inden-4-yl)ethanone	C ₁₇ H ₂₄ O	<chem>C(C)(=O)c1c(C(C)(C)C)ccc2C(C)(C)CCc12</chem>	/	0.89	
Musk #21	1-(3,5,5,8,8-Pentamethyl-5,6,7,8-tetrahydro-2-naphthalenyl)ethanone	C ₁₇ H ₂₄ O	<chem>C1(C)(C)c2c(C(C)(C)CC1)cc(C(C)=O)c(C)c2</chem>	17610-24-1	0.89	

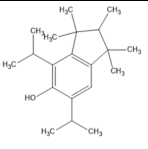
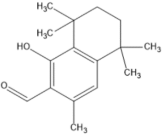
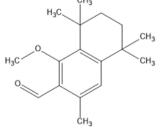
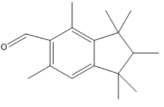
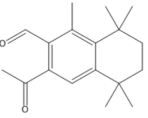
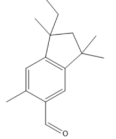
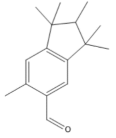
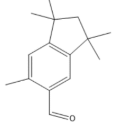
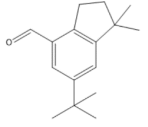
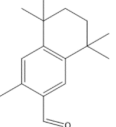
Musk #22	1-(3,5,5,8-Tetramethyl-5,6,7,8-tetrahydro-2-naphthalenyl)ethanone	C ₁₆ H ₂₂ O	<chem>C1(C)(C)c2c(C(C)CC1)cc(C(C)=O)c(C)c2</chem>	93162-97-1	1.43	
Musk #23	1-(5,5,8,8-Tetramethyl-5,6,7,8-tetrahydro-2-naphthalenyl)ethanone	C ₁₆ H ₂₂ O	<chem>C1(C)(C)c2c(C(C)(C)CC1)cc(C(C)=O)cc2</chem>	17610-21-8	1.54	
Musk #24	1-(3,8,8-trimethyl-5,6,7,8-tetrahydronaphthalen-2-yl)ethanone	C ₁₅ H ₂₀ O	<chem>C(C)(=O)c1c(C)cc2c(C(C)(C)CCC2)c1</chem>	/	1.92	
Musk #25	1-(3-Ethyl-8,8-dimethyl-5,6,7,8-tetrahydro-2-naphthalenyl)ethanone	C ₁₆ H ₂₂ O	<chem>C(C)(=O)c1c(CC)cc2c(C(C)(C)CCC2)c1</chem>	27413-60-1	1.35	
Musk #26	1-(3-(tert-butyl)-5,6,7,8-tetrahydronaphthalen-2-yl)ethanone	C ₁₆ H ₂₂ O	<chem>C(C)(=O)c1c(C(C)(C)C)cc2c(c1)CCCC2</chem>	/	1.35	
Musk #27	6,7-diisopropylchroman-2-one	C ₁₅ H ₂₀ O ₂	<chem>c1(C(C)C)c(C(C)C)cc2c(c1)CCC(=O)O2</chem>	/	3.43	
Musk #28	6,8-diisopropylchroman-2-one	C ₁₅ H ₂₀ O ₂	<chem>c12c(c(C(C)C)cc(C(C)C)c1)OC(=O)CC2</chem>	/	3.43	
Musk #29*	6,6,7,8,8-pentamethyl-1,3,4,6,7,8-hexahydrocyclopenta[g]isochromene	C ₁₇ H ₂₄ O	<chem>C1(C)(C)c2c(C(C)(C)C1C)cc1c(c2)CCOC1</chem>	/	0.99	

Musk #30	6,6,9,9-tetramethyl-3,4,7,8-tetrahydro-1H-benzo[g]isochromene	C ₁₇ H ₂₄ O	<chem>C1(C)(C)c2c(C(C)(C)CC1)cc1c(c2)CCOC1</chem>	1217-06-7	0.89	
Musk #31	4,6,6,8,8-pentamethyl-1,3,4,6,7,8-hexahydrocyclopenta[g]isochromene	C ₁₇ H ₂₄ O	<chem>C1(C)(C)c2c(C(C)(C)C1)cc1c(C(C)COC1)c2</chem>	/	0.99	
Musk #32*	6,6,8,8-tetramethyl-1,3,4,6,7,8-hexahydrocyclopenta[g]isochromene	C ₁₆ H ₂₂ O	<chem>C1(C)(C)c2c(C(C)(C)C1)cc1c(c2)CCOC1</chem>	/	1.49	
Musk #33	4,4,8,8-tetramethyl-1,3,4,6,7,8-hexahydrocyclopenta[g]isochromene	C ₁₆ H ₂₂ O	<chem>C1(C)(C)c2c(cc3C(C)(C)CCc3c2)COC1</chem>	/	1.49	

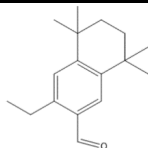
* means the SMs used in the test set;

** "/" means not available from NIST Library, ChemSpider, and Chemical Book.

Table S3-2 The predicted LC_{50} values of 15 SMs using the constructed CoMSIA model

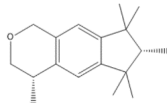
Molecular formula	Molecular structure	LC_{50} ($\times 10^{-6}$ mmol/pT) in mysid
$C_{18}H_{28}O$		0.398
$C_{16}H_{22}O_2$		0.836
$C_{17}H_{24}O_2$		0.533
$C_{17}H_{24}O$		0.815
$C_{18}H_{24}O_2$		0.731
$C_{16}H_{22}O$		1.486
$C_{16}H_{22}O$		0.932
$C_{15}H_{20}O$		1.3
$C_{16}H_{22}O$		1.016
$C_{16}H_{22}O$		1.459

C₁₇H₂₄O



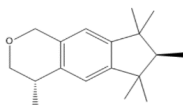
1.043

C₁₈H₂₆O



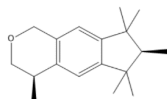
1.045

C₁₈H₂₆O



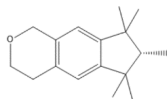
1.034

C₁₈H₂₆O



1.615

C₁₈H₂₆O



1.483

CHAPTER 4

FUNCTIONAL MODIFICATION OF HHCB: STRATEGY FOR OBTAINING ENVIRONMENTALLY FRIENDLY DERIVATIVES

This chapter has been published in the *Journal of Hazardous Materials* (2021), 416: 126116. I am the primary author of this paper, and am mainly responsible for the research initiation, data collection, model development, result analysis and generation of the manuscript. The co-author Wenwen Gu is mainly responsible for the research initiation, data collection, model development, result analysis and generation of the manuscript, Bing Chen helps to conduct the data analysis and polish the manuscript, Zhiwen Zhu helps to edit the manuscript and Baiyu Zhang is the principal investigator of the manuscript involved research project/funds and is mainly responsible for supervising me throughout the research and finalizing the manuscript.

Li, X., Gu, W., Chen, B., Zhu, Z., & Zhang, B. (2021). Functional Modification of HHCB: Strategy for Obtaining Environmentally Friendly Derivatives. *Journal of Hazardous Materials*, 416: 126116.

DOI: 10.1016/j.jhazmat.2021.126116

4.1 Introduction

Synthetic musks (SMs) as alternatives to the natural musk have been widely used in personal care products (PCPs), such as fragrances, shampoos, soaps, and household items (Duedahl-Olesen et al., 2005; Roosens et al., 2007). They are usually categorized in four categories, namely nitro, polycyclic, macrocyclic and alicyclic compounds (Homem et al., 2015b). Polycyclic musks dominate the SMs market with a market share of over 61% (Nakata et al., 2007). As one of the most widely used polycyclic musks, galaxolide (HHCB) is known as a high production-volume chemical whose production reached 1427 metric tons in 2000 in Europe (European Union Risk Assessment Report, 2008). On the other hand, HHCB is recognized as an emerging contaminant with potential human health concerns due to its ubiquitous existence, high lipophilicity ($\log K_{ow}$ of 6.26) and long persistence in the environment (Winkler et al., 1998; NORMAN List of Emerging Substances, 2020). HHCB has been frequently detected in natural waters, soil, air as well as sludge and effluent from the wastewater treatment plants (Zeng et al., 2005; Sumner et al., 2010; Zhang et al., 2020a). HHCB entered the food chain and gradually accumulated in organisms and had a medium-range transport (detected in the Arctic) (Xie et al., 2007; Peng et al., 2018; Peng et al., 2019; Ding et al., 2020; Ehiguese et al., 2021). HHCBs in liver tissues of seals, sea lions, Atlantic sharpnose shark, river otter, mink, common merganser, lesser scaup, greater scaup, and mallard and even the human body has been documented (Kannan et al., 2005). Recent studies highlighted the ecological risk of HHCB residues in the environment. It could significantly decrease the algal growth rate (Ding et al. 2020), bring oxidative stress to zebra mussels and lead to genetic damage (Parolini et al., 2015), as well as decrease the growth, survival, and reproduction of youth gastropod (*Potamopyrgus antipodarum*) (Pedersen et al., 2009). Besides the algae and arctic organisms,

HHCB could also pose potential risks to humans. Li et al. (2013) demonstrated that HHCB inhibited the production of progesterone and cortisol. The large consumption of HHCB and their ecological toxicity call for the systematic development of environmentally friendly HHCB alternatives with desired properties and functions, lower ecological toxicities (e.g., bio-toxicity, bio-accumulation ability, and mobility in this study), smaller human health risks and less environmental footprint.

The three-dimensional quantitative structure-activity relationship (3D-QSAR) is a robust method used to design new chemicals by investigating and virtual screening the three-dimensional properties of the ligands (Vilar et al., 2008; Winkler, 2018; Li et al., 2020a). Particularly, this tool can be used to correlate the chemical structures of designed molecules to their physiochemical activities for further prediction. Attempts in designing and screening fragrance molecules based on the quantitative structure-property relationships have been reported (Zhang et al., 2018c). Moreover, the 3D-QSAR model can be applied to evaluate the environmental behaviors of the designed chemicals and their ecological impacts on the environment. Gu et al. (2019) assessed the biological toxicity of polychlorinated naphthalene in the environment, determined their biodegradability in the environment with 3D-QSAR. The degradation of chemicals (e.g., polychlorinated biphenyl) has been evaluated and predicated by 3D-QSAR using the bioaccumulation factor (BCF) of pollutants (Zhao et al., 2018b). By establishing the relationships between HHCB molecular structure and its functional and environmental properties, HHCB alternatives could be designed with higher efficiency and less environmental impact by 3D-QSAR. The topic has never been reported yet.

Before acting as an additive in PCPs, an in-depth investigation of the toxicity of HHCB derivatives is of great importance. The toxicity of chemicals to mice or rats has been used to infer the toxicity to humans (Raveh et al., 1993). TOPKAT could provide abundant toxicity

information such as mutagenicity, carcinogenicity, skin irritancy, etc., and was found with good assessment reliability of the predictions (Ruiz et al., 2011). TOPKAT module has been used to predict the carcinogenicity and hepatotoxicity of acebutolol's by-products (Rakibe et al., 2018) and the genotoxicities of Salmonella (Snyder et al., 2004). Therefore, the TOPKAT was introduced as an emerging tool to advance the understanding of the toxicity of HHCB alternatives and facilitate the derivatives' screening process. Besides, the skin exposure toxicity of the developed derivatives to humans was also evaluated using molecular docking. The score obtained from molecular docking can be used to evaluate and reveal the fitness and the binding affinities between the ligand and the protein (Wang et al., 2003; Ling et al., 2018). After molecular docking, HHCB derivatives with lower skin exposure toxicity will be screened out as the optimum alternative of HHCB.

The HHCB by-products generated during treatment processes have been recognized with ecological impacts and pathological effects; such impacts and their transformation mechanisms in the environment remain to be unclear with few research attempts. For example, HHCB-lactone, one of the HHCB's by-products has been widely detected in the effluent of wastewater treatment plant (Bester, 2005; Horii et al., 2007; Reiner and Kannan, 2006). Its residence in the effluents after treatment, such as bioremediation (Martin et al., 2007) and disinfection (Kuhlich et al., 2011), have also been documented. As an environmentally friendly alternative to HHCB, the behaviors of newly designed HHCB derivatives and the ecological impacts of the generated by-products should be considered. Thus, this study simulated the transformation pathways of a representative HHCB derivative following the ones reported by HHCB molecule (Gatermann et al., 2002; Sanchez-Prado et al., 2004; Martin et al., 2007). The by-products' bio-toxicity, bio-accumulation ability and mobility of these new HHCB derivatives were predicted using the 3D-QSAR models. This study attempted to provide an in-depth investigation on the transformation

mechanism of newly generated HHCB alternatives to further limit their adverse environmental impact.

In addition, given that HHCB is an additive in PCPs for external use, the use of HHCB and other PCPs additives may have synergistic or antagonistic impacts on human health. A detailed assessment of such impacts could prevent the potential risks of HHCBs to humans by controlling their dermal absorption. Representative functional PCP additives (e.g., moisturizers and anti-photosensitivity materials) were selected in this study for such assessment. Molecular docking methodology can be used as a key tool to investigate the interactions between the ligand and the target protein with known 3D structures through the docking process (Morris et al., 2008). The constructed binding modes between the ligand (i.e., HHCB and its derivatives) and target skin protein without functional additives could reveal the potential risk of designed HHCB derivatives to humans. Their interaction with representative functional additives could be further assessed, verified, and screened to reduce the dermal adsorption risk of the designed HHCB derivatives using molecular dynamics simulations (Gu et al., 2020c). Taguchi experimental design was introduced into the molecular dynamics simulations as a statistic approach to facilitate the interaction evaluation, product screening and optimization process with higher efficiency. The synergistic or antagonistic impacts of HHCB derivatives and other PCPs additives were firstly accessed to control the possible dermal adsorption of HHCB derivatives and reduce their potential risks to human health.

Therefore, the objectives of this study include (1) building a 3D-QSAR model by using known functional property (half-life) and molecular structures of SMs for obtaining new HHCB derivatives; (2) screening the derivatives by using three environmental properties (bio-toxicity, bio-accumulation ability and mobility) 3D-QSAR models; (3) further screening the designed HHCB derivatives with less toxic to rats by using TOPKAT; (4) accessing the HHCB derivatives

- PCPs additives interactions for dermal adsorption control using Taguchi experimental design- molecular docking and molecular dynamics simulations; (5) analyzing the degradation pathways of the selected HHCB derivative, and assessing the mobility, bio-toxicity, and bio-accumulation ability of its transformation by-products. This study aims to provide a comprehensive view of HHCB's new derivatives, including designing, evaluating their environmental and human health risks, and predicting environmental behaviors of the degradation by-products.

4.2 Materials and Methods

4.2.1 Molecular design for obtaining functionally improved and environmentally friendly HHCB derivatives

The functional properties of a SM, namely the odor stability, musky scent, and odor intensity, determine their performance as an additive in personal care products (Rimkus, 1999). The half-life is a well-recognized parameter to reflect long-lasting capacity or odor stability (Clausen et al., 1986; Paasivirta et al., 2002; Bradbury et al., 2008). Therefore, the half-life of the newly designed molecule was selected as a functional property during 3D-QSAR modelling. The musky scent is another functional parameter for SMs. It is highly related to the molecular structure of polycyclic compounds (Rossiter, 1996). Therefore, the key structures that give musky scent were defined and remained in the designed HHCB derivative compounds. Odor intensity is also an important functional parameter for HHCB derivative screening. The worse its molecular steadiness, the higher the odor intensity of the fragrance (Woker, 2002; Nagendrappa, 2014). The molecular steadiness is generally represented by the positive frequency value and the energy gap of a compound (Gu et al., 2020c; Chaudhary, 2020). When

the polycyclic compound has a positive frequency value, the higher the energy gap value, the lower the odor intensity of the fragrance.

The bio-accumulation factor (BCF), LC_{50} and vapor pressure were selected as environmental properties of SMs in this study. Bioaccumulation refers to the accumulation of chemical substances in or within organisms when chemical substances are only derived from water. BCF is a factor that reflects the degree of bio-accumulation (Arnot and Gobas, 2006). LC_{50} stands for the lethal concentration of a chemical in air or water that kills 50% of the test living organisms during the observation period, and thus was chosen as the toxicity indicator. When the LC_{50} value increases, the toxicity of the chemical decreases. Vapor pressure is an important physical and chemical parameter for predicting the behavior of chemical substances in the atmosphere. It has been used as an evaluation indicator for long-distance atmospheric mobility of target chemicals. The higher the vapor pressure value, the higher the mobility of the chemicals (Gu et al., 2017).

Last but not least, TOPKAT model was used here to provide reliable toxicity information prediction such as mutagenicity, carcinogenicity, skin irritancy, etc. of HHCB alternatives and facilitate the derivatives' screening process. The potential human health risk of HHCB was expressed by LibDock Score of HHCB or its derivatives to human skin stratum corneum protein (4ZRY).

4.2.1.1 Construction of the 3D-QSAR model

3D-QSAR models were analyzed with the SYBYL[®]. The chemical structures (i.e., SMs with similar structures) and their half-lives (hours) in the air (obtained from EPI Suite software) (Zachary and Greenway, 2009) were used as independent and dependent variables, respectively, for 3D-QSAR model establishment. The data set (n=13) was composed of a training set (10 SMs

showed in Table S4-1) and a test set (4 SMs showed in Table S4-1) for 3D-QSAR model construction and validation, respectively, using CoMFA method (Chu and Li, 2019). The SM compound with the longest half-life (i.e., SM 1) was selected as a template molecule and was included in both sets.

The construction of 3D-QSAR and a follow-up molecular alignment were performed using the SYBYL[®]. The Sketch derivative module was used to optimize the 3D structure (e.g., geometries) of each SM (Nayyar et al., 2006) using the Tripos force field with Gasteiger-Hückel charges. The energy convergence gradient value of each molecule was minimized to 0.005 kJ/mol with Powell method at a maximum iteration of 10,000. The template molecule (i.e., SM 1) was then aligned to the other SMs using the Align Database command in SYBYL.

4.2.1.2 Design of HHCB derivatives with improved functional properties

HHCB has four stereoisomers, among which (4S, 7R) molecular configurations were the widely recognized and effective aroma source of HHCB (Fráter et al., 1999; Kraft and Fráter 2001). Therefore, (4S, 7R)-HHCB was selected in this study as an example for molecular modification. Representative structures and functional groups have been identified for molecules to exhibit musky scents. Such structures and functional groups were adopted and used as screening criteria to make sure the designed HHCB derivatives possess the desired scent. The relationships between the molecular structure of designed HHCB derivatives and the musky scent include: (1) The targeting compounds must be tricyclic isochroman derivatives; (2) The musky scent can be remained when a component contain 16-19 carbon atoms with the strongest musky scent when 17-18 carbon atoms appear; (3) The saturated ring of the selected derivative compound should contain two quaternary carbon atoms which are all part of the saturated ring; and (4) The methyl group on the oxygen ring of the compound must be located in the meta

position of the oxygen atom (Rossiter, 1996; Liu, 2004). Following such criteria, the key structures that gave musky scent would remain in the designed HHCB derivatives.

New HHCB derivatives with better odor stability were designed based on the descriptor fields information (i.e., steric and electrical fields) presented in the contour maps generated by the CoMFA model. Half-life, a term used to describe the time required for a quantity to reduce to half of its initial value, has been used to reflect the odor stability of a fragrance (Paasivirta et al., 2002; Bradbury et al., 2008). That information (i.e., field information and half-life) advanced the understanding of the physical and chemical properties of HHCB and its derivatives, and revealed the possible mono- and bis-substituted sites of the HHCB molecule with possible substitutional groups. The HHCB derivatives thus could be generated and their functional property (i.e., odor stability) could be determined through the generated contour map and assessed with the CoMFA model. The half-lives of the derivatives should not exceed 48 hours, a threshold set for avoiding obvious air migration of a chemical and the associated ecological concerns (Stockholm Convention on Persistent Organic Pollutants, 2001). The HHCB derivatives with the improved functional property (i.e., longer half-life than that of HHCB) were then selected and used for the following investigation.

Moreover, the order intensity of the aroma compounds was further evaluated using the molecular steadiness. The worse the molecular steadiness, the higher the odor intensity of a compound (Woker, 2002; Nagendrappa, 2014). The molecular steadiness of HHCB derivatives was reflected by their energy gap and positive frequency calculated by Gaussian[®] 09. The structures of HHCB and the new HHCB derivatives were optimized using density functional theory (DFT) (B3LYP/6-31G*) (Gu et al., 2020c). When the compound had a positive frequency value, the lower the energy gap value, the higher the odor intensity of the fragrance. The derivatives with higher odor intensity were selected and used for further investigation.

4.2.1.3 Design of HHCB derivatives with less environmental impacts using 3D-QSAR models

The selected derivatives were then assessed by three environmental property indicators, including biological toxicity (LC_{50}) in fish, migration ability ($\log_{\text{vapor pressure}}$, named as $\log VP$), and bioaccumulation ability ($\log BCF$). The HHCB molecule was used as a control. Two 3D-QSAR models were constructed to predict the $\log VP$ and $\log BCF$ of the new HHCB derivatives, respectively. The CoMSIA model of $\log VP$ consisted of a training set (15 SMs) and a test set (6 SMs). Musk 25 was selected as the template molecule and included in both sets. The CoMFA model of $\log BCF$ consisted of a training set (13 SMs) and a test set (4 SMs). Musk 83 was selected as the template molecule and included in both sets. The construction of two 3D-QSAR models (i.e., $\log VP$ and $\log BCF$) were the same as the method shown in Section 4.2.1.2. As for biological toxicity (LC_{50}), which could be obtained by prediction with EPI Suite software. HHCB derivatives with improved environmental properties (i.e., higher LC_{50} , lower $\log VP$ and $\log BCF$ than control) were then selected and used for further investigation.

4.2.1.4 Human health risk assessment of HHCB derivatives using toxicokinetic analysis and molecular docking

The molecules of HHCB and the screened HHCB derivatives in Section 4.2.2 were imported into Discovery Studio[®] 2020. The “Calculate molecular properties”, “Small molecules”, and “Toxicity prediction extensible” modules in the TOPKAT module were selected in order. A few other important parameters (e.g., rat inhalation LC_{50} , skin irritancy and ocular irritancy) were calculated as the toxicity endpoint parameters of the ecological risk assessment.

The toxicity of HHCB and their derivatives to humans were evaluated as the binding ability between chemical compounds (i.e., HHCB and the newly designed HHCB derivatives) and one

identical protein in humans using molecular docking with Discovery Studio[®] 2020. As a major protein in the epidermis, the mutation in the keratin proteins [e.g., keratin 1 (K1) or keratin 10 (K10)] has been considered as a well-recognized inducer of skin disorder, such as epidermolytic ichthyosis, and ichthyosis with confetti (Bunick and Milstone, 2017). The 4ZRY, one of the keratins, thus was chosen as the identical protein in this study. The LibDock Score was used to express the binding ability between chemical compounds and 4ZRY. The 4ZRY was obtained from the PDB database bank. Firstly, designed chemicals and target protein were loaded into the software. LibDock module was then used to define the selected protein as a receptor molecule. After that, potential binding sites can be found, modified, and defined by the module of Find Sites from Receptor Cavities. Finally, each chemical compound was integrated into the formed protein binding cavity for rapid docking with the ligand molecule. During the process, only “Docking Preferences” and “Max Hit to Save” were changed to “User Specified” and “10”, and the rest remained the same. The HHCb derivatives with lower toxicity were then subject to further studies.

4.2.2 Evaluation of behaviors of a selected representative HHCb derivative

4.2.2.1 Evaluation of its environmental behaviors

The derivative with the least human health risk was selected and then its degradation pathway was explored and compared with that of HHCb. The degradation methods for HHCb and the new derivative include photodegradation (Sanchez-Prado et al., 2004), biotransformation (Martin et al., 2007), chlorination (Kuhlich et al., 2011) and metabolic pathway of these compounds in algal cells (Ding et al., 2020). In addition, DFT calculations (Lee et al., 1988) were performed using the B3LYP/6-31G* basis set by Gaussian software (Frisch et al., 2013). All reactants, transition states, intermediates and by-products generated in

the photodegradation, biotransformation and chlorination processes, were optimized to obtain the optimal structure, and the energy barrier of each reaction path are calculated.

The human health risk of the above transformation by-products was also assessed using TOPKAT module in Discovery Studio[®] 2020. The methodology procedure is consistent with that of HHCB derivatives in Section 4.2.1.4.

4.2.2.2 Evaluation of the HHCB derivative and other PCP additives interactions and the related human health risk assessment

Taguchi experimental method was used to statistically design the experimental runs by using an orthogonal table. The orthogonal table is a regularly formalized and standardized table with the characteristics of the equal combination. Thus, the chance of the samples to be selected would be equal. This is a cost-efficient optimization method by statistical selection and analysis of a small amount of experimental data (Ayhan et al., 2020). Therefore, Taguchi experimental method was used in this study to obtain more representative and authoritative results with fewer runs.

After molecular docking of chemical compounds (i.e., HHCB and selected derivatives) with 4ZRY, the molecular dynamics simulation was performed to determine the binding energy of the above complexes by adding 12 moisturizers additives (i.e., DL-Pyroglutamic acid, D-Sorbose, vitamin A, vitamin E, lactic acid, urea, ceramide 3, linoleic acid, glycerol, phytosphingosine, ceramide 1) and three anti-photosensitivity materials (i.e., quercetin, vitamin B₃ and rutin) (Zhang et al., 2020b; Nezzal et al., 2009; Marques et al., 2016; Chanchal and Swarnlata, 2008; Hasegawa et al., 2008; Onoda et al., 2012; Choi and Lee, 2015; Lourith et al., 2016; Yamada et al., 2021; Choi et al., 2017; Cha et al., 2016; Müller et al., 2007; Fernández-Ponce et al., 2015; Minocha et al., 2018; Tomazelli et al., 2018). After comparing the binding

energy of different conditions, the conditions with lower binding energy (absolute value) were selected. The selected additives were used as the factors and adding or not adding were the two levels for screening the optimum additives combinations in Taguchi experimental design.

Molecular dynamics simulations of the chemical compounds (i.e., HHCb and the selected HHCb derivatives) were conducted by using the Dell PowerEdge R7425 server and Gromacs software. Detailed molecular dynamics settings were provided in Supplement Information. The simulation experiments were constructed by simulating the binding ability between one chemical compound (i.e., HHCb or one representative HHCb derivative) and 4ZRY. Besides the experimental groups, one control group without adding any additives was set up for comparison. Subsequently, the binding ability between the chemical compound (i.e., HHCb or one representative HHCb derivative) and 4ZRY complexes under the scenarios designed by Taguchi experimental method was simulated. Each binding energy was determined using the Molecular Mechanics/Poisson-Boltzmann Surface Area (MMPBSA) method. After obtaining the results, the absolute values of binding energy were used to illustrate whether the additives can help to reduce binding ability between the chemical compound (i.e., HHCb or one representative HHCb derivative) and 4ZRY. This provided valuable guidance for reducing the toxicity of the chemical compound (i.e., HHCb or one representative HHCb derivative) to human bodies, by adding some moistures or anti-photosensitivity materials while using SMs. The combined binding energy was calculated following the equation illustrated below (Gu et al., 2020c):

$$G_{\text{bind}} = G_{\text{complex}} - G_{\text{free-protein}} - G_{\text{free-ligand}} \quad (4-1)$$

The binding free energy of the molecule can be determined as follows:

$$G = E_{\text{gas}} - TS_{\text{gas}} + G_{\text{solvation}} \quad (4-2)$$

The solvation free energy can be calculated as follows:

$$G_{\text{solvation}} = G_{\text{polar}} + G_{\text{nonpolar}} \quad (4-3)$$

All the parameters shown in the above equations were defined and shown in the Supplementary Materials. The complex system between the chemical compound (i.e., HHCB or one representative HHCB derivative) and 4ZRY was placed in a cubic box with a side length of 14.885 nm, the GROMOS96 43a1 field was used for molecular constraint, and Na⁺ ions were added to neutralize the system charge. The energy minimization simulation was performed on the basis of the steepest gradient method, the temperature was set to 300K and the standard atmospheric pressure (1 bar) was used as the bath pressure.

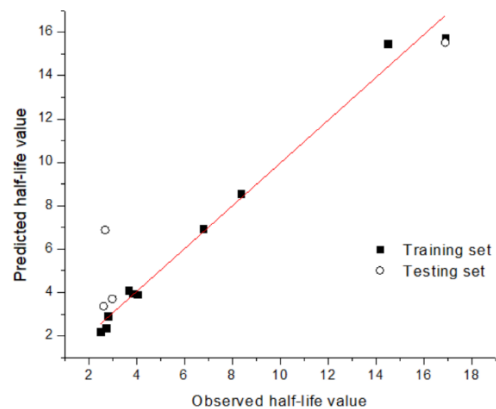
4.3 Results and Discussion

4.3.1 Evaluation of the constructed 3D-QSAR models for predicting HHCB functional and environmental properties

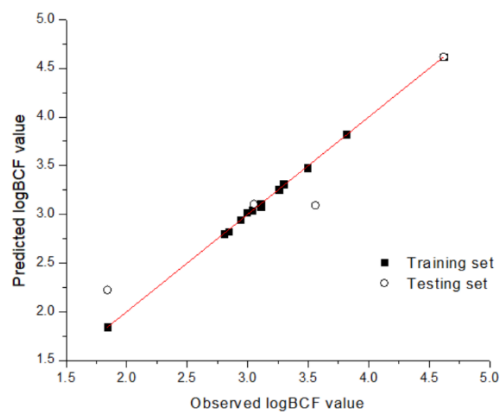
The statistical evaluation of three 3D-QSAR models is shown in Table 4-1. The cross-validation coefficient (q^2) for all the parameters (i.e., half-life, $\log VP$ and $\log BCF$) are higher than 0.5, indicating the credible predictive ability of three models (Salahinejad and Ghasemi, 2014). Relatively high values of non-cross-validation ($r^2 > 0.9$ and close to 1.000) and external test coefficient (R^2_{pred}) further proved the good predictive ability and the robustness of the generated models. The standard error of estimate (SEE) of three models were less than 0.95 confirmed the good fit ability and predictive ability of the models (Gu et al., 2019). Linear regression analysis was conducted based on the predicted and experimental values of three parameters (i.e., half-life, $\log VP$ and $\log BCF$) and the results are presented in Figure 4-1. The slopes of three regression models (i.e., half-life, $\log BCF$ and $\log VP$) were 0.9882, 0.9998 and 1.0001, indicating good internal predictive abilities of the generated 3D-QSAR models and proves their applicability in predicting the desired environmental properties of generated HHCB derivatives.

Table 4-1 Statistical parameters of the established 3D-QSAR models

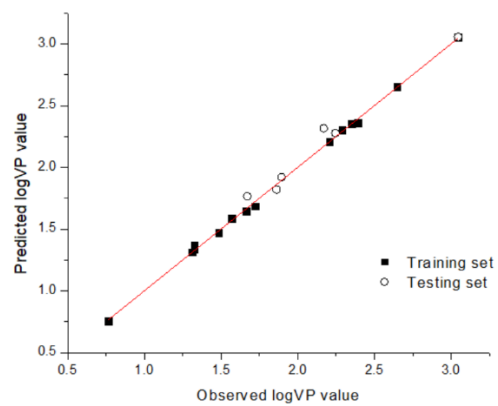
Target	Models	q^2	r^2	SEE	F	R^2_{pred}
HL	CoMFA	0.557	0.988	0.755	104.186	0.940
$\log VP$	CoMSIA	0.507	0.999	0.024	1668.465	0.947
$\log BCF$	CoMFA	0.546	0.999	0.022	1426.871	0.909



(1)



(2)

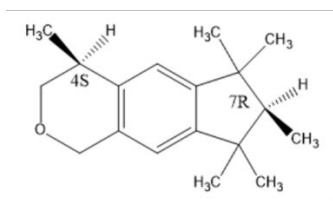


(3)

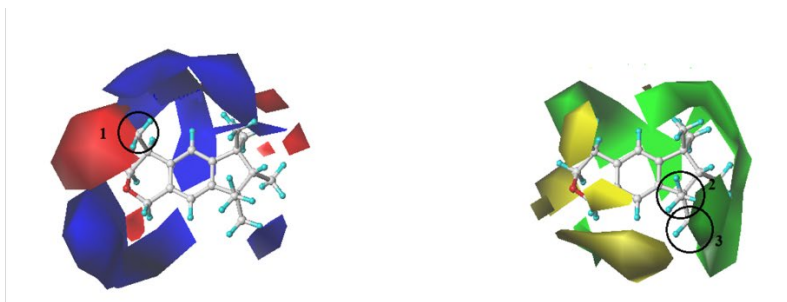
Figure 4-1 Plot of observed vs predicted values using the CoMFA model (1) Half-life: $y=0.9882x+0.07848$; (b) $\log BCF$: $y=0.9998x+3.3607 \times 10^{-5}$; (c) $\log VP$: $y=1.00013x+5.59253 \times 10^{-4}$

4.3.2 Determination of HHCb molecular substituted sites and groups based on contour maps of 3D-QSAR model

The contribution of descriptor fields to the functional property of HHCb molecule was assessed by the CoMFA model and the result indicated that electrostatic fields contribute (61.2%) to the half-life of HHCb compared to that of the steric field (38.8%). The electrostatic potential of HHCb is also presented in the contour maps (Figure 4-2), indicating the substituent effect to generate HHCb derivatives with better functionality. Substitution of more positively charged groups in blue areas and more negatively charged groups in red areas of the electrostatic field [Figure 4-2(b)] favored the extension of the half-life of newly designed HHCb products. Similarly, longer half-lives of HHCb derivatives were expected with substitutions of bigger molecular groups in the green area and smaller molecular groups in yellow [Figure 4-2(c)]. Three potential substituted areas, namely position 1 (CH₃), 2 (CH₃), and 3 (CH₃) were identified by the contour maps (Figure 4-2). Accordingly, located in red area, the positions 1 (CH₃) could be replaced with more negatively charged substituents (-C₂H₃, -CH₂NH₂, -NH₂, -OCH₃, -C₂H, -CH₂OH, -NO, -NO₂, -CHO, and -OOH), 2(CH₃), and 3(CH₃) surrounded by green color could be replaced with bigger molecular substituents (-C₂H₃, -C₂H, -OH, -COOH, -CH₂OH, -NO, -NO₂, -NH₂, -CH₂NH₂, and -OCH₃) to generate HHCb derivatives with longer half-lives. Thus, a total of 90 HHCb derivatives were generated. Among them, 20 HHCb derivatives were single-substituted molecules (only one -CH₃ was substituted) and the rest 70 were double-substituted (two -CH₃ were substituted).



(a)



(b)

(c)

Figure 4-2 The (a) molecular structure of (4S, 7R)-HHCb, contour maps of (b) HHCb (electrostatic field) and (c) HHCb (steric field)

4.3.3 HHCB derivatives with improved functional and environmental properties

The replacement of substituted groups and predicted results are shown in Table 4-2. We believed that all the 90 designed HHCB derivatives had musky scents after applying the criteria in the molecular designing process, as stated in Section 4.2.1.2. For the odor-lasting property, it was found that 26 new HHCB derivatives (shown in Table 4-3) had a longer half-life than that of HHCB. The increasing rate ranged from 9.98% to 49.89%. The longest half-life is 10.29 hours, much less than the 48-hour threshold as persistent organic pollutants, indicating that these 26 new derivatives can be used as musky compounds (Stockholm Convention on Persistent Organic Pollutants, 2001). These newly designed molecules had extended odor-lasting properties than the original HHCB when serving as SMs without ecological concerns. The odor intensity can be interpreted by the frequency and energy gap of HHCB derivatives were calculated using Gaussian 09 software based on density functional theory at the b3pw91/6-31G* unit level (Gu et al., 2019). When the compound had a positive frequency value, the higher the energy gap value, the lower the odor intensity of the fragrance. The results are listed in detail in Table 4-3. All the 26 derivative compounds reported a positive frequency and only three derivatives (Derivative 4, Derivative 21 and Derivative 68) showed an increased energy gap. Results revealed that all the rest 23 derivatives had the same or higher intensity levels compared to that of HHCB.

Two environmental 3D-QSAR models [i.e., bio-accumulation ($\log BCF$) and migration ($\log VP$)] were constructed in this study. The models were designed independently to predict the biological toxicity, bio-accumulation, and migration ability of the selected 26 HHCBs derivatives (Table 4-3).

Table 4-2 Predicted values of half-life for SMs' derivatives using CoMFA model

HHCB derivatives	Positions of substitution			half-life (hours)	Relative deviation
	1-position	2-position	3-position		
HHCB	-CH ₃ *	-CH ₃	-CH ₃	6.957	
Derivative 1	-C ₂ H ₃	-	-	2.988	-57.05%
Derivative 2	-CH ₂ NH ₂	-	-	3.933	-43.47%
Derivative 3	-NH ₂	-	-	4.024	-42.16%
Derivative 4	-OCH ₃	-	-	10.289	47.89%
Derivative 5	-C ₂ H	-	-	4.295	-38.26%
Derivative 6	-CH ₂ OH	-	-	9.904	42.36%
Derivative 7	-NO	-	-	7.844	12.75%
Derivative 8	-NO ₂	-	-	7.903	13.60%
Derivative 9	-CHO	-	-	3.143	-54.82%
Derivative 10	-COOH	-	-	3.411	-50.97%
Derivative 11	-	-C ₂ H ₃	-CH ₃	3.395	-51.20%
Derivative 12	-	-C ₂ H	-CH ₃	4.280	-38.48%
Derivative 13	-	-OH	-CH ₃	3.300	-52.57%
Derivative 14	-	-COOH	-CH ₃	2.685	-61.41%
Derivative 15	-	-CH ₂ OH	-CH ₃	4.320	-37.90%
Derivative 16	-	-NO	-CH ₃	6.665	-4.20%
Derivative 17	-	-NO ₂	-CH ₃	3.718	-46.56%
Derivative 18	-	-NH ₂	-CH ₃	6.740	-3.12%
Derivative 19	-	-CH ₂ NH ₂	-CH ₃	4.445	-36.11%
Derivative 20	-	-OCH ₃	-CH ₃	9.379	34.81%
Derivative 21	-	-C ₂ H ₃	-C ₂ H ₃	10.013	43.93%
Derivative 22	-	-C ₂ H ₃	-C ₂ H	9.155	31.59%
Derivative 23	-	-C ₂ H ₃	-OH	2.504	-64.01%
Derivative 24	-	-C ₂ H ₃	-COOH	2.982	-57.14%
Derivative 25	-	-C ₂ H ₃	-CH ₂ OH	4.771	-31.42%
Derivative 26	-	-C ₂ H ₃	-NO	2.864	-58.83%
Derivative 27	-	-C ₂ H ₃	-NO ₂	2.836	-59.24%
Derivative 28	-	-C ₂ H ₃	-NH ₂	4.695	-32.51%

Derivative 29	-	-C ₂ H ₃	-CH ₂ NH ₂	8.264	18.79%
Derivative 30	-	-C ₂ H ₃	-OCH ₃	2.975	-57.24%
Derivative 31	-	-C ₂ H	-C ₂ H ₃	6.267	-9.92%
Derivative 32	-	-C ₂ H	-C ₂ H	6.775	-2.62%
Derivative 33	-	-C ₂ H	-OH	6.700	-3.69%
Derivative 34	-	-C ₂ H	-COOH	8.719	25.33%
Derivative 35	-	-C ₂ H	-CH ₂ OH	9.087	30.62%
Derivative 36	-	-C ₂ H	-NO	7.678	10.36%
Derivative 37	-	-C ₂ H	-NO ₂	4.378	-37.07%
Derivative 38	-	-C ₂ H	-NH ₂	3.636	-47.74%
Derivative 39	-	-C ₂ H	-CH ₂ NH ₂	4.490	-35.46%
Derivative 40	-	-C ₂ H	-OCH ₃	3.130	-55.01%
Derivative 41	-	-OH	-C ₂ H ₃	4.288	-38.36%
Derivative 42	-	-OH	-C ₂ H	3.434	-50.64%
Derivative 43	-	-OH	-OH	8.887	27.74%
Derivative 44	-	-OH	-COOH	4.719	-32.17%
Derivative 45	-	-OH	-CH ₂ OH	3.051	-56.14%
Derivative 46	-	-OH	-NO	3.300	-52.57%
Derivative 47	-	-OH	-NO ₂	9.937	42.83%
Derivative 48	-	-OH	-NH ₂	4.595	-33.95%
Derivative 49	-	-OH	-CH ₂ NH ₂	4.526	-34.94%
Derivative 50	-	-OH	-OCH ₃	3.962	-43.05%
Derivative 51	-	-COOH	-C ₂ H ₃	5.899	-15.21%
Derivative 52	-	-COOH	-C ₂ H	9.135	31.31%
Derivative 53	-	-COOH	-OH	3.406	-51.04%
Derivative 54	-	-COOH	-COOH	5.829	-16.21%
Derivative 55	-	-COOH	-CH ₂ OH	3.978	-42.82%
Derivative 56	-	-COOH	-NO	3.696	-46.87%
Derivative 57	-	-COOH	-NO ₂	4.246	-38.97%
Derivative 58	-	-COOH	-NH ₂	5.979	-14.06%
Derivative 59	-	-COOH	-CH ₂ NH ₂	3.476	-50.04%
Derivative 60	-	-COOH	-OCH ₃	2.395	-65.57%
Derivative 61	-	-CH ₂ OH	-C ₂ H ₃	3.666	-47.30%

Derivative 62	-	-CH ₂ OH	-C ₂ H	8.294	19.22%
Derivative 63	-	-CH ₂ OH	-OH	4.158	-40.23%
Derivative 64	-	-CH ₂ OH	-COOH	7.801	12.13%
Derivative 65	-	-CH ₂ OH	-CH ₂ OH	9.131	31.25%
Derivative 66	-	-CH ₂ OH	-NO	8.845	27.14%
Derivative 67	-	-CH ₂ OH	-NO ₂	6.846	-1.60%
Derivative 68	-	-CH ₂ OH	-NH ₂	9.220	32.53%
Derivative 69	-	-CH ₂ OH	-CH ₂ NH ₂	8.355	20.09%
Derivative 70	-	-CH ₂ OH	-OCH ₃	8.192	17.75%
Derivative 71	-	-NO	-C ₂ H ₃	4.122	-40.75%
Derivative 72	-	-NO	-C ₂ H	4.697	-32.49%
Derivative 73	-	-NO	-OH	3.589	-48.41%
Derivative 74	-	-NO	-COOH	3.085	-55.66%
Derivative 75	-	-NO	-CH ₂ OH	7.651	9.98%
Derivative 76	-	-NO	-NO	5.820	-16.34%
Derivative 77	-	-NO	-NO ₂	8.373	20.35%
Derivative 78	-	-NO	-NH ₂	8.291	19.17%
Derivative 79	-	-NO	-CH ₂ NH ₂	9.180	31.95%
Derivative 80	-	-NO	-OCH ₃	3.794	-45.46%
Derivative 81	-	-NO ₂	-C ₂ H ₃	5.420	-22.09%
Derivative 82	-	-NO ₂	-C ₂ H	4.498	-35.35%
Derivative 83	-	-NO ₂	-OH	3.334	-52.08%
Derivative 84	-	-NO ₂	-COOH	3.244	-53.37%
Derivative 85	-	-NO ₂	-CH ₂ OH	3.414	-50.93%
Derivative 86	-	-NO ₂	-NO	4.040	-41.93%
Derivative 87	-	-NO ₂	-NO ₂	3.608	-48.14%
Derivative 88	-	-NO ₂	-NH ₂	9.418	35.37%
Derivative 89	-	-NO ₂	-CH ₂ NH ₂	3.113	-55.25%
Derivative 90	-	-NO ₂	-OCH ₃	5.182	-25.51%

*: “-” means the position keep the original molecular group.

Table 4-3 Functional and environmental properties of SMs' derivatives

HHCB and its derivatives	HL (functional property)	Change rate	Frequency	Energy gap(eV)	LC ₅₀ (bio-toxicity)	Change rate	logBCF (bio-accumulation)	Change rate	logVP (mobility)	Change rate
HHCB	6.957		44.87	6.01	0.032		3.093		2.198	
Derivative 4	10.289	47.89%	37.04	6.05	0.452	1312.50%	3.055	-1.23%	2.439	10.96%
Derivative 6	9.904	42.36%	34.29	5.96	0.065	103.13%	2.447	-20.89%	2.178	-0.91%
Derivative 7	7.844	12.75%	39.20	3.66	0.232	625.00%	2.777	-10.22%	1.744	-20.66%
Derivative 8	7.903	13.60%	33.39	4.91	0.591	1746.88%	2.988	-3.39%	1.991	-9.42%
Derivative 20	9.379	34.81%	43.11	6.01	0.452	1312.50%	2.502	-19.11%	2.152	-2.09%
Derivative 21	10.013	43.93%	39.12	6.02	0.008	-75.00%	2.745	-11.25%	2.206	0.36%
Derivative 22	9.155	31.59%	48.71	5.85	0.029	-9.38%	3.304	6.82%	1.856	-15.56%
Derivative 29	8.264	18.79%	29.57	5.96	0.660	1962.50%	3.010	-2.68%	2.143	-2.50%
Derivative 34	8.719	25.33%	43.45	6.00	12.976	40450.00%	2.952	-4.56%	1.956	-11.01%
Derivative 35	9.087	30.62%	46.54	3.58	1.532	4687.50%	3.228	4.36%	2.108	-4.09%
Derivative 36	7.678	10.36%	46.28	6.00	0.368	1050.00%	3.223	4.20%	2.331	6.05%
Derivative 43	8.887	27.74%	40.29	4.67	0.662	1968.75%	2.72	-12.06%	1.996	-9.19%
Derivative 47	9.937	42.83%	41.77	5.88	3.112	9625.00%	2.217	-28.32%	2.460	11.92%
Derivative 52	9.135	31.31%	40.89	6.01	17.976	56075.00%	2.638	-14.71%	1.956	-11.01%
Derivative 62	8.294	19.22%	44.25	5.95	1.532	4687.50%	2.491	-19.46%	1.799	-18.15%
Derivative 64	7.801	12.13%	41.55	5.97	212.303	663346.88%	2.530	-18.20%	1.905	-13.33%
Derivative 65	9.131	31.25%	28.03	3.55	6.568	20425.00%	3.400	9.93%	1.930	-12.19%
Derivative 66	8.845	27.14%	42.05	6.00	2.255	6946.88%	2.325	-24.83%	1.688	-23.20%
Derivative 68	9.220	32.53%	46.23	6.03	14.992	46750.00%	2.385	-22.89%	1.825	-16.97%
Derivative 69	8.355	20.09%	42.26	3.52	10.496	32700.00%	3.027	-2.13%	2.015	-8.33%
Derivative 70	8.192	17.75%	44.76	3.60	9.895	30821.88%	2.801	-9.44%	1.993	-9.33%
Derivative 75	7.651	9.98%	49.09	3.53	0.255	696.88%	2.779	-10.15%	1.938	-11.83%
Derivative 77	8.373	20.35%	39.59	3.67	0.698	2081.25%	2.724	-11.93%	2.392	8.83%
Derivative 78	8.291	19.17%	43.95	4.71	1.562	4781.25%	2.859	-7.57%	1.925	-12.42%
Derivative 79	9.180	31.95%	45.65	5.95	2.269	6990.63%	2.394	-22.60%	2.243	2.05%
Derivative 88	9.418	35.37%	42.12	6.00	4.469	13865.63%	2.998	-3.07%	2.594	18.02%

*LC₅₀ values predicted with EPI Suite software.

The increased value of $\log BCF$ means that the chemicals can be more easily accumulate in or on organisms. Twenty-four of the 26 selected derivatives reported lower $\log BCF$ values, and the $\log BCF$ of 13 derivatives decreased over 10% compared to the original HHCB. All of these 24 derivatives could be considered as a class of HHCB substitution with decreased hazard to humans and ecosystems.

Among the 26 new derivatives, the bio-toxicity of only five derivatives increased compared to that of HHCB. The toxicity value of 16 new molecules was reduced by more than 10%. Derivative 64 and Derivative 52 had the highest increase of LC_{50} value of 663346.88% and 56075.00%, respectively. These results indicated an obviously decreased bio-toxicity of some of the newly designed HHCB derivatives.

The CoMSIA model of $\log VP$ illustrated 16 new derivatives with decreased $\log VP$ higher than 10%, and 8 derivatives with decreased $\log VP$ less than 10%. Sixteen new derivatives were screened out with the above 3D-QSAR models with the improved functional property (i.e., longer half-lives), and less environmental impact in terms of lower toxicity, bio-accumulation, and mobility.

According to the above screening processes, 15 derivatives were selected for further analysis, including Derivative 6, Derivative 7, Derivative 8, Derivative 20, Derivative 29, Derivative 34, Derivative 43, Derivative 52, Derivative 62, Derivative 64, Derivative 66, Derivative 69, Derivative 70, Derivative 75, and Derivative 78.

4.3.4 Human health risk assessment of HHCB derivatives using toxicokinetic analysis and molecular docking

HHCB is widely used as a fragrance ingredient in various PCPs (Li et al., 2018). Skin contact and penetration are recognized as the most important human exposure to synthetic musk

compared with dietary and respiratory intake (Li et al., 2018; Roosens et al., 2007). Exposure to residential soil, drinking water, agricultural commodities, and residential air could be other uptake pathways of HHCB (Li and Jennings, 2017). Therefore, it was essential to assess the human health risk of designed SMs' derivatives after the screening of their functional and environmental risk properties. In this study, the toxicokinetic simulation and molecular docking were employed to investigate human health risk of the designed SMs' derivatives. The toxicokinetic simulation calculation procedures were performed using TOPKAT Extensible module (Blessy Christina et al., 2012; Rakibe et al., 2018), in Discovery Studio[®] 2020 software. The predicted toxicokinetic parameters of HHCB before and after modification are shown in Table 4-4.

The predicted results showed that all the 15 derivatives were at the same level with the target molecule HHCB in Ames mutagenicity, NTP rodent carcinogenicity, skin sensitization, ocular irritancy, and aerobic biodegradability. The toxicokinetic indexes generated by the model were compared with that of HHCB. The “Categories for substances hazardous to the aquatic environment” (Table S4-2) were also used as a reference for product evaluation. The NTP results of HHCB and its derivatives predicted in this study are lower than 0.8, indicating that they are not a carcinogen (Lv et al., 2021). Compared to HHCB, Derivative 6 reported a lower biotoxicity in terms of fathead minnow LC_{50} and daphnia EC_{50} index generated in the “Acute Oral, Inhalation and Percutaneous Toxicity Classification for Rats”. Though Derivative 6 showed varied results in other toxicokinetic parameters, Derivative 6 and HHCB remained in the same toxicity level following the United Nations guideline. Hence, Derivative 6 was set to become one substitute of choice for HHCB. Derivatives 8 and 29 failed in this screening because levels of their rat chronic oral LOAEL and fathead minnow LC_{50} (see Table S4-2) increased to Category 1 from Category 2.

Table 4-4 Toxicokinetic prediction and assessment of HHCB before and after modification using TOPKAT Extensible module

Compounds	Probability value								
	Ames mutagenicity	NTP Rodent Carcinogenicity							
		Male rat	Female rat	Male mouse	Female mouse	Male rat Non vs. Carc	Male rat Single vs. Mult	Female rat Non vs. Carc	Female rat Single vs. Mult
HHCB	0.2538/Non	0.6500/Carc	0.4293/Non	0.5563/Non	0.5991/Carc	0.2873/Non	Needless	0.3149/Carc	0.4408/Single
HHCB derivative 6	0.2451/Non	0.6936/Carc	0.3817/Non	0.5151/Non	0.6361/Carc	0.2919/Non	Needless	0.3039/Carc	0.4718/Single
HHCB derivative 7	0.3551/Non	0.6895/Carc	0.4532/Non	0.4595/Non	0.5997/Carc	0.2479/Non	Needless	0.3066/Carc	0.4720/Single
HHCB derivative 8	0.3901/Non	0.6481/Carc	0.4119/Non	0.5007/Non	0.5926/Non	0.2777/Non	Needless	0.3254/Carc	0.4635/Single
HHCB derivative 20	0.4528/Non	0.6744/Carc	0.4210/Non	0.4568/Non	0.5953/Non	0.2727/Non	Needless	0.2994/Carc	0.4540/Single
HHCB derivative 29	0.3218/Non	0.6558/Carc	0.3928/Non	0.4531/Non	0.6122/Carc	0.2617/Non	Needless	0.2852/Carc	0.4039/Single
HHCB derivative 34	0.2856/Non	0.6187/Carc	0.3977/Non	0.4142/Non	0.5392/Non	0.2806/Non	Needless	0.3267/Carc	0.3780/Single
HHCB derivative 43	0.4252/Non	0.6513/Carc	0.4014/Non	0.5511/Non	0.5929/Non	0.2751/Non	Needless	0.2869/Carc	0.4988/Single
HHCB derivative 52	0.2856/Non	0.6187/Carc	0.3977/Non	0.4142/Non	0.5392/Non	0.2806/Non	Needless	0.3267/Carc	0.3780/Single
HHCB derivative 62	0.3256/Non	0.6329/Carc	0.3877/Non	0.4660/Non	0.5888/Non	0.2870/Non	Needless	0.3636/Carc	0.4608/Single
HHCB derivative 64	0.3330/Non	0.6187/Carc	0.3935/Non	0.4748/Non	0.5839/Non	0.2651/Non	Needless	0.2854/Carc	0.4727/Single
HHCB derivative 66	0.5087/Non	0.6591/Carc	0.4208/Non	0.4744/Non	0.5961/Non	0.2698/Non	Needless	0.3064/Carc	0.4846/Single
HHCB derivative 69	0.3023/Non	0.6387/Carc	0.3814/Non	0.4895/Non	0.5936/Non	0.2512/Non	Needless	0.2813/Carc	0.3985/Single
HHCB derivative 70	0.4283/Non	0.6303/Carc	0.3939/Non	0.4694/Non	0.5968/Non	0.2561/Non	Needless	0.2751/Carc	0.4214/Single
HHCB derivative 75	0.5087/Non	0.6591/Carc	0.4208/Non	0.4744/Non	0.5961/Non	0.2698/Non	Needless	0.3064/Carc	0.4846/Single
HHCB derivative 78	0.5058/Non	0.7181/Carc	0.4234/Non	0.4504/Non	0.5975/Non	0.2660/Non	Needless	0.3201/Carc	0.4601/Single

Table 4-4 Toxicokinetic predictions of HHCB before and after modification using TOPKAT Extensible module (continued)

Compounds	Probability value				Developmental toxicity potential (DTP)	Rat oral LD_{50} * g/kg	Rat maximum tolerated dose-feed/Water g/kg	Rat maximum tolerated dose-gavage g/kg	Rat inhalational LC_{50} * mg/m ³ /h
	FDA Rodent Carcinogenicity								
	Male mouse Non vs. Carc	Male mouse Single vs. Mult	Female mouse Non vs. Carc	Female mouse Single vs. Mult					
HHCB	0.3014/Carc	0.2408/Mult	0.3146/Carc	0.5295/Mult	0.4704/Non	0.7165/Low	0.0403/High	0.3734/Low	25390.90/Mod
HHCB derivative 6	0.2806/Carc	0.2023/Mult	0.3118/Carc	0.5388/Mult	0.4798/Non	0.3971/Low	0.0584/Mod	0.3131/Low	16144.80/Mod
HHCB derivative 7	0.2628/Carc	0.1841/Mult	0.3114/Carc	0.4635/Mult	0.5174/Non	0.2268/Mod	0.0455/High	0.0681/Mod	6730.88/High
HHCB derivative 8	0.2760/Carc	0.2266/Mult	0.3114/Carc	0.5026/Mult	0.5038/Non	0.2587/Mod	0.0422/High	0.2983/Mod	12281.50/Mod
HHCB derivative 20	0.2864/Carc	0.2099/Mult	0.2859/Carc	0.4956/Mult	0.4667/Non	0.4836/Low	0.0262/High	0.2292/Mod	19946.50/Mod
HHCB derivative 29	0.2839/Carc	0.2301/Mult	0.2768/Carc	0.4449/Mult	0.5120/Non	0.2166/Mod	0.0557/Mod	0.1190/Mod	8877.98/Mod
HHCB derivative 34	0.3240/Carc	0.2022/Mult	0.3892/Carc	0.4135/Mult	0.4839/Non	0.5418/Low	0.1681/Mod	0.1688/Mod	7566.49/High
HHCB derivative 43	0.2797/Carc	0.2142/Mult	0.2964/Carc	0.4893/Mult	0.5120/Non	1.7707/Low	0.0820/Mod	0.1134/Mod	9986.59/Mod
HHCB derivative 52	0.3240/Carc	0.2022/Mult	0.3892/Carc	0.4135/Mult	0.4839/Non	0.5418/Low	0.1681/Mod	0.1688/Mod	7566.49/High
HHCB derivative 62	0.3519/Carc	0.2590/Mult	0.3983/Carc	0.4577/Mult	0.5195/Non	0.6782/Low	0.0615/Mod	0.2050/Mod	11226.80/Mod
HHCB derivative 64	0.2477/Non	Not available	0.2596/Carc	0.4973/Mult	0.4824/Non	0.4617/Low	0.2410/Mod	0.1856/Mod	6515.51/High
HHCB derivative 66	0.2606/Non	Not available	0.2994/Carc	0.4465/Mult	0.4918/Non	0.1565/Mod	0.0681/Mod	0.0509/Mod	4347.92/High
HHCB derivative 69	0.2692/Carc	0.2312/Mult	0.2541/Carc	0.5321/Mult	0.5333/Non	0.4382/Low	0.0805/Mod	0.4488/Low	4826.64/High
HHCB derivative 70	0.2765/Carc	0.2132/Mult	0.2518/Carc	0.5042/Mult	0.5185/Non	0.5629/Low	0.0401/High	0.1582/Mod	13052.90/Mod
HHCB derivative 75	0.2606/Non	Not available	0.2994/Carc	0.4465/Mult	0.4918/Non	0.1565/Mod	0.0681/Mod	0.0509/Mod	4347.92/High
HHCB derivative 78	0.2743/Carc	0.2046/Mult	0.2972/Carc	0.3979/Mult	0.4922/Non	0.0703/Mod	0.0571/Mod	0.0481/High	2409.95/High

* Assessment finished based on "Acute toxicity estimate (ATE) values and criteria for acute toxicity hazard categories" (Table S4-3), cited from the United Nations. Globally harmonized system of classification and labelling of chemicals (GHS) [M]. 8th ed. New York: United Nations, 2019.

Table 4-4 Toxicokinetic predictions of HHCB before and after modification using TOPKAT Extensible module (continued)

Compounds	Rat chronic oral LOAEL g/kg	Fathead minnow <i>LC</i> ₅₀ * g/L	Daphnia <i>EC</i> ₅₀ * mg/L	Probability value					
				Skin irritancy	Skin sensitization NEG vs. SENS	Skin sensitization MLD/MOD vs. SEV	Ocular irritancy SEV vs. MOD	Ocular irritancy (Non/Mild) vs. (Mod/Sev)	Aerobic biodegradability
HHCB	0.0152/High	0.0019/High	4.6778/High	0.9975/Yes	0.8374/SENS	0.9222/SEV	0.7927/SEV	0.9749/(Mod/Sev)	0.3009/Non
HHCB derivative 6	0.0086/High	0.0162/Central	18.5383/Central	0.9961/Yes	0.8070/SENS	0.8994/SEV	0.7285/SEV	0.9759/(Mod/Sev)	0.3751/Non
HHCB derivative 7	0.0114/High	0.0020/High	2.9244/High	0.9724/Non	0.8068/SENS	0.9185/SEV	0.7890/SEV	0.9748/(Mod/Sev)	0.3467/Non
HHCB derivative 8	0.0042/Hyper	0.0009/Extremely	4.1151/High	0.9964/Yes	0.8226/SENS	0.9160/SEV	0.8065/SEV	0.9756/(Mod/Sev)	0.2540/Non
HHCB derivative 20	0.0107/High	0.0039/High	3.7136/High	0.9975/Yes	0.8389/SENS	0.9284/SEV	Not available	Not available	0.3379/Non
HHCB derivative 29	0.0039/Hyper	0.0008/Extremely	2.7190/High	0.9972/Yes	0.8297/SENS	0.8742/SEV	0.7573/SEV	0.9758/(Mod/Sev)	0.4355/Non
HHCB derivative 34	0.0117/High	0.0010/High	20.3901/Central	0.9968/Yes	0.8048/SENS	0.9167/SEV	0.7397/SEV	0.9997/(Mod/Sev)	0.4517/Non
HHCB derivative 43	0.0155/High	0.1361/Low	19.7961/Central	0.9782/Yes	0.7935/SENS	0.9176/SEV	Needless	0.8103(Non/Mild)	0.3603/Non
HHCB derivative 52	0.0117/High	0.0015/High	20.3901/Central	0.9968/Yes	0.8048/SENS	0.9167/SEV	0.7397/SEV	0.9997/(Mod/Sev)	0.4517/Non
HHCB derivative 62	0.0111/High	0.0064/High	13.2885/Central	0.9970/Yes	0.8041/SENS	0.8994/SEV	0.7477/SEV	0.9997/(Mod/Sev)	0.3989/Non
HHCB derivative 64	0.0112/High	0.0244/Central	67.8145/Central	0.9762/Yes	0.8067/SENS	0.8904/SEV	0.7148/SEV	0.8286/(Mod/Sev)	0.4809/Non
HHCB derivative 66	0.0125/High	0.0139/Central	17.4594/Central	0.9707/Non	0.8187/SENS	0.9006/SEV	0.6908/SEV	0.8173/(Mod/Sev)	0.3351/Non
HHCB derivative 69	0.0080/High	0.0564/Central	9.2835/High	0.9781/Yes	0.7906/SENS	0.9062/SEV	0.7479/SEV	0.9995/(Mod/Sev)	0.4197/Non
HHCB derivative 70	0.0067/High	0.0236/Central	26.4007/Central	0.9969/Yes	0.7998/SENS	0.9042/SEV	0.7115/SEV	0.9747/(Mod/Sev)	0.3668/Non
HHCB derivative 75	0.0125/High	0.0139/Central	17.4594/Central	0.9707/Non	0.8187/SENS	0.9006/SEV	0.6908/SEV	0.9748/(Mod/Sev)	0.3351/Non
HHCB derivative 78	0.0181/High	0.0256/Central	6.2168/High	0.9699/Non	0.8145/SENS	0.9132/SEV	0.7023/SEV	0.9757/(Mod/Sev)	0.3478/Non

* Assessment finished based on "Ecotoxicological Hazard Classification" (Table S4-2), cited from the United Nations. Globally harmonized system of classification and labelling of chemicals (GHS) [M].8th ed. New

York: United Nations, 201

Generally, Derivatives 7, 34, 52, 62, 69, 70, 75 and 78 had certain advantages over HHCB except in rat oral LD_{50} (see acute toxicity hazard categories in Table S4-3), rat maximum tolerated dose-feed/water, rat maximum tolerated dose-gavage, and rat inhalational LC_{50} (see acute toxicity hazard categories in Table S4-3). Given that the main route for SMs' exposure to human bodies is focused on skin penetration, the above disadvantages of these HHCB derivatives could be ignored when added as additives in various PCPs and consumer goods. Furthermore, Derivatives 7, 75 and 78 showed no skin irritancy and lower bio-toxicity than that of HHCB, indicating Derivatives 6, 7, 75 and 78 passed toxicokinetic screening and can be recommended as substitutes of SMs.

Molecular docking was also performed to evaluate the skin exposure toxicity of HHCB and its derivatives to humans. One of the keratins, 4ZRY was chosen as the representative ligand of the stratum corneum in this study. The 4ZRY was selected as the target protein receptor and the binding capacity between the protein receptor and chemicals (i.e., HHCB and its derivatives) was expressed as the docking scoring function. Scoring functions can be used to evaluate the fitness between the ligand and the protein (Wang et al., 2003); analyze the differences of binding energy, and reveal the binding affinities of ligand and protein receptor (tilapia skin gelatin hydrolysates) (Ling et al., 2018). The higher LibDock score, the stronger the binding force (Gu et al., 2020c). The LibDock scores of HHCB and its derivatives to 4ZRY follow a sequence of 69.56, 77.58, 65.68, 77.52 and 79.74 for HHCB, Derivative 6, Derivative 7, Derivative 75 and Derivative 78, respectively, indicating only Derivative 7 decreased in the binding affinities compared with HHCB. In summary, after the screening through molecular dynamics followed by molecular docking, Derivative 7 emerged as the best candidate of HHCB's substitute with lower toxicity to human bodies.

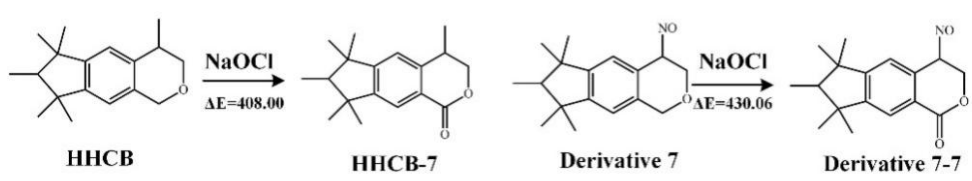
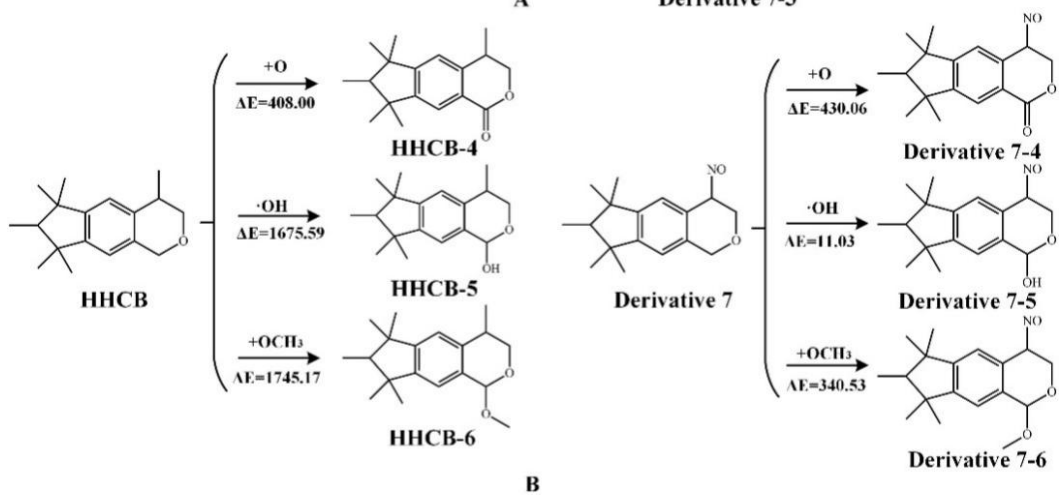
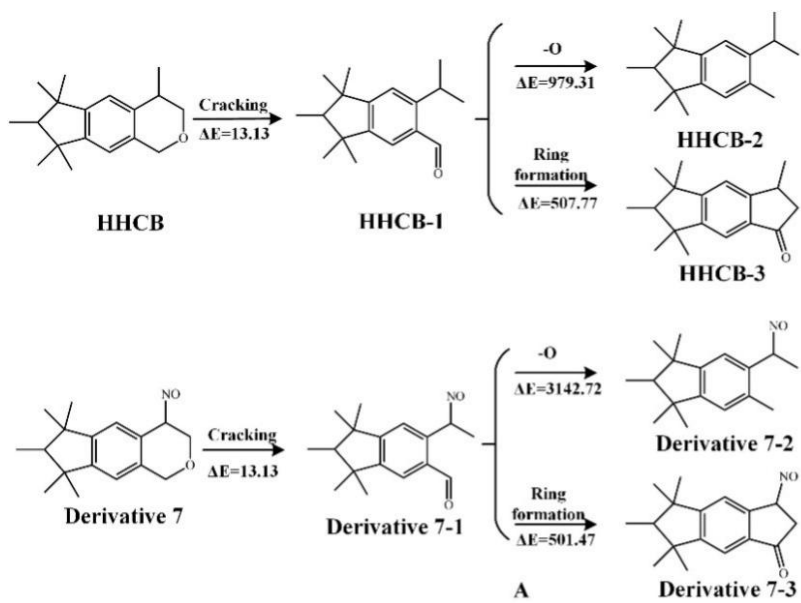
4.3.5 Environmental behavior evaluation of the selected representative HHCB derivative and its transformation by-products

If the designed HHCB derivatives were put into industrial production, the environmental characteristics of their transformation by-products must be considered. Among the designed molecules to replace HHCB, Derivative 7, as the best candidate of HHCB's substitute, was chosen for further analysis of its transformation mechanisms under various treatment processes. The HHCB's transformation mechanism includes photodegradation, biotransformation, chlorination, and metabolic pathways in algal cells (Sanchez-Prado et al., 2004; Martin et al., 2007; Kuhlich et al., 2011; Ding et al., 2020). The pathway of HHCB Derivative 7 was then simulated and deduced based on the information of HHCB (Figure 4-3).

The energy barrier (ΔE) indicates the minimum energy required for a chemical reaction to occur, so the lower the energy barrier, the more rapidly the system reaction will be (Hamelberg et al., 2004). Zhang et al. (2020c) calculated the energy barrier and found the transformation pathways of phthalate by-products. The energy barrier of each pathway was calculated and then these by-products' potential environmental risks were evaluated. According to Figure 4-3, ΔE of HHCB and Derivative 7 in the photodegradation process were similar. Specifically, in the transformation of HHCB to HHCB-1 and Derivative 7 to Derivative 7-1, ΔE is 13.13 kJ/mol. The ΔE of HHCB-1 to HHCB-3 and Derivative 7-1 to Derivative 7-3 are 507.77 and 501.47 kJ/mol, respectively. The ΔE value of Derivative 7-1 to Derivative 7-2 (3142.72 kJ/mol) was greater than that of HHCB-1 to HHCB-2 (979.31 kJ/mol), which meant the transformation of Derivative 7-1 to Derivative 7-2 required higher energy and the transforming process is more difficult than the transformation HHCB-1 to HHCB-2. In the biotransformation process, Derivative 7 showed a relatively easier transformation ability compared with HHCB. For the chlorination process, both these two chemicals have similar ΔE values. Among the degradation

treated by algal cells, the total barrier of path Derivative 7 to Derivative 7-12 was 4964.03 kJ/mol, which was almost 17 times greater than the total barrier of path HHCB to HHCB-12 (293.27 kJ/mol). Therefore, Derivative 7-12 may be difficult to form in the pathway of Derivative 7 to Derivative 7-12 (Zhang et al., 2020c). After deducing the by-products of Derivative 7, the environmental properties of its by-products were predicted using the constructed 3D-QSAR models. The results are shown in Table 4-5.

From Table 4-5, the by-products of Derivative 7 after biotransformation and chlorination exhibited an obvious decrease in bio-toxicity (higher LC_{50}), $\log BCF$ and $\log VP$ compared to that of HHCB. This may refer that biotransformation and chlorination can be the optimum choices for treating Derivative 7 once it enters the environment. Though these two methods may not be appropriate for treating HHCB. For example, after biotransformation, HHCB-4 had increased bio-toxicity (7.43%) and $\log BCF$ (16.10%), and HHCB-5 had increased $\log VP$ (22.98%) compared with HHCB. Photodegradation simulation results indicated that HHCB-3 [higher $\log BCF$ (12.38%) and $\log VP$ (5.41%)] and Derivative 7-3 [$\log BCF$ (5.82%) and $\log VP$ (21.75%)] had higher environmental concerns. HHCB-2 and Derivative 7-2 had much lower LC_{50} values (decreased around 90%) after photodegradation. Therefore, photodegradation may produce harmful by-products. Metabolic pathways of Derivative 7 in algal cells showed a strong ability to reduce the bio-toxicity; only one out of 10 by-products had a tiny increase (6.88%). However, nine out of 14 by-products of HHCB with higher bio-toxicity are as high as 108.86%. Only around 7% of HHCB's by-products had higher $\log BCF$ values, and half of Derivative 7's by-products had higher $\log BCF$ values with changing rate lower than 11.48%. In the same treatment, approximately half of by-products had increased mobility, ranging from 0.09% to 29.03%. The biodegradability of HHCB derivatives by alga was highly dependent on their chemical structures.



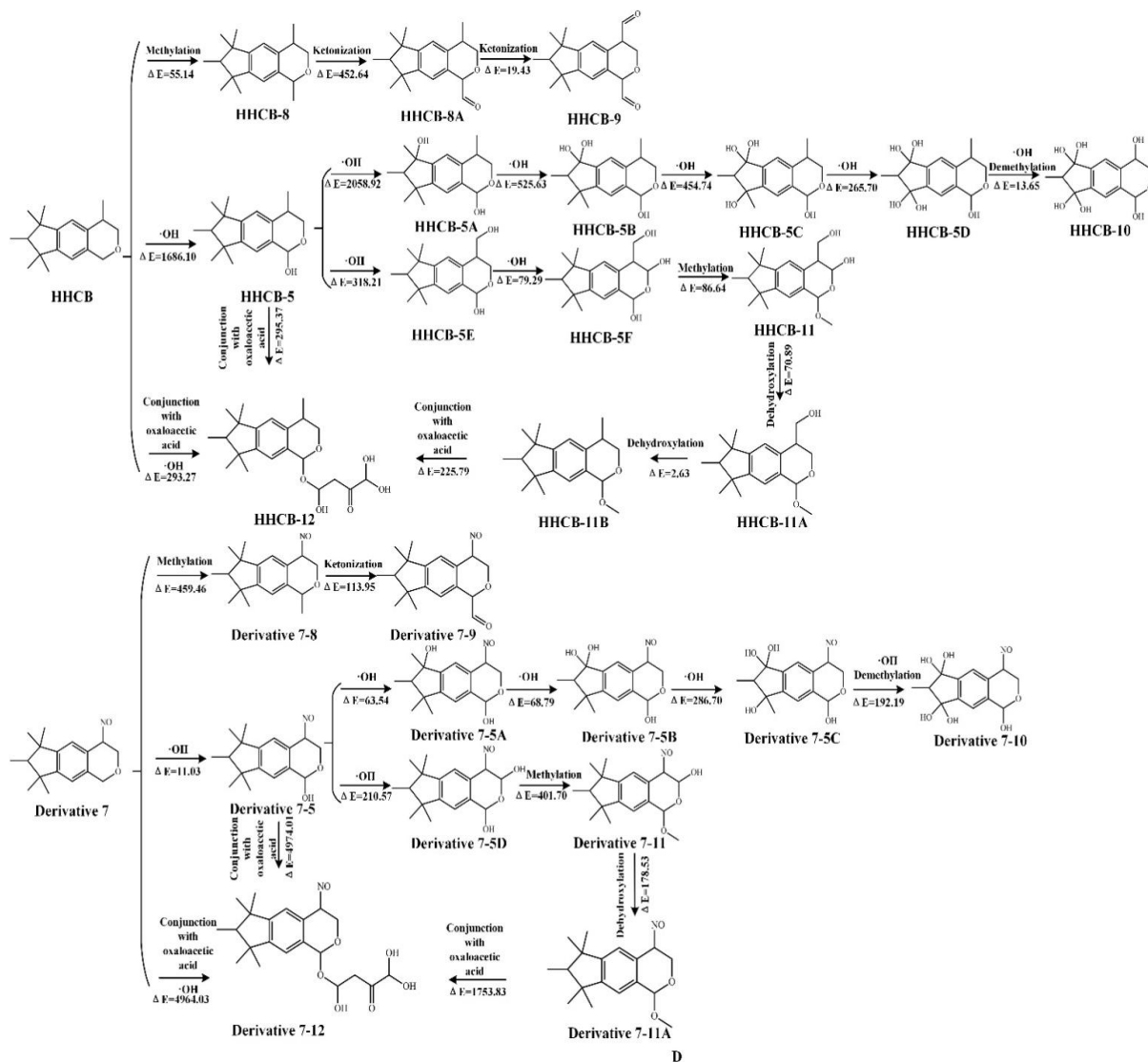


Figure 4-3 The photodegradation (A), biotransformation (B), chlorination (C) and metabolic pathways in algal cells (D) pathways of HHCB and Derivative 7. ΔE is in kJ/mol.

Table 4-5 The environmental properties of Derivative 7 by-products under different treatment methods

	Derivative 7 and its derivatives	LC ₅₀ (bio-toxicity)	Change rate	logBCF (bio-accumulation)	Change rate	logVP (mobility)	Change rate	HHCB and its derivatives	LC ₅₀ (bio-toxicity)	Change rate	logBCF (bio-accumulation)	Change rate	logVP (mobility)	Change rate
Photodegradation	Derivative 7	0.23		2.78		1.74		HHCB	0.03		3.09		2.20	
	Derivative 7-1	0.11	-53.02%	2.41	-22.24%	3.00	36.53%	HHCB-1	0.05	56.25%	2.49	-19.43%	1.96	-10.69%
	Derivative 7-2	0.03	-87.93%	1.97	-36.37%	1.66	-24.34%	HHCB-2	0.0018	-94.47%	2.86	-7.63%	1.85	-15.79%
	Derivative 7-3	0.27	15.95%	3.27	5.82%	2.68	21.75%	HHCB-3	0.04	25.00%	3.48	12.38%	2.32	5.41%
Biotransformation	Derivative 7-4	1.12	381.03%	2.53	-18.27%	2.07	-5.96%	HHCB-4	0.46	1337.50%	3.59	16.10%	2.07	-6.01%
	Derivative 7-5	2.52	986.21%	2.83	-8.66%	2.05	-6.64%	HHCB-5	0.33	931.25%	2.62	-15.23%	2.70	22.98%
Chlorination	Derivative 7-6	0.43	84.48%	2.78	-10.05%	2.14	-2.59%	HHCB-6	0.07	118.75%	2.59	-16.33%	1.76	-20.06%
	Derivative 7-7	1.12	381.03%	2.53	-18.27%	2.07	-5.96%	HHCB-7	0.46	1337.50%	3.59	16.10%	2.07	-6.01%
	Derivative 7-5A	26.45	11301.29%	3.28	6.01%	2.55	15.88%	HHCB-5A	7.76	24150.00%	1.61	-47.91%	0.85	-61.15%
	Derivative 7-5B	45.30	19426.29%	3.32	7.40%	2.66	21.16%	HHCB-5B	15.93	49681.25%	1.74	-43.61%	1.40	-36.44%
	Derivative 7-5C	193.66	83374.57%	3.37	8.86%	2.84	29.03%	HHCB-5C	111.60	348650.00%	1.78	-42.45%	1.48	-32.85%
Metabolic pathways in algal cells	Derivative 7-5D	1.75	655.60%	2.83	-8.44%	2.10	-4.55%	HHCB-5D	229.19	716118.75%	1.81	-41.51%	1.10	-49.95%
	Derivative 7-8	0.13	-43.97%	2.57	-16.81%	2.17	-1.41%	HHCB-5E	3.01	9306.25%	2.99	-3.33%	2.28	3.64%
	Derivative 7-9	0.83	259.48%	2.58	-16.68%	2.22	1.00%	HHCB-5F	71.99	224868.75%	2.88	-6.82%	2.27	3.18%
	Derivative 7-10	331.64	142850.00%	3.45	11.48%	2.43	10.42%	HHCB-8	0.01	-68.75%	3.17	2.39%	2.48	12.60%
	Derivative 7-11	0.55	137.07%	2.82	-8.92%	2.19	-0.36%	HHCB-8A	0.35	993.75%	2.56	-17.14%	2.46	12.10%
	Derivative 7-11A	0.43	84.48%	3.23	4.40%	1.50	-31.76%	HHCB-9	1.44	4400.00%	2.79	-9.76%	1.97	-10.33%
	Derivative 7-12	23.41	9989.22%	3.06	-0.94%	1.85	-15.88%	HHCB-10	12211.42	38160587.50%	2.76	-10.83%	2.37	7.87%
								HHCB-11	16.88	52650.00%	2.98	-3.75%	2.20	0.09%
							HHCB-11A	1.54	4712.50%	2.80	-9.63%	2.15	-2.18%	
							HHCB-11B	0.07	118.75%	2.69	-12.93%	2.58	17.42%	
							HHCB-12	4.72	14650.00%	2.40	-22.47%	2.37	7.69%	

Table 4-6 Toxicokinetic prediction and assessment of HHCB and Derivative 7's transformation products using TOPKAT Extensible module

Compounds	Probability value								
	Ames mutagenicity	NTP Rodent Carcinogenicity							
		Male rat	Female rat	Male mouse	Female mouse	Male rat Non vs. Carc	Male rat Single vs. Mult	Female rat Non vs. Carc	Female rat Single vs. Mult
HHCB	0.2538/Non	0.6500/Carc	0.4293/Non	0.5563/Non	0.5991/Carc	0.2873/Non	Needless	0.3149/Carc	0.4408/Single
HHCB-1	0.1629/Non	0.5444/Non	0.4562/Non	0.6057/Carc	0.5397/Non	0.3061/Non	Needless	0.3024/Carc	0.4563/Single
HHCB-2	0.2046/Non	0.5874/Non	0.4902/Non	0.5975/Carc	0.5436/Non	0.3577/Carc	0.5691/Mult	0.3153/Carc	0.4518/Single
HHCB-3	0.2076/Non	0.6294/Carc	0.4484/Non	0.5727/Carc	0.5349/Non	0.3157/Non	Needless	0.3046/Carc	0.4473/Single
HHCB-4	0.1282/Non	0.6481/Carc	0.5040/Non	0.6129/Carc	0.5758/Non	0.3515/Carc	0.5692/Mult	0.3186/Carc	0.4154/Single
HHCB-5	0.2668/Non	0.6181/Carc	0.4388/Non	0.5961/Carc	0.5664/Non	0.3217/Non	Needless	0.2784/Carc	0.5050/Single
HHCB-5A	0.4629/Non	0.5948/Non	0.4380/Non	0.5841/Carc	0.5401/Non	0.3028/Non	Needless	0.2624/Non	Needless
HHCB-5B	0.4391/Non	0.6173/Carc	0.4405/Non	0.5966/Carc	0.5601/Non	0.3168/Non	Needless	0.2538/Non	Needless
HHCB-5C	0.6300/Non	0.5848/Non	0.4653/Non	0.5636/Non	0.4648/Non	0.3173/Non	Needless	0.2665/Carc	0.5031/Single
HHCB-5D	0.6490/Non	0.5827/Non	0.4348/Non	0.5616/Non	0.5066/Non	0.3246/Non	Needless	0.2579/Non	Needless
HHCB-5E	0.2754/Non	0.6312/Carc	0.4134/Non	0.5909/Carc	0.5949/Non	0.3155/Non	Needless	0.2636/Non	Needless
HHCB-5F	0.2675/Non	0.5810/Non	0.4092/Non	0.6023/Carc	0.5655/Non	0.3255/Non	Needless	0.2920/Carc	0.4523/Single
HHCB-6	0.2881/Non	0.6387/Carc	0.4574/Non	0.5865/Carc	0.5861/Non	0.3359/Non	Needless	0.2876/Carc	0.4259/Single
HHCB-7	0.1282/Non	0.6481/Carc	0.5040/Non	0.6129/Carc	0.5758/Non	0.3515/Carc	0.5692/Mult	0.3186/Carc	0.4154/Single
HHCB-8	0.1843/Non	0.6346/Carc	0.4559/Non	0.5760/Carc	0.5855/Non	0.3048/Non	Needless	0.2935/Carc	0.4691/Single
HHCB-8A	0.2342/Non	0.6285/Carc	0.4551/Non	0.5736/Carc	0.5894/Non	0.3295/Non	Needless	0.2996/Carc	0.4803/Single
HHCB-9	0.3037/Non	0.6530/Carc	0.4583/Non	0.5042/Non	0.5936/Non	0.2682/Non	Needless	0.2791/Carc	0.4664/Single

HHCB-10	0.7118/Non	0.5958/Non	0.4122/Non	0.4320/Non	0.4661/Non	0.3021/Non	Needless	0.2628/Non	Needless
HHCB-11	0.2667/Non	0.5979/Non	0.4054/Non	0.5576/Non	0.5716/Non	0.3006/Non	Needless	0.2995/Carc	0.4914/Single
HHCB-11A	0.2632/Non	0.6580/Carc	0.4263/Non	0.5787/Carc	0.5974/Non	0.3276/Non	Needless	0.2718/Carc	0.4416/Single
HHCB-11B	0.2881/Non	0.6387/Carc	0.4574/Non	0.5865/Carc	0.5861/Non	0.3359/Non	Needless	0.2876/Carc	0.4259/Single
HHCB-12	0.1795/Non	0.5824/Non	0.3912/Non	0.5611/Non	0.5295/Non	0.2788/Non	Needless	0.2455/Non	Needless
Derivative 7	0.3551/Non	0.6895/Carc	0.4532/Non	0.4595/Non	0.5997/Carc	0.2479/Non	Needless	0.3066/Carc	0.4720/Single
Derivative 7-1	0.2893/Non	0.5722/Non	0.4663/Non	0.5546/Non	0.5562/Non	0.2679/Non	Needless	0.2866/Carc	0.5113/Single
Derivative 7-2	0.3927/Non	0.6207/Carc	0.5316/Carc	0.5322/Non	0.5495/Non	0.3157/Non	Needless	0.2939/Carc	0.4986/Single
Derivative 7-3	0.2663/Non	0.6535/Carc	0.4688/Non	0.5332/Non	0.5405/Non	0.2758/Non	Needless	0.2970/Carc	0.4789/Single
Derivative 7-4	0.1749/Non	0.6518/Carc	0.5340/Carc	0.5992/Carc	0.5669/Non	0.3027/Non	Needless	0.3186/Carc	0.4422/Single
Derivative 7-5	0.3749/Non	0.6243/Carc	0.4752/Non	0.5359/Non	0.5591/Non	0.2960/Non	Needless	0.2900/Carc	0.5041/Single
Derivative 7-5A	0.5552/Non	0.6370/Carc	0.4917/Non	0.5253/Non	0.5279/Non	0.2820/Non	Needless	0.2728/Carc	0.5035/Single
Derivative 7-5B	0.5395/Non	0.6492/Carc	0.4835/Non	0.5120/Non	0.5295/Non	0.2715/Non	Needless	0.2674/Carc	0.4903/Single
Derivative 7-5C	0.6972/Non	0.6082/Carc	0.4920/Non	0.4620/Non	0.4275/Non	0.3105/Non	Needless	0.2859/Carc	0.4820/Single
Derivative 7-5E	0.3749/Non	0.6017/Carc	0.4717/Non	0.5257/Non	0.5265/Non	0.3006/Non	Needless	0.3048/Carc	0.4979/Single
Derivative 7-6	0.3769/Non	0.6555/Carc	0.5027/Non	0.4961/Non	0.5840/Non	0.2830/Non	Needless	0.2948/Carc	0.4867/Single
Derivative 7-7	0.1749/Non	0.6518/Carc	0.5340/Carc	0.5992/Carc	0.5669/Non	0.3027/Non	Needless	0.3186/Carc	0.4422/Single
Derivative 7-8	0.2759/Non	0.6435/Carc	0.4922/Non	0.4860/Non	0.5815/Non	0.2729/Non	Needless	0.2821/Carc	0.4631/Single
Derivative 7-9	0.3149/Non	0.6414/Carc	0.4984/Non	0.5200/Non	0.5921/Non	0.2962/Non	Needless	0.3017/Carc	0.5011/Single
Derivative 7-10	0.7037/Non	0.6278/Carc	0.4852/Non	0.4630/Non	0.4281/Non	0.3225/Non	Needless	0.2708/Carc	0.4993/Single
Derivative 7-11	0.3603/Non	0.5881/Non	0.4728/Non	0.5450/Non	0.5372/Non	0.2943/Non	Needless	0.3208/Carc	0.5167/Mult
Derivative 7-11A	0.3769/Non	0.6555/Carc	0.5027/Non	0.4961/Non	0.5840/Non	0.2830/Non	Needless	0.2948/Carc	0.4867/Single
Derivative 7-12	0.2536/Non	0.5058/Non	0.4453/Non	0.3564/Non	0.4457/Non	0.2406/Non	Needless	0.2522/Non	Needless

Table 4-6 Toxicokinetic prediction and assessment of HHCB and Derivative 7's transformation products using TOPKAT Extensible module (continued)

Compounds	Probability value				Developmental toxicity potential (DTP)	Rat oral LD_{50} * g/kg	Rat maximum tolerated dose-feed/Water g/kg	Rat maximum tolerated dose-gavage g/kg	Rat inhalational LC_{50} * mg/m ³ /h
	FDA Rodent Carcinogenicity								
	Male mouse Non vs. Carc	Male mouse Single vs. Mult	Female mouse Non vs. Carc	Female mouse Single vs. Mult					
HHCB	0.3014/Carc	0.2408/Mult	0.3146/Carc	0.5295/Mult	0.4704/Non	0.7165/Low	0.0403/High	0.3734/Low	25390.90/Mod
HHCB-1	0.3549/Carc	0.2637/Mult	0.2824/Carc	0.4754/Mult	0.5047/Non	0.5162/Low	0.0765/Mod	0.7098/Low	23921.50/Mod
HHCB-2	0.3572/Carc	0.2570/Mult	0.2806/Carc	0.4670/Mult	0.4863/Non	0.1858/Mod	0.0456/High	1.0084/Low	63523.20/Low
HHCB-3	0.3184/Carc	0.2567/Mult	0.3104/Carc	0.5152/Mult	0.5158/Non	0.7335/Low	0.0714/Mod	0.4018/Low	22087.50/Mod
HHCB-4	0.3687/Carc	0.3367/Mult	0.2925/Carc	0.5519/Mult	0.4973/Non	0.9887/Low	0.0495/High	0.2796/Mod	24412.60/Mod
HHCB-5	0.3183/Carc	0.2356/Mult	0.2992/Carc	0.5646/Mult	0.5181/Non	0.4832/Low	0.0544/Mod	0.1283/Mod	16392.40/Mod
HHCB-5A	0.2837/Carc	0.2157/Mult	0.2773/Carc	0.4954/Mult	0.5175/Non	0.6824/Low	0.0781/Mod	0.0937/Mod	9603.61/Mod
HHCB-5B	0.2669/Carc	0.2867/Mult	0.3007/Carc	0.4573/Mult	0.5316/Non	1.1003/Low	0.1241/Mod	0.0495/High	5941.94/High
HHCB-5C	0.3010/Carc	0.2235/Mult	0.2913/Carc	0.4118/Mult	0.5239/Non	1.2508/Low	0.1837/Mod	0.0328/High	3536.86/High
HHCB-5D	0.3002/Carc	0.2467/Mult	0.2760/Carc	0.4048/Mult	0.5438/Toxic	2.5961/Non	0.2845/Mod	0.0188/High	2158.01/High
HHCB-5E	0.2912/Carc	0.2486/Mult	0.3011/Carc	0.4905/Mult	0.5202/Non	0.5435/Low	0.0882/Mod	0.1361/Mod	9582.69/Mod
HHCB-5F	0.2944/Carc	0.2468/Mult	0.2763/Carc	0.4451/Mult	0.5366/Toxic	0.5822/Low	0.1211/Mod	0.0299/High	4347.40/High
HHCB-6	0.3151/Carc	0.3142/Mult	0.3041/Carc	0.4555/Mult	0.4983/Non	0.5362/Low	0.0275/Mod	0.1365/Mod	20213.30/Mod
HHCB-7	0.3687/Carc	0.3367/Mult	0.2925/Carc	0.5519/Mult	0.4973/Non	0.9887/Low	0.0495/High	0.2796/Mod	24412.60/Mod
HHCB-8	0.3022/Carc	0.2786/Mult	0.3134/Carc	0.5103/Mult	0.5244/Non	0.3814/Low	0.0384/High	0.3097/Low	24421.90/Mod
HHCB-8A	0.3038/Carc	0.2715/Mult	0.3149/Carc	0.4631/Mult	0.5066/Non	0.4387/Low	0.0458/High	0.5361/Low	11737.20/Mod
HHCB-9	0.2956/Carc	0.2509/Mult	0.2976/Carc	0.4498/Mult	0.5228/Non	0.2942/Mod	0.0411/High	0.5241/Low	7290.72/High
HHCB-10	0.2647/Carc	0.2184/Mult	0.2635/Carc	0.4445/Mult	0.6258/Toxic	5.7362/Non	0.4189/Low	0.0127/High	1280.92/Hyper
HHCB-11	0.2411/Non	Needless	0.2780/Carc	0.4894/Mult	0.5377/Toxic	0.3437/Low	0.0543/Mod	0.0250/High	5782.11/High

HHCB-11A	0.2904/Carc	0.2387/Mult	0.2800/Carc	0.5118/Mult	0.5178/Non	0.3193/Low	0.0396/High	0.1138/Mod	12774.60/Mod
HHCB-11B	0.3151/Carc	0.3142/Mult	0.3041/Carc	0.4555/Mult	0.4983/Non	0.5362/Low	0.0275/High	0.1365/Mod	20213.30/Mod
HHCB-12	0.3012/Carc	0.2119/Mult	0.2396/Non	Needless	0.5278/Non	0.5920/Low	0.1949/Mod	0.0348/High	4044.33/High
Derivative 7	0.2628/Carc	0.1841/Mult	0.3114/Carc	0.4635/Mult	0.5174/Non	0.2268/Mod	0.0455/High	0.0681/Mod	6730.88/High
Derivative 7-1	0.2796/Carc	0.2118/Mult	0.2850/Carc	0.3738/Mult	0.5297/Non	0.4280/Low	0.0824/Mod	0.1514/Mod	6880.30/High
Derivative 7-2	0.3164/Carc	0.2187/Mult	0.2887/Carc	0.4572/Mult	0.5430/Toxic	0.0989/Mod	0.0592/Mod	0.0879/Mod	14274.10/Mod
Derivative 7-3	0.2703/Carc	0.2179/Mult	0.3158/Carc	0.4447/Mult	0.5408/Toxic	0.6744/Low	0.0798/Mod	0.0763/Mod	6481.74/High
Derivative 7-4	0.2970/Carc	0.3493/Mult	0.2946/Carc	0.4211/Mult	0.5159/Non	0.5071/Low	0.0558/Mod	0.0509/Mod	7187.33/High
Derivative 7-5	0.2635/Carc	0.2432/Mult	0.3197/Carc	0.4242/Mult	0.5531/Toxic	0.1648/Mod	0.0612/Mod	0.0234/High	4331.16/High
Derivative 7-5A	0.2457/Non	Needless	0.3121/Carc	0.3357/Mult	0.5604/Toxic	0.2129/Mod	0.0880/Mod	0.0170/High	2536.76/High
Derivative 7-5B	0.2505/Non	Needless	0.3149/Carc	0.3561/Mult	0.5563/Toxic	0.3431/Low	0.1397/Mod	0.0090/High	1568.82/Hyper
Derivative 7-5C	0.2651/Carc	0.2336/Mult	0.3207/Carc	0.3496/Mult	0.5704/Toxic	0.5416/Low	0.2066/Mod	0.0060/High	933.48/Hyper
Derivative 7-5E	0.2706/Carc	0.2022/Mult	0.3198/Carc	0.3630/Mult	0.5532/Toxic	0.4300/Low	0.0827/Mod	0.0054/High	1947.29/Hyper
Derivative 7-6	0.2643/Carc	0.2695/Mult	0.3015/Carc	0.3970/Mult	0.5434/Toxic	0.1824/Mod	0.0309/High	0.0248/High	5327.81/High
Derivative 7-7	0.2970/Carc	0.3493/Mult	0.2946/Carc	0.4211/Mult	0.5159/Non	0.5071/Low	0.0558/Mod	0.0509/Mod	7187.33/High
Derivative 7-8	0.2829/Carc	0.2602/Mult	0.3220/Carc	0.4149/Mult	0.5528/Toxic	0.1265/Mod	0.0432/High	0.0564/Mod	6455.13/High
Derivative 7-9	0.2675/Carc	0.2372/Mult	0.3164/Carc	0.4014/Mult	0.5432/Toxic	0.2244/Mod	0.0515/Mod	0.0973/Mod	3447.06/High
Derivative 7-10	0.2690/Carc	0.2354/Mult	0.2851/Carc	0.3769/Mult	0.5885/Toxic	1.0957/Low	0.3199/Low	0.0034/Hyper	569.42/Hyper
Derivative 7-11	0.2392/Non	Needless	0.2933/Carc	0.3789/Mult	0.5712/Toxic	0.2055/Mod	0.0370/High	0.0045/Hyper	2590.06/High
Derivative 7-11A	0.2643/Carc	0.2695/Mult	0.3015/Carc	0.3970/Mult	0.5434/Toxic	0.1824/Mod	0.0309/High	0.0248/High	5327.81/High
Derivative 7-12	0.2494/Non	0.2637/Mult	0.2344/Non	Needless	0.5829/Toxic	0.5684/Low	0.2874/Mod	0.0014/Hyper	518.80/Hyper

* Assessment finished based on "Acute toxicity estimate (ATE) values and criteria for acute toxicity hazard categories" (Table S4-3), cited from the United Nations. Globally harmonized system of classification and labelling of chemicals (GHS) [M].8th ed. New York: United Nations, 2019.

Table 4-6 Toxicokinetic prediction and assessment of HHCB and Derivative 7's transformation products using TOPKAT Extensible module (continued)

Compounds	Rat chronic oral LOAEL g/kg	Fathead minnow LC_{50} * g/L	Daphnia EC_{50} * mg/L	Probability value					
				Skin irritancy	Skin sensitization NEG vs. SENS	Skin sensitization MLD/MOD vs. SEV	Ocular irritancy SEV vs. MOD	Ocular irritancy (Non/Mild) vs. (Mod/Sev)	Aerobic biodegradability
HHCB	0.0152/High	0.0019/High	4.6778/High	0.9975/Yes	0.8374/SENS	0.9222/SEV	0.7927/SEV	0.9749/(Mod/Sev)	0.3009/Non
HHCB-1	0.0196/High	0.0001/Extremely	2.9480/High	0.9975/Yes	0.8204/SENS	0.9274/SEV	0.6778/MOD	0.8149/(Mod/Sev)	0.3527 /Non
HHCB-2	0.0094/High	0.0002/Extremely	1.5214/High	0.9953/Yes	0.8369/SENS	0.9278/SEV	0.6983/SEV	0.8160/(Mod/Sev)	0.2285/Non
HHCB-3	0.0167/High	0.0010/Extremely	7.3176/High	0.9963/Yes	0.8152/SENS	0.9241/SEV	Needless	0.7627/Mild	0.3431/Non
HHCB-4	0.0172/High	0.0010/Extremely	11.3007/Central	0.9969/Yes	0.7896/SENS	0.9281/SEV	Needless	0.8917/Non	0.4363/Non
HHCB-5	0.0087/High	0.0121/Central	19.0288/Central	0.9953/Yes	0.7760/SENS	0.9120/SEV	0.7111/SEV	0.8319/(Mod/Sev)	0.3681/Non
HHCB-5A	0.0080/High	0.0790/Central	31.4062/Central	0.9770/Yes	0.8037/SENS	0.9130/SEV	0.6993/SEV	0.8299/(Mod/Sev)	0.3382/Non
HHCB-5B	0.0114/High	0.2783/Low	31.0746/Central	0.9768/Yes	0.7935/SENS	0.9140/SEV	0.6815/SEV	0.8285/(Mod/Sev)	0.3341/Non
HHCB-5C	0.0124/High	1.5147/Low	48.0794/Central	0.9748/Yes	0.7930/SENS	0.9058/SEV	0.6655/MOD	0.8283/(Mod/Sev)	0.3572/Non
HHCB-5D	0.0223/High	6.2364/Low	59.5967/Central	0.9751/Yes	0.7638/SENS	0.8958/SEV	0.6618/MOD	0.8280/(Mod/Sev)	0.3657/Non
HHCB-5E	0.0077/High	0.0329/Central	20.5078/Central	0.9766/Yes	0.8002/SENS	0.8960/SEV	0.6955/SEV	0.8356/(Mod/Sev)	0.3699/Non
HHCB-5F	0.0090/High	0.0341/Central	21.7603/Central	0.9768/Yes	0.8044/SENS	0.9002/SEV	0.6796/MOD	0.8347/(Mod/Sev)	0.3509/Non
HHCB-6	0.0100/High	0.0012/High	3.0047/High	0.9965/Yes	0.8152/SENS	0.9177/SEV	0.6773/MOD	0.8142/(Mod/Sev)	0.3474/Non
HHCB-7	0.0172/High	0.0010/	11.3007/Central	0.9969/Yes	0.8194/SENS	0.9281/SEV	Needless	0.8917/Non	0.4363/Non
HHCB-8	0.0057/High	0.0011/High	5.1680/High	0.9972/Yes	0.8251/SENS	0.9131/SEV	Needless	0.9696/Non	0.3144/Non
HHCB-8A	0.0085/High	0.0014/High	9.4040/High	0.9968/Yes	0.8336/SENS	0.9202/SEV	0.6459/MOD	0.8185/(Mod/Sev)	0.4077/Non
HHCB-9	0.0080/High	0.0027/High	10.5729/Central	0.9968/Yes	0.8152/SENS	0.9199/SEV	0.6167/MOD	0.8181/(Mod/Sev)	0.4445/Non
HHCB-10	0.0169/High	34.9903/Low	121.2230/Low	0.9717/Non	0.8414/NEG	Needless	0.6756/MOD	0.8165/(Mod/Sev)	0.4273/Non
HHCB-11	0.0052/High	0.0109/Central	8.4734/High	0.9756/Yes	0.7803/SENS	0.8937/SEV	0.7003/SEV	0.8297/(Mod/Sev)	0.3786/Non
HHCB-11A	0.0045/Hyper	0.0106/Central	11.7682/Central	0.9960/Yes	0.7293/SENS	0.8868/SEV	0.6989/SEV	0.8322/(Mod/Sev)	0.3797/Non

HHCB-11B	0.0100/High	0.0012/High	3.0047/High	0.9965/Yes	0.7893/SENS	0.9177/SEV	0.6773/MOD	0.8142/(Mod/Sev)	0.3474/Non
HHCB-12	0.0043/Hyper	0.0432/Central	34.6483/Central	0.9947/Yes	0.8274/SENS	0.8891/SEV	0.6372/MOD	0.8244/(Mod/Sev)	0.4571/Non
Derivative 7	0.0114/High	0.0020/High	2.9244/High	0.9724/Non	0.8068/SENS	0.9185/SEV	0.7890/SEV	0.9748/(Mod/Sev)	0.3467/Non
Derivative 7-1	0.0300/High	0.0001/ Extremely	1.4254/High	0.9703/Non	0.8044/SENS	0.9239/SEV	0.6163/MOD	0.8237/(Mod/Sev)	0.3452/Non
Derivative 7-2	0.0148/High	0.0004/ Extremely	1.4396/High	0.9661/Non	0.8113/SENS	0.9232/SEV	0.6487/MOD	0.8220/(Mod/Sev)	0.2602/Non
Derivative 7-3	0.0168/High	0.0011/High	3.6072/High	0.9673/Non	0.7839/SENS	0.9186/SEV	Needless	0.7636/Mild	0.3555/Non
Derivative 7-4	0.0130/High	0.0011/High	7.2309/High	0.9688/Non	0.7932/SENS	0.9235/SEV	Needless	0.8747/Non	0.4441/Non
Derivative 7-5	0.0052/High	0.0130/Central	11.7945/Central	0.9629/Non	0.7965/SENS	0.9089/SEV	0.6560/MOD	0.8262/(Mod/Sev)	0.3936/Non
Derivative 7-5A	0.0058/High	0.0843/Central	19.5037/Central	0.9607/Non	0.7993/SENS	0.9115/SEV	0.6316/MOD	0.8253/(Mod/Sev)	0.3409/Non
Derivative 7-5B	0.0082/High	0.2971/Low	19.2983/Central	0.9627/Non	0.7753/SENS	0.9136/SEV	0.5991/MOD	0.8275/(Mod/Sev)	0.3319/Non
Derivative 7-5C	0.0101/High	1.6163/Low	26.5547/Central	0.9560/Non	0.7839/SENS	0.8977/SEV	0.5888/MOD	0.8222/(Mod/Sev)	0.3793/Non
Derivative 7-5E	0.0099/High	0.0149/Central	6.3398/High	0.9633/Non	0.7776/SENS	0.9179/SEV	0.6318/MOD	0.8306/(Mod/Sev)	0.3528/Non
Derivative 7-6	0.0060/High	0.0013/High	1.8570/High	0.9682/Non	0.8065/SENS	0.9088/SEV	Needless	0.8053/Mild	0.3506/Non
Derivative 7-7	0.0130/High	0.0011/High	7.2309/High	0.9688/Non	0.7932/SENS	0.9235/SEV	Needless	0.8747/Non	0.4441/Non
Derivative 7-8	0.0051/High	0.0012/High	3.2574/High	0.9707/Non	0.8113/SENS	0.9108/SEV	Needless	0.9718/Non	0.3418/Non
Derivative 7-9	0.0063/High	0.0015/High	5.9996/High	0.9683/Non	0.7807/SENS	0.9129/SEV	Needless	0.8104/Mild	0.4115/Non
Derivative 7-10	0.0162/High	6.6448/Low	31.5335/Central	0.9579/Non	0.8008/SENS	0.8875/SEV	0.6037/MOD	0.8218/(Mod/Sev)	0.3726/Non
Derivative 7-11	0.0051/High	0.0048/High	3.6481/High	0.9681/Non	0.7641/SENS	0.9115/SEV	0.6365/MOD	0.8289/(Mod/Sev)	0.3660/Non
Derivative 7-11A	0.0060/High	0.0013/High	1.8570/High	0.9682/Non	0.8021/SENS	0.9088/SEV	Needless	0.8053/Mild	0.3506/Non
Derivative 7-12	0.0057/High	0.0514/Central	9.5646/High	0.9643/Non	0.8072/SENS	0.8591/ (MLD/MOD)	0.5545/MOD	0.8205/(Mod/Sev)	0.4130/Non

* Assessment finished based on "Ecotoxicological Hazard Classification" (Table S4-2), cited from the United Nations. Globally harmonized system of classification and labelling of chemicals (GHS) [M].8th ed. New York: United Nations, 2019.

Human health risk assessment of these transformation by-products was also calculated using the toxicokinetic analysis. The results showed that the derivatives were at the same level with their own precursors in Ames mutagenicity, NTP rodent carcinogenicity, skin sensitization, ocular irritancy, and aerobic biodegradability. According to Table 4-6, five photodegradation transformation products (HHCB-1, HHCB-2, HHCB-3, Derivative 7-1 and Derivative 7-2) and two chlorination transformation products (HHCB-7 and Derivative 7-7) have higher toxicity levels to fathead minnow (from high to extremely high) than their precursors. Therefore, further attention should be paid to the proper treatment of the by-products generated by these two processes. Almost all the transformation products of HHCB and Derivative 7 from biotransformation and metabolic pathways in algal cells keep the same toxicity level with their precursors. Thus there are no significant changes compared with their precursors. Toxicity analysis results also revealed that all the transformation products become noncarcinogenic in the female mouse. An obvious improvement of Derivative 7 is that all its transformation products will not lead to skin irritancy, while all HHCB's transformation products lead to skin irritancy.

4.3.6 Evaluation of the HHCB derivative and other PCP additives interactions and the related human health risk assessment

Derivative 7 as an ideal newly designed molecule was further evaluated for its potential risks to human bodies. SMs mainly enter human bodies by directly applying on skins through daily usage. From the literature, two methods have been found to prevent the pathway from entering the human body. These methods include improving the function of skin barrier and adding substances that inhibit photosensitivity.

Zhang et al. (2017a) investigated the transdermal permeation dynamics and distribution of

HHCB and found that 70% of HHCB remained dominantly in the stratum corneum after 24 hours. Stratum corneum is a selectively permeable, heterogeneous, complex outer layer of the epidermis that resists desiccation and environmental challenge. To improve the skin barrier function, upgrading moisturization is an optimum option to restrain the entrance of HHCB into human bodies (Rawlings and Harding, 2004). On the other hand, Fang et al. (2017) found that polycyclic musk such as AHTN can act as a photosensitizer that significantly increases photo-induced oxidative damage to amino acids. Because the use of these photosensitizers can accelerate the injury to cells and other organisms and even may lead to human skin cancer (Robinson et al., 2013). Thus, to overcome the risks bring by photosensitizers, substances that inhibit photosensitivity could be added when applying SMs.

One of the keratins, 4ZRY was chosen as the representative ligand of the stratum corneum in this study. The binding energy of SMs with 4ZRY could reflect the strength of the interaction between the protein and the SM molecules. Therefore, the molecular dynamics simulation was employed in this study to simulate the effects of moisturizers and anti-photosensitivity materials addition on the binding ability of SMs with 4ZRY. Thus, the best skincare additive combination that helps prevent SM molecules from causing toxicity risks to the human body could be screened. The binding energy of SMs before and after modification with 4ZRY under the presence of each additive is obtained and summarized in Table 4-7, respectively.

According to Table 4-7, 12 out of 15 additives for Derivative 7-4ZRY presented a decreased binding energy (absolute value), and 4 out of 15 additives for HHCB-4ZRY presented a decreased binding energy (absolute value). Thus, 12 compounds were then selected as the additives (including 12 additives for Derivative 7-4ZRY and 4 additives for HHCB-4ZRY) that significantly decrease the binding ability between Derivative 7 and 4ZRY (4.27%-30.22%), HHCB and 4ZRY (0.89%-15.26%), respectively. As a result, a Taguchi experimental design (12

factors, 2 levels) was set out to screen the optimum additives combinations, which helped to prevent SMs enter human bodies through skin permeation after modification.

In the Taguchi experimental design, SNR (signal to noise ratio) is used to identify control factors that reduce variability in products or processes by minimizing the effects of uncontrollable factors (noise factors), is the parameter to evaluate robustness (Castorena-Cortés et al., 2009; Gu et al., 2020c). The larger the SNR is, the smaller the binding energy of the system is, and thus less effect to the system is attributed from the experimental design conditions. Thus, the parameter SNR was selected as the evaluating indicator of the binding energy between ligand molecule HHCB before and after modification with receptor molecule 4ZRY (Table 4-8).

Figure 4-4 gives an overview of all the combination groups of additives from a Taguchi experimental design and the heat map provides a continuous value of binding energy. The blue and white color indicates whether to add additives or not, and the light purple to dark purple shows the binding energy of Derivative 7-4ZRY or HHCB-4ZRY with a different combination of 12 additives. In Table 4-8, the binding energy of Derivative 7-4ZRY with all combination groups present decreased from 1.83% to 30.57%, and significant improvement (more than 15%) in toxicity inhibition was found for 12 out of 32 combination groups. As for HHCB-4ZRY, the binding energy of only eight combination groups decreased (3.99%-10.77%) compared to the blank group. Twenty-four out of 32 combination groups were found to be effective to reduce the HHCB toxicity to keratins after molecular modification, ranging from 0.81% to 32.66%. For example, the addition of rutin + lactic acid + glycerol + vitamin B₃ + phytosphingosine + ceramide 3 to HHCB before and after modification could bring the toxicity of HHCB to keratins down to 32.66%. A screening of selected commonly used functional additives in cosmetics and PCPs proved that a proper introduction of the right additive combination would lower the risk to the skin. This study also provided a new insight to reduce the human health risk by restraining the pathway of SMs entering human bodies.

Table 4-7 The binding energy of HHCB-4ZRY and Derivative 7-4ZRY with additives present

Additives		Before modification (HHCB)		After modification (Derivative 7)	
		Binding energy	Change rate	Binding energy	Change rate
Anti-photosensitivity materials	Quercetin	-136.98	2.81%	-134.66	-6.55%
	Rutin	-141.48	6.19%	-125.28	-13.06%
	Vitamin B ₃	-131.24	-1.49%	-129.04	-10.45%

Moisturizers	DL-Pyroglutamic acid	-145.64	9.31%	-168.44	16.90%
	Lactic Acid	-170.04	27.63%	-100.79	-30.05%
	Glycerol	-132.05	-0.89%	-136.35	-5.37%
	Urea	-112.91	-15.26%	-117.82	-18.23%
	Vitamin E	-135.64	1.81%	-137.94	-4.27%
	D-Sorbose	-154.57	16.01%	-118.61	-17.69%
	Phytosphingosine	-152.16	14.21%	-129.04	-10.44%
	Vitamin A	-113.17	-15.06%	-116.86	-18.90%
	Linoleic Acid	-177.20	33.00%	-100.55	-30.22%
	Vitamin C	-137.09	2.90%	-147.31	2.24%
	Ceramide 3	-146.21	9.74%	-129.69	-10.00%
Ceramide 1	-139.85	4.97%	-151.34	5.04%	

Blank		-133.23		-144.09	

Table 4-8 Calculation of binding energy and signal to noise ratio (SNR) of the HHCB-4ZRY and Derivative 7-4ZRY complexes
in the molecular dynamics simulation system from a Taguchi experimental design

No.	Taguchi experimental design *												HHCB-4ZRY complex			Derivative 7-4ZRY complex			Improvement rate of binding energy after modification
	A	B	C	D	E	F	G	H	I	J	K	L	Binding energy (kJ/mol)	Change rate (without added)	SNR	Binding energy (kJ/mol)	Change rate (without added)	SNR	
1	1	1	1	1	1	1	1	1	1	1	1	1	-139.87	-4.98%	42.91	-134.09	6.94%	42.55	4.13%
2	1	1	1	1	0	1	1	1	1	0	0	0	-175.54	-31.75%	44.89	-134.59	6.59%	42.58	23.33%
3	1	1	1	0	1	1	0	0	0	1	1	1	-171.73	-28.89%	44.70	-125.73	12.74%	41.99	26.79%
4	1	1	1	0	0	1	0	0	0	0	0	0	-139.97	-5.05%	42.92	-108.07	25.00%	40.67	22.79%
5	1	1	0	1	1	0	1	0	0	1	0	0	-164.88	-23.75%	44.34	-132.82	7.82%	42.47	19.44%
6	1	1	0	1	0	0	1	0	0	0	1	1	-120.62	9.47%	41.63	-116.22	19.34%	41.31	3.65%
7	1	1	0	0	1	0	0	1	1	1	0	0	-134.19	-0.71%	42.55	-108.81	24.48%	40.73	18.91%
8	1	1	0	0	0	0	0	1	1	0	1	1	-147.83	-10.95%	43.40	-102.26	29.03%	40.19	30.82%
9	1	0	1	1	1	0	0	1	0	0	1	0	-137.62	-3.29%	42.77	-127.77	11.33%	42.13	7.16%
10	1	0	1	1	0	0	0	1	0	1	0	1	-152.89	-14.76%	43.69	-131.59	8.68%	42.38	13.93%
11	1	0	1	0	1	0	1	0	1	0	1	0	-121.83	8.56%	41.71	-115.32	19.97%	41.24	5.34%
12	1	0	1	0	0	0	1	0	1	1	0	1	-124.08	6.87%	41.87	-140.89	2.22%	42.98	-13.55%
13	1	0	0	1	1	1	0	0	1	0	0	1	-136.09	-2.14%	42.68	-118.01	18.10%	41.44	13.28%
14	1	0	0	1	0	1	0	0	1	1	1	0	-158.72	-19.13%	44.01	-120.07	16.67%	41.59	-24.35%
15	1	0	0	0	1	1	1	1	0	0	0	1	-136.42	-2.39%	42.70	-121.52	15.67%	41.69	10.92%
16	1	0	0	0	0	1	1	1	0	1	1	0	-124.87	6.28%	41.93	-141.45	1.83%	43.01	-13.28%
17	0	1	1	1	1	0	0	0	1	0	0	1	-189.62	-42.32%	45.56	-127.69	11.38%	42.12	32.66%
18	0	1	1	1	0	0	0	0	1	1	1	0	-133.91	-0.50%	42.54	-129.78	9.93%	42.26	3.08%
19	0	1	1	0	1	0	1	1	0	0	0	1	-147.15	-10.44%	43.36	-139.01	3.53%	42.86	5.53%
20	0	1	1	0	0	0	1	1	0	1	1	0	-142.01	-6.59%	43.05	-140.86	2.24%	42.98	0.81%
21	0	1	0	1	1	1	0	1	0	0	1	0	-139.67	-4.83%	42.90	-134.66	6.54%	42.58	3.59%
22	0	1	0	1	0	1	0	1	0	1	0	1	-126.19	5.29%	42.02	-124.30	13.74%	41.89	1.50%
23	0	1	0	0	1	1	1	0	1	0	1	0	-153.18	-14.97%	43.70	-115.39	19.92%	41.24	24.67%
24	0	1	0	0	0	1	1	0	1	1	0	1	-141.15	-5.94%	42.99	-116.57	19.10%	41.33	17.41%

25	0	0	1	1	1	1	1	0	0	1	0	0	-127.91	3.99%	42.14	-155.84	8.16%	43.85	-21.84%
26	0	0	1	1	0	1	1	0	0	0	1	1	-122.47	8.08%	41.76	-136.52	5.25%	42.70	-11.47%
27	0	0	1	0	1	1	0	1	1	1	0	0	-142.28	-6.79%	43.06	-116.02	19.48%	41.29	18.46%
28	0	0	1	0	0	1	0	1	1	0	1	1	-134.50	-0.95%	42.57	-135.55	5.92%	42.64	-0.78%
29	0	0	0	1	1	0	1	1	1	1	1	1	-143.20	-7.48%	43.12	-125.04	13.22%	41.94	12.68%
30	0	0	0	1	0	0	1	1	1	0	0	0	-118.88	10.77%	41.50	-134.37	6.74%	42.57	-13.03%
31	0	0	0	0	1	0	0	0	0	1	1	1	-134.79	-1.17%	42.59	-100.04	30.57%	40.00	25.78%
32	0	0	0	0	0	0	0	0	0	0	0	0	-133.23	0.00%	42.49	-144.09	0.00%	43.17	-8.15%

* 1) A: quercetin; B: rutin; C: lactic acid; D: glycerol; E: vitamin B₃; F: urea; G: vitamin E; H: D-Sorbose; I: phytosphingosine; J: vitamin A; K: linoleic acid; L: ceramide 3;

2) "1" means added, "0" means no added.

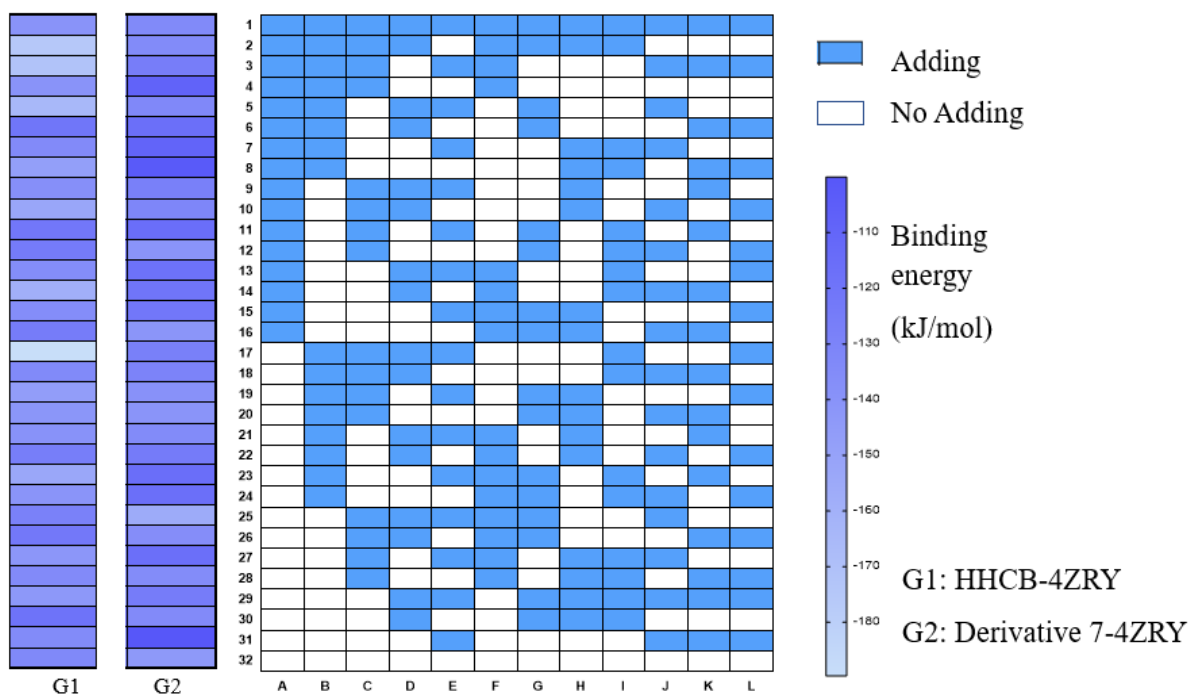


Figure 4-4 Binding energy of HHCB-4ZRY and Derivative 7-4ZRY complexes from a Taguchi experimental design

4.3.7 Potential applications of HHCB derivatives

As an economical substitution of natural musk fragrance, HHCB has been considered as a key polycyclic musk widely adopted for PCPs formation. According to United States Environmental Protection Agency (US EPA) (2014), a rapid increase in HHCB consumption in the United States has been reported, with an amount of 2.8, 3.1, 3.52 and 3.74 million lbs in 2000, 2004, 2008 and 2011, respectively. HHCB has thus been placed on the “High Production Volume List” by the US EPA (Ehiguese et al., 2021). A similar trend of production was also reported in European and Asian countries. However, after usage, HHCB in PCPs cannot be fully mitigated by the wastewater treatment plant. The existence of HHCBs in the sewage effluents, sludge, surface waters and sediments have thus been widely observed (Zeng et al., 2005; Kannan et al., 2005; Sumner et al., 2010). Díaz-Garduño et al. (2017) found that fragrances accounted for approximately 40% among 175 chemicals (pharmaceutically active compounds, PCPs and regulated compounds) in the effluent of wastewater treatment plants.

The toxicity assessment of HHCB has been flourishing in recent years, whose ecological toxicity, adverse human health impacts have been recognized. HHCB has been proved to have a potential risk to organisms. Researchers found that the exposure of HHCB with a concentration of 0.005 mmol/L led to higher zebrafish embryos mortality, decreased heart rate, lowered hatching rate and disturbances in thyroid hormone secretion and regulation in developmental zebrafish embryos (Ming et al., 2020). After using PCPs contained HHCB, HHCB was found to remain in the stratum corneum after 24 hours (Zhang et al., 2017a). Fan et al. (2019) compared the toxicity

differences of the three most popular SMs and found that musk ketone was the most toxic to aquatic organisms, followed by HHCB and AHTN.

Development of environmentally friendly and lower human health risks HHCB equivalents, therefore, are of great importance. Derivative 7 obtained and examined in this study has been recognized as a promising HHCB alternative. It exhibited improved functional properties (i.e., better odor stability and higher odor intensity with musky scent maintained), less environmental impacts and lower human health risk. When mixed with proper additives commonly used in PCPs (e.g., moisturizers and anti-photosensitivity materials), the toxicity of this HHCB derivative could be further reduced. The newly designed molecule has shown its potential applicability as an alternative to HHCB for the formation of fragrances, shampoos, soaps, and household items.

4.4 Summary

In this chapter, 3D-QSAR models were constructed to obtain HHCB's new derivatives and predict their functional properties, bio-toxicity, bio-accumulation ability and mobility. Among the 90 newly designed derivatives, Derivatives 6, 7, 75 and 78 were believed to have a better production potential due to their better functional properties, lower bio-toxicity, as well as smaller $\log BCF$ and $\log VP$ values. The transformation processes (i.e., photodegradation, biotransformation and chlorination) of HHCB and the selected Derivative 7 were deduced and environmental properties of the transformation products generated in each process were further evaluated. Human health risks of HHCB, Derivative 7 and their transformation products were assessed

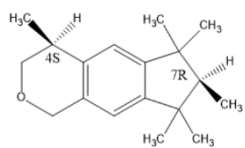
using molecular docking, density functional theory and molecular dynamics. Additives assisted SMs (i.e., Derivative 7 and HHCB) skin penetration prevention were assessed integrated with the Taguchi experimental design. The results proved that an additive combination of rutin, lactic acid, glycerol, vitamin B₃, phytosphingosine, and ceramide 3 with HHCB, as well as an additive combination of vitamin B₃, vitamin A, linoleic acid, and ceramide 3 with Derivative 7 could significantly reduce the toxicity of these two SMs molecules to keratins at a rate 32.66% and 30.57%, respectively. Derivative 7 has been recognized as an environmentally friendly HHCB derivative with improved functional properties (odor lasting, intensity and musky scent) and lower human health risk, and its associated additive formula with less human health toxicity was optimized. It is the first comprehensive study regarding the design of functionally improved and environmentally friendly HHCB alternatives, helping to better understand their environmental behaviors and human health risks, and facilitating their treatment after usage. The strategy showcased in this study could also serve as a valuable tool for the future designing of other PCPs.

Appendices

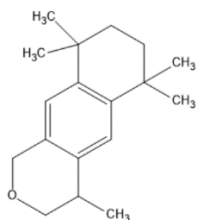
Table S4-1 Molecular structures of the training set and test set used in 3D-QSAR modelling

No.	Molecular structure	No.	Molecular structure	No.	Molecular structure
Musk 1 a ¹² b ¹		Musk 27 c ²		Musk 52	
Musk 2 b ¹ c ¹		Musk 28		Musk 53	
Musk 3 c ¹		Musk 29		Musk 55	
Musk 4 a ¹ b ¹		Musk 30		Musk 56	
Musk 5 a ¹		Musk 31 c ²		Musk 57	

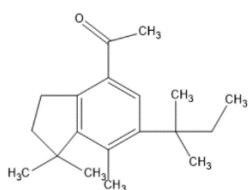
Musk 6
a¹ b²



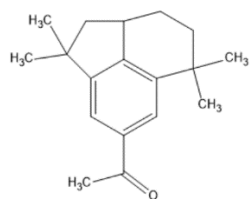
Musk 7
a¹



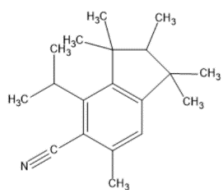
Musk 8
a¹ c¹



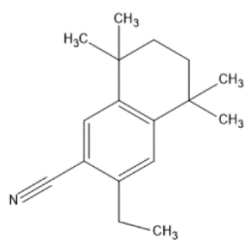
Musk 9
a¹



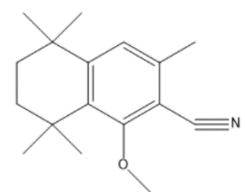
Musk 10
a¹ c¹



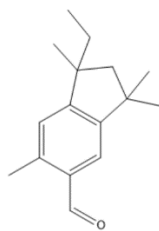
Musk 11
b¹ c¹



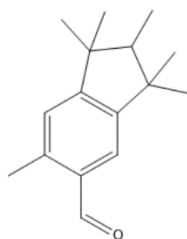
Musk 12
a¹



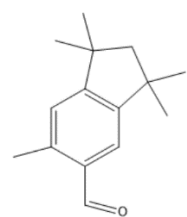
Musk 32



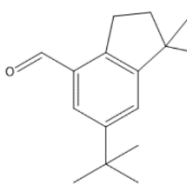
Musk 33



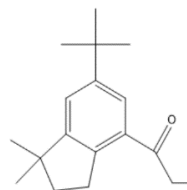
Musk 34



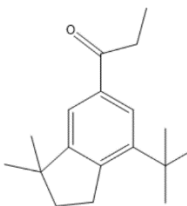
Musk 35



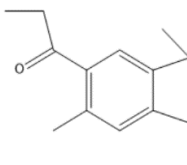
Musk 36



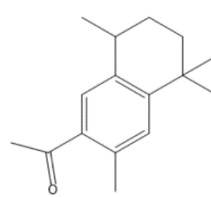
Musk 37



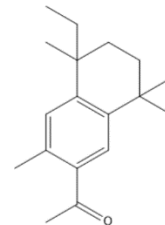
Musk 38
c²



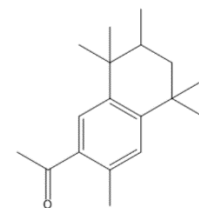
Musk 58



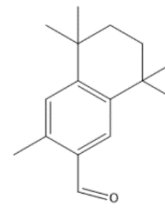
Musk 59



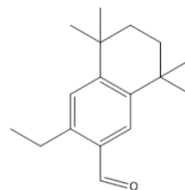
Musk 60



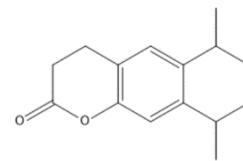
Musk 61



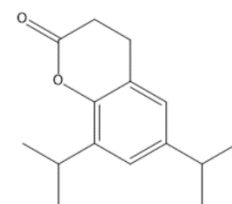
Musk 62

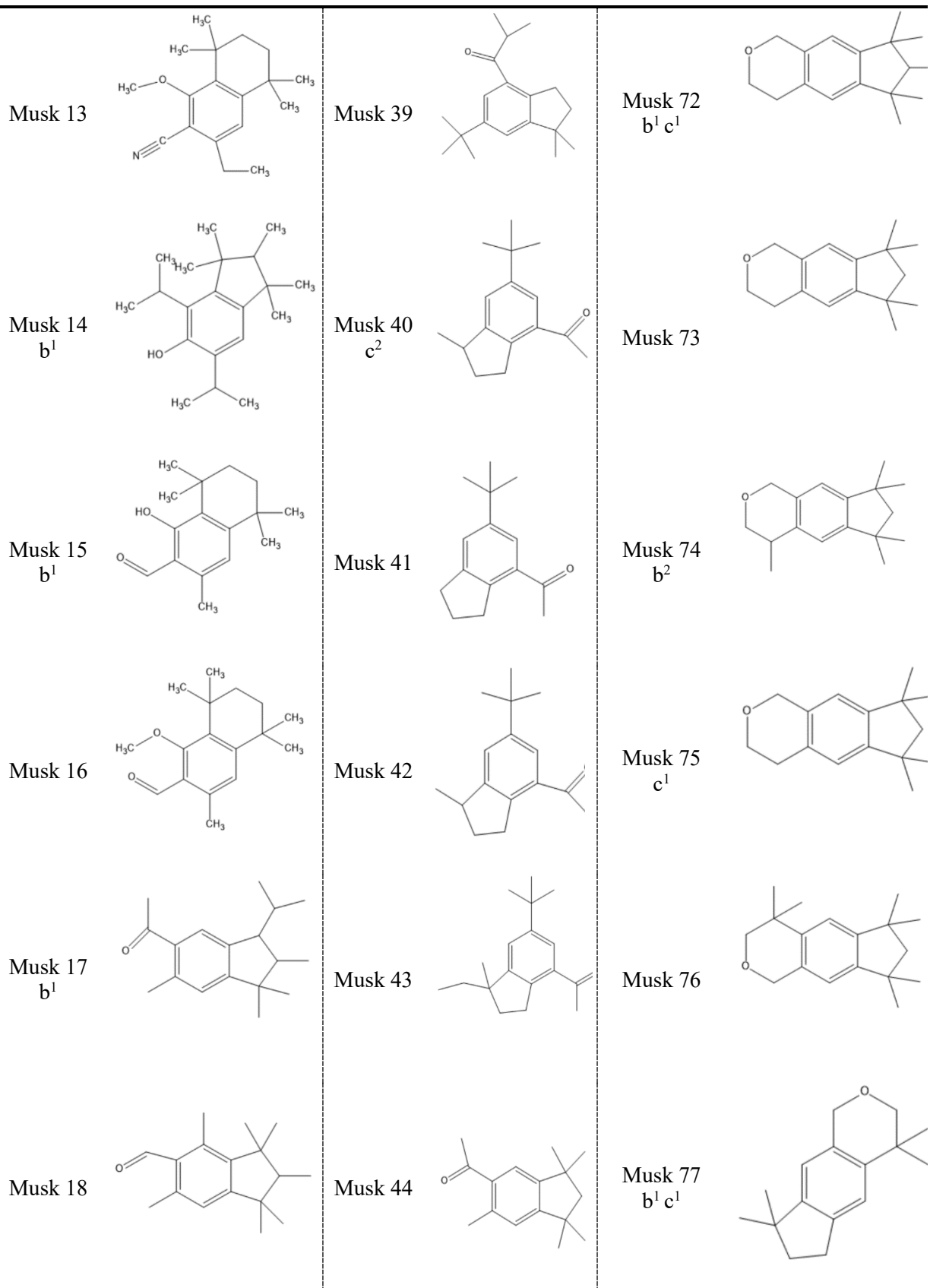


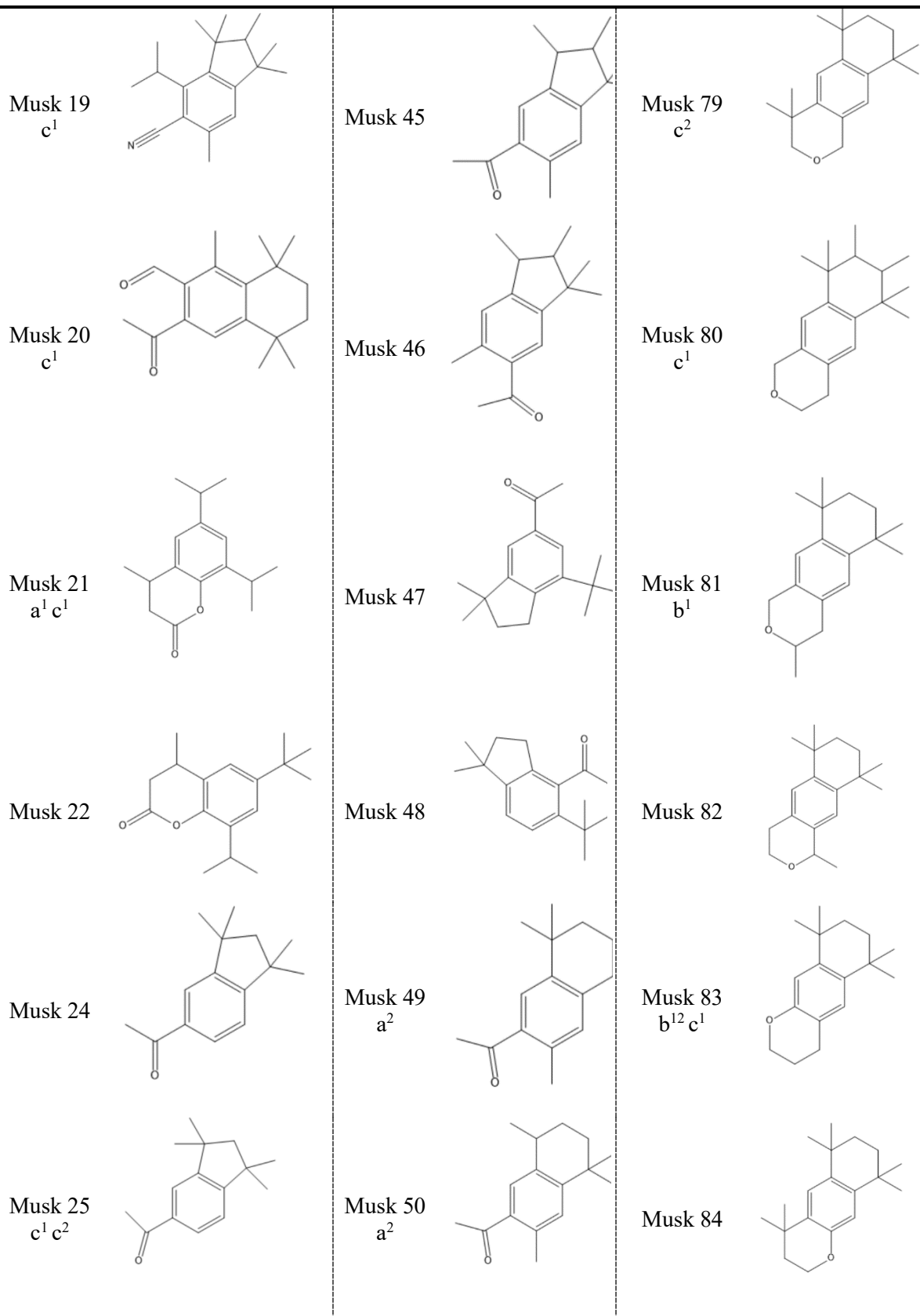
Musk 65
b¹ c¹



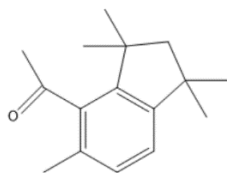
Musk 66
b²



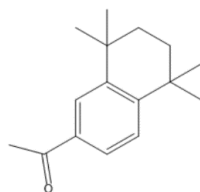




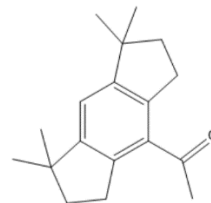
Musk 26



Musk 51
a²



Musk 89
b¹



(1) Molecular structures used in the 3D-QSAR model for predicting a: Half-life; b: $\log BCF$; c: $\log VP$;

(2) ¹ means training set; ² means testing set.

Table S4-2 Categories of substance hazardous level to the aquatic environment

Data or item	Harmful subdivision level and its assign score value				Note
	Category 1	Category 2	Category 3	Category 4	
Acute toxicity LC_{50}/EC_{50} , mg/L	≤1	>1~10	>10~100	>100	1
Degradation	—	—	—	—	2
Chronic toxicity $NOEC/EC_x$, mg/L (Rapidly degradable substances)	≤0.01	>0.01~0.1	>0.1~1	—	3
Chronic toxicity $NOEC/EC_x$, mg/L (Non-rapidly degradable substances)	≤0.1	>0.1~1	—	—	

Note 1: Include 96 hr LC_{50} (for fish); 48 hr EC_{50} (for crustacea); 72 or 96 hr EC_{50} (for algae or other aquatic plants).

Note 2: Substances are considered rapidly degradable in the environment if the following criteria hold true:

- (a) if in 28-day ready biodegradation studies, the following levels of degradation are achieved:
 - (i) tests based on dissolved organic carbon: 70%;
 - (ii) tests based on oxygen depletion or carbon dioxide generation: 60% of theoretical maxima; These levels of biodegradation must be achieved within 10 days of the start of degradation which point is taken as the time when 10% of the substance has been degraded, unless the substance is identified as a complex, multi-component substance with structurally similar constituents. In this case, and where there is sufficient justification, the 10-day window condition may be waived and the pass level applied at 28 days.

(b) if in those cases where only BOD and COD data are available, when the ratio of BOD/COD is ≥ 0.5 ;

or

- (c) if other convincing scientific evidence is available to demonstrate that the substance can be degraded (biotically and/or abiotically) in the aquatic environment to a level >70% within a 28-day period.

Note 3: (a) Include Chronic $NOEC$ or EC_x (for fish); Chronic $NOEC$ or EC_x (for crustacea); Chronic $NOEC$ or EC_x (for algae or other aquatic plants);

- (b) If the following occurs, chronic toxicity reference Note 1 Acute toxicity classification:
 - (i) substances for which adequate chronic toxicity data are not available and the substance is not rapidly degradable.
 - (ii) the experimentally determined BCF is ≥ 500 (or, if absent, the $\log K_{ow} \geq 4$).

Cited from United Nations. Globally harmonized system of classification and labelling of chemicals (GHS) [M]. 8th ed. New York: United Nations, 2019.

Table S4-3 Acute toxicity estimate (ATE) values and criteria for acute toxicity hazard evaluation

Toxicity classification	Oral LD_{50} mg/kg	Acute Dermal LD_{50} mg/kg	Acute Inhalation LC_{50}
Category 1	$ATE \leq 5$	$ATE \leq 50$	Gases: $ATE \leq 100$ ppmV Vapours: $ATE \leq 0.5$ mg/L Dusts and Mists: $ATE \leq 0.05$ mg/L
Category 2	$5 < ATE \leq 50$	$50 < ATE \leq 200$	Gases: $100 < ATE \leq 500$ ppmV Vapours: $0.5 < ATE \leq 2.0$ mg/L Dusts and Mists: $0.05 < ATE \leq 0.5$ mg/L
Category 3	$50 < ATE \leq 300$	$200 < ATE \leq 1000$	Gases: $500 < ATE \leq 2500$ ppmV Vapours: $2.0 < ATE \leq 10$ mg/L Dusts and Mists: $0.5 < ATE \leq 1.0$ mg/L
Category 4	$300 < ATE \leq 2000$	$1000 < ATE \leq 2000$	Gases: $2500 < ATE \leq 20000$ ppmV Vapours: $10 < ATE \leq 20$ mg/L Dusts and Mists: $1.0 < ATE \leq 5.0$ mg/L
Category 5	$2000 < ATE \leq 5000$	$2000 < ATE \leq 5000$	Equivalent doses for inhalation*

* a) The substance is classified in this category if reliable evidence is already available that indicates the LD_{50} or LC_{50} to be in the range of Category 5 values or other animal studies or toxic effects in humans indicate a concern for human health of an acute nature.

b) The substance is classified in this category, through extrapolation, estimation or measurement of data, if assignment to a more hazardous category is not warranted, and:

- reliable information is available indicating significant toxic effects in humans; or
- any mortality is observed when tested up to Category 4 values by the oral, inhalation, or dermal routes; or
- where expert judgment confirms significant clinical signs of toxicity, when tested up to Category 4 values, except for diarrhoea, piloerection or an ungroomed appearance; or
- where expert judgment confirms reliable information indicating the potential for significant acute effects from other animal studies.

Cited from United Nations. Globally harmonized system of classification and labelling of chemicals (GHS) [M]. 8th ed. New York: United Nations, 2019.

S4.2.2.2 Human health risk control of HHCB derivatives using molecular dynamics simulation

All parameters in the equations of Section 4.2.2.2 were defined (Gu et al., 2021a) below:

$$G_{\text{bind}} = G_{\text{complex}} - G_{\text{free-protein}} - G_{\text{free-ligand}} \quad (4-S1)$$

G_{bind} - Binding free energy of the system / The combined binding free energy;

G_{complex} - Binding free energy of the complex;

$G_{\text{free-protein}}$ - Binding free energy of the protein;

$G_{\text{free-ligand}}$ - Binding free energy of the ligand molecule;

where the binding energy of the molecule is calculated as:

$$G = E_{\text{gas}} - TS_{\text{gas}} + G_{\text{solvation}} \quad (4-S2)$$

G - Binding free energy of the molecule;

E_{gas} - The energy of gas phase;

TS_{gas} - The energy of gas phase transition state;

$G_{\text{solvation}}$ - Binding free energy of the solvation;

where the free solvation energy is further decomposed into polar and nonpolar components:

$$G_{\text{solvation}} = G_{\text{polar}} + G_{\text{nonpolar}} \quad (4-S3)$$

G_{polar} - Binding free energy of the polar solvation;

G_{nonpolar} - Binding free energy of the nonpolar solvation.

CHAPTER 5

INHALATION AND INGESTION OF SMS IN PREGNANT WOMEN: IN SILICO SPONTANEOUS ABORTION RISK EVALUATION AND CONTROL

This chapter has been published in *Environment International* (2022): 158, 106911. I am the primary author of this paper, and am mainly responsible for the conceptualization, methodology, software, formal analysis, investigation, writing - original draft preparation, writing - review & editing of the manuscript. The co-author Yuanyuan Zhao is mainly responsible for the conceptualization, methodology, software, formal analysis, investigation, writing - original draft preparation, writing - review & editing of the manuscript, Bing Chen helps to conduct the formal analysis and writing - review & editing, Zhiwen Zhu and Tahir Husain help to edit the manuscript, Qiao Kang helps on the data curation, and Baiyu Zhang is the principal investigator of the manuscript involved writing - review & editing, supervision, project administration, and funding acquisition.

Li, X., Zhao, Y., Chen, B., Zhu, Z., Kang, Q., Husain, T., & Zhang, B. (2022). Inhalation and ingestion of Synthetic musks in pregnant women: In silico spontaneous abortion risk evaluation and control. *Environ. Int.*, 158, 106911.

DOI: 10.1016/j.envint.2021.106911

5.1 Introduction

Synthetic musks (SMs) are a class of pharmaceutical and personal care products with a typical musky fragrance, excellent fixation properties, and low prices. (Artola-Garicano et al., 2003a). However, these daily necessities have been detected in various environmental samples due to their extension application and limited removal effect via traditional sewage treatment processes (Katuri et al., 2020; Rico et al., 2021). Villa et al. (2014) reported the existence of galaxolide (HHCB) and tonalide (AHTN) in both fresh snowfall and water samples in the Northern Italian Alps, indicating the long-distance mobility of SMs. In addition, the highly lipophilic SMs have a bioaccumulation effect in the environment, which can be transmitted and enriched through the food chain, and finally enter the organisms. The detection of HHCB, AHTN, musk xylene (MX) and musk ketone (MK) in seafood (i.e., fish, oysters, shellfish, salmon, and eels) produced in Northern Spain and the southwest coast in Europe were reported (Vallecillos et al., 2015a; Saraiva et al., 2016). SMs have also been detected in human blood and breast milk. In Vienna, Austria, Hutter et al. (2010) determined the exposure levels of 11 SMs in human blood and found that the detection rates of HHCB and MX in human blood were 89% and 62%, at concentrations as high as 6900 ng/L and 190 ng/L, respectively. SMs in the atmosphere can enter the blood system through breathing or skin interaction, thereby causing potential harm to human health (Gao et al., 2016). Thirteen kinds of SMs were identified in 1237 human breast milk collected from 12 provinces in China (Yin et al., 2016). Among these breast milk samples, the average detected concentration of HHCB was as high as 18.03 ng/g. Hu et al. (2010) concluded that SMs may be transferred from pregnant women to their children. SMs widely present in the environment, so it is inevitable that they could enter human's body through inhalation and ingestion (Sousa et al., 2020). Therefore, it is important to study the potential risks brought from SMs to human beings, especially groups that need special attention such as pregnant

women.

Studies have shown that SMs have environmental hormone effects. For example, Taylor et al. (2014) found that human exposure was negatively correlated with the level of progesterone. Li et al. (2013) used the human adrenocortical carcinoma cell line H295R to evaluate the effects of HHCB and AHTN on seven types of sterol hormones and ten types of sterol synthesis pathway genes in humans. They confirmed the inhibition of HHCB and AHTN on human progesterone synthesis and cortisol. In addition, HHCB and AHTN can also be used as selective estrogen receptor modulators to impede human estrogen activities (Schreurs et al., 2002). Progesterone is a natural hormone secreted by the corpus luteum of women (Ward et al., 2020). During pregnancy, the corpus luteum of the ovary regulates the endometrium by secreting an appropriate amount of progesterone, so that the endometrium changes from the proliferative stage to the secretory stage to facilitate embryo implantation and development (Tang et al., 2019). If the levels of progesterone cannot be properly maintained, threatened miscarriage or even miscarriage will eventually occur (Feng et al. 2017; Wang et al., 2020). In addition, the continuously rising of estrogen levels during normal pregnancy is an important sign to ensure a safe pregnancy. Experimental and clinical studies on a variety of non-primate species have shown that the withdrawal of progesterone could lead to the changes in gene expression that initiate parturition at term (Andersson et al., 2008). Feng et al. (2017) pointed out that if pregnant women cannot maintain appropriate progesterone levels, threatened abortion or even miscarriage would eventually occur. Therefore, proper levels of progesterone and estrogen can ensure and maintain women's normal pregnancy as well as safe and smooth development of embryos. As the inhibition of HHCB and AHTN on human progesterone and estrogen activities, it is necessary to conduct an in-depth investigation on the evaluation and reduction of the spontaneous abortion risk. This topic has never been tackled before.

A healthy dietary is an effective method to control the risk of spontaneous abortion. Di Cintio (2001) indicated that the risk of spontaneous abortion was inversely and significantly related to green vegetables, fruit, milk, cheese, eggs and fish consumption. In recent years, studies have shown that women should pay attention to balance nutritional intake during pregnancy to maintain a normal metabolism (Sununtnasuk and Fiedler, 2017; Lander et al., 2019). Supplements of vitamins are suggested, which can help improve immunity and promote fetal growth (Wang et al., 2018). Thus, a proper supplementary diet plan could be beneficial for lowering the potential risk of SMs to pregnant women. To prove such hypothesis, multiple supplementary diet plans were selected in this study to investigate whether these supplements can reduce the harm of musk to pregnant women.

Besides, developing molecules with lower human health risks have been long adopted. Obtaining SM alternatives through molecular modification might help to reduce the possible spontaneous abortion risk and maintain their functional properties (odor). The three-dimensional quantitative structure-activity relationship (3D-QSAR) is a robust method used to design new chemicals (Winkler, 2018). Through investigating and virtual screening, the three-dimensional properties of the ligands, the chemical and biological activities of the target molecule can be predicted. Such properties enable the application of 3D-QSAR in evaluating and predicting the biological toxicity, bioconcentration, long-range transport potential, biodegradability of chemical compounds (Gu et al., 2019; Li et al., 2021a; Jiang and Li, 2016; Yang et al., 2021). However, there are extremely limited studies using 3D-QSAR models to predict the toxicity of SMs and modify SMs molecular structures to obtain new SMs derivatives with lower risks to humans especially pregnant women.

The objective of this study is thus to evaluate and control abortion risk of SMs to pregnant women through conducting 3D-QSAR model-based risk prediction and SM molecular modification, as well as establishing supplementary diet plans. Progesterone and

estrogen were adopted for evaluating the health of fetus. A progesterone-estrogen integrated factor was established based on the G1-anti-entropy weight method (G1) (Wang et al., 2021) during 3D-QSAR modelling. LibDock scores were used to reflect the binding ability of SMs with progesterone and estrogen for performance evaluation of the supplementary diet plans and SM derivatives. The findings would help to provide a theoretical circumvention system for mitigating the potentially spontaneous abortion caused by long-term exposure of SMs to pregnant women.

5.2 Methodology

5.2.1 Establishment of relationships between SMs and their abortion risk to pregnant women

LibDock score, a parameter that reflects the binding ability of ligand and the receptor, has been commonly used to describe toxicity (Fang et al., 2019). It can be calculated by molecular docking, and then used as inputs for other modelling processes (Akula et al., 2006; Gu et al., 2021b; Ren et al., 2021). A higher LibDock score means a greater capacity of ligand-protein binding (Ren et al., 2019). The wide existence of SMs in the environment can adversely affect the production and activity of progesterone and estrogen (Schreurs et al., 2002, Li et al., 2013). Proper levels of progesterone and estrogen can maintain women's normal pregnancy and ensure the safe and smooth development of embryos. If pregnant women cannot maintain appropriate progesterone levels, threatened abortion or even miscarriage would eventually occur (Feng et al. 2017). Specifically, the higher the LibDock score, the stronger the interaction between SMs (or their derivatives) and the two receptors, the stronger its inhibitory effect on progesterone and estrogen, and the higher the abortion risks. In this study, the LibDock scores reflecting the binding affinity between SMs and two proteins (i.e., progesterone and estrogen) were obtained in Discovery Studio[®] 2020 to

represent the abortion risks. The “LibDock module” was used to define the selected protein as a receptor molecule. The “Find Sites from Receptor Cavities” under the “Define module” was then selected to identify the possible binding site in the receptor that can be further defined and modified. Finally, the ligand molecule was integrated into the formed protein binding cavity for rapid docking. During the docking process, the “User Specified” in “Docking Preferences” was used and the “Max Hit to Save” was set as 10 (Zhao et al., 2020).

The reliability of the LibDock scores of SMs and target receptors (i.e., progesterone and estrogen) generated by molecular docking needs to be further verified (the structures of target receptors are shown in Figure S5-1). A correlation between the LibDock scores and the binding energy between SMs and target receptors was used to reflect the reliability of LibDock. The molecular dynamics simulation, a proven accurate method that has been widely applied to reflect the binding abilities of chemicals and target proteins (Alonso et al., 2006; Gu et al., 2020b; Zhao et al., 2020; Qiu et al., 2020), was thus selected as a verification tool. Molecular dynamics simulation can dynamically describe the movement of the ligand and receptor in the defined composite system. The binding ability between them can be characterized by the binding energy based on the estimation of the molecular force field. The smaller the binding energy is, the stronger the binding ability exhibited between the ligand and the receptor (Zhao et al., 2020). The detailed steps of molecular dynamics simulations were provided in the supplementary materials (S5-1.1)

To prove the reliability of LibDock score as an effective binding ability indicator, the molecular docking between the protein Acetylcholinesterase (AChE) and SMs was conducted and compared with the binding energy generated from molecular dynamics simulation in this study to establish the correlation using two-dimensional quantitative structure-activity relationship (2D-QSAR) modelling (detailed information was shown in the supplementary material S5-1.2).

5.2.2 Reduction of spontaneous abortion risk by supplementary diet plans assisted with L₁₂ Taguchi experiment design

The supplementary diet plan was investigated to reduce the abortion risk from SMs. A total of 10 anti-fetus supplementary (i.e., vitamin C, carotene, niacin, folic acid, vitamin A, vitamin E, ovalbumin, vitamin B₁₂, vitamin B₂, and vitamin B₆) were investigated. The L₁₂ Taguchi design module in the Minitab software package was used to establish the ten factors (A: vitamin C; B: carotene; C: niacin; D: folic acid; E: vitamin A; F: vitamin E; G: ovalbumin; H: vitamin B₁₂; I: vitamin B₂; J: vitamin B₆) at two levels (without, with). The L₁₂ orthogonal array which comprised of 12 experiments was used (Mensah et al., 2019). Twelve supplementary diet plans were evaluated for the reduced spontaneous abortion risk from inhaling and ingesting the selected SMs, including phantolide (PHAN), celestolide (ADBI), tonalide (AHTN), galaxolide (HHCB) and musk ketone (MK). The LibDock score of SMs and target proteins (progesterone and estrogen) without supplementary were calculated by molecular docking, and then binding ability without supplementary uptake was used as control. The supplementary diet plans used SMs and two proteins (progesterone and estrogen) as targets, selecting the signal-to-noise ratio (the smaller, the better) as the evaluation criteria for verification. (Gu et al., 2020b). Eventually, the three most effective diet plans were selected for further analysis in section 5.2.4.

5.2.3 Reduction of spontaneous abortion risk by designing SM derivatives through 3D-QSAR modelling

5.2.3.1. Model construction and evaluation

Two single factor 3D-QSAR models and one multi-activity 3D-QSAR model were constructed in this study using the SYBYL-X2.0 software for designing SM derivatives. The principles and advantages of choosing 3D-QSAR model as the molecular modification method were provided in supplementary materials (S5-1.3). To establish the 3D-QSAR

models, the molecular structures and LibDock scores of SMs' estrogen activity (SM-E), SMs' progesterone activity (SM-P), and SMs' combined activities (estrogen and progesterone) (SM-C) were selected as independent and dependent variables, respectively. As the inputs of the multi-activity 3D-QSAR model, the LibDock scores of SM-C were obtained based on G1-anti-entropy weight method by calculating the comprehensive weights of the combined parameters (progesterone and estrogen). A single weight setting cannot guarantee the objectivity and comprehensiveness of the results. This study thus comprehensively considered subjective and objective weights, and finally used joint weights for characterization. Progesterone plays a crucial role in regulating and maintaining gestation (Lim, 2020). Therefore, the subjective weighting for progesterone and estrogen was set as 0.7 and 0.3, respectively. The objective weightings of progesterone and estrogen were both set as 0.5. According to the G1-anti-entropy weight method, the comprehensive weighting can be calculated as 0.6 and 0.4 for progesterone and estrogen, respectively. All the obtained data were normalized before calculating the objective weightings. Detailed calculation regarding the G1-anti-entropy weight method can be found in the supplementary material (S5-1.4).

The 39 SMs' molecular structures used for model construction (Table S5-1) were drawn and optimized in SYBYL- X2.0. For estrogen 3D-QSAR model, the whole data set (n=23) was divided into a training set (18 compounds) for 3D-QSAR model generation and a test set (5 compounds) for model validation. The target compound (SM-25) with the highest value was selected as the template molecule. For progesterone 3D-QSAR model, the whole data set (n=39) consisted of a training set (30 compounds) and a test set (10 compounds). The template compound is SM-43. In the multi-activity 3D-QSAR model, the whole data set (n=31) included a training set (24 compounds) and a test set (7 compounds) for model validation. The template compound is MK (details are shown in S5-1.5). The optimization

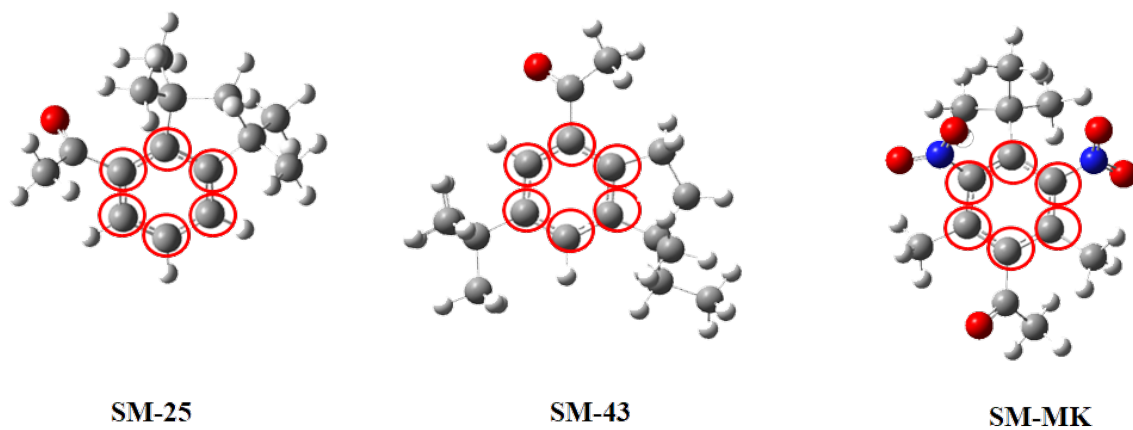


Figure 5-1 The structure and the alignment of the common molecular skeleton of template molecules SM-25, SM-43 and MK

of SMs was performed using the Tripos force field and Gasteiger-Hückel charges (Safavi-Sohi and Ghasemi, 2013). The Powell's method was used with a maximum of 10,000 optimizations and an energy convergence gradient value of 0.005 kJ/mol, and all the rest parameters were set to default values (Li et al., 2021b). For each 3D-QSAR model, the template SM molecules with common molecular skeletons were labeled (shown in Figure 5-1).

For each constructed model, the LibDock scores of the SMs (both in training and test sets) were introduced to performance evaluation and molecular validation by SYBYL-X2.0. Partial least-squares regression analysis was applied to establish the relationships between the structures and abortion risks of the associated compounds (Li et al., 2020b). The leave-one-out method was used to cross-validate the training set and determined the values of cross-validation coefficient q^2 (Nnadi et al., 2018). The non-cross-validation analysis was then conducted to obtain the non-cross-validation r^2 , F-test value (F), and standard error of estimate value (SEE) (Cheng et al., 2018). The standard error of prediction (SEP) of the cross-validation of the input and predictive values of the selected SMs (test set) and the external predictive set cross-checking coefficient (R^2_{pred}) were used as the parameters for indicating the ability for external prediction of the constructed comparative molecular similarity indices analysis (CoMSIA) model (Zhao et al., 2020).

5.2.3.2. Design of derivatives with reduced abortion risk and improved environmental and functional properties

Among the 39 molecular structures, SM-6 (i.e., (4S, 7R)-HHCB) and MK, two of most widely used SMs, were selected as precursors for molecular modification. New derivatives with lower abortion risk were designed based on the descriptor fields information (i.e., hydrogen bond donor and acceptor, electrostatic, steric, and hydrophobic fields) presented in the contour maps generated by the CoMSIA model. To verify that these derivative

molecules can be generated and stably exist in the environment, the frequency of these new derivatives was calculated using Gaussian 09[®] software based on density functional theory at the b3pw91/6-31G* unit level (Gu et al., 2019).

The derivatives with lower abortion risk and positive frequency were then assessed by two environmental property indicators, including migration ability ($\log_{\text{vapor pressure}}$, named as $\log VP$), and bioaccumulation ability ($\log BCF$), predicted by 3D-QSAR models (Li et al., 2021a). Besides the ecological impacts, the functional properties of SMs, including odor stability, musky scent, and odor intensity (Li et al., 2021a) were also predicted to determine their performance as an additive in personal care products.

5.2.4 Reduction of spontaneous abortion risk by integration of supplementary diet plans and molecular modification

After a comprehensive screening in section 5.2.3, the derivative with the lowest abortion risk and most improved environmental and functional properties was selected. This derivative and the three highly recommended supplementary diet plans obtained from section 5.2.2 were then used to demonstrate the integration of SM molecular modification and supplementary diet plans for further reduction of the abortion risk. Molecular docking of the new derivative using progesterone and estrogen as indicators with/without each selected supplementary diet plan was conducted. Results were compared to obtain the best abortion risk reduction plan.

5.3 Results and Discussion

5.3.1 Establishment of relationships between SMs and their abortion risk to pregnant women

The relationships between SMs and their abortion risk to pregnant women were represented by LibDock scores, a parameter reflecting the binding ability between the two.

LibDock scores of SMs docked to estrogen receptor (SM-E) and SMs docked to progesterone (SM-P) were obtained using the molecular docking method in Discovery Studio® 2020. After obtaining the LibDock scores of SM-P and SM-E, the LibDock scores of SM-C were calculated based on G1-anti-entropy weight method by calculating the comprehensive weights of the combined parameters (LibDock scores of progesterone and estrogen). These LibDock scores of SM-P, SM-E and SM-C were shown in Table S5-2. As shown in Table S5-2, except for SM-25 and SM-30, the LibDock scores of the remaining 37 SMs with estrogen (SM-E) were higher than those of progesterone. The average LibDock score of SMs with estrogen (1.954) was also higher than that of progesterone (1.912). The findings illustrated that estrogen was more affected by SMs than progesterone.

The LibDock scores and binding energies of SMs and AChE enzymes were calculated to demonstrate the feasibility of using the LibDock scores between SMs and two proteins (progesterone and estrogen) to represent the abortion risk. The constructed 2D-QSAR model provided the correlation of LibDock scores-binding energies of 74 SMs and the AChE enzyme obtained from shrimps (Table 5-1). An equation was established as follows:

$$\text{LibDock Score} = -0.215 \text{ Binding Energy} + 54.317 \quad (5-1)$$

In the 2D-QSAR model of SMs molecular toxicity to shrimp, R is 0.463 ($n=74$, $\alpha=0.01$, $r_{\min}=0.463 > r_0: 0.298$), which meets the statistical requirements. Statistical significance is 0.000 (<0.05), demonstrating it is a significance test (Calao-Ramos et al., 2021). As predicted (in section 5.2.1), the above statistical results exhibited a significant negative correlation between the LibDock score and the binding energy of SMs and the AChE enzyme. In other words, the greater the docking score, the smaller the binding energy. The results showcased a good correlation between the docking score values and binding energies when predicting the toxicity of SMs to shrimp. It is thus reasonable to use LibDock scores to replace binding energies to represent the abortion risk.

Table 5-1 The LibDock scores and binding energies of 74 complexes (SMs to the AChE enzyme)

SM complexes	LibDock scores	Binding energy (kJ/mol)	SMs complexes	LibDock scores	Binding energy (kJ/mol)
SM-1	86.28	-106.44	SM-45	79.30	-102.51
SM-2	72.03	-117.14	SM-46	63.82	-107.94
SM-3	72.04	-116.68	SM-47	66.69	-83.55
SM-4	74.54	-72.77	SM-48	56.18	-107.11
SM-5	87.33	-58.19	SM-49	72.86	-111.38
SM-6	97.28	-137.39	SM-50	70.70	-99.38
SM-8	79.92	-134.33	SM-51	80.07	-131.44
SM-9	75.16	-95.10	SM-52	70.91	-137.57
SM-10	74.94	-126.22	SM-53	63.42	-112.84
SM-11	79.31	-101.18	SM-55	81.28	-114.93
SM-12	58.44	-90.98	SM-56	80.70	-140.83
SM-13	69.93	-133.16	SM-57	80.75	-134.35
SM-15	91.42	-117.05	SM-58	70.70	-110.24
SM-16	60.40	-107.38	SM-59	78.63	-115.52
SM-17	86.28	-30.58	SM-60	57.11	-99.22
SM-18	90.71	-117.15	SM-61	88.92	-134.18
SM-19	74.94	-120.51	SM-62	87.68	-131.49
SM-20	67.35	-70.47	SM-63	74.54	-103.72
SM-25	64.78	-68.85	SM-64	75.59	-133.89
SM-26	58.02	-85.89	SM-65	100.10	-150.55
SM-27	60.45	-122.33	SM-66	97.99	-136.05
SM-28	64.28	-91.66	SM-72	96.03	-134.89
SM-29	89.13	-106.11	SM-73	98.34	-151.70
SM-31	79.84	-150.15	SM-74	88.55	-142.90
SM-32	88.76	-125.56	SM-75	82.48	-124.71
SM-33	89.89	-119.55	SM-76	77.08	-109.28
SM-34	78.62	-105.20	SM-77	82.07	-137.29
SM-35	86.29	-103.93	SM-80	78.39	-106.16
SM-36	89.77	-136.99	SM-81	86.69	-163.48
SM-37	78.50	-128.63	SM-82	96.83	-131.94
SM-38	77.85	-119.71	SM-83	95.26	-121.29
SM-39	84.30	-138.01	SM-84	78.40	-146.75
SM-40	78.07	-99.33	SM-85	90.11	-149.07
SM-41	84.06	-94.91	SM-86	97.28	-147.56
SM-42	78.25	-116.99	SM-87	80.11	-122.57
SM-43	79.29	-120.58	SM-88	96.71	-135.04
SM-44	73.42	-86.62	SM-89	64.24	-82.83

5.3.2 Reduction of spontaneous abortion risk by supplementary diet plans

5.3.2.1 Design and evaluation of supplementary diet plans

The LibDock scores of five SMs including Phantolide (PHAN), celestolide (ADBI), tonalide (AHTN), galaxolide (HHCB), and musk ketone (MK) to two proteins (i.e., progesterone and estrogen) with the addition of supplementary diet plans were obtained using molecular docking. For each SM and one target protein, 12 supplementary diet plans were designed respectively using L₁₂ Taguchi experimental design. A total of 120 groups (12 supplementary plans × 5 SMs × 2 proteins) were designed. The LibDock score as an indicator of binding ability was used to reflect the risk of spontaneous abortion. The lower the LibDock score, the lower risk of spontaneous abortion.

Results of docking with progesterone receptor protein (Figure 5-2) show that the LibDock score of PHAN, ADBI, AHTN, HHCB, and MK to progesterone receptor protein without any supplementary diet plan (control group) is 89.2688, 92.4485, 92.8215, 91.0730, and 71.5961, respectively. LibDock scores of these SMs under the other 11 supplementary diet plans were compared with these of the control group. Among them, the LibDock scores of PHAN and progesterone receptor protein under 9 supplementary diet plans were decreased from 0.82% to 28.03%. The LibDock scores of ADBI and progesterone receptor protein under 10 supplementary diet plans were decreased from 4.48% to 23.69%. The LibDock scores of AHTN and progesterone receptor protein under 10 supplementary diet plans were decreased from 0.27% to 23.49%. Under 8 supplementary diet plans, the LibDock scores of HHCB and progesterone receptor protein were decreased from 7.11% to 20.86%. The LibDock scores of MK and progesterone receptor protein under 10 supplementary diet plans were reduced from 5.28% to 47.63%.

The LibDock scores (Figure 5-2) of PHAN, ADBI, AHTN, HHCB, and MK to estrogen receptor protein without any supplementary diet plan (control group) was 79.8070, 86.4039,

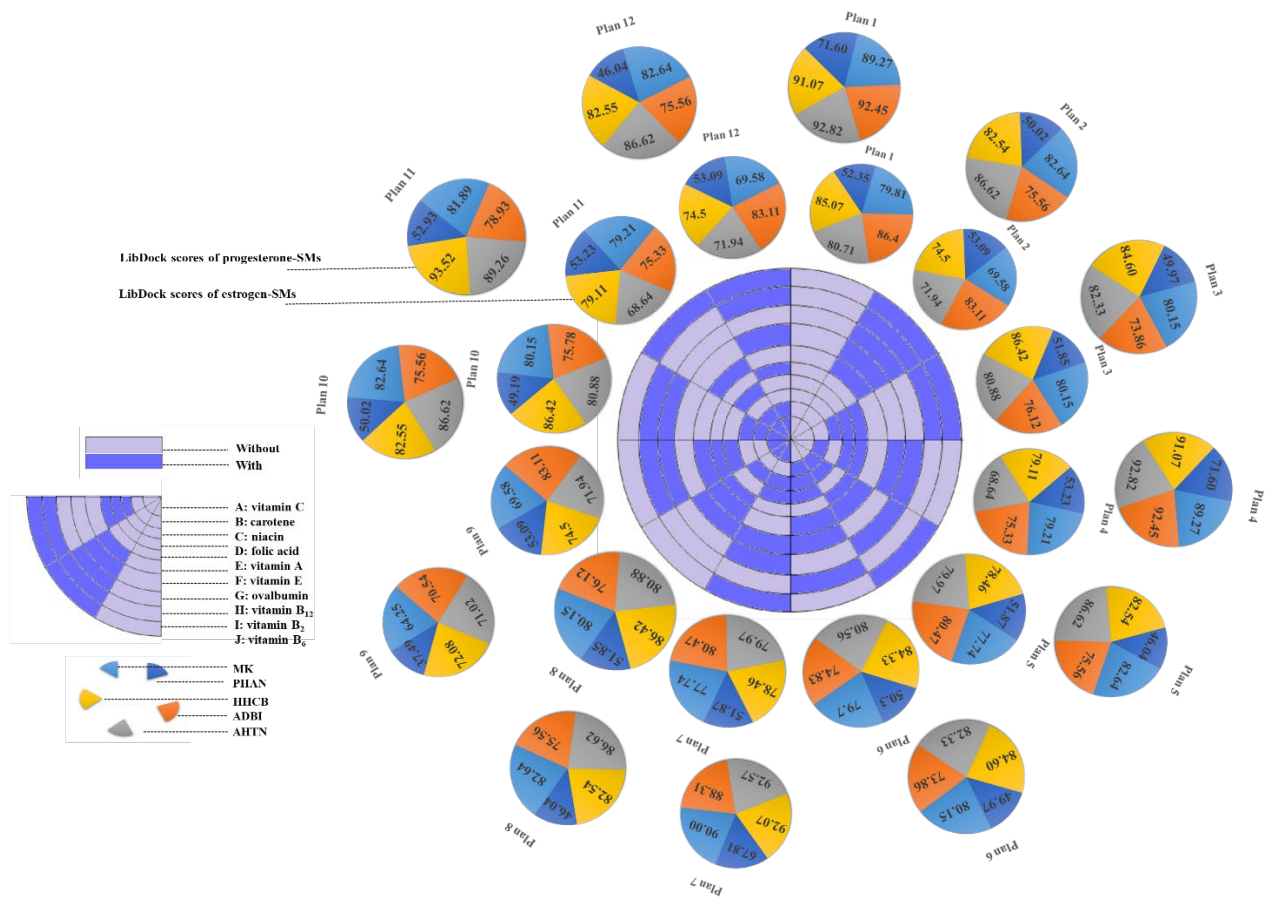


Figure 5-2 LibDock scores of SMs with progesterone and estrogen under supplementary diet plans based on L₁₂ Taguchi experimental design.

80.7110, 85.0710, and 52.3487, respectively. Compared with the control group of estrogen, the LibDock scores of PHAN, ADBI, AHTN, HHCB to estrogen under 8 supplementary diet plans were further reduced. The LibDock score values decreased between 0.13%~12.81%, 3.81%~13.40%, 0.19%~14.96%, and 0.87%~12.43% for PHAN, ADBI, AHTN, HHCB, respectively. Similarly, the LibDock scores of MK to estrogen receptor protein under 10 supplementary diet plans were decreased from 0.91% to 6.03%. The molecular docking results show that under the above-mentioned supplementary diet plans, the binding ability of SMs with progesterone and estrogen could be significantly inhibited. Thereby, such diet can help to reduce the risk of spontaneous abortion caused by SMs. Three recommended supplementary diet plans (i.e., P8, P9, and P12) with lower LibDock score values compared with control group were selected for further analysis.

To verify whether the supplementary diet plans can reduce the risk of SMs to two proteins at the same time, the comprehensive LibDock scores (SM-C) were calculated using the G1 method. The signal-to-noise ratio (SNR) is used to identify control factors that reduce variability in products or processes by minimizing the effects of uncontrollable factors (noise factors). The smaller the SNR is, the larger the binding energy of the system is, and thus less effect to the system is attributed from the experimental design conditions (Li et al., 2021a). Therefore, the SNR was used as evaluating indicator for the binding energy of SM-C. In Table S5-3, Delta is the absolute average of two signal-to-noise ratios under levels 1 and 2 (with/ without supplement diet). The “Ranking” reflects the importance of 10 anti-fetus supplementary components (i.e., vitamin C, carotene, niacin, folic acid, vitamin A, vitamin E, ovalbumin, vitamin B₁₂, vitamin B₂, and vitamin B₆ as A-J). According to Table S5-3, the rank of the external stimulation conditions influences the binding energy of PHAN-two proteins from large to small was: vitamin B₂, followed by vitamin E, vitamin B₆, vitamin C, vitamin A, vitamin B₁₂, niacin,

ovalbumin, carotene, and folic acid. For ADBI, the most effective supplement was niacin, followed by carotene, vitamin E, vitamin B₂, folic acid, vitamin A, vitamin C, ovalbumin, vitamin B₆, and vitamin B₁₂. For AHTN, the most effective supplement was vitamin B₂ followed by vitamin E, vitamin A, niacin, carotene, folic acid, vitamin B₆, vitamin B₁₂, ovalbumin, and vitamin C. For HHCB, the most effective supplement was vitamin B₁₂, followed by niacin, vitamin B₆, vitamin E, vitamin A, ovalbumin, vitamin B₂, vitamin C, carotene, and folic acid. For MK, the most effective supplementary was niacin followed by vitamin B₂, vitamin E, vitamin C, folic acid, ovalbumin, vitamin B₁₂, vitamin B₆, vitamin A, and carotene. Based on the results, it can be deduced that vitamin E, vitamin B₂, niacin, vitamin A and vitamin B₆ can not only provide the necessary nutrients for human health but also can be integrated into the supplementary diet for pregnant women for a reduced spontaneous abortion risk brought by SMs.

5.3.2.2. Validation of reliability LibDock scores reflecting spontaneous abortion risk reduction by supplementary diet plans

The reliability of LibDock scores obtained by molecular docking were further validated through their comparison with associated binding energies generated by molecular dynamics simulation. Two complexes (HHCB docking with progesterone and MK docking with progesterone), and three recommended supplementary diet plans were selected for conducting molecular dynamics simulation. Results showed that the binding energy of HHCB molecule and progesterone of the control group (without any supplementary diet) was -78.15 kJ/mol, and the binding energy of the selected diet plan 8, 9, and 12 (P8, P9, and P12) was -60.98 kJ/mol, -53.10 kJ/mol, and -72.39 kJ/mol, respectively. Comparing with the control group, the binding energy of P8, P9, and P12 was reduced by 21.97%, 32.05%, and 7.37%, respectively. The

binding energy of MK molecule and progesterone in the control group was -50.9820 kJ/mol. The binding energy of P8, P9, and P12 was -39.79 kJ/mol, -45.46 kJ/mol, and -47.27 kJ/mol, respectively, with a reduction of 21.95%, 10.84%, and 7.28%, respectively, compared with the control group. The above findings show a consistent trend of the LibDock scores indicated in section 5.3.2.1. This further validated that the LibDock score can replace binding energy to reflect the SM-caused spontaneous abortion risk.

5.3.3 Reduction of spontaneous abortion risk by designing SM derivatives through 3D-QSAR modelling

5.3.3.1 Construction and evaluation of 3D-QSAR models

The single and multi-activity 3D-QSAR models were constructed using SYBYL-X2.0 software for designing SM derivatives. The constructed multi-activity 3D-QSAR model overcomes the limitations of generating molecules based on a single-effect model because it focuses on the multiple effects of pollutants. The two constructed single-activity 3D-QSAR models were used to provide more accuracy (substitution sites information from the contour maps) for designing derivatives and verifying the results of the multi-activity 3D-QSAR model.

Molecular structure of SMs and LibDock scores of SM to the target protein (i.e., estrogen, progesterone, estrogen-progesterone) were used as the inputs for constructing 3D-QSAR models. The LibDock scores of the selected SMs molecule to estrogen receptor (SM-E) and progesterone (SM-P), progesterone and estrogen (SM-C) were shown in Table S5-2.

To evaluate the predictive ability of the constructed models, the model evaluation parameters were given and shown in Table 5-2. Generally, we believe that a model can be confirmed to have a credible predictive ability when its cross-validation coefficient $q^2 > 0.5$ and the non-cross-validation $r^2 > 0.9$ and close to 1.000 (Salahinejad et al., 2014). In this study, q^2

Table 5-2 Statistical parameters for performance evaluation of the constructed 3D-QSAR models.

Models	SEE^{*1}	F^{*2}	$R^2_{pred}^{*3}$
SM-P	0.003	213.974	0.975
SM-E	0.001	2215.361	0.728
SM-C	0.016	2245.224	0.665

Note: ^{*1} refers to standard error of estimate; ^{*2} refers to F-value; ^{*3} refers to external test coefficient.

(for progesterone, estrogen as well as the SM-C) is 0.756, 0.760, and 0.754, respectively. The r^2 of progesterone, estrogen as well as the SM-C is 0.991, 1.000, and 0.995, respectively. These results indicated that the model has a good predictive ability. In addition, low standard error of estimate (*SEE*), high F-test value and high external test coefficient R^2_{pred} (greater than 0.6) were also obtained, representing a good fit ability and predictive ability of the model. Figure S5-2 showed the scattered dots figure of the training set and test set of SM-E, SM-P and SM-C models. In the regression model, r^2 of SM-E, SM-P and SM-C were 0.9997, 0.9923, and 0.9797, respectively, indicating a good internal predictive ability of the generated 3D-QSAR models and proving their applicability in predicting the abortion risks of SM derivatives.

5.3.3.2 Design of SM derivatives with reduced abortion risks using 3D-QSAR models

Based on the constructed 3D-QSAR models, including the SM-P CoMSIA, SM-E CoMSIA and the SM-C CoMSIA ones, the contribution of the hydrophobic, acceptor, electrostatic and steric field was obtained and shown in Table S5-4, respectively. HHCB and MK are two of the most widely used SMs in the world market (Li et al., 2021b) with toxicity concerns (Fan et al., 2019). Therefore, HHCB and MK were adopted as example SMs to construct all the three 3D-QSAR models. All the contour maps in the three 3D-QSAR models were considered for the determination of SMs molecular modification sites and groups. In order to ensure the integrity of the functional property (i.e., musky odor) and parent structure of SMs (Li et al., 2021a), this study firstly selected the methyl groups (-CH₃) that can be substituted on the branched chains for modification. The contour maps were then used to determine the modified sites of HHCB and MK. Figure 5-3 shows the contour maps of three 3D-QSAR models of HHCB and MK. Figure 5-3 shows the contour maps of three 3D-QSAR models of HHCB and MK. In the electrostatic field, the blue area indicates that the addition of negative groups is beneficial to decrease the LibDock score of SMs, and the red area indicates that the addition of positive groups is beneficial to the LibDock score of SMs. In the steric field, the green area indicates

that the introduction of smaller molecular groups in this area can decrease the LibDock score, while the yellow area indicates that the introduction of bigger molecular groups in this area can increase the LibDock score of SMs. In the acceptor field, the purple area suggested that the introduction of hydrogen bond acceptors in this area can increase the LibDock score, while the red area showed that the introduction of hydrogen bond acceptors in this area could decrease the LibDock score of SMs. In the hydrophobic field, the yellow area emphasizes that the introduction of hydrophobic groups in this area can increase the LibDock score, while the white area indicates that the introduction of hydrophilic groups in this area can increase the LibDock score of SMs.

The contour maps indicated the available HHCB or MK molecular modification sites. Through modifying of the applicable groups for substations at the available sites, SM derivatives could be generated. The groups for HHCB and MK substitution were identified and numbered based on the information collected from the contour maps (i.e., Figure 5-3), and was highlighted in Figure 5-4. The substitution sites were named as 1-, 2-, and 3-, for HHCB (Figure 5-4a), and 1-, 2-, 6-, 7-, and 9- for MK, respectively (Figure 5-4b). The 1-, 2-, and 3- of HHCB were surrounded by yellow, white and purple, suggesting substitution of $-OCH_3$ and $-NO_2$. For MK molecule, 1-position was surrounded by white, purple, 2-position was surrounded by purple, 6- and 7- sites were surrounded by yellow, white and purple, and 9- position was surrounded by yellow. Thus, $-OCH_3$, and $-NO_2$ can be introduced at the 1-, 7-position substituent of MK. The $-NH_2$, $-COOH$, $-OH$, $-CHO$, $-COCH_3$, $-CONH_2$, $-NO_2$, and $-OCH_3$ can be introduced at the 2-position substituent of MK. The $-NO_2$ can be introduced at the 6-position, and $-COOH$, $-C_3H_7$, $-C_4H_9$, $-C_5H_{11}$, and $-CH_2OH$ can be introduced at the 9-position substituent of MK. A total of 69 derivatives (i.e., 26 HHCB and 43 MK ones) were generated. HHCB derivatives include Derivative-1 to Derivative-26 and MK derivatives include Derivative-27 to Derivative-69. Derivatives with lower LibDock scores and decreased abortion risks were eventually selected.

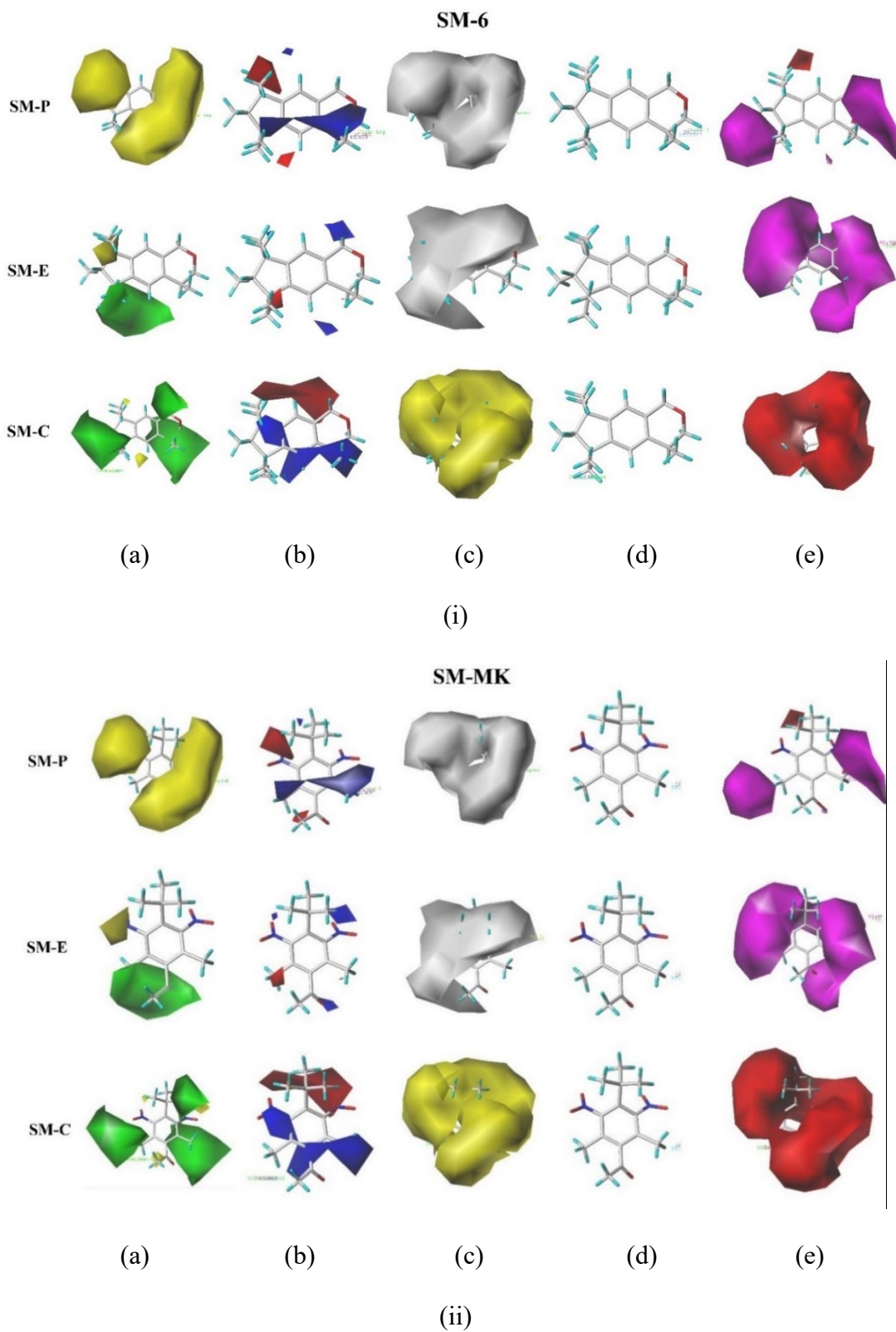


Figure 5-3 (i) The contour maps of HHCB; (ii) the contour maps of MK

*(a): steric field, (b): electrostatic field, (c): hydrophobic field, (d): donor field, (e): acceptor field.

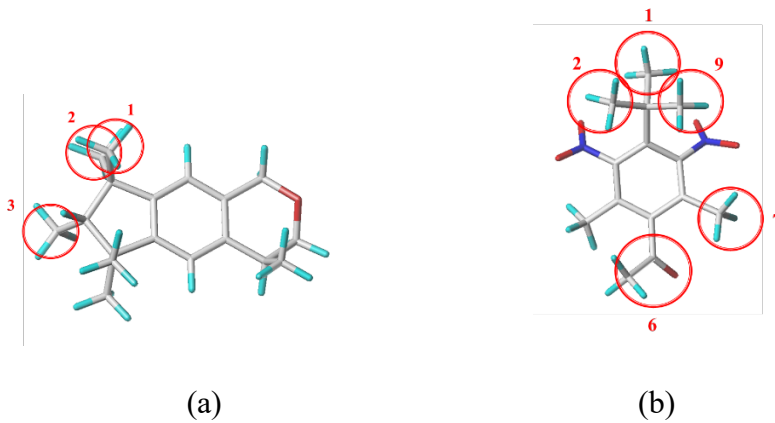
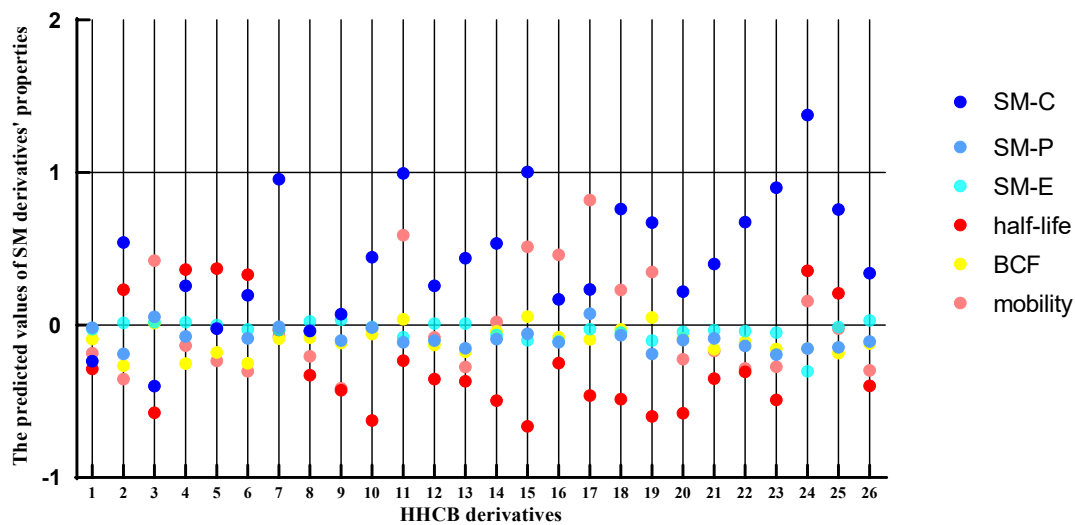


Figure 5-4 The substituted sites of HHCB (a) and MK (b).

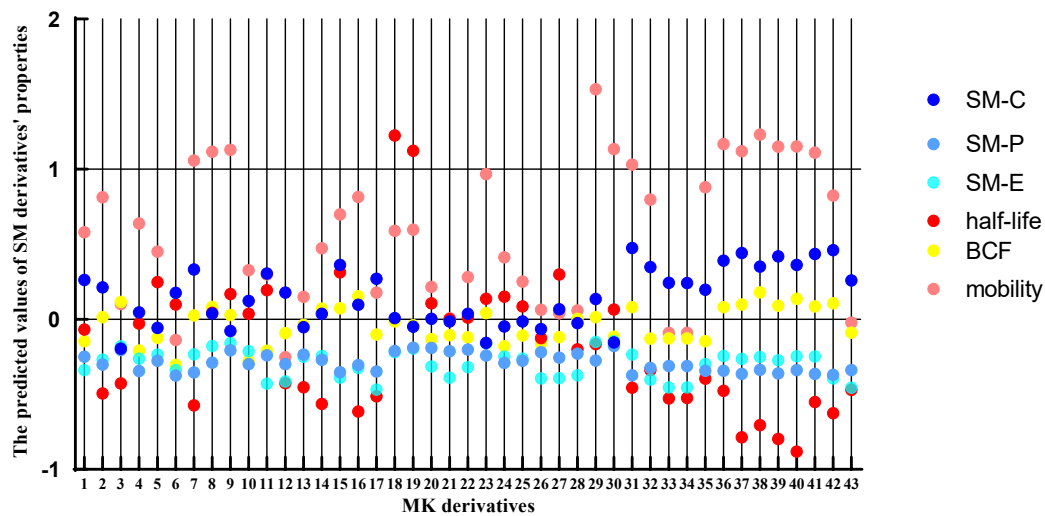
5.3.3.3 Selection of SM derivatives with lower abortion risks and improved environmental and functional properties

The 69 designed SM derivatives were further screened to obtain the ones with low abortion risk (low LibDock scores). Among designed derivatives, 3 ones, namely Derivative-6 (of HHCB), Derivative-24 (of HHCB) and Derivative-53 (of MK) were selected based on their lower LibDock scores as results of the 3D-QSAR models. A sharp reduction of the binding ability (137.67%) between the molecule and progesterone-estrogen was reported on Derivative-24. Further, Derivative-24 showed a lower SM-E (-3.78%) and SM-P (-8.02%) value compared with that of HHCB. The DS software was then used to calculate the LibDock scores of Derivative-24 with progesterone and estrogen, in order to verify the consistency of the predicted value obtained from 3D-QSAR models. The LibDock score (obtained from DS software) of Derivative-24 with estrogen (82.36) and progesterone (83.00) was decreased 3.18% and 8.87%, respectively. It is basically consistent with the 3D-QSAR model prediction results, indicating that the 3D-QSAR models constructed in this paper are extremely reliable. Therefore, Derivative-24 was regarded as a better molecule than all others for abortion risk reduction.

Besides the prediction of abortion risk, improved environmental properties were considered. The bioconcentration factor ($\log BCF$) and mobility ($\log VP$) of SMs were used to reflect the environmental properties in the 3D-QSAR models. According to Figure 5-5, Derivative-6 has lower environmental concerns (-25.15% of $\log BCF$ and -30.35% of $\log VP$). Derivative-53 has a similar performance to Derivative-6 but with a tiny increase of $\log VP$ (increased 3.87% compared to MK). Derivative-24 with the best performance of decreasing binding ability, and lower bioconcentration ability (-15.49%) were selected as the optimum SM derivative for further analysis. In Figure 5-5, the change rate of $\log BCF$ as an example can be calculated as follow:



(a)



(b)

Figure 5-5 The predicted values of change rates of LibDock scores (SM-C, SM-P, and SM-E), functional and environmental properties of (a) HHCB derivatives and (b) MK derivatives.

$$\text{Change rate of } \log BCF (\%) = (\log BCF \text{ value of SM derivatives} - \log BCF \text{ value of SM precursor}) / \log BCF \text{ value of SM precursor} \quad (5-2)$$

In addition, functional properties of the selected Derivative-24, including odor stability, musky scent, and odor intensity, were also predicted. Derivative-24 was proved has musky scents by using the criteria from Li et al. (2021a). The odor stability was reflected using the half-life with an increase of 35.58% for Derivative-24, and Derivative-24 had a musky scent after applying the criteria suggested by Li et al. (2021a). The odor intensity was used to reflect using the frequency value of a molecular structure, which could be calculated using Gaussian 09[®] software based on density functional theory (Gu et al., 2019). According to Li et al. (2021a), when the polycyclic compound has a positive frequency value, the higher the energy gap value, the lower the odor intensity of the fragrance. Derivative-24 with the energy gap of 4.42eV and a positive frequency value of 28.77 was suggested to have a stronger odor intensity compared with HHCB (the energy gap, 6.01 eV). Thus, Derivative-24 was selected with lower abortion risks and improved environmental and functional properties.

5.3.3.4 Toxic mechanism of SMs before and after molecular modification

The mechanism for the reduced abortion risk of SM derivatives was investigated. Progesterone, which plays a major regulatory role in preventing pregnant women from abortion, was taken as the target protein (Figure 5-6). During the binding process of HHCB with progesterone, the main types of amino acids involved in the interaction were isoleucine (ILE: non-polar, hydrophobic), aspartic acid (ASP: negatively charged in polarity, hydrophilic), valine (VAL: non-polar, hydrophobic), leucine (LEU: non-

polar, hydrophobic), phenylalanine (PHE: non-polar, hydrophobic), Glutamine (GLN: polar uncharged, hydrophilic), proline (PRO: non-polar, hydrophobic), methionine (MET: non-polar, hydrophobic), serine (SER: extremely Uncharged, hydrophilic), tryptophan (TRP: non-polar, hydrophobic), glycine (GLY: polar uncharged, hydrophilic), arginine (ARG: polar positively charged, affinity Water-based), glutamic acid (GLU: negatively charged in polarity, hydrophilic), and lysine (LYS: positively charged in polarity, hydrophilic) (Gu et al., 2020b). During the binding process of SM-24 with progesterone, the main types of amino acids involved in the interaction were isoleucine (ILE: non-polar, hydrophobic), phenylalanine (PHE: non-polar, hydrophobic), serine (SER: polar uncharged, hydrophilic), valine (VAL: Non-polar, hydrophobic), phenylalanine (PHE: non-polar, hydrophobic), arginine (ARG: polar positively charged, hydrophilic), glutamic acid (GLU: polar negatively charged, hydrophilic). The above analysis results showed that during the binding process of HHCB with progesterone, there were 17 key amino acids formed around the HHCB molecule, and the formation rates of hydrophilic and hydrophobic amino acids were 41.18% and 58.82%, respectively. There were 12 key amino acids formed around the SM-24 molecule, and the formation rates of hydrophilic and hydrophobic amino acids are 50.00% and 50.00%, respectively. The key amino acids formed around the HHCB are more than those of Derivative-24, showing that there are more interactions between HHCB and progesterone. This result fully explained the reason why the LibDock score of HHCB to progesterone is smaller than that of Derivative-24 to progesterone. In addition, the formation rate of hydrophilic amino acids around Derivative-24 was

higher than that of HHCB. The hydrophilic environment may reduce the interaction between SMs and progesterone. This reduced the abortion risk in pregnant women.

In addition, the formation rate of hydrophilic amino acids around Derivative-24 was higher than that of HHCB. The hydrophilic environment may reduce the interaction between SMs and progesterone. This reduced the risk of spontaneous abortion in pregnant women. The above ligand-acceptor interaction mechanism provided new ideas for the development of SMs derivative. During the development of new compounds, not only the steric field, electrostatic field, hydrophobic field, hydrogen bond donor field and acceptor field, but also the influence of factors such as hydrophilicity and hydrophobicity on the molecular activity of SMs derivatives should be considered.

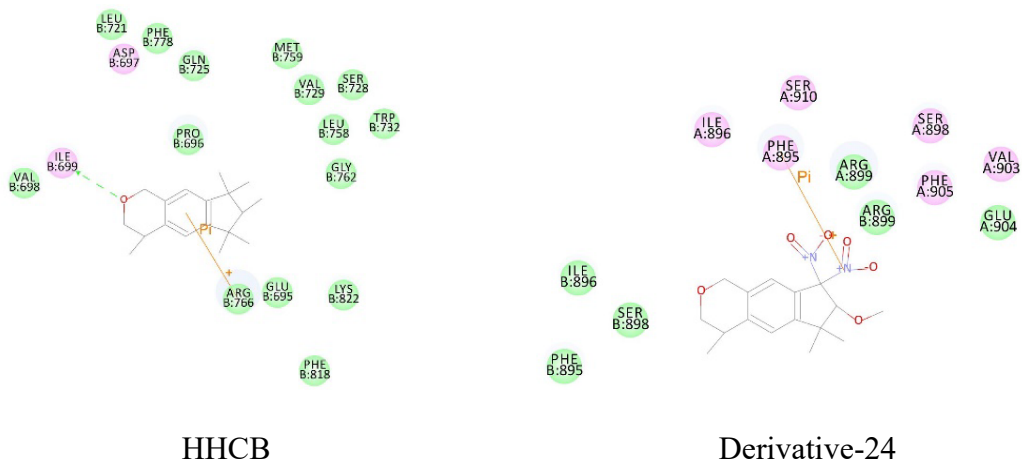


Figure 5-6 Verification of the binding mechanism of HHCB and its derivatives with progesterone.

5.3.4 Reduction of spontaneous abortion risk by integration of supplementary diet plans and molecular modification

The effectiveness of supplementary diet plans on SM derivatives was investigated in this study. The LibDock scores of SM derivative (i.e., Derivative-24) to the target protein (i.e., progesterone or estrogen) under the three highly recommended supplementary diet plans (i.e., P8, P9, and P12) were calculated using the molecular docking method.

The molecular docking results showed that the LibDock scores of Derivative-24 with progesterone and estrogen without supplementary diet plans were 83.00 and 82.36, respectively. Among the three supplementary diet plans, the LibDock scores for Derivative-24 with progesterone (73.58) and estrogen (80.06) in P8 were decreased by 11.35% and 2.80%, respectively, compared with the blank control group. In P9, the LibDock scores for Derivative-24 with progesterone (72.28) and estrogen (78.39) were decreased by 12.92% and 4.82%, respectively, compared with the blank control group. In P12, the LibDock scores for Derivative-24 with progesterone (66.58) and estrogen (78.79) were decreased by 19.78% and 4.33%, respectively, compared with the blank control group. The above results indicated that the three groups of optimal supplementary diet plans could effectively inhibit the binding ability of Derivative-24 with progesterone and estrogen receptor proteins. Among the three supplementary diet plans, the supplementations mainly included vitamin C, niacin, vitamin A, vitamin E, and ovalbumin in P8; vitamin C, folic acid, vitamin A, vitamin E, vitamin B₁₂, and vitamin B₂ in P9; vitamin C, carotene, vitamin A, ovalbumin, vitamin B₂, vitamin B₆ in

P12. The results showed that vitamin C and vitamin A were the main factors inhibiting the binding of Derivative-24 to progesterone and estrogen. According to the nutrient composition table, spinach and apples are rich in vitamin C and vitamin A, respectively. Therefore, it is recommended that pregnant women should eat more foods rich in vitamin C and vitamin A, which can effectively reduce the spontaneous abortion risk caused by SMs.

The LibDock scores of the HHCB with progesterone and estrogen without the supplementary diet plan were 91.07 and 85.07, respectively. Compared with HHCB, the LibDock scores of Derivative-24 with progesterone and estrogen decreased 8.02% and 3.78%, respectively. The LibDock scores of Derivative-24 with progesterone under the three supplementary diet plans were reduced by 19.21%, 20.64%, and 26.89%, respectively. The LibDock scores of Derivative-24 with estrogen under the three supplementary diet plans were reduced by 5.90%, 7.85%, and 7.38%, respectively. These results proved that, the abortion risk of HHCB derivatives (i.e., Derivative-24) under supplementary diet plans was much lower than that without supplementary diet plans. Therefore, there was a significant synergistic effect of supplementary diet plans and molecular modification. Both supplementary diet plans and molecular modification can help to effectively inhibit the binding ability between SMs and progesterone and estrogen, resulting in lower risks of spontaneous abortion in pregnant women.

5.4 Summary

SMs have been identified as substances with emerging risks to human health in recent years. Human exposure to SMs, particularly for special groups such as pregnant

women, through using personal care products could encourage the bioaccumulation of SMs and pose a hidden threaten to abortion. Nevertheless, effective risk control measures remain to be blank. In this chapter, a theoretical circumvention strategy was established to reduce such abortion risk through 1) adopting a supplementary diet; 2) developing environmentally friendly new SMs derivatives; and 3) integration of (1) and (2) using molecular docking and 3D-QSAR models. The relationship between a healthy diet and the reduction of spontaneous abortion risk was firstly confirmed. The multi-activity 3D-QSAR model was developed as an innovative tool for the design and screening of SMs derivatives with better functional ability, lower environmental risks and lower abortion risk (i.e., lower binding ability between SM and two hormones progesterone and estrogen). In the end, a significant synergistic effect was identified between supplementary diet plans and molecular modification. The integration of the optimum chemical, Derivative-24, proved a much lower abortion risk than HHCB under each of the selected three supplementary food regulation plans. Such results demonstrated the proposed theoretical circumvention strategy could serve as the comprehensive abortion risk control measure through effectively inhibiting the interaction between SMs with progesterone and estrogen. It also provided scientific support for designing new pharmaceutical and personal care products.

Appendices

S5-1. Methodology

S5-1.1 Detailed steps of molecular dynamics simulation

Molecular dynamics simulations were conducted by using the Dell PowerEdge R7425 server and GROMACS software. The simulation experiments were constructed by simulating the binding ability between SMs (or SM derivatives) and target proteins (i.e., progesterone and estrogen) (Figure S5-1). Each binding energy was obtained using the Molecular Mechanics/Poisson-Boltzmann Surface Area (MMPBSA) method. The absolute values of binding energy were further used to represent the abortion risks. This provided valuable guidance for evaluating the abortion risks of SMs to pregnant women. The combined binding energy was calculated following the equation illustrated below (Gu et al., 2020b):

$$G_{\text{bind}} = G_{\text{complex}} - G_{\text{free-protein}} - G_{\text{free-ligand}} \quad (5-S1)$$

The binding free energy of the molecule can be determined as follows:

$$G = E_{\text{gas}} - TS_{\text{gas}} + G_{\text{solvation}} \quad (5-S2)$$

The solvation free energy can be calculated as follows:

$$G_{\text{solvation}} = G_{\text{polar}} + G_{\text{nonpolar}} \quad (5-S3)$$

S5-1.2 Establishment of relationships between SMs and their abortion risks to pregnant women

AChE is an important hydrolase widely existed in vertebrates and invertebrates in the process of nerve conduction. Exposure of AChE to sublethal concentrations of chemical pollutants will severely inhibit its conduction activity. Therefore, AChE was selected as the target protein to reflect the toxic effects of SMs on shrimps and uses

molecular docking and molecular dynamics methods to calculate the docking score and binding energy between SMs molecules and shrimps. The three-dimensional structure of AChE (ID: 2PH9) was collected from the PDB database.

AChE enzymes and 74 SMs molecules were loaded into Discovery Studio[®] 2020 software to obtain the docking score. After docking, the complexes of 74 SMs molecules and AChE enzyme were used as the ligand complex structure for the molecular dynamic (MD) simulation. The MD of the complex was performed using the GROMACS software, and the molecular mechanics Poisson-Poltz was used. The Mann Surface Area (MM-PBSA) method was used to calculate the binding energy of the simulation results (Westermaier et al., 2017). Specifically, MD needs to be carried out in boundary conditions. The Gromos96 force field was selected, and the protein-ligand complex was placed in a cube box (11.45 nm×11.45 nm×11.45 nm). The shortest distance between the box boundary and the complex was 1nm, and the side length of the box was 11.45nm. The box was then filled with water (SPC216). In order to make the entire system appear electrically neutral, sodium ions were added to replace the water molecules in the box. The simulation process consisted of four steps, namely energy minimization, canonical ensemble (NVT) temperature control, (isothermal–isobaric) NPT pressure control and MD balance simulation. The method used for energy minimization was the steepest descent method. When the energy converged to 1000 kJ/mol, the system energy was considered to have reached an equilibrium state. During the NVT and NPT processes, the protein-ligand complex was restricted by position. The pre-equilibrium conditions were set up as 300 K and 1 bar. The complexes of 74

SMs and AChE enzyme were conducted under 100 ps simulation. In the MD balance simulation, the position restriction was lifted. Under the conditions of well-balanced temperature and pressure, the two sets of complexes were simulated by the Leapfrog Newton integration method at 200 ps, with a simulation step of 2 fs and a simulation step of 100,000 steps. The binding energy results of the 74 complexes were calculated using MM-PBSA method. From 100 ps to 200 ps, frame extraction was performed every 10 ps, and a conformation was selected to calculate the binding energy. A total of 11 conformations were selected. The final binding free energy result was an average of 11 conformations. The MM-PBSA method is mainly used to calculate the van der Waals interaction, electrostatic interaction, non-polar solvation energy and polar solvation energy, to obtain the value of binding energy (Gu et al., 2020b).

In this study, the LibDock scores of SMs molecule and AChE enzyme in shrimp were used as the dependent variable, and the binding energy between the two was used as the independent variable. The gradual regression method was adopted to perform multiple linear regression to construct a Libdock scores-binding energy model using the two-dimensional quantitative structure-activity relationship (2D-QSAR) method. The 2D-QSAR model was conducted through SPSS analysis in PASW software. The relationship between Libdock scores and binding energy was then analyzed through the obtained correlation results.

S5-1.3 The principle and advantages of 3D-QSAR model

The 3D-QSAR model can be used to predict the performance or activities of unknown compounds based on the quantitative changes between structure and activity

(Kubinyi^a, 1997). In detail, a 3D-QSAR model can be firstly constructed according to the relationship between the structural characteristics and biological activities of compounds, and then the contour maps can be obtained (Kubinyi, 1997b). According to the information provided by the contour maps, we can accurately locate the modification sites that have a greater impact on the biological activity of the compound, and further obtain new compounds through the modification and transformation on the basis of existing compounds (Hou et al., 2020). After obtaining new compounds through molecular modification, the biological activities of new compounds can be predicted according to the established 3D-QSAR model. In a summary, there are two advantages of using the 3D-QSAR model as the molecular modification method. A model can be constructed only using the relationship between the compound and its biological activity based on the structural characteristics of the compound and the obtained contour maps. The 3D-QSAR models can also predict the biological activity of the designed derivatives, which assist in discovering and terminating the research on derivatives with unsatisfactory modification results to minimize the research costs and new compound development risks.

S5-1.4 Construction of 3D-QSAR models for designing SM derivatives with lower spontaneous abortion risk

a. Min-Max normalization

The Min-max standardization method was used in this study. After normalization, values of the LibDock scores were between 0 and 1. For every feature, the minimum value of that feature gets transformed into a 0, the maximum value gets transformed

into a 1, and every other value gets transformed into a decimal between 0 and 1. It is a deviation standardization, which makes the results fall to the interval [0, 1]. In the equations, “i” represents the molecule, and “j” represents protein in this study.

$$b_{ij} = \frac{x_{ij} - \min(x_i)}{\max(x_i) - \min(x_i)} \quad (\text{Higher better}) \quad (5-S4)$$

$$b_{ij} = \frac{\max(x_i) - x_{ij}}{\max(x_i) - \min(x_i)} \quad (\text{Lower better}) \quad (5-S5)$$

After standardization, the evaluation index should be:

$$0 \leq b_{ij} \leq 1 \quad (5-S6)$$

Then the matrix is normalized to $B = [b_{ij}]_{i \times j}$ (5-S7)

$$B = \begin{bmatrix} b_{11} & b_{12} & \cdots & b_{1j} \\ b_{21} & b_{22} & \cdots & b_{2j} \\ \vdots & \vdots & \ddots & \vdots \\ b_{i1} & b_{i2} & \cdots & b_{ij} \end{bmatrix} \quad (5-S8)$$

b. Determination of weighting of progesterone and estrogen

The G1 method is a comprehensive evaluation method to obtain the subjective and objective weights of various variables through the sequential analysis and the anti-entropy weight method. Then the subjective and objective weights were used to calculate the comprehensive weight of each indicator through the comprehensive weight function (Wang et al., 2021). Rajuddin et al. (2021) found the incidence of threatened abortion correlated to progesterone with the correlation strength of -0.838. To highlight the importance of progesterone, the subjective weight for progesterone and estrogen were set up as 0.3 and 0.7, respectively. The objective weight was calculated

based on anti-entropy weight method. Anti-entropy weight method is a developed method of entropy weight method. When the system is under n kinds of conditions, the probability of each condition is $(1, 2, \dots, n)$. The entropy can be calculated as

$$h'_t = -\sum_{i=1}^m p_{ij} \ln p_{ij} \quad (5-S9)$$

In which, $p_{ij} = \frac{b_{ij}}{\sum_{i=1}^i b_{ij}}$, b_{ij} are the elements of the standard index set $B = [b_{ij}]_{i \times j}$.

$$\lim_{p_{ij} \rightarrow 0} p_{ij} \ln p_{ij} = 0, \text{ when } p_{ij} = 0 \quad (5-S10)$$

$$\sum_{i=0}^i p_{ij} = 1, \text{ when } 0 \leq p_{ij} \leq 1 \quad (5-S11)$$

Calculate the anti-entropy of the criteria as follows,

$$h_t = -\sum_{i=1}^i p_{ij} \ln(1 - p_{ij}) \quad (5-S12)$$

The objective of each index s_j can be calculated:

$$s_j = \frac{1-h_t}{n-\sum_{i=1}^i h_t} \quad (1 \leq t \leq n) \quad (5-S13)$$

c. Determination of the comprehensive weights of the combined parameters (progesterone and estrogen)

The objective weighting w_j determined by the entropy method is combined with the subjective weighting j determined by the empirical method. The comprehensive weighting w_j of each detection type is finally determined as:

$$w_j = \xi s_j + (1 - \xi) o_j \quad (j = 1, 2) \quad (5-S14)$$

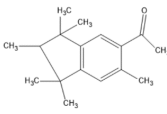
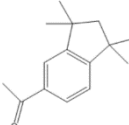
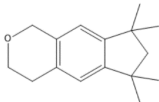
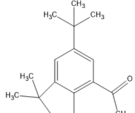
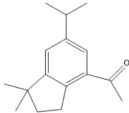
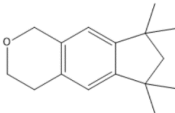
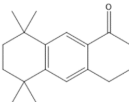
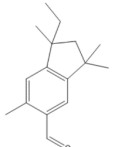
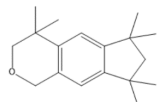
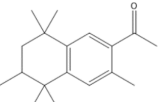
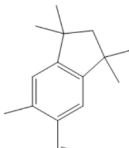
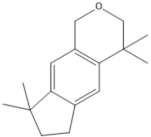
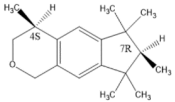
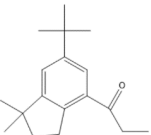
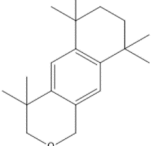
where ξ is the preference coefficient of the subjective weighting $\xi \in [0,1]$. A larger ξ

value indicates that the research focuses more on subjective weighting; conversely, a lower ξ indicates that decision makers should pay more attention to objective weighting.

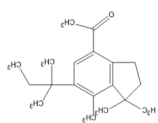
The indexes of combined effects can be then calculated as,

$$Z = B \cdot D = \begin{bmatrix} b_{11} & b_{12} & \cdots & b_{1j} \\ b_{21} & b_{22} & \cdots & b_{2j} \\ \vdots & \vdots & \ddots & \vdots \\ b_{i1} & b_{i2} & \cdots & b_{ij} \end{bmatrix} \cdot \begin{bmatrix} \omega_1 \\ \omega_2 \\ \vdots \\ \omega_j \end{bmatrix} = [e_1 \quad e_2 \quad \cdots \quad e_j] \quad (5-S15)$$

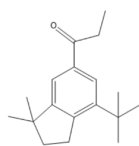
Table S5-1. Molecular structures of the training set and test set used in 3D-QSAR modelling

No.	Molecular structure	No.	Molecular structure	No.	Molecular structure
Musk-1 a ¹ b ¹ c ¹		Musk-25 a ¹ b ¹² c ¹		Musk-73 a ¹ c ²	
Musk-2 a ¹ b ¹ c ¹		Musk-30 a ² c ¹		Musk-75 a ¹ c ²	
Musk-3 a ¹ b ¹ c ¹		Musk-32 a ² b ² c ¹		Musk-76 a ¹ b ¹ c ¹	
Musk-4 a ¹ b ¹ c ¹		Musk-34 a ² b ² c ¹		Musk-77 a ¹	
Musk-6 a ¹ b ¹ c ¹		Musk-36 a ¹ c ²		Musk-79 a ¹ c ²	

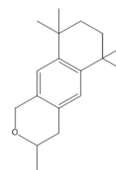
Musk-8
 $a^1 b^2$



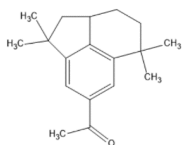
Musk-37
 a^1



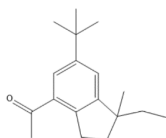
Musk-81
 $a^2 b^1 c^1$



Musk-9
 $a^1 c^2$



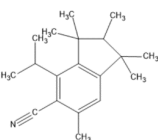
Musk-43
 a^{12}



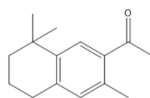
Musk-82
 $a^1 b^1 c^1$



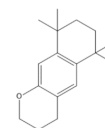
Musk-10
 $a^1 b^2 c^1$



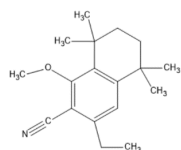
Musk-55
 $a^1 b^1 c^1$



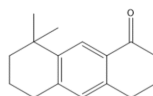
Musk-83
 $a^1 b^1 c^1$



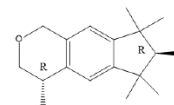
Musk-13
 $a^1 c^1$



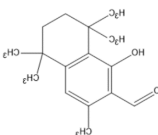
Musk-56
 a^1



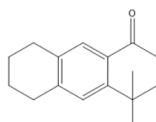
Musk-85
 $a^2 b^1 c^1$



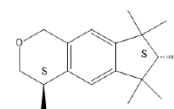
Musk-15
 $A^2 c^2$



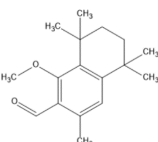
Musk-57
 $a^1 c^2$



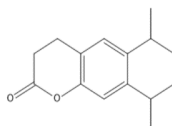
Musk-86
 $a^2 b^1 c^1$



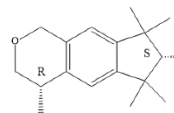
Musk-16
 $a^1 b^1 c^1$



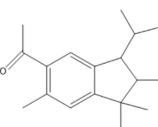
Musk-65
 a^2



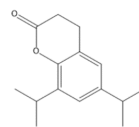
Musk-87
 a^2



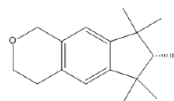
Musk-17
 $a^1 b^2 c^1$



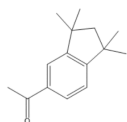
Musk-66
 $b^1 c^1$



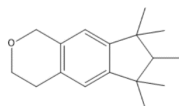
Musk-88
 $a^1 b^1 c^1$



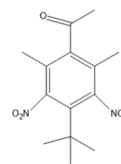
Musk-24
a¹



Musk-72
a¹ b¹ c¹



Musk
ketone
a¹ b¹ c¹²



(1) Molecular structures used in the 3D-QSAR models for predicting a: progesterone;
b: estrogen; c: multi-activity;

(2) ¹ means training set; ² means test set.

(3) CAS number of HHCB: 1222-05-5, CAS number of MK: 81-14-1.

Table S5-2. LibDock scores of SM-P, SM-E and SM-C

SMs	SM-P	SM-E	SM-C	SMs	SM-P	SM-E	SM-C	SMs	SM-P	SM-E	SM-C
SM-1	1.902	1.951	0.356	SM-25	1.951	1.904	0.480	SM-73	1.933	1.947	0.323
SM-2	1.937	1.966	0.226	SM-30	1.973	1.957	0.201	SM-75	1.917	1.919	0.473
SM-3	1.912	1.967	0.264	SM-32	1.933	1.950	0.306	SM-76	1.914	1.951	0.336
SM-4	1.907	1.968	0.268	SM-34	1.897	1.927	0.474	SM-77	1.858	1.935	0.498
SM-6	1.930	1.959	0.269	SM-36	1.897	1.985	0.196	SM-79	1.935	1.962	0.246
SM-8	1.951	1.989	0.087	SM-37	1.988	1.988	0.019	SM-81	1.914	1.957	0.305
SM-9	1.900	1.978	0.227	SM-43	1.907	1.992	0.149	SM-82	1.914	1.957	0.305
SM-10	1.908	1.979	0.211	SM-55	1.921	1.939	0.381	SM-83	1.931	1.959	0.269
SM-13	1.912	1.979	0.202	SM-56	1.947	1.962	0.226	SM-85	1.934	1.959	0.262
SM-15	1.868	1.947	0.426	SM-57	1.862	1.934	0.496	SM-86	1.930	1.959	0.269
SM-16	1.868	1.940	0.458	SM-65	1.948	1.972	0.177	SM-87	1.912	1.959	0.299
SM-17	1.910	1.962	0.289	SM-66	1.933	1.984	0.143	SM-88	1.895	1.946	0.387
SM-24	1.886	1.924	0.504	SM-72	1.899	1.951	0.360	MK	1.719	1.855	1.000

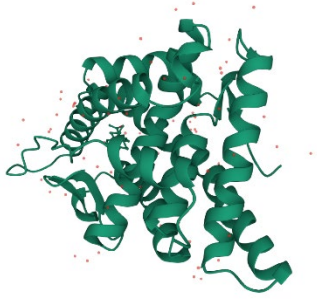
Table S5-3. Signal-to-noise ratios of ten factors and two levels in the supplementary diet plans

SMs	Factors	A	B	C	D	E	F	G	H	I	J
PHAN	Level 1	-16.64	-14.21	-12.52	-14.22	-16.46	-18.20	-15.21	-16.18	-19.49	-17.62
	Level 2	-12.04	-14.46	-16.15	-14.46	-12.22	-10.47	-13.46	-12.50	-9.19	-11.06
	Delta	4.60	0.25	3.63	0.24	4.24	7.73	1.75	3.67	10.30	6.56
	Ranking	4	9	7	10	5	2	8	6	1	3
ADBI	Level 1	-19.01	-19.86	-20.18	-19.45	-19.20	-19.82	-18.36	-18.04	-19.58	-18.32
	Level 2	-4.02	-3.17	-2.85	-3.58	-3.83	-3.21	-4.66	-4.99	-3.45	-4.70
	Delta	14.98	16.70	17.33	15.87	15.37	16.62	13.70	13.05	16.12	13.62
	Ranking	7	2	1	5	6	3	8	10	4	9
AHTN	Level 1	-15.88	-17.97	-10.26	-17.63	-18.19	-18.45	-16.00	-16.21	-18.46	-16.51
	Level 2	-12.36	-10.28	-17.98	-10.61	-10.05	-9.79	-12.25	-12.04	-9.78	-11.73
	Delta	3.52	7.69	7.72	7.02	8.14	8.66	3.76	4.17	8.69	4.78
	Ranking	10	5	4	6	3	2	9	8	1	7
HHCB	Level 1	-9.95	-9.58	-6.50	-9.10	-10.33	-10.87	-10.22	-11.69	-10.13	-10.91
	Level 2	-7.58	-7.95	-11.03	-8.44	-7.21	-6.67	-7.32	-5.85	-7.41	-6.63
	Delta	2.37	1.63	4.53	0.66	3.12	4.20	2.90	5.85	2.72	4.28
	Ranking	8	9	2	10	5	4	6	1	7	3
MK	Level 1	-21.61	-10.19	-23.97	-8.64	-9.81	-22.13	-8.70	-9.40	-23.29	-20.09
	Level 2	-8.27	-19.69	-5.91	-21.24	-20.07	-7.75	-21.18	-20.48	-6.95	-9.79
	Delta	13.35	9.50	18.05	12.59	10.27	14.39	12.47	11.09	16.70	10.31
	Ranking	4	10	1	5	9	3	6	7	2	8

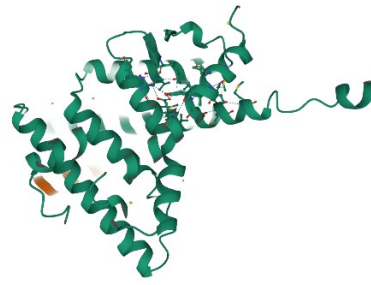
Note: Factor A-J refers to vitamin C, carotene, niacin, folic acid, vitamin A, vitamin E, ovalbumin, vitamin B₁₂, vitamin B₂, and vitamin B₆, respectively;
 Level 1: with supplement diet;
 Level 2: without supplement diet.

Table S5-4. The contributions of hydrophobic, acceptor, donor, electrostatic, and steric fields
in 3D-QSAR models

Models	Hydrophobic field	Acceptor field	Donor field	Electrostatic field	Steric field
SM-P	0.262	0.285	0.000	0.122	0.331
SM-E	0.260	0.325	0.000	0.058	0.357
SM-C	0.248	0.290	0.000	0.086	0.377



Estrogen



Progesterone

Figure S5-1 The structures of estrogen and progesterone

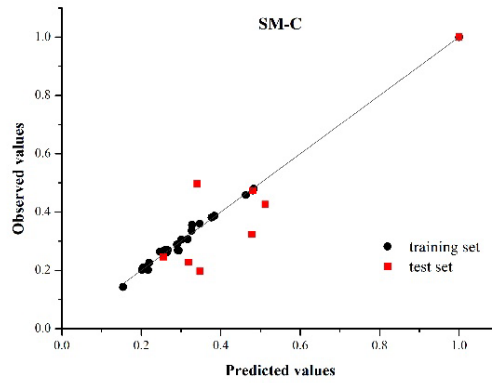
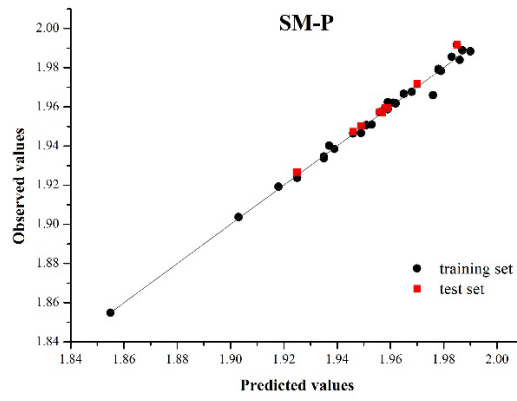
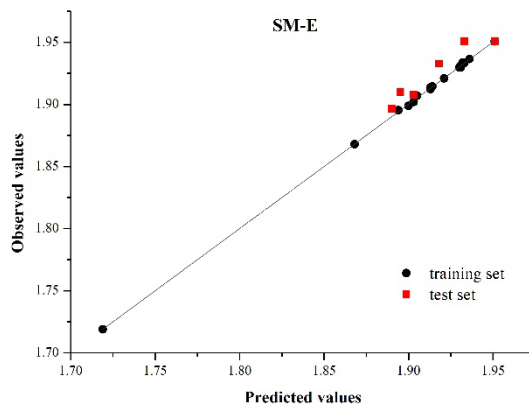


Figure S5-2 The scattered dots figure of training set and test set of SM-E, SM-P, and SM-C models

CHAPTER 6

DERMAL EXPOSURE TO SYNTHETIC MUSKS: HUMAN HEALTH RISK ASSESSMENT, MECHANISM, AND CONTROL STRATEGY

This chapter has been submitted to *Ecotoxicology and Environmental Safety*, and the status now is found to be minor revision required. I am the primary author of this paper, and am mainly responsible for the conceptualization, methodology, software, formal analysis, investigation, writing - original draft preparation, writing - review & editing of the manuscript. The co-author Wei He is mainly responsible for the conceptualization, methodology, software, formal analysis, investigation, writing - original draft preparation, writing - review & editing of the manuscript, Yuanyuan Zhao is mainly responsible for the methodology, software, formal analysis, investigation of the manuscript the manuscript, Bing Chen helps to conduct the formal analysis and writing - review & editing, Zhiwen Zhu helps to edit the manuscript, Qiao Kang helps on the data curation, and Baiyu Zhang is the principal investigator of the manuscript involved writing - review & editing, supervision, project administration, and funding acquisition.

6.1 Introduction

Synthetic musks (SMs) are a group of aromatic compounds that are commonly used as additives in personal care products (PCPs) and have been recognized as emerging contaminants due to their negative impacts on human health and ecological systems. SMs can enter human bodies via various routes and dermal absorption has been identified as the major exposure pathway (Nakata et al., 2015). SM molecules, especially galaxolide (HHCB) and tonalide (AHTN) can enter into the stratum corneum, and gradually remain and accumulate in human keratin (Brunn and Amberg-Müller, 2004; Zhang et al., 2017). The bioaccumulation of SMs in the human body played a key role in causing potential health concerns such as sun allergy, neurotoxicity (Tseng and Tsai, 2019; Sousa et al., 2021). It has also been found that HHCB and AHTN could inhibit the production of progesterone and may lead to abortion risks to pregnant women (Wang et al., 2020; Li et al., 2022). It is thus of great importance to reduce the adverse impact of SMs on humans through assessing the potential risks of SMs via dermal interactions, exploring the underlying mechanism of SMs accumulation in human bodies, and developing effective control strategies, which have never been tackled previously.

Despite the recently identified adverse impacts of SMs, proper indicators for assessing their human health risks remains to be poorly studied. Stratum corneum is considered as the first and foremost barrier for the SM molecules, which could retain 70.0% and 70.3% of the HHCB and AHTN molecules after 24-h period. The

percutaneous absorption rates of HHCB and AHTN were 11.4% and 11.3%, respectively (Zhang et al., 2017). Cells of the stratum corneum contain a large volume fraction of keratin. Thus, the bioaccumulation ability of SMs in human keratin was used as a representative parameter in assessing the human health risk of SMs. Thanks to the advancement in quantum chemistry, the interactions of molecules could be simulated and interpreted at a molecular level. Molecular dynamics simulation has been used to reflect the accumulation of SM molecules onto keratin by calculating the binding energy generated during this process (Li et al., 2022). Research attempts have been conducted using binding energy as the key parameter in risk assessment of the toxicity of tamoxifen, the comparative cytotoxicity of halogenated aromatic disinfection byproducts, the aquatic toxicity of microplastic and other environmental and human health risks of chemicals (Flynn et al., 2017; Zhang et al., 2020; Chen et al., 2021; Li et al., 2022). However, the binding energy of SMs to human keratin proteins has never been used to assess the human health risk of SMs.

Further, it is imperative to understand the bioaccumulation mechanisms of SMs in skin keratin, which could extend the knowledge of the risk control of SMs. The molecular structural features of chemical molecules (e.g., physicochemical, electronic, and topological parameters) are in close association with their physical-chemical properties, which determines their behaviors in the environment (Ertan et al., 2009; Mombelli and Devillers, 2010; Mukherjee et al., 2022). The two-dimensional quantitative structure-activity relationship (2D-QSAR) models could explain the

change in the biological activity of the molecule caused by the change of its own parameters based on mathematical statistics (Villaverde et al., 2018). For example, Yang et al. (2019) found that the interaction between adjacent bonds was one of the key factors influencing the toxicity of dioxins. Ni et al. (2018) indicated that the bioaccumulation of polycyclic aromatic hydrocarbons in rice was affected by the molecular weight. Bordás et al. (2011) summarized that the Lowest unoccupied molecular orbital energy (E_{LUMO}) is an important factor for predicting bioconcentration factors. The 2D-QSAR modelling could facilitate the in-depth understanding of molecular structural features of SMs could serve as a cornerstone for understanding their bioaccumulation mechanisms in skin keratin. However, 2D-QSAR aided bioaccumulation analysis has never been investigated.

Eliminating or reducing the source of exposure has been considered as an effective strategy for SMs control, which can be achieved by developing SMs with lower human health risks or reducing their entrance into human bodies. A significant predictive tool is desired to provide affluence information about the exact molecular characteristics essential for bioaccumulation ability in innovative chemical design and pathway control. The three-dimensional quantitative structure-activity relationship (3D-QSAR) is an in-silico method used to design chemicals with lower adverse impacts or improved functional properties (Winkler, 2018; Gu et al., 2019; Li et al., 2021a). Derivatives that have a less environmental impact (e.g., bio-toxicity, mobility, bio-accumulation ability in organisms, degradation effects) have been designed with 3D-QSAR models (Gu et

al., 2019; Zhang et al., 2021), whose corresponding bioaccumulation ability in the human body, however, was overlooked. The development of SM derivatives with less bioaccumulation ability is important for reducing the human health risk caused by dermal exposure. In addition, previous molecular design of improved SM properties used half-lives of SMs to reflect their long-lasting capacity or odor stability, which cannot well reflect the odor sensitivity of SMs to humans directly. The binding energy of SMs with a proper olfactory protein might be a potential indicator to replace half-lives for screening SMs with improved odor sensitivity, though its applicability in designing SMs derivatives needs to be further examined.

As an effective exposure reduction strategy, adding other ingredients in the PCPs could lead to a further reduction of human health risks caused by SMs. AHTN, a widely used SM, has been proved as a photosensitizer (Fang et al., 2017). The damage of skin by such photosensitizing substances can be inhibited by using sunscreen products (Mujtaba et al., 2018; Mota et al., 2019). Li et al. (2021) proved that adding selective moisturizers ingredients and anti-photosensitivity materials can reduce the toxicity of HHCB to skin keratin. The wide varieties of PCPs additives on the market highlighted the importance of extending the screening of proper candidates to prevent the potential risks of SMs accumulation in human keratin. It is thus essential to evaluate the mainly widely used additives in PCPs to achieve such assessment.

In this study, we assessed the human health risk using the binding energy of SMs and target keratin as the key parameter and investigated the bioaccumulation

mechanisms of SMs in human keratin using the 2D-QSAR method. We further developed the control strategies by modifying existing SM molecules with less human health risk using 3D-QSAR modelling and then determining appropriate PCP ingredients that helped to prevent the bioaccumulation of SMs in humans. This study used in-silico methods to provide an in-depth investigation of human health risks assessment, mechanism, and risk control of SMs through dermal exposure.

6.2 Materials and Methods

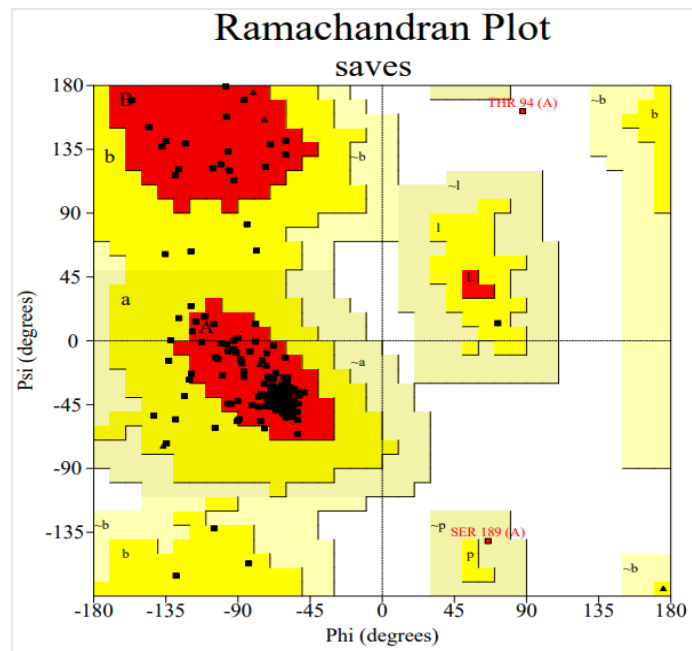
6.2.1 Human health risk assessment of functional SMs using molecular docking and molecular dynamics simulations

The binding energies of SMs-human skin keratin protein (4ZRY) (PDB Protein Data Bank) and SMs-human olfactory receptor (OR5AN1) were calculated in this study as the human health risk (bioaccumulation ability) and functional property (odor sensitivity) indicators, respectively. Keratin protein is one of the main components of the stratum corneum, in which SMs have been detected (Zhang et al., 2017; Li et al., 2021a). The mutations of keratin could lead to skin disease (e.g., confetti Ichthyosis) (Bunick and Milstone, 2017). Among the keratin proteins, 4ZRY was selected as the research objective in this study. The bioaccumulation ability of SMs was assessed using the binding energy of SMs to human skin keratin protein (4ZRY) (Li et al., 2022).

On the other hand, the smells of odorant molecules are conferred by their distinctive structural features. Molecules with a particular structure could enter the complementary sites of nasal receptors and trigger the corresponding signals that can

be processed by the brain (Zarzo, 2007). The protein OR5AN1 selected in this study is an important human olfaction receptor for musk (Ahmed et al., 2018). This protein was thus used to simulate its activation process by musky molecules based on molecular recognition between receptor and ligand. The impact of molecular structures on molecular aroma intensity could also be explained.

The human olfactory protein OR5AN1 was constructed by the homology modelling method using the structure of protein OR5AN1 generated from chimpanzee (SWISS-MODEL website). The 6TOD (Orexin receptor) was used as a template, and SAVES 6.0 was used to evaluate the structural quality of the constructed protein. The stereochemical properties of the protein were then analyzed through PROCHEK and the Lagrange diagram of the constructed protein was shown in Figure 6-1. It can be seen from Figure 6-1 that the amino acids in the residues in most favored regions account for more than 90% of the amino acids in the Ramachandran Plot, indicating that the constructed protein is of good quality and can be used as human olfactory protein.



Plot statistics

Residues in most favoured regions [A,B,L]	247	91.5%
Residues in additional allowed regions [a,b,l,p]	21	7.8%
Residues in generously allowed regions [~a,~b,~l,~p]	1	0.4%
Residues in disallowed regions	1	0.4%
	----	-----
Number of non-glycine and non-proline residues	270	100.0%
Number of end-residues (excl. Gly and Pro)	2	
Number of glycine residues (shown as triangles)	13	
Number of proline residues	8	

Total number of residues	293	

Based on an analysis of 118 structures of resolution of at least 2.0 Angstroms and R-factor no greater than 20%, a good quality model would be expected to have over 90% in the most favoured regions.

Figure 6-1 The Ramachandran Plot of human olfactory protein (OR5AN1)

After obtaining the structures of 4ZRY and OR5AN1, 79 SMs were docked with 4ZRY or OR5AN1 receptors, respectively, via Discovery Studio® 2021 to obtain new complexes. Then molecular dynamics simulation was applied to determine the binding energy (ΔG) through Groningen Machine for Chemical Simulations (GROMACS, Berendsen Laboratory, Göttingen University, Göttingen, Germany) package. The Dell PowerEdge R7425 server was used to perform molecular dynamics simulation calculations in Gromacs software. The SMs were firstly docked to keratin and olfactory proteins, and the new complexes were then filled in a periodic twelve cubes with 10 nm on the side. The GROMOS96 43a1 force field was used for molecular confinement, and Na⁺ ion was added to neutralize the system charge (Li et al., 2022). The above-mentioned composite systems were set as a group and the energy minimization simulation based on the steepest gradient method was performed. The size of the pressure bath was set to a constant standard atmospheric pressure of 1 bar. The higher the binding energy SMs-4ZRY, the easier SMs could be accumulated in the human skin. Similarly, the higher the binding energy SMs-OR5AN1 has, the stronger the olfactory sensitivity is. The obtained binding energies were used to assess the bioaccumulation ability and odor sensitivity of SMs and will further be used as inputs for 3D-QSAR models construction.

6.2.2 Exploration of SM bioaccumulation mechanism through 2D-QSAR modelling

The 2D-QSAR models could explain the change in the biological activity of the

molecule caused by the change of its own molecular structural features (e.g., physicochemical, electronic, and topological parameters) based on mathematical statistics (Mombelli and Devillers, 2010; Villaverde et al., 2018; Mukherjee et al., 2022). Researchers have found the bioaccumulation ability of a chemical is relevant to its own molecular structural features (Bordás et al., 2011; Ni et al., 2018). The descriptors (i.e., geometric, electronic, physical and chemical, spectral and topological parameters) of the SMs were obtained through PaDEL-descriptor software, Gaussian and ChemDraw software. The calculated 32 SM descriptors and their meanings are shown in Table 6-1.

The 2D-QSAR model analysis method explains the change in the biological activity of the molecule caused by the change of its own parameters based on mathematical statistics (Villaverde et al., 2018). The binding energy of SMs-keratin (4ZRY) and SMs-olfactory (OR5AN1) was chosen as the dependent variable, and the SMs' descriptors shown in Table 6-1 were chosen as the independent variables to construct two 2D-QSAR models of the interaction of SMs-4ZRY and SMs-OR5AN1. For each 2D-QSAR model (SMs-4ZRY or SMs-OR5AN1), 60 SMs were randomly selected as the training set, and the rest 19 SMs were used as the test set. Based on the training and test set, the 2D-QSAR models were then constructed using the regression analysis method for multiple linear regression. The principal component analysis was used to screen out the SMs' descriptors with more significance to binding ability (Du et al., 2019). The Kaiser-Meyer Olkin (KMO) and spherical test methods were then used to verify the stability of the descriptors. The descriptors with the highest R or KMO

value (test results for the partial correlation between test variables) were removed until the number of descriptors met the modeling scale. The molecular features that played the key role in SM-Protein (i.e., keratin and olfactory) interactions were further identified using the constructed 2D-QSAR models. The coefficient of the SM indicator in the model is positive, indicating that the higher the value, the better the SMs' ability to attach to the protein receptor.

The sensitivity analysis method was used in this study to screen the main influencing factors of the constructed 2D-QSAR model of the interaction of SMs with keratin and olfactory proteins. The influence of the selected 32 SM descriptors on the bioaccumulation ability or odor sensitivity and their uncertainty could then be generated. The sensitivity coefficient represents the proportion of the predicted value change rate to the input parameter change rate (Yu et al., 2017), and its general expression is:

$$SC_i = (\Delta Y_i / Y_i) / (\Delta X_i / X_i) \quad (6-1)$$

in which, SC_i means the sensitivity coefficient of input i , $\Delta X_i / X_i$ indicates the rate of change of input parameters, and $\Delta Y_i / Y_i$ is the rate of change of the corresponding forecast results.

Table 6-1 The definition of 32 SM descriptors

Categories	Descriptors	Definition	Categories	Descriptors	Definition
Geometric parameters	DM	Dipole Moment	Physical and chemical parameters	BP	Boiling Point
	Q _{xx}	Quadrupole moment Q _{xx}		MP	Melting Point
	Q _{yy}	Quadrupole moment Q _{yy}		CT	Critical Temp
	Q _{zz}	Quadrupole moment Q _{zz}		CP	Critical Pres
	Q _{xy}	Quadrupole moment Q _{xy}		CV	Critical Vol
	Q _{xz}	Quadrupole moment Q _{xz}		G	Gibbs Energy
	Q _{yz}	Quadrupole moment Q _{yz}		LogP	Oil-water distribution factor
Mol Wt	Molecular weight	HL	Herry's Law		
MR	Stereoscopic effect parameter	HF	Heat of Form		
Electronic parameters	TE	Total Energy	Spectral parameters	Freq	Frequency
	q ⁺	Most positive Milliken charge number		I	Infrared
	q ⁻	Most negative Milliken charge number		R	Raman
	qH ⁺	Most positive hydrogen ion charge number	tSPA	Topological surface area	
	LUMO	Lowest unoccupied molecular orbital	Topological parameters	TR	Topological radius
	HOMO	Highest occupied molecular orbital		TD	Topological diameter
	EG	Energy gap		TS	Topological shape

6.2.3 Control of SM human health risk

6.2.3.1 Control of human health risk for SMs by designing new SM derivatives

The three-dimensional quantitative structure-activity relationship (3D-QSAR) is an *in silico* method used to design chemicals with lower adverse impacts or improved functional properties (Li et al., 2021; Zhang et al., 2021). In this study, three 3D-QSAR models (i.e., SMs-4ZRY, SMs-OR5AN1 and multi-activity 3D-QSAR model) were constructed for designing functional SM derivatives with lower human health risk through SYBYL-X2.0 software. The inputs used for model constructs include the molecular structures of SMs, the binding energies of SMs and single human protein (4ZRY or OR5AN1), and combined proteins (4ZRY and OR5AN1) (SMs-C). The binding energy of SMs-C was calculated with the values of SM-4ZRY and SM-OR5AN1 and integrated using the Improved Grey Correlation Analysis (Zhang and Zhao, 2007). Given that both binding energies were equally important, the subjective weighting factors for these two factors were defined as 0.5 each. The objective weightings of 4ZRY and OR5AN1 were both set as 0.5. Detailed calculations regarding the Improved Grey Correlation Analysis were given in the supplementary material (S6-1.2).

The detailed 3D-QSAR model construction information (i.e., molecules used training set and test set) was given in Table S6-1. The data set for SMs-4ZRY 3D-QSAR model consists of 51 molecules (i.e., 40 SMs training set and a 11 SMs test set). The data set for SMs-OR5AN1 model includes 63 SMs (i.e., 50 SMs training set and a 13

SMs test set). The multi-activity 3D-QSAR model (SMs-C) used 39 molecules (i.e., 29 SMs training set and a 10 SMs test set) as the database. The molecules with the highest binding energy were selected as the template molecule for the corresponding template in the 3D-QSAR model, namely SM-20 for SMs-4ZRY, SM-7 for SMs-OR5AN1, and SM-55 for SMs-C. The Tripos force field and Gasteiger-Hückel charges were used to perform the optimization of the targeting molecules (Reihaneh and Jahan, 2013), with a maximum of 10,000 optimizations and 0.005 kJ/mol energy convergence gradient through the Powell's method (Li et al., 2022). The template SM molecules (i.e., SM-20, SM-7, and SM-55) with circled common skeletons were presented in Figure S6-1.

6.2.3.2 Control of human health risk for SMs by adding other PCP ingredients

In this study, eight categories (i.e., chelating agent, moisturizer, surfactant, preservative, essence, thickener agent, colorant and pearlescent agent) of 20 ingredients (i.e., EDTA-Na₂, EDTA-Na₄, Glycerin, Sorbitol, Octyl glucose, dodecyl dimethyl betaine (BS-12), cocamidopropyl betaine (CAPB), alkyl ethoxylate sulfate (AES), sodium benzoate, dimethyloldimethyl (DMDM), methylisothiazolinone (MIT), AHTN, HHCB, PHAN, hydroxyethyl cellulose (HEC), yellow collagen, Lemon yellow, Carmine, EGDS, and glycolmonostearate (EGMS)) in the body wash were selected (Siew et al., 2021; Ngan et al., 2020; Cressey et al., 2012; Ngo et al., 2021; Crudden, 1999; Fowler et al., 1997; Kakizawa and Miyake, 2019; Bujak et al., 2015; López-Sánchez et al., 2021; Schlichte and Katta, 2014; Eissa et al., 2012; Conkle et al., 2018; Tai et al., 2014). Each category contains at least two kinds of additives (shown in Table

6-4). The ingredients from body wash products are screened out based on the results obtained from the 2D-QSAR mechanism analysis, and then the potential human health risk for the body wash product containing the SM before and after modification could be assessed with these screened ingredients present. After the target SM (or the optimum SM derivative) and each ingredient were docked to 4ZRY, the binding energy of each new complex (SM-ingredient-4ZRY) was calculated through molecular dynamics simulation.

6.3 Results and Discussion

6.3.1 Human health risk assessment of SMs

The binding energy of SMs-4ZRY, SMs- OR5AN1, and SMs-4ZRY-OR5AN1 (SMs-C) were obtained and shown in Table S6-2. The binding energy of SMs-4ZRY ranged from 50.87 to 133.37, and the binding energy of SMs-OR5AN1 ranged from 82.52 to 165.559. To verify whether the SMs-C correlates to the SMs-4ZRY, SMs-OR5AN1, the correlation coefficient was calculated and the curve fittings of SMs-4ZRY and SMs-C SMs-OR5AN1 and SMs-C were given in Figure S6-2. According to the correlation coefficient table, when the Significance level equals 0.01, the correlation coefficient should be greater than 0.281. The correlation coefficient of both SMs-4ZRY and SMs-C (0.5252), and SMs-OR5AN1 and SMs-C (0.3682) were greater than 0.2813, indicating the calculated values of SMs-C was highly correlated with both SMs-4ZRY and SMs-OR5AN1.

6.3.2 SM bioaccumulation mechanism

6.3.2.1 The construction and evaluation of 2D-QSAR models

The obtained formulas of the two constructed 2D-QSAR models are given in Table 6-2. The SMS-4ZRY model reflects the bioaccumulation ability of SMS on human keratin, and the SMS-OR5AN1 model represents the odor sensitivity. According to the results shown in Table 6-2, the correlation coefficient R are 0.618 and 0.541 for SMS-4ZRY and SMS-OR5AN1 respectively ($n=60$, $p=0.001$, $r_{min}=0.618/0.541 > r_0=0.4078$), which meets the statistical requirements. Both models in the table are statistically significant ($Sig=0.000$) (Gu et al., 2020). The KMO values were 0.658 (SMS-4ZRY) and 0.620 (SMS-OR5AN1) (>0.6), indicating that the models had good robustness (Hernández-Martínez et al., 2021). It can be seen from Figure S6-3 that the training set, test set molecule experimental value and model prediction value fit well in the constructed 2D-QSAR models ($n=79$, $p=0.001$, $r_{min}=0.618/0.620 > r_0=0.370$). The results further verified the reliability of the constructed 2D-QSAR models.

In the SMS-4ZRY 2D-QSAR model, the positive coefficients of descriptors include Q_{YY} (quadrupole moment), TE (total energy), CT (critical temp), CV (critical vol) and TR (topological radius), which means the bioaccumulation ability of SMS increases. A rising MW, HOMO, EG, CP, G, I, R and TD of SMS gave a lower binding ability between SMS and 4ZRY, indicating a reduced interaction between SMS and human keratin. Similarly, in the SMS-OR5AN1 2D-QSAR model, it can be found that when SMS' QYZ, LUMO, HL, I, HOMO, and CP decrease (or SMS' MW, TE, QH, BP, and MP increase), the binding ability between SMS and olfactory protein increases, indicating the improvement of SMS' odor sensitivity to human.

Table 6-2 The obtained 2D-QSAR formulas of SMs-4ZRY and SMs-OR5AN1

2D-QSAR models	Formulas
SMs-4ZRY	$\text{Binding Energy} = -60.274 + 0.543 \times Q_{YY} - 0.068 \times MW + 0.409 \times TE - 31.867 \times \text{HOMO} - 28.012 \times EG + 0.327 \times CT - 2.872 \times CP + 0.108 \times CV - 0.014 \times G - 0.044 \times I - 0.002 \times R + 3.857 \times TR - 2.674 \times TD$
SMs-OR5AN1	$\text{Binding Energy} = -3.557 - 1.064 \times Q_{yz} + 0.033 \times MW + 0.233 \times TE + 12.617 \times QH - 44.114 \times LUMO - 13.899 \times EG + 0.075 \times BP - 6.203 \times HL - 0.006 \times I - 0.018 \times R - 16.651 \times \text{HOMO} + 0.106 \times MP - 0.247 \times CP$

6.3.2.2 The domain analysis of the established 2D-QSAR models

The domain analysis of the 2D-QSAR model helps to determine the reliable prediction range of the model (Mukherjee et al., 2022). Standardized residual, an indicator for model predictability, is the calculated value of residual divided by its standard deviation with an acceptable value between -3 to 3 (Wang et al., 2009). The distance between the molecule and the X centroid is named lever, and it can be defined as,

$$h_i = X_i(X^T X)^{-1}X_i^{(T)} \quad (6-2)$$

$$h^* = 3(p + 1)/n \quad (6-3)$$

in which, h^* is the warning lever value (0.7 in this study), p represents the number of influencing parameters in 2D-QSAR model, and n represents the number of SMs used training set. William's diagram is a diagram of the relationship between standardized residuals and leverage (Figure S6-4). It can be seen from William's Figure S6-4 that all data points of the 2D-QSAR model of the interaction between musk molecules and keratin are within the applicable range, and no data deviate from the defined interval. In the SMs-4ZRY 2D-QSAR model, the levered value of two molecules in the training set, and the lever value of one molecule in the test set exceed the warning lever value. However, the small standardized residuals of the above three molecules proved that they were not outliers (Gramatica et al., 2007). Thus, the 2D-QSAR models constructed in this paper have good robustness and a wide range of applications.

6.3.2.3 Determination of main factors influencing bioaccumulation ability and

olfactory sensitivity of SMs based on sensitivity analysis

The sensitivity of all descriptors and determining the main influencing descriptors was conducted through the sensitivity analysis method (Du et al., 2019). The influence degree of the bioaccumulation and olfactory sensitivity of SMs was calculated by increasing each descriptor's value by 10%, 20%, 30%, 40%, and 50%, respectively. The significance of each descriptor was described by the sensitivity, and the sensitivity coefficient of each descriptor is shown in Figure 6-2.

In Figure 6-2 (a), among the 13 descriptors in SMs-4ZRY 2D-QSAR model, the absolute values of the sensitivity coefficients of CT, TE and CV are greater than 1, and CT has the highest value of 4.242. Thus, CT, TE, and CV parameters are the main factors affecting the SMs accumulated in human keratein. According to Figure 6-2 (b), TE, BP and MP with the highest absolute values of the sensitivity coefficients are more significant than 0.5. Thus TE, BP, and MP have been confirmed as the main factors influencing odor sensitivity.

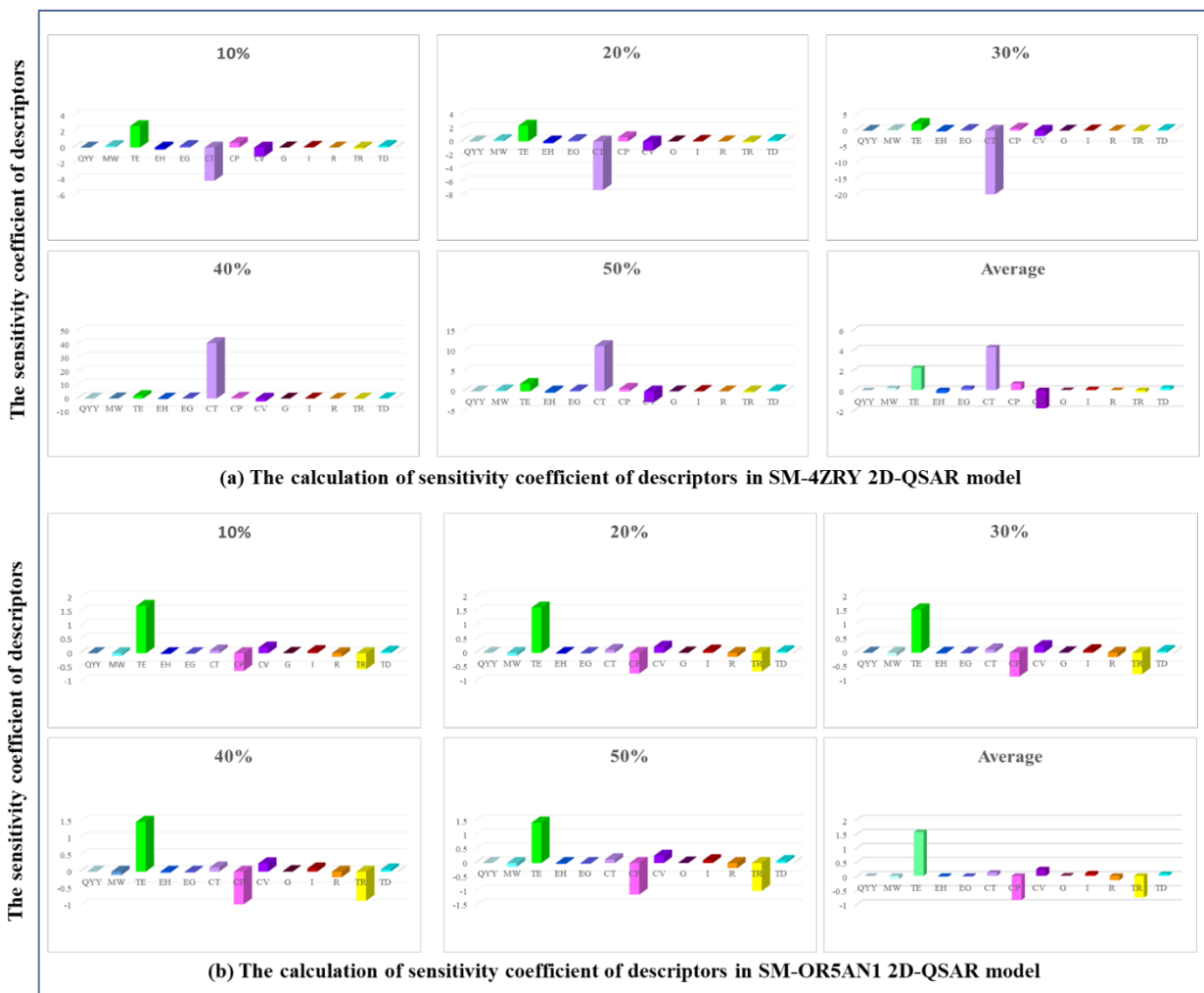


Figure 6-2 The influence degree on the bioaccumulation and olfactory sensitivity of SMs

6.3.2.4 Mechanism influencing SM bioaccumulation ability and olfactory sensitivity

Based on the results in section 6.3.2.3, the main factors affecting the interaction between musk molecules and keratin are CT, TE and CV. Hall and Story (1996) indicated that hydrogen bond and dipole were the main factors affecting the critical temperature. The dipole represents the polarity of the molecule (Al-Malah, 2011). The change of the polarity of the molecule could affect the hydrophobic interaction between the molecule and the receptor (Bunmahotama et al., 2020). The molecule and the receptor are combined through hydrogen bonding and hydrophobic interaction (Davis and Teague, 1999) and the total energy of the molecule is proportional to its reactivity (Bello and Nava, 2004). According to the volume theory (Wezel and Opperhuizen, 1995), the SM molecule first penetrates the cell membrane and then enters the lipid bilayer structure of the cell. An increasing SM concentration could lead to the expansion of their volumes at the skin surface till a critical volume arrives, which could block the ion channel. The binding ability of SMs to keratin is thus further reduced. Therefore, as the CT, TE, and CV of the SMs decrease, the reactivity of the SMs decreases, and the bioaccumulation ability of SMs in human keratin decreases.

In addition, the main factors affecting the interaction between SMs and olfactory protein are BP, MP and TE. It has been approved that the dipole moment and polarity of a molecule are negatively related to the boiling point and melting point of the molecule (Glazier et al., 2010; Rabideau et al., 2020). As stated above, decreased

polarity can increase in the hydrophobic effect of the molecule. Similar to the analysis of the mechanism of the interaction between SMs and keratin, the TE positive correlation with the binding energy of SMs-olfactory protein. Therefore, the increasing of TE, BP and MP enhance the reactivity of SMs and olfactory proteins, and improve the binding ability of SMs to OR5AN1, leading to enhanced SMs olfactory sensitivity to human beings.

6.3.3 Control of SM human health risk

6.3.3.1 Control of SM human health risk by designing new SM derivatives

(1) 3D-QSAR model evaluation

The multi-activity 3D-QSAR model was introduced into this study to consider multiple activities that could be brought by SMs, by improving the odor sensitivity and reducing the bioaccumulation ability together. In this study, the constructed SMs-4ZRY and SMs-OR5AN1 models were used to design new SM derivatives and provide more information about the modified sites from the contour maps (Li et al., 2022). The q^2 (cross-validation coefficient) and r^2 (non-cross-validation coefficient) of all the three models are greater than 0.5 and 0.9, respectively (Table S6-3). According to Salahinejad and Ghasemi (2014) and Meng et al. (2020), all the three 3D-QSAR models constructed in this study have good predictability. Besides, the high F-test value indicated that the model fits the data well. and the high external test coefficient R^2_{pred} (greater than 0.6) (Table S6-3), proves a good predictive ability of the constructed models (Li et al., 2022).

(2) 3D-QSAR aided design of SM derivatives with reduced human health risk and enhanced functional properties

The hydrophobic, acceptor, donor, electrostatic and steric field were the main descriptors used in this study for molecular modification, whose information were provided in the contour maps. The contributions of the fields for each 3D-QSAR model (i.e., SMs-4ZRY CoMFA, SMs-OR5AN1 CoMFA and the SMs-C CoMSIA) were provided in Table S6-4. Three mostly adopted SMs in personal care products, namely SM-6 (i.e., (4S,7R)-HHCB), SM-2 (i.e., TRASE) and SM-1 (i.e., PHAN), were chosen as precursors (Chen et al., 2014; Schmitt et al., 2013; Li et al., 2016b) for molecular modification. PHAN was selected as the example to explain as it was used in all the 3D-QSAR model constructions. Figure S6-5 illustrated the contour maps of PHAN generated by three 3D-QSAR models, whose modification information was presented. The contour maps of HHCB and TRASE were given in the supplementary materials (Figure S6-6).

The color in fields represents different meanings. For example, the binding energy could be increased when a hydrogen bond is introduced into the purple acceptor field, whereas the addition of a hydron bond in the red area could lead to the reduction of the binding energy of SMs. Similarly, the introduction of hydrophobic groups into the yellowish hydrophobic field could enhance the binding energy. In contrast, the white area emphasizes that the binding energy of SMs-proteins would increase if using hydrophilic groups. The blue and red in the electrostatic field are related to the positive groups or negative groups. The green and yellow from the steric fields are correlated to the size of the modified groups (Li et al., 2022).

The available modification sites of PHAN were obtained from the contour maps. SM derivatives were generated by changing the appropriate groups for substations at the available sites. The available modification sites of PHAN were identified based on

the contour maps in Figure S6-5, and were numbered and highlighted in Figure 6-3. A total of 693 SMs derivatives (i.e., 89 HHCB derivatives, 70 TRASE derivatives and 534 PHAN derivatives) were designed based on the available modification sites provided in the contour maps (the modified sites of each molecule are given in Tables S2-1, S2-2, and S2-3). Derivatives with lower binding energy (decreased bioaccumulation risks) and improved olfactory sensitivity were eventually selected.

From the 693 SM derivatives, four PHAN derivatives (i.e., PHAN-55, PHAN-58, PHAN-357, and PHAN-358) were screened out with lower bioaccumulation risk, improved odor stability and higher binding energy of SMs-C (Table 6-3). Among the four SM derivatives, PHAN-58 has the best performance. A significantly lower binding ability between PHAN-58 and skin keratin 4ZRY was found with a decreased rate of 17.15%. The odor sensitivity of this new derivative improves about eight percent, which means it has similar or stronger odor sensitivity than that of PHAN. Therefore, PHAN-58 was selected as the optimum SM derivative for further analysis and investigation.

Table 6-3 The predicted environmental properties of PHAN derivatives using 3D-QSAR models

Name	The binding energy of SMs-C	Change rates	The binding energy of SMs-OR5AN1	Change rates	The binding energy of SMs-4ZRY	Change rates
PHAN	0.543		139.272		88.910	
PHAN-55	0.586	7.89%	147.763	6.10%	79.614	-10.45%
PHAN-58	0.59	8.62%	150.283	7.91%	73.57	-17.25%
PHAN-357	0.642	18.20%	144.932	4.06%	86.748	-2.43%
PHAN-358	0.619	13.96%	144.892	4.04%	82.408	-7.31%

6.3.3.2 Control of SM human health risk by adding other PCP ingredients

SMs as odor additives are commonly used with other ingredients in personal care products. In this study, eight categories of 20 widely used ingredients from bodywash products were selected (Table 6-4). The molecular dynamics simulation was employed to simulate the effects of the ingredients on the binding ability of PHAN (or PHAN-58) with 4ZRY. Thus, the best body wash ingredient combination that helps prevent the human health risk of SM could be screened.

Based on the results obtained in section 6.3.2, total energy (TE) was found as the main and common factor in both SMs-4ZRY 2D-QSAR model and SMs-OR5AN1 2D-QSAR model. Therefore, the TE values of the ingredients were calculated by Gaussian[®] 09 and the results are listed in Table 6-4.

In each category, the lowest components were screened out to form a new group. According to section 6.3.3.1, when the TE value decreases, the bioaccumulation ability decreases. To prove this result, the additives in Table 6-4 with lower TE values from each category were selected, including AES, DMDM, EDTA-Na₄, EGDS, HEC, lemon yellow and octyl glucose as group A. PHAN-58 was selected as one of the best performance SM derivatives. After molecular docking of the chemicals (i.e., PHAN and PHAN-58) with 4ZRY (or OR5AN1), the binding energies of the new complexes (with the addition of group A) were calculated through molecular dynamics simulation. The total energy values of PHAN and PHAN-58 were also obtained through the Gaussian[®] 09 software.

The results showed that the TE of PHAN-58 and PHAN was -849.594 and -737.511 a.u., respectively, and the binding energy of PHAN-58-4ZRY and PHAN-4ZRY was -65.551 and -88.906 kJ/mol, respectively. The newly generated SM molecule PHAN-58 had a lower TE value and reported a lower binding energy value of PHAN-58-4ZRY, which meets the criteria of “decreased positive TE value, which means the bioaccumulation ability of SMs decreases.” Besides, the binding energy of PHAN-58-4ZRY with group A additives (-51.324) was reduced by 21.70% (PHAN-58-OR5AN1 with group A additives increased by 8.97%) compared with PHAN-58 without additives. So does PHAN, which reported a decreased binding energy by 6.32% when adding the additives. When applied to the skin with selected additives, the binding energy of PHAN-58-4ZRY was -51.324 kJ/mol, almost half the binding energy of PHAN only (-88.906 kJ/mol). This can be explained that the designed SM derivative (PHAN-58) with the supplement of group A (the lower TE value additives) has a much lower bioaccumulation ability in human keratein than PHAN itself. A new perception of reducing the bioaccumulation ability by inhibiting the dermal exposure pathway of SMs entering human bodies was proposed in this paper.

Table 6-4 The total energy of body wash components atomic units (a.u.)

Category	Name	Total energy
Chelating agents	EDTA-Na ₂	-1424.35
	EDTA-Na ₄	-1740.99
Colorants	Lemon yellow	-2784.48
	Carmines	-2450.66
Essences	AHTN	-776.82
	HHCB	-776.81
	PHAN	-737.51
Moisturizers	Glycerin	-344.23
	Sorbitol	-686.36
	Octyl glucose	-1001.65
Pearlescent agents	EGDS	-1733.12
	EGMS	-979.61
Preservatives	Sodium benzoate	-582.58
	DMDM	-684.40
	MIT	-682.79
Surfactants	BS-12	-834.75
	CAPB	-1082.08
	AES	-1458.28
Thickener agents	HEC	-2715.85
	Yellow collagen	-1493.23

Summary

In this study, the human health risk of SMs was assessed using binding energy as the indicator through molecular dynamics simulation. The bioaccumulation ability of SMs was adopted to evaluate the human health risk-associated mechanism. Results indicated that the CT, TE, and CV were the main factors affecting the bioaccumulation ability of SMs to 4ZRY, and TE, BP, and MP are the main factors that influence the binding of SMs and olfactory proteins in humans. The total energy was confirmed as the most important molecular structural factor influencing bioaccumulation ability. Two single-factor and one multi-factors 3D-QSAR models were established to design new SM derivatives with lower bioaccumulation ability but higher odor sensitivity. Among the 693 designed SM derivatives, PHAN-58 merged as the optimum derivative with a decreased bioaccumulation ability of 17.25%. Besides the design of new derivatives, adding other ingredients with PHAN/ PHAN-58 was another strategy to control the human health risk. The lower TE value ingredients combination, group A (i.e., AES, DMDM, EDTA-Na₄, EGDS, HEC, lemon yellow, and octyl glucose) was selected. A significant reduction of the bioaccumulation ability of PHAN-58-4ZRY was achieved by the addition of group A (i.e., a reduction of 42.272% compared with that of PHAN without group A). This study provided a molecular-level insight into the interactions between SMs and skin proteins for the first time and facilitated the design of new SM molecules and PCP ingredients with reduced human health risk. There are no ethical concerns (e.g., human and animal subjects) in this study. The findings would help generate new personal care products with fewer environmental concerns.

Appendices

S6-1.2 Improved Grey Correlation Analysis

(1) Grey Correlation Analysis

Grey Correlation Analysis is used to solve the problems presented in gray systems and assist the analysis, modelling, prediction, decision-making, and control process. According to Wang et al. (2019), the Grey Correlation Analysis reveals the relationship between two discrete sequences in grey space and requires fewer data and less calculation. Yang and Zhang (2007) used the Grey Correlation Analysis to investigate the influence of particle fractions of slag powder on the compressive strength of slag cement composed of 50% slag powder and 50% Portland cement.

The Grey Correlation Analysis was used in this study to obtain the integrated value of the binding energy of 4ZRY and OR5AN1. There is an observation matrix X_i and a positive ideal quantities X^+ . The grey correlation coefficient $\gamma(x_j^+, x_{ij})$ can be calculated as below:

$$\gamma(x_j^+, x_{ij}) = \frac{m + \xi M}{\Delta_{ij}^+ + \xi M} \quad (6-S1)$$

In which, “i” represents the SM molecule, “j” represents proteins (4ZRY or OR5AN1), $m = \min_i \min_j (\Delta_{ij}^+)$, $M = \max_i \max_j (\Delta_{ij}^+)$. In order to reduce the influence of extreme values on the evaluation results, the resolution coefficient ξ is introduced, and $\xi \in [0,1]$. The “ ξ ” and Δ_{ij}^+ can be calculated using equations 2 and 3:

$$\xi = \frac{\sigma}{\mu} \quad (6-S2)$$

In which σ is the standard deviation, and μ is the average value of X_{ij} .

$$\Delta_{ij}^+ = |x_j^+ - x_{ij}| \quad (6-S3)$$

In which x_j^+ is the ideal value. In this study, the x_j^+ for 4ZRY and OR5AN1 was set as 80% of the minimum value of X_{ij} and 120% of the maximum value of the X_{ij} , respectively.

(2) Grey Correlation Analysis combined with technique for order preference by similarity to an ideal solution (TOPSIS)

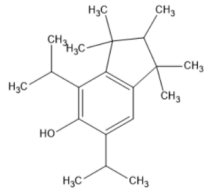
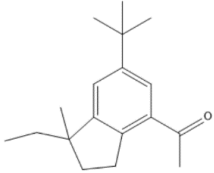
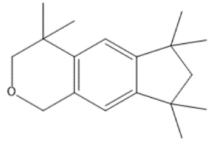
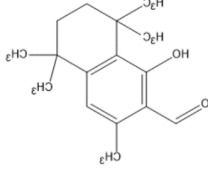
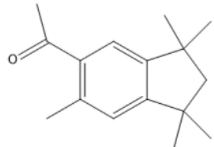
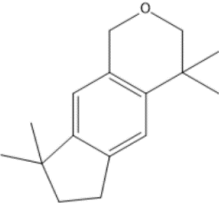
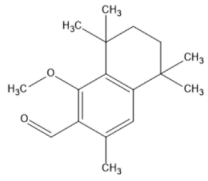
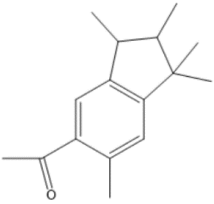
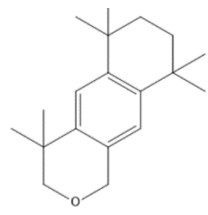
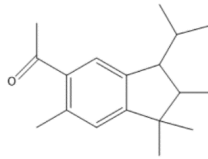
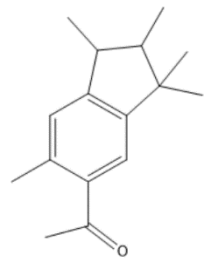
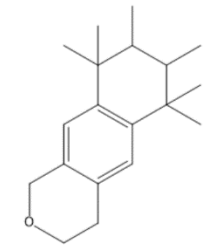
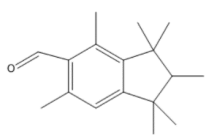
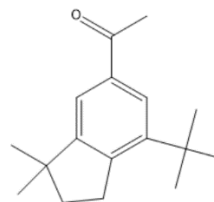
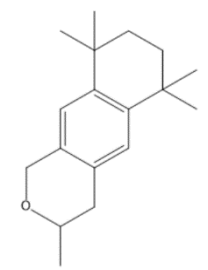
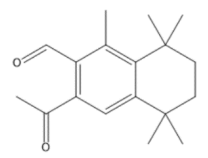
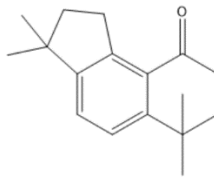
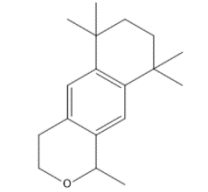
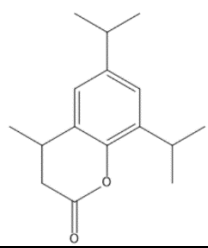
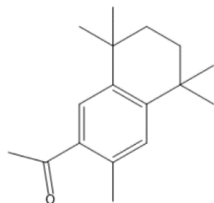
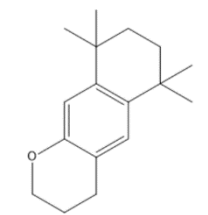
Grey Correlation Analysis is a maximum relevance evaluation method. The higher γ_{mi}^+ means the more accurate the comprehensive evaluation X_i . To calculate the negative ideal vector X^- , the equation is as follows:

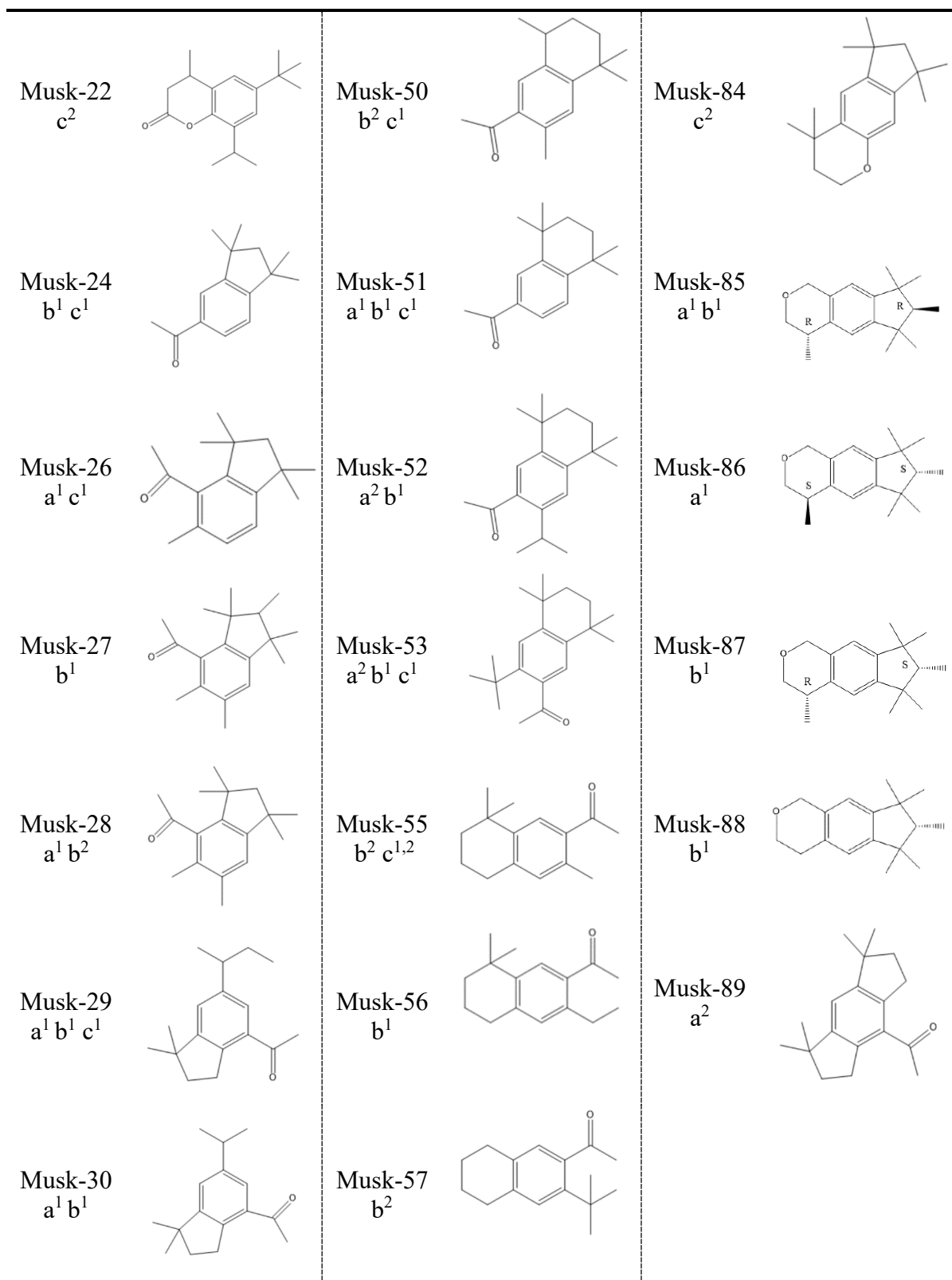
$$\gamma(x_j^-, x_{ij}) = \frac{m + \xi M}{\Delta_{ij}^- + \xi M} \quad (6-S4)$$

Table S6-1 Molecular structures of the training set and test set used in 3D-QSAR modelling.

No.	Molecular structure	No.	Molecular structure	No.	Molecular structure
Musk-1 a ¹ b ¹ c ¹		Musk-31 a ¹ b ¹		Musk-59 a ¹ b ¹	
Musk-2 c ¹		Musk-32 a ¹ b ² c ¹		Musk-60 b ¹	
Musk-4 b ² c ¹		Musk-33 a ¹ b ¹		Musk-61 a ¹ b ¹ c ¹	
Musk-5 a ¹ b ¹ c ¹		Musk-34 a ¹ b ¹		Musk-62 a ² b ¹	
Musk-6 a ¹ c ¹		Musk-35 a ¹ b ¹ c ¹		Musk-63 b ¹ c ¹	

Musk-7 b ^{1,2}		Musk-36 a ¹ b ² c ¹		Musk-64 a ¹ b ²	
Musk-8 b ¹ c ¹		Musk-37 b ¹ c ²		Musk-65 c ¹	
Musk-9 b ¹		Musk-38 a ² b ¹ c ²		Musk-66 a ¹ b ¹	
Musk-10 a ¹ b ¹		Musk-39 a ² b ¹ c ¹		Musk-72 a ² b ²	
Musk-11 a ¹ b ¹		Musk-40 a ¹ b ¹ c ¹		Musk-73 a ¹ b ¹ c ²	
Musk-12 a ¹		Musk-41 b ¹ c ²		Musk-74 a ¹ b ²	
Musk-13 a ¹ b ¹		Musk-42 a ² b ¹ c ²		Musk-75 b ¹ c ¹	

Musk-14 $a^2 b^1$		Musk-43 $a^1 b^2 c^2$		Musk-76 b^1	
Musk-15 $a^1 c^1$		Musk-44 $a^2 b^1$		Musk-77 $a^1 b^1 c^1$	
Musk-16 a^1		Musk-45 $a^1 b^1$		Musk-79 $a^1 b^2$	
Musk-17 $b^1 c^1$		Musk-46 $a^2 b^1$		Musk-80 $a^1 b^1$	
Musk-18 $b^1 c^1$		Musk-47 $a^1 c^1$		Musk-81 $b^1 c^1$	
Musk-20 $a^{1,2}$		Musk-48 $a^1 b^1 c^1$		Musk-82 $a^1 b^2 c^2$	
Musk-21 c^1		Musk-49 $a^1 b^1$		Musk-83 $a^1 c^2$	



(1) Molecular structures used in the 3D-QSAR models for predicting a: 4ZRY; b: OR5AN1; c: multi-activity;

(2) ¹ means training set; ² means test set.

Table S6-2 The binding energy of SMs-4ZRY, SMs-OR5AN1 and SMs-C

SMs	The binding energy of SMs-4ZRY	The binding energy of SMs-OR5AN1	The binding energy of SMs-C	SMs	The binding energy of SMs-4ZRY	The binding energy of SMs-OR5AN1	The binding energy of SMs-C
1	88.91	139.272	0.543	43	84.97	93.546	0.434
2	110.67	135.775	0.476	44	107.04	107.934	0.402
3	85.23	131.603	0.526	45	107.89	93.812	0.374
4	75.62	135.657	0.582	46	101.46	93.753	0.387
5	125.14	117.870	0.397	47	103.64	107.255	0.408
6	120.99	161.034	0.602	48	111.23	102.619	0.384
7	104.96	165.559	0.670	49	118.09	100.623	0.368
8	106.85	161.637	0.631	50	96.31	104.930	0.420
9	97.64	158.374	0.626	51	85.47	102.034	0.448
10	91.54	141.139	0.543	52	101.94	123.577	0.453
11	61.65	119.709	0.626	53	103.39	136.861	0.495
12	88.37	136.512	0.534	55	50.97	98.840	0.718
13	101.78	137.405	0.501	56	74.58	89.837	0.474
14	94.96	127.929	0.483	57	87.99	103.548	0.442
15	132.91	110.023	0.368	58	103.64	107.982	0.410
16	99.79	105.170	0.412	59	116.06	102.921	0.376
17	108.09	116.076	0.419	60	80.11	115.962	0.500
18	83.67	117.434	0.489	61	96.18	97.343	0.406
19	66.33	115.214	0.576	62	103.17	106.681	0.408
20	133.37	110.193	0.368	63	80.43	117.707	0.503
21	121.68	99.571	0.361	64	111.64	99.020	0.376
22	96.13	107.221	0.426	65	83.67	87.663	0.429
24	109.38	100.105	0.382	66	102.05	82.520	0.368
25	100.82	98.828	0.398	72	96.16	101.197	0.413
26	89.24	83.323	0.404	73	112.87	117.412	0.414
27	77.13	126.225	0.542	74	110.24	106.556	0.393
28	77.52	117.162	0.514	75	85.52	99.851	0.443

29	104.89	104.722	0.400	76	103.83	118.861	0.435
30	97.56	90.112	0.390	77	85.71	93.617	0.432
31	63.91	121.240	0.611	79	107.71	131.678	0.467
32	76.03	100.859	0.485	80	103.96	116.194	0.428
33	118.68	96.817	0.360	81	109.45	109.872	0.402
34	57.24	99.613	0.628	82	90.06	126.049	0.491
35	108.65	96.563	0.377	83	103.35	102.980	0.400
36	78.21	97.758	0.469	84	94.35	124.928	0.476
37	86.81	113.030	0.467	85	64.36	110.242	0.579
38	121.73	132.270	0.445	86	54.21	123.808	0.725
39	104.25	110.694	0.414	87	53.66	114.528	0.708
40	97.01	95.837	0.401	88	64.76	113.671	0.584
41	88.04	86.893	0.413	89	115.83	94.425	0.361
42	101.56	95.542	0.390				

Table S6-3 The assessment of the constructed 3D-QSAR models.

Models	q^2	r^2	F^{*1}	$R^2_{\text{pred}}^{*2}$
SMs-4ZRY	0.726	0.999	3589.073	0.697
SMs-OR5AN1	0.701	0.992	494.045	0.775
SMs-C	0.758	0.992	330.303	0.936

Note: ^{*1} refers to F-value; ^{*2} refers to external test coefficient.

Table S6-4 The contributions of hydrophobic, acceptor, donor, electrostatic, and steric fields in 3D-QSAR models.

Models	Hydrophobic field	Acceptor field	Donor field	Electrostatic field	Steric field
SMs-4ZRY	/	/	/	0.658	0.342
SMs-OR5AN1	/	/	/	0.362	0.638
SMs-C	0.167	0.382	0.008	0.006	0.377

Table S6-5-1 The substitution sites of galaxolide (HHCB)

NO.	Site-4	Site-5	Site-6	NO.	Site-4	Site-5	Site-6
1	COOH			46	COOH		NH ₂
2	C ₂ H ₅			47	C ₂ H ₅		NH ₂
3	CH=CH ₂			48	CH=CH ₂		NH ₂
4	OCH ₃			49	OCH ₃		NH ₂
5	CH ₂ OH			50	CH ₂ OH		NH ₂
6	C=-CH			51	C=-CH		NH ₂
7	OH			52	OH		NH ₂
8	CHO			53	CHO		NH ₂
9		OCH ₃		54		OCH ₃	OH
10			OH	55		OCH ₃	CHO
11			CHO	56		OCH ₃	COOH
12			COOH	57		OCH ₃	NH ₂
13			NH ₂	58	COOH	OCH ₃	OH
14	COOH	OCH ₃		59	C ₂ H ₅	OCH ₃	OH
15	C ₂ H ₅	OCH ₃		60	CH=CH ₂	OCH ₃	OH
16	CH=CH ₂	OCH ₃		61	OCH ₃	OCH ₃	OH
17	OCH ₃	OCH ₃		62	CH ₂ OH	OCH ₃	OH
18	CH ₂ OH	OCH ₃		63	C=-CH	OCH ₃	OH
19	C=-CH	OCH ₃		64	OH	OCH ₃	OH
20	OH	OCH ₃		65	CHO	OCH ₃	OH
21	CHO	OCH ₃		66	COOH	OCH ₃	CHO
22	COOH		OH	67	C ₂ H ₅	OCH ₃	CHO
23	C ₂ H ₅		OH	68	CH=CH ₂	OCH ₃	CHO
24	CH=CH ₂		OH	69	OCH ₃	OCH ₃	CHO
25	OCH ₃		OH	70	CH ₂ OH	OCH ₃	CHO
26	CH ₂ OH		OH	71	C=-CH	OCH ₃	CHO
27	C=-CH		OH	72	OH	OCH ₃	CHO
28	OH		OH	73	CHO	OCH ₃	CHO
29	CHO		OH	74	COOH	OCH ₃	COOH
30	COOH		CHO	75	C ₂ H ₅	OCH ₃	COOH
31	C ₂ H ₅		CHO	76	CH=CH ₂	OCH ₃	COOH
32	CH=CH ₂		CHO	77	OCH ₃	OCH ₃	COOH
33	OCH ₃		CHO	78	CH ₂ OH	OCH ₃	COOH
34	CH ₂ OH		CHO	79	C=-CH	OCH ₃	COOH
35	C=-CH		CHO	80	OH	OCH ₃	COOH
36	OH		CHO	81	CHO	OCH ₃	COOH

37	CHO	CHO	82	COOH	OCH ₃	NH ₂
38	COOH	COOH	83	C ₂ H ₅	OCH ₃	NH ₂
39	C ₂ H ₅	COOH	84	CH=CH ₂	OCH ₃	NH ₂
40	CH=CH ₂	COOH	85	OCH ₃	OCH ₃	NH ₂
41	OCH ₃	COOH	86	CH ₂ OH	OCH ₃	NH ₂
42	CH ₂ OH	COOH	87	C=-CH	OCH ₃	NH ₂
43	C=-CH	COOH	88	OH	OCH ₃	NH ₂
44	OH	COOH	89	CHO	OCH ₃	NH ₂
45	CHO	COOH				

Table S6-5-2 The substitution sites of traseolide (TRASE)

NO.	Site-1	Site-3	Site-4	NO.	Site-1	Site-3	Site-4
1	OCH ₃			36	NO ₂		COOH
2	NO ₂			37	NO ₂		CHO
3		COOH		38	NO ₂		NH ₂
4		C ₂ H ₅		39		COOH	OH
5		CH=CH ₂		40		COOH	COOH
6		OCH ₃		41		COOH	CHO
7		CH ₂ OH		42		COOH	NH ₂
8		C=-CH		43		C ₂ H ₅	OH
9		OH		44		C ₂ H ₅	COOH
10		CHO		45		C ₂ H ₅	CHO
11			OH	46		C ₂ H ₅	NH ₂
12			COOH	47		CH=CH ₂	OH
13			CHO	48		CH=CH ₂	COOH
14			NH ₂	49		CH=CH ₂	CHO
15	OCH ₃	COOH		50		CH=CH ₂	NH ₂
16	OCH ₃	C ₂ H ₅		51		OCH ₃	OH
17	OCH ₃	CH=CH ₂		52		OCH ₃	COOH
18	OCH ₃	OCH ₃		53		OCH ₃	CHO
19	OCH ₃	CH ₂ OH		54		OCH ₃	NH ₂
20	OCH ₃	C=-CH		55		CH ₂ OH	OH
21	OCH ₃	OH		56		CH ₂ OH	COOH
22	OCH ₃	CHO		57		CH ₂ OH	CHO
23	NO ₂	COOH		58		CH ₂ OH	NH ₂
24	NO ₂	C ₂ H ₅		59		C=-CH	OH
25	NO ₂	CH=CH ₂		60		C=-CH	COOH
26	NO ₂	OCH ₃		61		C=-CH	CHO
27	NO ₂	CH ₂ OH		62		C=-CH	NH ₂
28	NO ₂	C=-CH		63		OH	OH
29	NO ₂	OH		64		OH	COOH
30	NO ₂	CHO		65		OH	CHO
31	OCH ₃		OH	66		OH	NH ₂
32	OCH ₃		COOH	67		CHO	OH
33	OCH ₃		CHO	68		CHO	COOH
34	OCH ₃		NH ₂	69		CHO	CHO
35	NO ₂		OH	70		CHO	NH ₂

Table S6-5-3 The substitution sites of phantolide (PHAN)

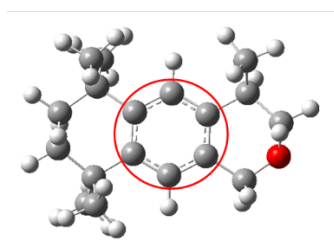
No.	Site-2	Site-3	Site-4	Site-5	Site-6	No.	Site-2	Site-3	Site-4	Site-5	Site-6	No.	Site-2	Site-3	Site-4	Site-5	Site-6
1	CH=CH ₂					179	CHO				NH ₂	357		C ₂ H ₅		CHO	
2	CH ₂ NH ₂					180	CHO				CH ₂ OH	358		C ₂ H ₅		COOH	
3	OCH ₃					181	CHO				C=-CH	359		C ₃ H ₇		NH ₂	
4	NH ₂					182	CHO				OH	360		C ₃ H ₇		OH	
5	CH ₂ OH					183	CHO				CHO	361		C ₂ H ₅			CH=CH ₂
6	C=-CH					184	CHO				COOH	362		C ₂ H ₅			CH ₂ NH ₂
7	OH					185	CHO				CH=CH ₂	363		C ₂ H ₅			OCH ₃
8	CHO					186	COOH				CH ₂ NH ₂	364		C ₂ H ₅			NH ₂
9	COOH					187	COOH				OCH ₃	365		C ₂ H ₅			CH ₂ OH
10		C ₂ H ₅				188	COOH				NH ₂	366		C ₂ H ₅			C=-CH
11		C ₃ H ₇				189	COOH				CH ₂ OH	367		C ₂ H ₅			OH
12			CH=CH ₂			190	COOH				C=-CH	368		C ₂ H ₅			CHO
13			CH ₂ NH ₂			191	COOH				OH	369		C ₂ H ₅			COOH
14			OCH ₃			192	COOH				CHO	370		C ₃ H ₇			NH ₂
15			NH ₂			193	COOH				COOH	371		C ₃ H ₇			OH
16			CH ₂ OH			194	COOH				CH=CH ₂	372			CH=CH ₂	CH=CH ₂	
17			C=-CH			195			OCH ₃		CH ₂ NH ₂	373			CH=CH ₂	CH ₂ NH ₂	
18			OH			196			OCH ₃		OCH ₃	374			CH=CH ₂	OCH ₃	
19			CHO			197			OCH ₃		NH ₂	375			CH=CH ₂	NH ₂	
20			COOH			198			OCH ₃		CH ₂ OH	376			CH=CH ₂	CH ₂ OH	
21				CH=CH ₂		199			OCH ₃		C=-CH	377			CH=CH ₂	C=-CH	
22				CH ₂ NH ₂		200			OCH ₃		OH	378			CH=CH ₂	OH	
23				OCH ₃		201			OCH ₃		CHO	379			CH=CH ₂	CHO	
24				NH ₂		202			OCH ₃		COOH	380			CH=CH ₂	COOH	
25				CH ₂ OH		203			OCH ₃		CH=CH ₂	381			CH ₂ NH ₂	CH=CH ₂	
26				C=-CH		204			NH ₂		CH ₂ NH ₂	382			CH ₂ NH ₂	CH ₂ NH ₂	
27				OH		205			NH ₂		OCH ₃	383			CH ₂ NH ₂	OCH ₃	
28				CHO		206			NH ₂		NH ₂	384			CH ₂ NH ₂	NH ₂	
29				COOH		207			NH ₂		CH ₂ OH	385			CH ₂ NH ₂	CH ₂ OH	
30					CH=CH ₂	208			NH ₂		C=-CH	386			CH ₂ NH ₂	C=-CH	
31					CH ₂ NH ₂	209			NH ₂		OH	387			CH ₂ NH ₂	OH	
32					OCH ₃	210			NH ₂		CHO	388			CH ₂ NH ₂	CHO	
33					NH ₂	211			NH ₂		COOH	389			CH ₂ NH ₂	COOH	
34					CH ₂ OH	212			NH ₂		CH=CH ₂	390			OCH ₃	CH=CH ₂	
35					C=-CH	213			CH ₂ OH		CH ₂ NH ₂	391			OCH ₃	CH ₂ NH ₂	
36					OH	214			CH ₂ OH		OCH ₃	392			OCH ₃	OCH ₃	
37					CHO	215			CH ₂ OH		NH ₂	393			OCH ₃	NH ₂	
38					COOH	216			CH ₂ OH		CH ₂ OH	394			OCH ₃	CH ₂ OH	

39	CH=CH ₂	C ₂ H ₅	217	CH ₂ OH	C=-CH	395	OCH ₃	C=-CH
40	CH ₂ NH ₂	C ₂ H ₅	218	CH ₂ OH	OH	396	OCH ₃	OH
41	CH ₂ NH ₂	C ₃ H ₇	219	CH ₂ OH	CHO	397	OCH ₃	CHO
42	OCH ₃	C ₂ H ₅	220	CH ₂ OH	COOH	398	OCH ₃	COOH
43	OCH ₃	C ₃ H ₇	221	CH ₂ OH	CH=CH ₂	399	NH ₂	CH=CH ₂
44	NH ₂	C ₂ H ₅	222	C=-CH	CH ₂ NH ₂	400	NH ₂	CH ₂ NH ₂
45	NH ₂	C ₃ H ₇	223	C=-CH	OCH ₃	401	NH ₂	OCH ₃
46	CH ₂ OH	C ₂ H ₅	224	C=-CH	NH ₂	402	NH ₂	NH ₂
47	OH	C ₂ H ₅	225	C=-CH	CH ₂ OH	403	NH ₂	CH ₂ OH
48	OH	C ₃ H ₇	226	C=-CH	C=-CH	404	NH ₂	C=-CH
49	CHO	C ₂ H ₅	227	C=-CH	OH	405	NH ₂	OH
50	COOH	C ₂ H ₅	228	C=-CH	CHO	406	NH ₂	CHO
51	CH=CH ₂	CH=CH ₂	229	C=-CH	COOH	407	NH ₂	COOH
52	CH=CH ₂	CH ₂ NH ₂	230	C=-CH	CH=CH ₂	408	CH ₂ OH	CH=CH ₂
53	CH=CH ₂	OCH ₃	231	OH	CH ₂ NH ₂	409	CH ₂ OH	CH ₂ NH ₂
54	CH=CH ₂	NH ₂	232	OH	OCH ₃	410	CH ₂ OH	OCH ₃
55	CH=CH ₂	CH ₂ OH	233	OH	NH ₂	411	CH ₂ OH	NH ₂
56	CH=CH ₂	C=-CH	234	OH	CH ₂ OH	412	CH ₂ OH	CH ₂ OH
57	CH=CH ₂	OH	235	OH	C=-CH	413	CH ₂ OH	C=-CH
58	CH=CH ₂	CHO	236	OH	OH	414	CH ₂ OH	OH
59	CH=CH ₂	COOH	237	OH	CHO	415	CH ₂ OH	CHO
60	CH ₂ NH ₂	CH=CH ₂	238	OH	COOH	416	CH ₂ OH	COOH
61	CH ₂ NH ₂	CH ₂ NH ₂	239	OH	CH=CH ₂	417	C=-CH	CH=CH ₂
62	CH ₂ NH ₂	OCH ₃	240	CHO	CH ₂ NH ₂	418	C=-CH	CH ₂ NH ₂
63	CH ₂ NH ₂	NH ₂	241	CHO	OCH ₃	419	C=-CH	OCH ₃
64	CH ₂ NH ₂	CH ₂ OH	242	CHO	NH ₂	420	C=-CH	NH ₂
65	CH ₂ NH ₂	C=-CH	243	CHO	CH ₂ OH	421	C=-CH	CH ₂ OH
66	CH ₂ NH ₂	OH	244	CHO	C=-CH	422	C=-CH	C=-CH
67	CH ₂ NH ₂	CHO	245	CHO	OH	423	C=-CH	OH
68	CH ₂ NH ₂	COOH	246	CHO	CHO	424	C=-CH	CHO
69	OCH ₃	CH=CH ₂	247	CHO	COOH	425	C=-CH	COOH
70	OCH ₃	CH ₂ NH ₂	248	CHO	CH=CH ₂	426	OH	CH=CH ₂
71	OCH ₃	OCH ₃	249	COOH	CH ₂ NH ₂	427	OH	CH ₂ NH ₂
72	OCH ₃	NH ₂	250	COOH	OCH ₃	428	OH	OCH ₃
73	OCH ₃	CH ₂ OH	251	COOH	NH ₂	429	OH	NH ₂
74	OCH ₃	C=-CH	252	COOH	CH ₂ OH	430	OH	CH ₂ OH
75	OCH ₃	OH	253	COOH	C=-CH	431	OH	C=-CH
76	OCH ₃	CHO	254	COOH	OH	432	OH	OH
77	OCH ₃	COOH	255	COOH	CHO	433	OH	CHO
78	NH ₂	CH=CH ₂	256	COOH	COOH	434	OH	COOH

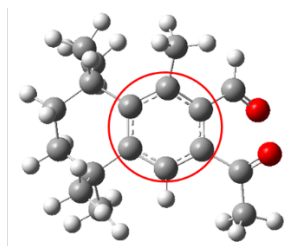
79	NH ₂	CH ₂ NH ₂	257		COOH	435	CHO	CH=CH ₂
80	NH ₂	OCH ₃	258	CH=CH ₂	CH=CH ₂	436	CHO	CH ₂ NH ₂
81	NH ₂	NH ₂	259	CH=CH ₂	CH ₂ NH ₂	437	CHO	OCH ₃
82	NH ₂	CH ₂ OH	260	CH=CH ₂	OCH ₃	438	CHO	NH ₂
83	NH ₂	C=-CH	261	CH=CH ₂	NH ₂	439	CHO	CH ₂ OH
84	NH ₂	OH	262	CH=CH ₂	CH ₂ OH	440	CHO	C=-CH
85	NH ₂	CHO	263	CH=CH ₂	C=-CH	441	CHO	OH
86	NH ₂	COOH	264	CH=CH ₂	OH	442	CHO	CHO
87	CH ₂ OH	CH=CH ₂	265	CH=CH ₂	CHO	443	CHO	COOH
88	CH ₂ OH	CH ₂ NH ₂	266	CH=CH ₂	COOH	444	COOH	CH=CH ₂
89	CH ₂ OH	OCH ₃	267	CH ₂ NH ₂	CH=CH ₂	445	COOH	CH ₂ NH ₂
90	CH ₂ OH	NH ₂	268	CH ₂ NH ₂	CH ₂ NH ₂	446	COOH	OCH ₃
91	CH ₂ OH	CH ₂ OH	269	CH ₂ NH ₂	OCH ₃	447	COOH	NH ₂
92	CH ₂ OH	C=-CH	270	CH ₂ NH ₂	NH ₂	448	COOH	CH ₂ OH
93	CH ₂ OH	OH	271	CH ₂ NH ₂	CH ₂ OH	449	COOH	C=-CH
94	CH ₂ OH	CHO	272	CH ₂ NH ₂	C=-CH	450	COOH	OH
95	CH ₂ OH	COOH	273	CH ₂ NH ₂	OH	451	COOH	CHO
96	C=-CH	CH=CH ₂	274	CH ₂ NH ₂	CHO	452	COOH	COOH
97	C=-CH	CH ₂ NH ₂	275	CH ₂ NH ₂	COOH	453		CH=CH ₂ CH=CH ₂
98	C=-CH	OCH ₃	276	OCH ₃	CH=CH ₂	454		CH=CH ₂ CH ₂ NH ₂
99	C=-CH	NH ₂	277	OCH ₃	CH ₂ NH ₂	455		CH=CH ₂ OCH ₃
100	C=-CH	CH ₂ OH	278	OCH ₃	OCH ₃	456		CH=CH ₂ NH ₂
101	C=-CH	C=-CH	279	OCH ₃	NH ₂	457		CH=CH ₂ CH ₂ OH
102	C=-CH	OH	280	OCH ₃	CH ₂ OH	458		CH=CH ₂ C=-CH
103	C=-CH	CHO	281	OCH ₃	C=-CH	459		CH=CH ₂ OH
104	C=-CH	COOH	282	OCH ₃	OH	460		CH=CH ₂ CHO
105	OH	CH=CH ₂	283	OCH ₃	CHO	461		CH=CH ₂ COOH
106	OH	CH ₂ NH ₂	284	OCH ₃	COOH	462		CH ₂ NH ₂ CH=CH ₂
107	OH	OCH ₃	285	NH ₂	CH=CH ₂	463		CH ₂ NH ₂ CH ₂ NH ₂
108	OH	NH ₂	286	NH ₂	CH ₂ NH ₂	464		CH ₂ NH ₂ OCH ₃
109	OH	CH ₂ OH	287	NH ₂	OCH ₃	465		CH ₂ NH ₂ NH ₂
110	OH	C=-CH	288	NH ₂	NH ₂	466		CH ₂ NH ₂ CH ₂ OH
111	OH	OH	289	NH ₂	CH ₂ OH	467		CH ₂ NH ₂ C=-CH
112	OH	CHO	290	NH ₂	C=-CH	468		CH ₂ NH ₂ OH
113	OH	COOH	291	NH ₂	OH	469		CH ₂ NH ₂ CHO
114	CHO	CH=CH ₂	292	NH ₂	CHO	470		CH ₂ NH ₂ COOH
115	CHO	CH ₂ NH ₂	293	NH ₂	COOH	471		OCH ₃ CH=CH ₂
116	CHO	OCH ₃	294	CH ₂ OH	CH=CH ₂	472		OCH ₃ CH ₂ NH ₂
117	CHO	NH ₂	295	CH ₂ OH	CH ₂ NH ₂	473		OCH ₃ OCH ₃
118	CHO	CH ₂ OH	296	CH ₂ OH	OCH ₃	474		OCH ₃ NH ₂
119	CHO	C=-CH	297	CH ₂ OH	NH ₂	475		OCH ₃ CH ₂ OH

120	CHO	OH		298	CH ₂ OH	CH ₂ OH	476	OCH ₃	C=-CH
121	CHO	CHO		299	CH ₂ OH	C=-CH	477	OCH ₃	OH
122	CHO	COOH		300	CH ₂ OH	OH	478	OCH ₃	CHO
123	COOH	CH=CH ₂		301	CH ₂ OH	CHO	479	OCH ₃	COOH
124	COOH	CH ₂ NH ₂		302	CH ₂ OH	COOH	480	NH ₂	CH=CH ₂
125	COOH	OCH ₃		303	C=-CH	CH=CH ₂	481	NH ₂	CH ₂ NH ₂
126	COOH	NH ₂		304	C=-CH	CH ₂ NH ₂	482	NH ₂	OCH ₃
127	COOH	CH ₂ OH		305	C=-CH	OCH ₃	483	NH ₂	NH ₂
128	COOH	C=-CH		306	C=-CH	NH ₂	484	NH ₂	CH ₂ OH
129	COOH	OH		307	C=-CH	CH ₂ OH	485	NH ₂	C=-CH
130	COOH	CHO		308	C=-CH	C=-CH	486	NH ₂	OH
131	COOH	COOH		309	C=-CH	OH	487	NH ₂	CHO
132	OCH ₃		CH=CH ₂	310	C=-CH	CHO	488	NH ₂	COOH
133	OCH ₃		CH ₂ NH ₂	311	C=-CH	COOH	489	CH ₂ OH	CH=CH ₂
134	OCH ₃		OCH ₃	312	OH	CH=CH ₂	490	CH ₂ OH	CH ₂ NH ₂
135	OCH ₃		NH ₂	313	OH	CH ₂ NH ₂	491	CH ₂ OH	OCH ₃
136	OCH ₃		CH ₂ OH	314	OH	OCH ₃	492	CH ₂ OH	NH ₂
137	OCH ₃		C=-CH	315	OH	NH ₂	493	CH ₂ OH	CH ₂ OH
138	OCH ₃		OH	316	OH	CH ₂ OH	494	CH ₂ OH	C=-CH
139	OCH ₃		CHO	317	OH	C=-CH	495	CH ₂ OH	OH
140	OCH ₃		COOH	318	OH	OH	496	CH ₂ OH	CHO
141	NH ₂		CH=CH ₂	319	OH	CHO	497	CH ₂ OH	COOH
142	NH ₂		CH ₂ NH ₂	320	OH	COOH	498	C=-CH	CH=CH ₂
143	NH ₂		OCH ₃	321	CHO	CH=CH ₂	499	C=-CH	CH ₂ NH ₂
144	NH ₂		NH ₂	322	CHO	CH ₂ NH ₂	500	C=-CH	OCH ₃
145	NH ₂		CH ₂ OH	323	CHO	OCH ₃	501	C=-CH	NH ₂
146	NH ₂		C=-CH	324	CHO	NH ₂	502	C=-CH	CH ₂ OH
147	NH ₂		OH	325	CHO	CH ₂ OH	503	C=-CH	C=-CH
148	NH ₂		CHO	326	CHO	C=-CH	504	C=-CH	OH
149	NH ₂		COOH	327	CHO	OH	505	C=-CH	CHO
150	CH ₂ OH		CH=CH ₂	328	CHO	CHO	506	C=-CH	COOH
151	CH ₂ OH		CH ₂ NH ₂	329	CHO	COOH	507	OH	CH=CH ₂
152	CH ₂ OH		OCH ₃	330	COOH	CH=CH ₂	508	OH	CH ₂ NH ₂
153	CH ₂ OH		NH ₂	331	COOH	CH ₂ NH ₂	509	OH	OCH ₃
154	CH ₂ OH		CH ₂ OH	332	COOH	OCH ₃	510	OH	NH ₂
155	CH ₂ OH		C=-CH	333	COOH	NH ₂	511	OH	CH ₂ OH
156	CH ₂ OH		OH	334	COOH	CH ₂ OH	512	OH	C=-CH
157	CH ₂ OH		CHO	335	COOH	C=-CH	513	OH	OH
158	CH ₂ OH		COOH	336	COOH	OH	514	OH	CHO
159	C=-CH		CH=CH ₂	337	COOH	CHO	515	OH	COOH
160	C=-CH		CH ₂ NH ₂	338	COOH	COOH	516	CHO	CH=CH ₂

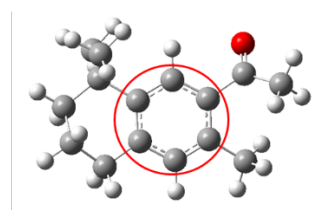
161	C=-CH	OCH ₃	339	C ₂ H ₅	CH=CH ₂	517	CHO	CH ₂ NH ₂
162	C=-CH	NH ₂	340	C ₂ H ₅	CH ₂ NH ₂	518	CHO	OCH ₃
163	C=-CH	CH ₂ OH	341	C ₂ H ₅	OCH ₃	519	CHO	NH ₂
164	C=-CH	C=-CH	342	C ₂ H ₅	NH ₂	520	CHO	CH ₂ OH
165	C=-CH	OH	343	C ₂ H ₅	CH ₂ OH	521	CHO	C=-CH
166	C=-CH	CHO	344	C ₂ H ₅	C=-CH	522	CHO	OH
167	C=-CH	COOH	345	C ₂ H ₅	OH	523	CHO	CHO
168	OH	CH=CH ₂	346	C ₂ H ₅	CHO	524	CHO	COOH
169	OH	CH ₂ NH ₂	347	C ₂ H ₅	COOH	525	COOH	CH=CH ₂
170	OH	OCH ₃	348	C ₃ H ₇	NH ₂	526	COOH	CH ₂ NH ₂
171	OH	NH ₂	349	C ₃ H ₇	OH	527	COOH	OCH ₃
172	OH	CH ₂ OH	350	C ₂ H ₅	CH=CH ₂	528	COOH	NH ₂
173	OH	C=-CH	351	C ₂ H ₅	CH ₂ NH ₂	529	COOH	CH ₂ OH
174	OH	OH	352	C ₂ H ₅	OCH ₃	530	COOH	C=-CH
175	OH	CHO	353	C ₂ H ₅	NH ₂	531	COOH	OH
176	OH	COOH	354	C ₂ H ₅	CH ₂ OH	532	COOH	CHO
177	CHO	CH=CH ₂	355	C ₂ H ₅	C=-CH	533	COOH	COOH
178	CHO	CH ₂ NH ₂	356	C ₂ H ₅	OH			



SM-7

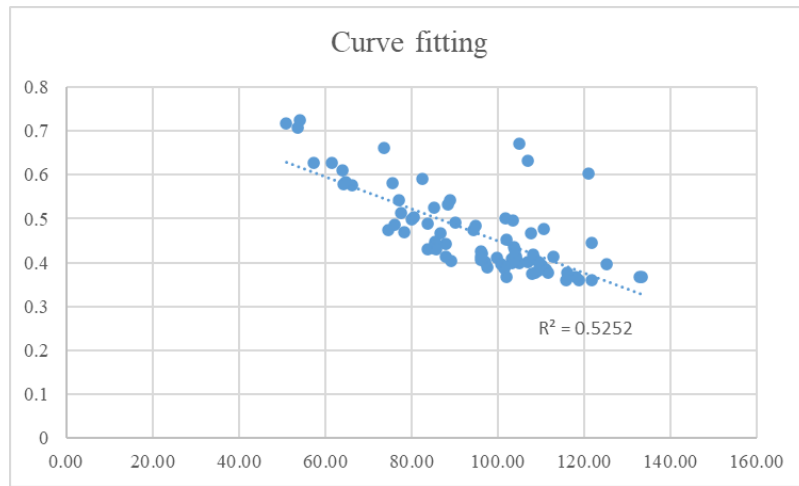


SM-20

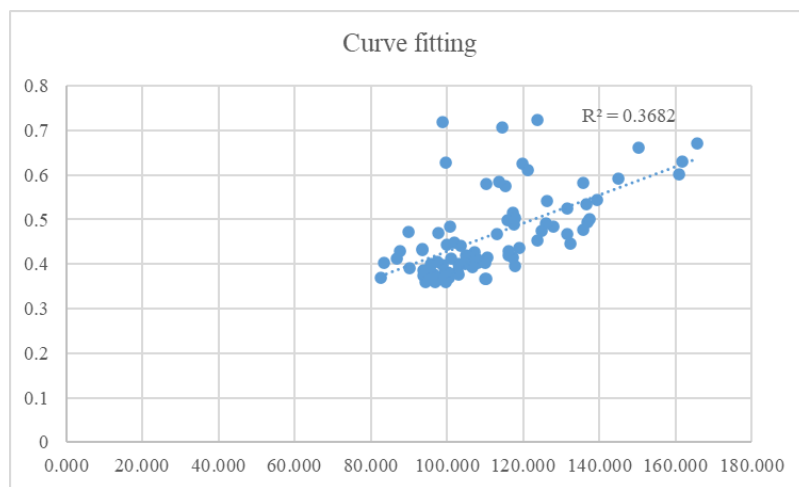


SM-55

Figure S6-1 The fingerprinting structures of template molecules SM-7, SM-20 and SM-55.

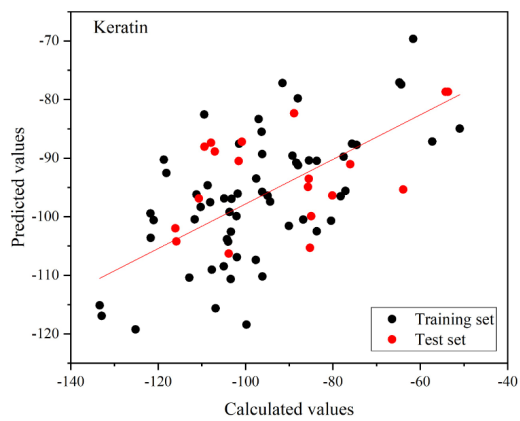


(a) SMs-4ZRY and SMs-C

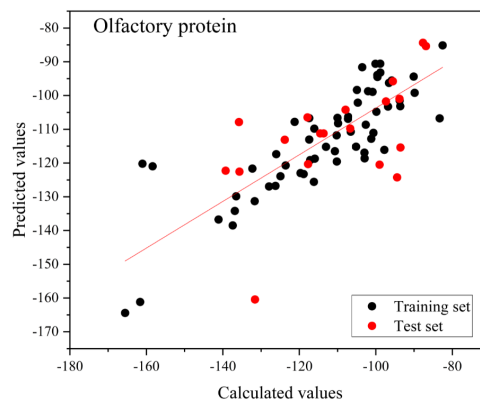


(b) SMs-OR5AN1 and SMs-C

Figure S6-2 The curve fitting of single factor and the multi-factors

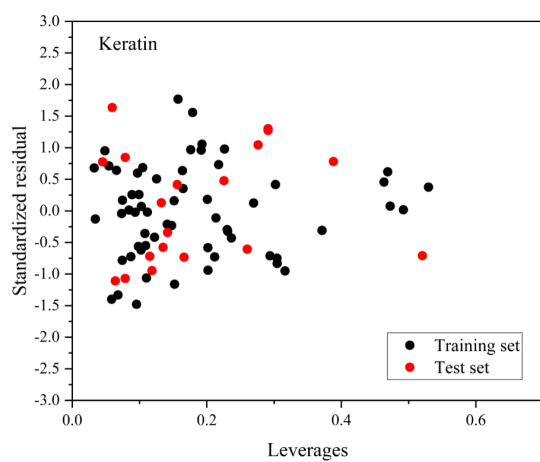


(a) Docked to 4ZRY

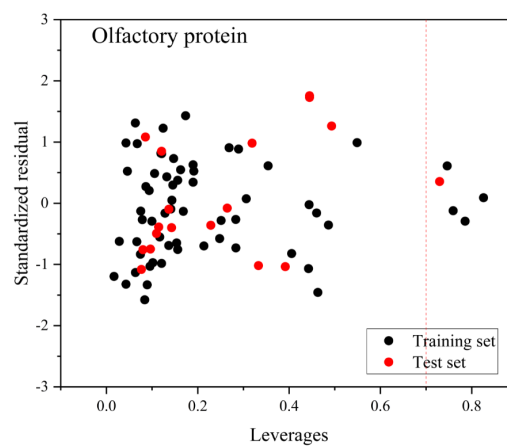


(b) Docked to OR5AN1

Figure S6-3 Linear fitting graph of 2D-QSAR models



(a) Docked to keratin



(b) Docked to olfactory protein

Figure S6-4 2D-QSAR model application domain William's diagram

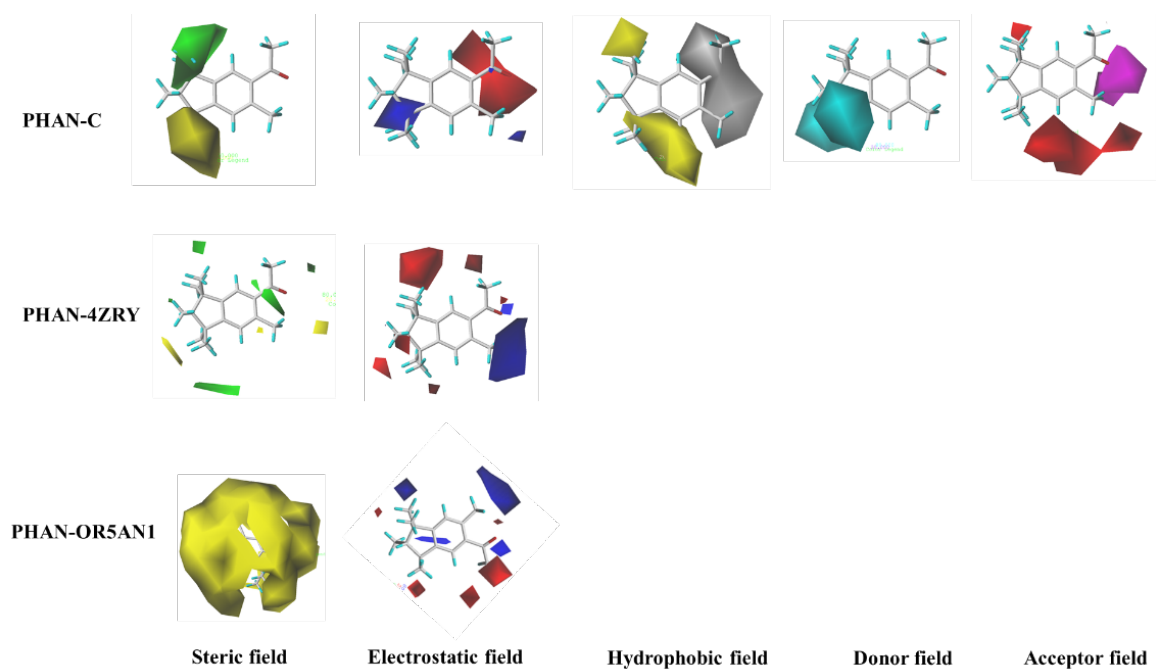


Figure S6-5 The contour maps of PHAN in 3D-QSAR models

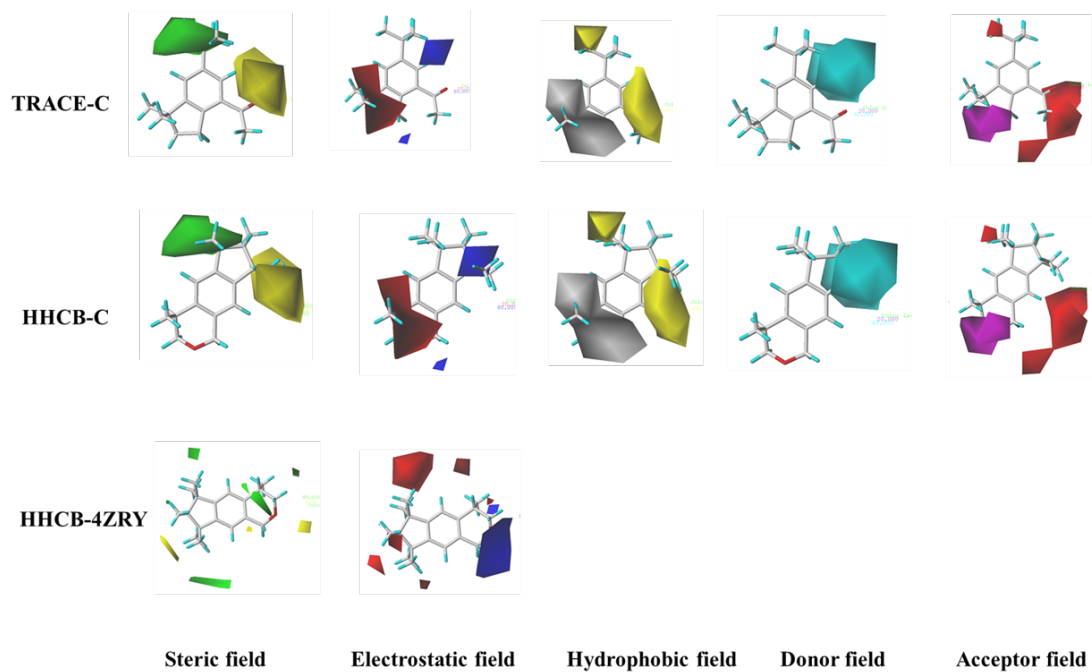


Figure S6-6 The contour maps of TRASE and HHCB in 3D-QSAR models

CHAPTER 7

CONCLUSIONS AND RECOMMENDATIONS

7.1 Conclusions

The primary focus of the thesis was to develop an in-silico framework for designing environmentally friendly, lower human health risks, and functional improved SM derivatives. Through the whole thesis, eight single factor 3D-QSAR models were constructed, covering environmental impacts (i.e., biotoxicity, mobility, and bioaccumulation ability), human health impacts (i.e., abortion risk of progestogen, abortion risk of estrogen, and bioaccumulation ability in skin keratin) and functional properties (i.e., half-life and odor sensitivity). Two multi-activity 3D-QSAR models were developed in this study as well with different mathematic approaches (i.e., G1-anti-entropy weight method and Improved Grey Correlation Analysis). Besides, molecular docking in Discovery Studio[®] 2020, molecular dynamics simulations in Dell PowerEdge R7425 server and Gromacs software, density functional theory in Gaussian software (in Compute Canada), TOPKAT module in Discovery Studio[®] 2020, full factorial experiment design, and Taguchi experiment design were used to supplement various toxicity analysis of SM derivatives. This study provided a comprehensive assessment of SM derivatives from designing, environmental and functional properties evaluation, simulation of derivatives' by-products from different treatment pathways. The thesis can be summarized as follows:

Chapter 2 provided a thorough review of classification, applications, occurrence and distributions, and typical synthetic routes of SMs. In addition, the review summarizes bioaccumulation (marine or river aquatic organisms and humans) and toxicity (physio toxicity and genotoxicity), as well as associated environmental risk assessment and pollution control. Finally, this chapter puts forward the environmental protection strategy, molecular modification, assessment, and screening of environmentally friendly SMs in the following studies.

In Chapter 3, the environmental risks of SMs treatment methods (i.e., biodegradation,

photodegradation, advanced oxidation (UV and ozone aided), and chlorination) were assessed by predicting the biotoxicity (LC_{50}) of SM by-products. LC_{50} in mysid and SM molecular structures were used as inputs to construct the 3D-QSAR model. The molecular structures of SMs (i.e., HHCB, AHTN, ADBI, PHAN, MK and TRASE) transformation by-products were collected from chlorination experiments (conducted in this study) and other treatment methods (collected from literature). After comparing the LC_{50} values of SM by-products and their precursors, a new finding showed that ozonation might propose more risk than the rest treatment methods to the environment (biotoxicity of SM by-product increased 179.16% than its precursors). Thus, special attention should be focused on the ozonation of SMs in the environment. The SM by-products with higher biotoxicity than their precursors were found in all the investigated treatment methods. Therefore, further treatment for SMs or designing new SM molecules are encouraged in future studies.

Chapter 4 gave a comprehensive view of designing environmentally friendly and functional improved SM derivatives. One optimum derivative with longer-lasting odor, lower environmental impacts, and lower human health risk comparing that of HHCB was designed and screened out. Three 3D-QSAR models (i.e., half-life, $\log VP$ and $\log BCF$) were constructed to obtain HHCB's new derivatives and predict their functional properties, mobility and bio-accumulation ability. The molecular docking, density functional theory, molecular dynamics integrated with Taguchi experimental design, and TOPKAT module were used for assessing the environmental properties of SM derivative, and thus, one optimum derivative was screened out. The degradation pathways (i.e., photodegradation, biotransformation, chlorination and metabolic pathways in algal cells) of the optimum SM derivative were simulated. By predicting the by-products' environmental properties, this chapter gives a clear and ahead perspective of the designed HHCB derivatives before it becomes an additive in PCPs.

A theoretical circumvention strategy proposed in Chapter 5 could be served as the comprehensive abortion risk control measure by effectively inhibiting the interaction between SMs with progesterone and estrogen. The resulted information gives a new sight of using integrated supplementary diet plans and molecular modification methods to reduce abortion risk. In this chapter, a theoretical circumvention strategy was established to reduce such abortion risk through adopting a supplementary diet, based on Taguchi experimental design and molecular dynamics simulations. Besides, three 3D-QSAR models (SM-C, SM-P and SM-C) were constructed to design lower abortion risk SM derivatives. Among the three 3D-QSAR models, SM-C is the first multi-factor 3D-QSAR model based on the G1-anti-entropy weighting method. The combining of supplementary diet plan and 3D-QSAR model verify the effectiveness of the proposed theoretical circumvention strategy as a comprehensive abortion risk control measure. The LibDock score of the optimum HHCB derivative under supplementary diet plan was reduced by 26.89%, compared with that of PHAN without a supplementary diet plan.

Chapter 6 provided a molecular-level insight into the interactions between SMs and skin keratin. In silico methods were established to reduce the human health risk of SMs from dermal exposure by investigating the risk mechanisms, designing lower bioaccumulation ability SMs and suggesting proper PCP ingredients using molecular docking, molecular dynamics simulation, and quantitative structure-activity relationship (QSAR) models. Three 3D-QSAR models and one 2D-QSAR model were constructed to design lower human health risk SM derivatives and explore the mechanism of what are molecular structure features affect the SMs accumulated in human keratin. The bioaccumulation risk of the selected PHAN derivative with a lower total energy ingredients group present could be reduced as higher as 42.272%, compared with that of PHAN without any additives based on the mechanism analysis.

7.2 Research Contributions

The major research contributions of this work can be summarized in the following aspects:

1) **The first study on biological toxicity of synthetic musks (SMs) transformation by-products predicted by the 3D-QSAR model.**

This area remains unexplored due to the rare identification of broad SM by-products and the lack of effective toxicity evaluation and management tools. This study tackled six commonly used SMs (i.e., galaxolide (HHCB), tonalide (AHTN), phantolide (PHAN), traseolide (TRASE), celestolide (ADBI) and musk ketone (MK)). Fifty-eight SM by-products of biodegradation, photodegradation, advanced oxidation (UV and ozone aided), and chlorination were identified by literature review and lab experiment. A 3D-QSAR model was first proposed to predict the toxicity of these by-products based on lethal concentration (LC_{50}) of mysid for SMs structures. The research outputs led to valuable reference data and useful guidance for understanding the fate of SMs and improving treatment strategies for mitigation of these emerging contaminants.

2) **The first study regarding the advancement of methodologies for creating and screening environmentally friendly SMs, evaluating their environmental properties, and managing the associated human health risks.**

HHCB was selected as it is one of the most widely used SMs and it has been recognized as an emerging contaminant by NORMAN. This study established the relationships between HHCB molecular structure and its functional/ environmental properties to design molecules of HHCB derivatives. This area remains unexplored due to the rare identification of effective parameters representing the odor property of SM when regulating their biotoxicity, bioaccumulation ability, mobility and stability. The assessment and control of the risks of HHCB to the human body were also conducted in this study, which has never been tackled before. The transformation by-products of the selected HHCB derivatives were further recognized and their associated environmental properties were predicted. This study provides the theoretical basis for the

design of functionally improved and environmentally friendly HHCB alternatives, helps to better understand their environmental behaviors, and facilitates their treatment after usage.

3) **The first study regarding the theoretical circumvention strategy to reduce the abortion risk of SMs to pregnant women through designing the supplementary diet plan and environmentally friendly SMs derivatives.** HHCB and MK were selected as they are one of the most widely used SMs and have been recognized as emerging contaminants by NORMAN. This study established the relationships between HHCB and MK molecular structures and their associated potential abortion risk so as to design molecules of HHCB and MK derivatives and further provided a supplementary diet plan to reduce the abortion risk in pregnant women. In addition, the assessment and control of environmental (i.e., bioaccumulation ability and mobility) and functional properties (i.e., odor stability, musky scent, and odor intensity) of HHCB derivatives were conducted. A significant synergistic effect was identified between supplementary diet plans and molecular modification. This study identified an effective strategy for inhibiting the interaction between SMs with progesterone and estrogen, and helped to provide scientific support for designing new pharmaceutical and personal care products.

4) **The first study regarding reducing the human health risk (represented by bioaccumulation ability) of SMs via dermal exposure.** A significant reduction of bioaccumulation ability of designed PHAN derivatives with lower total energy ingredients group was found compared with that of PHAN without any additives. The first study on the bioaccumulation mechanism of how the SMs influence the bioaccumulation ability of SMs in human skin is also proposed. This study used in silico methods to provide an in-depth investigation of human health risks assessment, mechanism, and risk control of SMs through dermal exposure.

7.3 Recommendations for Further Work

- 1) SMs as additives used in personal care products, accompanied by other additives like moisturizers, whitening agents, proteins, silicone, and so on. The interaction between these additives should be further conducted to reveal the environmental impacts, the human health risks of the products as a whole.
- 2) In-depth investigation should be pursued on the monitoring and evaluation of environmental behaviors of SMs (e.g., evaporation, natural biodegradation and photo-oxidation, their interaction with different contaminants and their migration among different media) to facilitate proper risk assessment and pollution control.
- 3) In addition, the bioaccumulation of SMs in the organisms and their toxicological impact on the surrounding environment are required. Till now, SMs have not been included in routine monitoring programs. An understanding of the pollution thresholds of SMs is of great importance to facilitate the management and the promulgation of appropriate laws and regulations.
- 4) The designed optimum SM derivatives should further be synthesized in the lab, and their environmental properties can then be detected using experimental technologies. This step will help to verify the SM derivatives' environmental properties predicted by *in silico* methods in this study.

REFERENCES

- Abramsson-Zetterberg, L., & Slanina, P. (2002). Macrocyclic musk compounds—an absence of genotoxicity in the Ames test and the in vivo Micronucleus assay. *Toxicol. Lett.*, *135*(1-2), 155-163. [https://doi.org/10.1016/S0378-4274\(02\)00257-6](https://doi.org/10.1016/S0378-4274(02)00257-6)
- Adeppa, K., Rupainwar, D. C., & Misra, K. (2010). Development of an improved method for conversion of thiuram disulfides into N, N-dialkylcarbamoyl halides and derivatives. *Synthetic Commun.*, *41*(2), 285-290. <https://doi.org/10.1080/00397910903537331>
- Aguirre, J., Bizkarguenaga, E., Iparraguirre, A., Fernández, L. Á., Zuloaga, O., & Prieto, A. (2014). Development of stir-bar sorptive extraction–thermal desorption–gas chromatography–mass spectrometry for the analysis of musks in vegetables and amended soils. *Anal. Chim. Acta.*, *812*, 74-82. <https://doi.org/10.1016/j.aca.2013.12.036>
- Ahmed, L., Zhang, Y., Block, E., Buehl, M., Corr, M. J., Cormanich, R. A., Gundala, R., Matsunami, H., O'Hagan, D., Ozbi, M., Pan, Y., Sekharan, S., Ten, N., Wang, M., Zhang, Q., Zhang, R., Batista, V.S., & Zhuang, H. (2018). Molecular mechanism of activation of human musk receptors OR5AN1 and OR1A1 by (R)-muscone and diverse other musk-smelling compounds. *Proc. Natl. Acad. Sci. U.S.A.*, *115*(17), E3950-E3958. <https://doi.org/10.1073/pnas.1713026115>
- Akula, N., Lecanu, L., Greeson, J., & Papadopoulos, V. (2006). 3D QSAR studies of AChE inhibitors based on molecular docking scores and CoMFA. *Bioorg. Med. Chem. Lett.*, *16*(24), 6277-6280. <https://doi.org/10.1016/j.bmcl.2006.09.030>
- Alaa, A. M., Asiri, Y. A., & Al-Agamy, M. H. (2011). Design, synthesis and antibacterial activity of fluoroquinolones containing bulky arenesulfonyl fragment: 2D-QSAR and docking study. *Eur. J. Med. Chem.*, *46*(11), 5487-5497. <https://doi.org/10.1016/j.ejmech.2011.09.011>
- Al-Malah, K. I. (2011). Aqueous solubility of a simple (single-carbon) organic molecule as a function of its size & dipole moment. *J. Mol. Model.*, *17*(5), 1029-1034. <https://doi.org/10.1007/s00894-010-0800-y>
- Alonso, H., Bliznyuk, A. A., & Gready, J. E. (2006). Combining docking and molecular dynamic simulations in drug design. *Med. Res. Rev.*, *26*(5), 531-568. <https://doi.org/10.1002/med.20067>
- Aminot, Y., Munsch, C., Héas-Moisan, K., Pollono, C., & Tixier, C. (2021). Levels and trends of synthetic musks in marine bivalves from French coastal areas. *Chemosphere*, *268*, 129312. <https://doi.org/10.1016/j.chemosphere.2020.129312>
- Andersson, S., Minjarez, D., Yost, N. P., & Word, R. A. (2008). Estrogen and progesterone metabolism in the cervix during pregnancy and parturition. *J. Clin. Endocrinol. Metab.*, *93*(6), 2366-2374. <https://doi.org/10.1210/jc.2007-2813>
- Andresen, J. A., Muir, D., Ueno, D., Darling, C., Theobald, N., & Bester, K. (2007). Emerging pollutants in the North Sea in comparison to Lake Ontario, Canada, data. *Environ. Toxicol. Chem.*, *26*(6), 1081-1089. <https://doi.org/10.1897/06-416R.1>
- Ansari, H. R. (1973). Cyclisation of optically active dihydromyrcenes (2, 6-dimethyl-2, 7-octadiene): A stereospecific ring contraction. *Tetrahedron*, *29*(11), 1559-1564. [https://doi.org/10.1016/S0040-4020\(01\)83397-4](https://doi.org/10.1016/S0040-4020(01)83397-4)
- Arbulu, M., Sampedro, M. C., Unceta, N., Gómez-Caballero, A., Goicolea, M. A., & Barrio, R. J. (2011). A retention time locked gas chromatography–mass spectrometry method based on stir-bar sorptive extraction and thermal desorption for automated determination of synthetic musk fragrances in natural and wastewaters. *J. Chromatog.*

- A., *J. Chromatogr. A*, *1218*(20), 3048-3055. <https://doi.org/10.1016/j.chroma.2011.03.012>
- Arnot, J.A., & Gobas, F.A. (2006). A review of bio-concentration factor (BCF) and bio-accumulation factor (BAF) assessments for organic chemicals in aquatic organisms. *Environ. Rev.*, *14* (4), 257-297. <https://doi.org/10.1139/a06-005>
- Arsenault, G., Konstantinov, A., Marvin, C. H., MacInnis, G., McAlees, A., McCrindle, R., Riddell, N., Tomy, G.T., & Yeo, B. (2007). Synthesis of the two minor isomers, δ - and ϵ -1, 2, 5, 6, 9, 10-hexabromocyclododecane, present in commercial hexabromocyclododecane. *Chemosphere*, *68*(5), 887-892. <https://doi.org/10.1016/j.chemosphere.2007.02.005>
- Artola-Garicano, E., Borkent, I., Damen, K., Jager, T., & Vaes, W. H. (2003b). Sorption kinetics and microbial biodegradation activity of hydrophobic chemicals in sewage sludge: Model and measurements based on free concentrations. *Environ Sci Technol.* *37*(1), 116-122. <https://doi.org/10.1021/es020115y>.
- Artola-Garicano, E., Borkent, I., Hermens, J. L., & Vaes, W. H. (2003a). Removal of two polycyclic musks in sewage treatment plants: freely dissolved and total concentrations. *Environ. Sci. Technol.*, *37*(14), 3111-3116. <https://doi.org/10.1021/es020226x>
- Ayhan, V., Çangal, Ç., Cesur, İ., Çoban, A., Ergen, G., Çay, Y., Kolip, A., & Özsert, İ. (2020). Optimization of the factors affecting performance and emissions in a diesel engine using biodiesel and EGR with Taguchi method. *Fuel*, *261*, 116371. <https://doi.org/10.1016/j.fuel.2019.116371>
- Bachelot, M., Li, Z., Munaron, D., Le Gall, P., Casellas, C., Fenet, H., & Gomez, E. (2012). Organic UV filter concentrations in marine mussels from French coastal regions. *Sci. Total Environ.*, *420*, 273-279. <https://doi.org/10.1016/j.scitotenv.2011.12.051>
- Balk, F., & Ford, R. A. (1999). Environmental risk assessment for the polycyclic musks AHTN and HHCB in the EU: I. Fate and exposure assessment. *Toxicol. Lett.*, *111*(1-2), 57-79. [https://doi.org/10.1016/S0378-4274\(99\)00169-1](https://doi.org/10.1016/S0378-4274(99)00169-1)
- Bello-Ramírez, A.M., & Nava-Ocampo, A.A. (2004). A QSAR analysis of toxicity of Aconitum alkaloids. *Fundam. Clin. Pharmacol.*, *18*(6), 699-704. <https://doi.org/10.1111/j.1472-8206.2004.00280.x>
- Berendsen, H. J., Postma, J. V., van Gunsteren, W. F., DiNola, A. R. H. J., & Haak, J. R. (1984). Molecular dynamics with coupling to an external bath. *J. Chem. Phys.*, *81*(8), 3684-3690. <https://doi.org/10.1063/1.448118>
- Besha, A. T., Gebreyohannes, A. Y., Tufa, R. A., Bekele, D. N., Curcio, E., & Giorno, L. (2017). Removal of emerging micropollutants by activated sludge process and membrane bioreactors and the effects of micropollutants on membrane fouling: A review. *J. Environ. Chem. Eng.*, *5*(3), 2395-2414. <https://doi.org/10.1016/j.jece.2017.04.027>
- Bester, K. (2004). Retention characteristics and balance assessment for two polycyclic musk fragrances (HHCB and AHTN) in a typical German sewage treatment plant. *Chemosphere*, *57*(8), 863-870. <https://doi.org/10.1016/j.chemosphere.2004.08.032>
- Bester, K. (2005). Polycyclic musks in the Ruhr catchment area—transport, discharges of waste water, and transformations of HHCB, AHTN and HHCB-lactone. *J. environ. monit.*, *7*(1), 43-51. [10.1039/B409213A](https://doi.org/10.1039/B409213A)
- Bester, K. (2009). Analysis of musk fragrances in environmental samples. *J. Chromatogr. A*, *1216*(3), 470-480. <https://doi.org/10.1016/j.chroma.2008.08.093>
- Blessy Christina, N. M. M., Meraj, K., & Bhaskar, M. (2012). In silico studies of indazole pyridine analogs as potent inhibitors of akt protein in cancer. *Int. J. Pharm. Sci. Rev.*

Res. 17(2), 56-61.

- Borch, J., Axelstad, M., Vinggaard, A. M., & Dalgaard, M. (2006). Diisobutyl phthalate has comparable anti-androgenic effects to di-n-butyl phthalate in fetal rat testis. *Toxicol. Lett.* 163(3), 183-190. <https://doi.org/10.1016/j.envres.2011.01.015>.
- Bordás, B., Bélai, I., & Kőmíves, T. (2011). Theoretical molecular descriptors relevant to the uptake of persistent organic pollutants from soil by zucchini. A QSAR study. *J. Agric. Food Chem.*, 59(7), 2863-2869. <https://doi.org/10.1021/jf1038772>
- Bradbury, L. M., Gillies, S. A., Brushett, D. J., Waters, D. L., & Henry, R. J. (2008). Inactivation of an aminoaldehyde dehydrogenase is responsible for fragrance in rice. *Plant Mol. Biol.*, 68(4-5), 439-449. <https://doi.org/10.1007/s11103-008-9381-x>
- Brausch, J. M., & Rand, G. M. (2011). A review of personal care products in the aquatic environment: environmental concentrations and toxicity. *Chemosphere*, 82(11), 1518-1532. <https://doi.org/10.1016/j.chemosphere.2010.11.018>
- Brunn, H., Bitsch, N., & Amberg-Müller, J. (2004). Toxicology of synthetic musk compounds in man and animals. In *Series Anthropogenic Compounds*. 259-280. Springer, Berlin, Heidelberg. <https://doi.org/10.1007/b14121>
- Buerge, I. J., Buser, H. R., Müller, M. D., & Poiger, T. (2003). Behavior of the polycyclic musks HHCB and AHTN in lakes, two potential anthropogenic markers for domestic wastewater in surface waters. *Environ. Sci. Technol.*, 37(24), 5636-5644. <https://doi.org/10.1021/es0300721>
- Bujak, T., Wasilewski, T., & Nizioł-Lukaszewska, Z. (2015). Role of macromolecules in the safety of use of body wash cosmetics. *Colloids Surf. B.*, 135, 497-503. <https://doi.org/10.1016/j.colsurfb.2015.07.051>
- Bunick, C. G., & Milstone, L. M. (2017). The X-ray crystal structure of the keratin 1-keratin 10 helix 2B heterodimer reveals molecular surface properties and biochemical insights into human skin disease. *J. Investig. Dermatol.*, 137(1), 142-150. <https://doi.org/10.1016/j.jid.2016.08.018>
- Bunmahotama W., Lin T. F., & Yang X. (2020). Prediction of adsorption capacity for pharmaceuticals, personal care products and endocrine disrupting chemicals onto various adsorbent materials. *Chemosphere*, 238: 124658. <https://doi.org/10.1016/j.chemosphere.2019.124658>
- Butte, W., Schmidt, S., & Schmidt, A. (1999). Photochemical degradation of nitrated musk compounds. *Chemosphere*, 38(6), 1287-1291. [https://doi.org/10.1016/S0045-6535\(98\)00529-3](https://doi.org/10.1016/S0045-6535(98)00529-3)
- Calao-Ramos, C., Bravo, A. G., Paternina-Urbe, R., Marrugo-Negrete, J., & Díez, S. (2021). Occupational human exposure to mercury in artisanal small-scale gold mining communities of Colombia. *Environ. Int.*, 146, 106216. <https://doi.org/10.1016/j.envint.2020.106216>.
- Canterino, M., Marotta, R., Temussi, F., & Zarrelli, A. (2008). Photochemical behaviour of musk tibetene. *Environ. Sci. Pollut. Res.*, 15(3), 182-187. <https://doi.org/10.1065/espr2007.12.464>
- Carlsson, G., & Norrgren, L. (2004). Synthetic musk toxicity to early life stages of zebrafish (*Danio rerio*). *Arch. Environ. Contam. Toxicol.*, 46(1), 102-105. <https://doi.org/10.1007/s00244-003-2288-2>
- Carlsson, G., Örn, S., Andersson, P. L., Söderström, H., & Norrgren, L. (2000). The impact of musk ketone on reproduction in zebrafish (*Danio rerio*). *Mar. Environ. Res.*, 50(1-5), 237-241. [https://doi.org/10.1016/S0141-1136\(00\)00075-1](https://doi.org/10.1016/S0141-1136(00)00075-1)
- Castorena-Cortés, G., Roldán-Carrillo, T., Zapata-Peñasco, I., Reyes-Avila, J., Quej-Aké, L., Marín-Cruz, J., & Olguín-Lora, P. (2009). Microcosm assays and Taguchi experimental design for treatment of oil sludge containing high concentration of

- hydrocarbons. *Bioresour. Technol.*, 100(23), 5671-5677.
<https://doi.org/10.1016/j.biortech.2009.06.050>
- Castro, M., Fernandes, J. O., Pena, A., & Cunha, S. C. (2018). Occurrence, profile and spatial distribution of UV-filters and musk fragrances in mussels from Portuguese coastline. *Mar. Environ. Res.*, 138, 110-118.
<https://doi.org/10.1016/j.marenvres.2018.04.005>
- Cavalheiro, J., Prieto, A., Monperrus, M., Etxebarria, N., & Zuloaga, O. (2013). Determination of polycyclic and nitro musks in environmental water samples by means of microextraction by packed sorbents coupled to large volume injection-gas chromatography–mass spectrometry analysis. *Anal. Chim. Acta.*, 773, 68-75.
<https://doi.org/10.1016/j.aca.2013.02.036>
- Cha, H. J., He, C., Zhao, H., Dong, Y., An, I. S., & An, S. (2016). Intercellular and intracellular functions of ceramides and their metabolites in skin. *Int. J. Mol. Med.*, 38(1), 16-22. <https://doi.org/10.3892/ijmm.2016.2600>
- Chan, W. Y., Chau, F. T., Lee, K. K., Kwong, W. H., & Yew, D. T. (2004). Substitution for natural musk in Pien Tze Huang does not affect its hepatoprotective activities. *Hum. Exp. Toxicol.*, 23(1), 35-47. <https://doi.org/10.1191/0960327104ht4140a>
- Chanchal, D., & Swarnlata, S. (2008). Novel approaches in herbal cosmetics. *J. Cosmet. Dermatol.*, 7(2), 89-95. <https://doi.org/10.1111/j.1473-2165.2008.00369.x>
- Chang, J. W., Yan, B. R., Chang, M. H., Tseng, S. H., Kao, Y. M., Chen, J. C., & Lee, C. C. (2014). Cumulative risk assessment for plasticizer-contaminated food using the hazard index approach. *Environ. Pollut.*, 189, 77-84.
<https://doi.org/10.1016/j.envpol.2014.02.005>
- Chase, D. A., Karnjanapiboonwong, A., Fang, Y., Cobb, G. P., Morse, A. N., & Anderson, T. A. (2012). Occurrence of synthetic musk fragrances in effluent and non-effluent impacted environments. *Sci. Total Environ.*, 416, 253-260.
<https://doi.org/10.1016/j.scitotenv.2011.11.067>
- Chaudhary, M. K., Srivastava, A., Singh, K. K., Tandon, P., & Joshi, B. D. (2020). Computational evaluation on molecular stability, reactivity, and drug potential of frovatriptan from DFT and molecular docking approach. *Comput. Theor. Chem.*, 1191, 113031. <https://doi.org/10.1016/j.comptc.2020.113031>
- Che, J. S., Yu, R. P., Song, Q. J., Wang, L. P., & Wu, S. F. (2011). Determination of synthetic musks in the sediment of the Taihu lake by using accelerated solvent extraction (ASE) and GC/MS. *Int. J. Environ. Anal. Chem.*, 91(4), 387-399.
<https://doi.org/10.1080/03067311003782633>
- Chen, C., Zhou, Q., Liu, S., & Xiu, Z. (2011). Acute toxicity, biochemical and gene expression responses of the earthworm *Eisenia fetida* exposed to polycyclic musks. *Chemosphere* 83(8), 1147-1154. <https://doi.org/10.1016/j.chemosphere.2011.01.006>
- Chen, D., Zeng, X., Sheng, Y., Bi, X., Gui, H., Sheng, G., & Fu, J. (2007). The concentrations and distribution of polycyclic musks in a typical cosmetic plant. *Chemosphere*, 66(2), 252-258.
<https://doi.org/10.1016/j.chemosphere.2006.05.024>
- Chen, F., Ying, G. G., Ma, Y. B., Chen, Z. F., Lai, H. J., & Peng, F. J. (2014). Field dissipation and risk assessment of typical personal care products TCC, TCS, AHTN and HHCB in biosolid-amended soils. *Sci. Total Environ.*, 470, 1078-1086.
<https://doi.org/10.1016/j.scitotenv.2013.10.080>
- Chen, X., Li, X., & Li, Y. (2021). Toxicity inhibition strategy of microplastics to aquatic organisms through molecular docking, molecular dynamics simulation and molecular modification. *Ecotoxicol. Environ. Saf.*, 226, 112870.
<https://doi.org/10.1016/j.ecoenv.2021.112870>

- Chen, Y., Cai, X., Jiang, L., & Li, Y. (2016). Prediction of octanol-air partition coefficients for polychlorinated biphenyls (PCBs) using 3D-QSAR models. *Ecotox. Environ. Safe.* 124, 202-212. <https://doi.org/10.1016/j.ecoenv.2015.10.024>
- Chen, Z., Sun, W., & Zhao, L. (2018). Combustion mechanisms and kinetics of fuel additives: A reaxff molecular simulation. *Energy Fuels*, 32(11), 11852-11863. <https://doi.org/10.1021/acs.energyfuels.8b02035>
- Cheng, Q., Chen, Q., Xu, J. H., & Yu, H. L. (2018). A 3D-QSAR assisted activity prediction strategy for expanding substrate spectra of an aldehyde ketone reductase. *Mol. Catal.*, 455, 224-232. <https://doi.org/10.1016/j.mcat.2018.06.013>.
- Chisvert, A., & Salvador, A. (Eds.). (2007). *Analysis of cosmetic products*. Elsevier.
- Choi, H. K., Cho, Y. H., Lee, E. O., Kim, J. W., & Park, C. S. (2017). Phytosphingosine enhances moisture level in human skin barrier through stimulation of the filaggrin biosynthesis and degradation leading to NMF formation. *Arch. Dermatol. Res.*, 309(10), 795-803. <https://doi.org/10.1007/s00403-017-1782-8>
- Choi, S. M., & Lee, B. M. (2015). Safety and risk assessment of ceramide 3 in cosmetic products. *Food Chem. Toxicol.*, 84, 8-17. <https://doi.org/10.1016/j.fct.2015.07.012>
- Chou, Y. J., & Dietrich, D. R. (1999). Interactions of nitromusk parent compounds and their amino-metabolites with the estrogen receptors of rainbow trout (*Oncorhynchus mykiss*) and the South African clawed frog (*Xenopus laevis*). *Toxicol. Lett.*, 111(1-2), 27-36. [https://doi.org/10.1016/S0378-4274\(99\)00168-X](https://doi.org/10.1016/S0378-4274(99)00168-X)
- Chu, Z., & Li, Y. (2019). Designing modified polybrominated diphenyl ether BDE-47, BDE-99, BDE-100, BDE-183, and BDE-209 molecules with decreased estrogenic activities using 3D-QSAR, pharmacophore models coupled with resolution V of the 210-3 fractional factorial design and molecular docking. *J. Hazard. Mater.*, 364, 151-162. <https://doi.org/10.1016/j.jhazmat.2018.10.027>
- Clara, M., Gans, O., Windhofer, G., Krenn, U., Hartl, W., Braun, K., Scharf, S., & Scheffknecht, C. (2011). Occurrence of polycyclic musks in wastewater and receiving water bodies and fate during wastewater treatment. *Chemosphere*, 82(8), 1116-1123. <https://doi.org/10.1016/j.chemosphere.2010.11.041>
- Clausen, G. H., Fanger, P. O., Cain, W. S., & Leaderer, B. P. (1986). Stability of body odor in enclosed spaces. *Environ. Int.*, 12(1-4), 201-205. [https://doi.org/10.1016/0160-4120\(86\)90031-0](https://doi.org/10.1016/0160-4120(86)90031-0)
- Conkle, J. L., Del Valle, C. D. B., & Turner, J. W. (2018). Are we underestimating microplastic contamination in aquatic environments?. *Environ. Manage.*, 61(1), 1-8. <https://doi.org/10.1007/s00267-017-0947-8>
- Correia, P., Cruz, A., Santos, L., & Alves, A. (2013). Human dermal exposure to galaxolide from personal care products. *Int. J. Cosmet. Sci.*, 35(3), 299-309. <https://doi.org/10.1111/ics.12043>
- Covaci, A., Harrad, S., Abdallah, M. A. E., Ali, N., Law, R. J., Herzke, D., & de Wit, C. A. (2011). Novel brominated flame retardants: a review of their analysis, environmental fate and behaviour. *Environ. Int.*, 37(2), 532-556. <https://doi.org/10.1016/j.envint.2010.11.007>
- Crespo, A., Martí, M. A., Estrin, D. A., & Roitberg, A. E. (2005). Multiple-steering QM-MM calculation of the free energy profile in chorismate mutase. *J. Am. Chem. Soc.*, 127(19), 6940-6941. <https://doi.org/10.1021/ja0452830>
- Cressey, B. D., Kumar, N., & Scheinman, P. L. (2012). Contact allergy to sorbitans: a follow-up study. *Dermatol.*, 23(4), 158-161. [10.1097/DER.0b013e318260d75f](https://doi.org/10.1097/DER.0b013e318260d75f)
- Crudden, J. J. (1999). The properties and industrial applications of N-acyl ED3A chelating surfactants. *Special Publications of the Royal Society of Chemistry*, 230, 130-150.
- Cunha, S. C., Fernandes, J. O., Vallecillos, L., Cano-Sancho, G., Domingo, J. L., Pocurull,

- E., Borrull, F., Maulvault, A., Ferrari, F., & Kotterman, M. (2015). Co-occurrence of musk fragrances and UV-filters in seafood and macroalgae collected in European hotspots. *Environ. Res.*, *143*, 65-71. <https://doi.org/10.1016/j.envres.2015.05.003>
- Davis A M, & Teague S J. (1999). Hydrogen bonding, hydrophobic interactions, and failure of the rigid receptor hypothesis. *Angew. Chem. Int. Ed.*, *38*(6): 736-749. [https://doi.org/10.1002/\(SICI\)1521-3773\(19990315\)38:6<736::AID-ANIE736>3.0.CO;2-R](https://doi.org/10.1002/(SICI)1521-3773(19990315)38:6<736::AID-ANIE736>3.0.CO;2-R)
- Deng, J. L. (1987). Basic method of grey system. *Huangzhong Polytechnical Institute Press, Wuhan, China.*
- Di Cintio, E., Parazzini, F., Chatenoud, L., Surace, M., Benzi, G., Zanconato, G., & La Vecchia, C. (2001). Dietary factors and risk of spontaneous abortion. *Eur. J. Obstet. Gynecol. Reprod. Biol.*, *95*(1), 132-136. [https://doi.org/10.1016/S0301-2115\(00\)00363-8](https://doi.org/10.1016/S0301-2115(00)00363-8).
- Díaz-Garduño, B., Pintado-Herrera, M. G., Biel-Maeso, M., Rueda-Márquez, J. J., Lara-Martín, P. A., Perales, J. A., Manzano, M.A., Garrido-Pérez, C., & Martín-Díaz, M. L. (2017). Environmental risk assessment of effluents as a whole emerging contaminant: Efficiency of alternative tertiary treatments for wastewater depuration. *Water Res.*, *119*, 136-149. <https://doi.org/10.1016/j.watres.2017.04.021>
- DiFrancesco, A. M., Chiu, P. C., Standley, L. J., Allen, H. E., & Salvito, D. T. (2004). Dissipation of fragrance materials in sludge-amended soils. *Environ. Sci. Technol.*, *38*(1), 194-201. <https://doi.org/10.1021/es034618v>
- Ding, T., Li, W., Cai, M., Jia, X., Yang, M., Yang, B., & Li, J. (2020). Algal toxicity, accumulation and metabolic pathways of galaxolide. *J. Hazard. Mater.*, *384*, 121360. <https://doi.org/10.1016/j.jhazmat.2019.121360>
- Dong, H., Tang, H., Chen, D., Xu, T., & Li, L. (2014). Analysis of 7 synthetic musks in cream by supported liquid extraction and solid phase extraction followed by GC-MS/MS. *Talanta*, *120*, 248-254. <https://doi.org/10.1016/j.talanta.2013.11.086>
- Draisci, R., Marchiafava, C., Ferretti, E., Palleschi, L., Catellani, G., & Anastasio, A. (1998). Evaluation of musk contamination of freshwater fish in Italy by accelerated solvent extraction and gas chromatography with mass spectrometric detection. *J. Chromatogr. A*, *814*(1-2), 187-197. [https://doi.org/10.1016/S0021-9673\(98\)00396-3](https://doi.org/10.1016/S0021-9673(98)00396-3)
- Du, M., Zhang, D., Hou, Y., Zhao, X., & Li, Y. (2019). Combined 2D-QSAR, principal component analysis and sensitivity analysis studies on fluoroquinolones' genotoxicity. *Int. J. Environ. Res. Public Health*, *16*(21), 4156. <https://doi.org/10.3390/ijerph16214156>
- Duedahl-Olesen, L., Cederberg, T., Pedersen, K. H., & Højgård, A. (2005). Synthetic musk fragrances in trout from Danish fish farms and human milk. *Chemosphere*, *61*(3), 422-431. <https://doi.org/10.1016/j.chemosphere.2005.02.004>
- Duedahl-Olesen, L., Cederberg, T., Pedersen, K. H., & Højgård, A. (2005). Synthetic musk fragrances in trout from Danish fish farms and human milk. *Chemosphere*, *61*(3), 422-431. <https://doi.org/10.1016/j.chemosphere.2005.02.004>
- Ehiguese, F. O., González-Delgado, M. J., Garrido-Perez, C., Araújo, C. V., & Martín-Díaz, M. L. (2021). Effects and Risk Assessment of the Polycyclic Musk Compounds Galaxolide® and Tonalide® on Marine Microalgae, Invertebrates, and Fish. *Processes*, *9*(2), 371. <https://doi.org/10.3390/pr9020371>
- Eissa, A. M., Khosravi, E., & Cimecioglu, A. L. (2012). A versatile method for functionalization and grafting of 2-hydroxyethyl cellulose (HEC) via click chemistry. *Carbohydr. Polym.*, *90*(2), 859-869. <https://doi.org/10.1016/j.carbpol.2012.06.012>
- Emig, M., Reinhardt, A., & Mersch-Sundermann, V. (1996). A comparative study of five

- nitro musk compounds for genotoxicity in the SOS chromotest and Salmonella mutagenicity. *Toxicol. Lett.*, *85*(3), 151-156. [https://doi.org/10.1016/0378-4274\(96\)03667-3](https://doi.org/10.1016/0378-4274(96)03667-3)
- Ertan, T., Yildiz, I., Tekiner-Gulbas, B., Bolelli, K., Temiz-Arpaci, O., Ozkan, S., Kaynak, F., Yalcin, I., & Aki, E. (2009). Synthesis, biological evaluation and 2D-QSAR analysis of benzoxazoles as antimicrobial agents. *Eur. J. Med. Chem.*, *44*(2), 501-510. <https://doi.org/10.1016/j.ejmech.2008.04.001>
- European Union Risk Assessment Report, 2008. <https://echa.europa.eu/documents/10162/947def3b-bbbf-473b-bc19-3bda7a8da910> (Accessed 6 March 2021).
- UNION, P. (2009). Regulation (EC) No 1223/2009 of the European parliament and of the council. *Official Journal of the European Union L*, *342*, 59.
- Fan, B., Wang, X., Li, J., Gao, X., Li, W., Huang, Y., & Liu, Z. (2019). Deriving aquatic life criteria for galaxolide (HHCB) and ecological risk assessment. *Sci. Total Environ.*, *681*, 488-496. <https://doi.org/10.1016/j.scitotenv.2019.05.033>
- Fang, H., Gao, Y., Wang, H., Yin, H., Li, G., & An, T. (2017). Photo-induced oxidative damage to dissolved free amino acids by the photosensitizer polycyclic musk tonalide: Transformation kinetics and mechanisms. *Water Res.*, *115*, 339-346. <https://doi.org/10.1016/j.watres.2017.03.006>
- Fang, Y., Cai, L., Lin, F., & Lu, Z. (2008). Degradation of synthetic musk ketone in water with ozone oxidation. *Chinese Journal of Environmental Engineering*. *2*(8), 1049-1052 (in Chinese). <https://kns.cnki.net/kcms/detail/detail.aspx?dbcode=CJFD&dbname=CJFD2008&file name=HJJZ200808008&v=zFRMwSVP%25mmd2FVYN1b%25mmd2Fyz89Byia%25mmd2FGZAwMQkCD9scNRrpUD4yf6SDne5mG1kcNQH13nU2>.
- Fang, Y., Chen, S., Lin, D., Yao, S. (2019). A new tetrapeptide biomimetic chromatographic resin for antibody separation with high adsorption capacity and selectivity. *J. Chromatogr. A*, *1604*, 460474. <https://doi.org/10.1016/j.chroma.2019.460474>.
- Federle, T., Sun, P., Dyer, S., & Kiel, B. (2014). Probabilistic assessment of environmental exposure to the polycyclic musk, HHCB and associated risks in wastewater treatment plant mixing zones and sludge amended soils in the United States. *Sci. Total Environ.*, *493*, 1079-1087. <https://doi.org/10.1016/j.scitotenv.2014.03.058>
- Fenet, H., Arpin-Pont, L., Vanhoutte-Brunier, A., Munaron, D., Fiandrino, A., Bueno, M.J.M., Boillot, C., Casellas, C., Mathieu, O. & Gomez, E. (2014). Reducing PEC uncertainty in coastal zones: A case study on carbamazepine, oxcarbazepine and their metabolites. *Environ. Int.*, *68*, 177-184. <https://doi.org/10.1016/j.envint.2014.03.025>
- Feng, X., Chen, L., Li, N., Zhao, Y., Han, Q., Wang, X., Wang, W., Ma, L., & Zhao, X. (2017). Metabolomics biomarker analysis of threatened abortion in polycystic ovary syndrome: a clinical discovery study. *Rsc. Adv.*, *7*(83), 52923-52929.
- Fernández-Ponce, M. T., Masmoudi, Y., Djerafi, R., Casas, L., Mantell, C., de la Ossa, E. M., & Badens, E. (2015). Particle design applied to quercetin using supercritical anti-solvent techniques. *J. Supercrit. Fluids*, *105*, 119-127. <https://doi.org/10.1016/j.supflu.2015.04.014>
- Flynn, M., Heale, K. A., & Alisaraie, L. (2017). Mechanism of off-target interactions and toxicity of tamoxifen and its metabolites. *Chem. Res. Toxicol.*, *30*(7), 1492-1507. <https://doi.org/10.1021/acs.chemrestox.7b00112>
- Fontal, M., van Drooge, B. L., & Grimalt, J. O. (2016). A rapid method for the analysis of methyl dihydrojasmonate and galaxolide in indoor and outdoor air particulate matter. *J. Chromatogra. A.*, *1447*, 135-140.

- <https://doi.org/10.1016/j.chroma.2016.04.028>
- Ford, R. A., Api, A. M., & Newberne, P. M. (1990). 90-day dermal toxicity study and neurotoxicity evaluation of nitromusks in the albino rat. *Food Chem. Toxicol.*, *28*(1), 55-61. [https://doi.org/10.1016/0278-6915\(90\)90136-B](https://doi.org/10.1016/0278-6915(90)90136-B)
- Fowler, J. F., Fowler, L. M., & Hunter, J. E. (1997). Allergy to cocamidopropyl betaine may be due to amidoamine: a patch test and product use test study. *Contact Dermat.*, *37*(6), 276-281. <https://doi.org/10.1111/j.1600-0536.1997.tb02464.x>
- Fráter, G., Müller, U., & Kraft, P. (1999). Preparation and olfactory characterization of the enantiomerically pure isomers of the perfumery synthetic Galaxolide®. *Helv. Chim. Acta*, *82*(10), 1656-1665. [https://doi.org/10.1002/\(SICI\)1522-2675\(19991006\)82:10<1656::AID-HLCA1656>3.0.CO;2-M](https://doi.org/10.1002/(SICI)1522-2675(19991006)82:10<1656::AID-HLCA1656>3.0.CO;2-M)
- Frisch, J. M., Trucks, W. G., & Schlegel, B. H. (2013). Gaussian 09, Revision D. 01, Gauss. Inc., Wallingford CT.
- Fromme, H., Lahrz, T., Piloty, M., Gebhart, H., Oddoy, A., & Rüden, H. (2004). Occurrence of phthalates and musk fragrances in indoor air and dust from apartments and kindergartens in Berlin (Germany). *Indoor Air*, *14*(3), 188-195. [10.1111/j.1600-0668.2004.00223.x](https://doi.org/10.1111/j.1600-0668.2004.00223.x)
- Fromme, H., Otto, T., & Pilz, K. (2001). Polycyclic musk fragrances in different environmental compartments in Berlin (Germany). *Water Res.*, *35*(1), 121-128. [https://doi.org/10.1016/S0043-1354\(00\)00233-5](https://doi.org/10.1016/S0043-1354(00)00233-5)
- Gao, M., Liu, Y., Dong, Y., & Song, Z. (2021). Effect of polyethylene particles on dibutyl phthalate toxicity in lettuce (*Lactuca sativa* L.). *J. Hazard. Mater.* *401*, 123422. <https://doi.org/10.1016/j.jhazmat.2020.123422>.
- Gao, Y., Ji, Y., Li, G., Mai, B., & An, T. (2016). Bioaccumulation and ecotoxicity increase during indirect photochemical transformation of polycyclic musk tonalide: A modeling study. *Water Res.*, *105*, 47-55. <https://doi.org/10.1016/j.watres.2016.08.055>
- García-Jares, C., Llompart, M., Polo, M., Salgado, C., Macías, S., & Cela, R. (2002). Optimisation of a solid-phase microextraction method for synthetic musk compounds in water. *J. Chromatogra. A.*, *963*(1-2), 277-285. [https://doi.org/10.1016/S0021-9673\(02\)00649-0](https://doi.org/10.1016/S0021-9673(02)00649-0)
- Gatermann, R., Biselli, S., Hühnerfuss, H., Rimkus, G. G., Hecker, M., & Karbe, L. (2002). Synthetic musks in the environment. Part 1: Species-dependent bioaccumulation of polycyclic and nitro musk fragrances in freshwater fish and mussels. *Arch. Environ. Contam. Toxicol.*, *42*(4), 437-446. <https://doi.org/10.1007/s00244-001-0041-2>
- Gatermann, R., Hellou, J., Hühnerfuss, H., Rimkus, G., & Zitko, V. (1999). Polycyclic and nitro musks in the environment: A comparison between Canadian and European aquatic biota. *Chemosphere*, *38*(14), 3431-3441. [https://doi.org/10.1016/S0045-6535\(98\)00564-5](https://doi.org/10.1016/S0045-6535(98)00564-5)
- Gatermann, R., Hühnerfuss, H., Rimkus, G., Attar, A., & Kettrup, A. (1998). Occurrence of musk xylene and musk ketone metabolites in the aquatic environment. *Chemosphere* *36*(11), 2535-2547. [https://doi.org/10.1016/S0045-6535\(97\)10208-9](https://doi.org/10.1016/S0045-6535(97)10208-9).
- Gautschi, M., Bajgrowicz, J. A., & Kraft, P. (2001). Fragrance chemistry—milestones and perspectives. *Chi. Internat. J. Chem.*, *55*(5), 379-387. Assessed by (<https://www.ingentaconnect.com/content/scs/chimia/2001/00000055/00000005/art00002?crawler=true>)
- Glazier, S., Marano, N., & Eisen, L. (2010). A closer look at trends in boiling points of hydrides: Using an inquiry-based approach to teach intermolecular forces of attraction. *J. Chem. Educ.*, *87*(12), 1336-1341. <https://doi.org/10.1021/ed100691n>
- Godayol, A., Besalú, E., Anticó, E., & Sanchez, J. M. (2015a). Monitoring of sixteen

- fragrance allergens and two polycyclic musks in wastewater treatment plants by solid phase microextraction coupled to gas chromatography. *Chemosphere*, 119, 363-370. <https://doi.org/10.1016/j.chemosphere.2014.06.072>
- Godayol, A., Gonzalez-Olmos, R., Sanchez, J. M., & Anticó, E. (2015b). Assessment of the effect of UV and chlorination in the transformation of fragrances in aqueous samples. *Chemosphere*, 125, 25-32. <https://doi.org/10.1016/j.chemosphere.2015.01.009>
- Gómez, M. J., Herrera, S., Solé, D., García-Calvo, E., & Fernández-Alba, A. R. (2011). Automatic searching and evaluation of priority and emerging contaminants in wastewater and river water by stir bar sorptive extraction followed by comprehensive two-dimensional gas chromatography-time-of-flight mass spectrometry. *Anal. Chem.*, 83(7), 2638-2647. <https://doi.org/10.1021/ac102909g>
- Gooding, M. P., Newton, T. J., Bartsch, M. R., & Hornbuckle, K. C. (2006). Toxicity of synthetic musks to early life stages of the freshwater mussel *Lampsilis cardium*. *Arch. Environ. Contam. Toxicol.*, 51(4), 549-558. <https://doi.org/10.1007/s00244-005-0223-4>
- Gramatica, P., Giani, E., & Papa, E. (2007). Statistical external validation and consensus modeling: a QSPR case study for *K_{OC}* prediction. *J. Mol. Graph. Model.*, 25(6): 755-766. <https://doi.org/10.1016/j.jmglm.2006.06.005>
- Groz, M. P., Bueno, M. M., Rosain, D., Fenet, H., Casellas, C., Pereira, C., Maria, V., Bebianno, M.J., & Gomez, E. (2014). Detection of emerging contaminants (UV filters, UV stabilizers and musks) in marine mussels from Portuguese coast by QuEChERS extraction and GC-MS/MS. *Sci. Total Environ.* 493, 162-169. <https://doi.org/10.1016/j.scitotenv.2014.05.062>
- Gu W., Li Q, & Li Y. (2020a). Law and mechanism analysis of biodegradability of polychlorinated naphthalenes based on principal component analysis, QSAR models, molecular docking and molecular dynamics simulation. *Chemosphere*, 243: 125427. <https://doi.org/10.1016/j.chemosphere.2019.125427>
- Gu, W., Chen, Y., & Li, Y. (2017). Attenuation of the atmospheric migration ability of polychlorinated naphthalenes (PCN-2) based on three-dimensional QSAR models with full factor experimental design. *Bull. Environ. Contam. Toxicol.*, 99(2), 276-280. <https://doi.org/10.1007/s00128-017-2123-5>
- Gu, W., Li, Q., & Li, Y. (2020c). Environment-friendly PCN derivatives design and environmental behavior simulation based on a multi-activity 3D-QSAR model and molecular dynamics. *J. Hazard. Mater.*, 393, 122339. <https://doi.org/10.1016/j.jhazmat.2020.122339>
- Gu, W., Li, X., Du, M., Ren, Z., Li, Q., & Li, Y. (2021a). Identification and regulation of ecotoxicity of polychlorinated naphthalenes to aquatic food Chain (green algae-Daphnia magna-fish). *Aquatic Toxicology*, 233, 105774.
- Gu, W., Li, X., Li, Q., Hou, Y., Zheng, M., & Li, Y. (2021b). Combined remediation of polychlorinated naphthalene-contaminated soil under multiple scenarios: An integrated method of genetic engineering and environmental remediation technology. *J. Hazard. Mater.* 405, 124139. <https://doi.org/10.1016/j.jhazmat.2020.124139>
- Gu, W., Zhao, Y., Li, Q., & Li, Y. (2019). Environmentally friendly polychlorinated naphthalenes (PCNs) derivatives designed using 3D-QSAR and screened using molecular docking, density functional theory and health-based risk assessment. *J. Hazard. Mater.* 363, 316-32. <https://doi.org/10.1016/j.jhazmat.2018.09.060>
- Gu, W., Zhao, Y., Li, Q., & Li, Y. (2020b). Plant-microorganism combined remediation of polychlorinated naphthalenes contaminated soils based on molecular directed transformation and taguchi experimental design-assisted dynamics simulation. *J.*

- Hazard. Mater.*, 396, 122753. <https://doi.org/10.1016/j.jhazmat.2020.122753>.
- Guo, R., Lee, I. S., Kim, U. J., & Oh, J. E. (2010). Occurrence of synthetic musks in Korean sewage sludges. *Sci. Total Environ.*, 408(7), 1634-1639. <https://doi.org/10.1016/j.scitotenv.2009.12.009>
- Hall, B., Tozer, S., Safford, B., Coroama, M., Steiling, W., Leneuve-Duchemin, M. C., McNamara, C., & Gibney, M. (2007). European consumer exposure to cosmetic products, a framework for conducting population exposure assessments. *Food Chem. Toxicol.*, 45(11), 2097-2108. <https://doi.org/10.1016/j.fct.2007.06.017>
- Hall, L. H., & Story, C. T. (1996). Boiling point and critical temperature of a heterogeneous data set: QSAR with atom type electrotopological state indices using artificial neural networks. *J. Chem. Inf. Model.*, 36(5), 1004-1014. <https://doi.org/10.1021/ci960375x>
- Hamelberg, D., Mongan, J., & McCammon, J. A. (2004). Accelerated molecular dynamics: a promising and efficient simulation method for biomolecules. *J. Chem. Phys.*, 120(24), 11919-11929. <https://doi.org/10.1063/1.1755656>
- Hasegawa, S., Azuma, M., & Takahashi, K. (2008). Stabilization of enzyme activity during the esterification of lactic acid in hydrophobic ethers and ketones as reaction media that are miscible with lactic acid despite their high hydrophobicity. *Enzyme Microb. Technol.*, 43(3), 309-316. <https://doi.org/10.1016/j.enzmictec.2008.03.017>
- Heberer, T. (2002). Occurrence, fate, and assessment of polycyclic musk residues in the aquatic environment of urban areas—a review. *Acta Hydroch. Hydrob.*, 30(5-6), 227-243. <https://doi.org/10.1002/aheh.200390005>
- Hernández-Martínez, A., Martínez-Vázquez, S., Rodríguez-Almagro, J., Khan, K. S., Delgado-Rodríguez, M., & Martínez-Galiano, J. M. (2021). Validation of perinatal post-traumatic stress disorder questionnaire for Spanish women during the postpartum period. *Sci. Rep.*, 11(1), 1-8.
- Homem, V., Alves, A., Alves, A., & Santos, L. (2016). Ultrasound-assisted dispersive liquid–liquid microextraction for the determination of synthetic musk fragrances in aqueous matrices by gas chromatography–mass spectrometry. *Talanta*, 148, 84-93. <https://doi.org/10.1016/j.talanta.2015.10.049>
- Homem, V., Avelino Silva, J., Cunha, C., Alves, A., & Santos, L. (2013). New analytical method for the determination of musks in personal care products by QuEChERS extraction followed by GC–MS. *Journal of Separation Science*, 36(13), 2176-2184. <https://doi.org/10.1002/jssc.201300190>
- Homem, V., Magalhães, I., Alves, A., & Santos, L. (2017). Assessing seasonal variation of synthetic musks in beach sands from Oporto coastal area: A case study. *Environ. Pollut.*, 226, 190-197. <https://doi.org/10.1016/j.envpol.2017.04.022>
- Homem, V., Silva, E., Alves, A., & Santos, L. (2015a). Scented traces—Dermal exposure of synthetic musk fragrances in personal care products and environmental input assessment. *Chemosphere*, 139, 276-287. <https://doi.org/10.1016/j.chemosphere.2015.06.078>
- Homem, V., Silva, J. A., Ratola, N., Santos, L., & Alves, A. (2015b). Long lasting perfume—A review of synthetic musks in WWTPs. *J. Environ. Manage.*, 149, 168-192. <https://doi.org/10.1016/j.jenvman.2014.10.008>
- Hong, J. H., Lee, J. Y., Ha, H. J., Lee, J. H., Oh, S. R., Lee, Y. M., Lee, M. Y., & Zoh, K. D. (2021). Occurrence and Sources of Synthetic Musk Fragrances in the Sewage Treatment Plants and the Han River, Korea. *Water*, 13(4), 392. <https://doi.org/10.3390/w13040392>
- Horii, Y., Reiner, J. L., Loganathan, B. G., Kumar, K. S., Sajwan, K., & Kannan, K. (2007). Occurrence and fate of polycyclic musks in wastewater treatment plants in Kentucky

- and Georgia, USA. *Chemosphere*, 68(11), 2011-2020.
<https://doi.org/10.1016/j.chemosphere.2007.04.054>
- Hou, Y., Zhao, Y., Li, Q., & Li, Y. (2020). Highly biodegradable fluoroquinolone derivatives designed using the 3D-QSAR model and biodegradation pathways analysis. *Ecotoxicol. Environ. Saf.*, 191, 110186.
<https://doi.org/10.1016/j.ecoenv.2020.110186>
- Hu, X. L., Liu, G., Wei, Y. T., Wang, Y. H., Zhang, T. X., Yang, S., Hu, D. F., & Liu, S. Q. (2018). Regional and seasonal effects on the gastrointestinal parasitism of captive forest musk deer. *Acta Trop.* 177, 1-8.
<https://doi.org/10.1016/j.actatropica.2017.09.021>.
- Hu, X., & Zhou, Q. (2011c). Comparisons of microwave-assisted extraction, simultaneous distillation-solvent extraction, Soxhlet extraction and ultrasound probe for polycyclic musks in sediments: recovery, repeatability, matrix effects and bioavailability. *Chromatographia*, 74(5), 489-495. <https://doi.org/10.1007/s10337-011-2084-5>
- Hu, Z., Shi, Y., & Cai, Y. (2011a). Reprint of: Concentrations, distribution, and bioaccumulation of synthetic musks in the Haihe River of China. *Chemosphere*, 85(2), 262-267.
<https://doi.org/10.1016/j.chemosphere.2011.09.002>
- Hu, Z., Shi, Y., Niu, H., Cai, Y., Jiang, G., & Wu, Y. (2010). Occurrence of synthetic musk fragrances in human blood from 11 cities in China. *Environ. Toxicol. Chem.*, 29(9), 1877-1882. <https://doi.org/10.1002/etc.258>
- Hu, Z., Shi, Y., Zhang, S., Niu, H., & Cai, Y. (2011b). Assessment of synthetic musk fragrances in seven wastewater treatment plants of Beijing, China. *Bull. Environ. Contam. Toxicol.*, 86(3), 302-306. <https://doi.org/10.1007/s00128-011-0215-1>
- Huang, W., Xie, Z., Yan, W., Mi, W., & Xu, W. (2016). Occurrence and distribution of synthetic musks and organic UV filters from riverine and coastal sediments in the Pearl River estuary of China. *Mar. Pollut. Bull.*, 111(1-2), 153-159.
<https://doi.org/10.1016/j.marpolbul.2016.07.018>
- Hutter, H. P., Wallner, P., Hartl, W., Uhl, M., Lorbeer, G., Gminski, R., Mersch-Sundermann, V., & Kundi, M. (2010). Higher blood concentrations of synthetic musks in women above fifty years than in younger women. *Int. J. Hyg. Environ. Health.*, 213(2), 124-130. <https://doi.org/10.1016/j.ijheh.2009.12.002>
- Hutter, H. P., Wallner, P., Moshhammer, H., Hartl, W., Sattelberger, R., Lorbeer, G., & Kundi, M. (2009). Synthetic musks in blood of healthy young adults: relationship to cosmetics use. *Sci. Total Environ.*, 407(17), 4821-4825.
<https://doi.org/10.1016/j.scitotenv.2009.05.026>
- Hutter, H. P., Wallner, P., Moshhammer, H., Hartl, W., Sattelberger, R., Lorbeer, G., & Kundi, M. (2005). Blood concentrations of polycyclic musks in healthy young adults. *Chemosphere*, 59(4), 487-492.
<https://doi.org/10.1016/j.chemosphere.2005.01.070>
- Janzen, N., Dopp, E., Hesse, J., Richards, J., Türk, J., & Bester, K. (2011). Transformation products and reaction kinetics of fragrances in advanced wastewater treatment with ozone. *Chemosphere*, 85(9), 1481-1486.
<https://doi.org/10.1016/j.chemosphere.2011.08.043>
- Jiang, L., & Li, Y. (2016). Modification of PBDEs (BDE-15, BDE-47, BDE-85 and BDE-126) biological toxicity, bio-concentration, persistence and atmospheric long-range transport potential based on the pharmacophore modeling assistant with the full factor experimental design. *J. Hazard. Mater.*, 307, 202-212.
<https://doi.org/10.1016/j.jhazmat.2015.12.031>

- Jo, J., Lee, J. Y., Lee, H. E., Son, Y. G., Yoo, J. W., Ahn, D. S., & Ahn, Y. G. (2021). Determination of twelve synthetic musk compounds in estuary and coastal areas near Han River of Korea by improved liquid–liquid extraction coupled with GC/MS. *Int. J. Environ. Anal. Chem.*, 1-12. <https://doi.org/10.1080/03067319.2021.1995723>
- Johnson, A. C., & Sumpter, J. P. (2001). Removal of endocrine-disrupting chemicals in activated sludge treatment works. *Environ. Sci. Technol.*, 35(24), 4697-4703. <https://doi.org/10.1021/es010171j>
- Juksu, K., Liu, Y., Zhao, J., Yao, L., Sarin, C., Sreesai, S., Klomjek, P., Traitangwong, A., & Ying, G. (2020). Emerging contaminants in aquatic environments and coastal waters affected by urban wastewater discharge in Thailand: An ecological risk perspective. *Ecotox. Environ. Safe.* 204, 110952. <https://doi.org/10.1016/j.ecoenv.2020.110952>.
- Kakizawa, Y., & Miyake, M. (2019). Creation of new functions by combination of surfactant and polymer-complex coacervation with oppositely charged polymer and surfactant for shampoo and body wash. *J. Oleo Sci.*, 68, 525-539. <https://doi.org/10.5650/jos.ess19081>
- Kallenborn, R., Gatermann, R., Planting, S., Rimkus, G. G., Lund, M., Schlabach, M., & Burkow, I. C. (1999). Gas chromatographic determination of synthetic musk compounds in Norwegian air samples. *J. Chromatogr. A.*, 846(1-2), 295-306. [https://doi.org/10.1016/S0021-9673\(99\)00259-9](https://doi.org/10.1016/S0021-9673(99)00259-9)
- Kamat, V. P., Hagiwara, H., Katsumi, T., Hoshi, T., Suzuki, T., & Ando, M. (2000). Ring closing metathesis directed synthesis of (R)-(-)-muscone from (+)-citronellal. *Tetrahedron*, 56(26), 4397-4403. [https://doi.org/10.1016/S0040-4020\(00\)00333-1](https://doi.org/10.1016/S0040-4020(00)00333-1)
- Kang, C. S., Lee, J. H., Kim, S. K., Lee, K. T., Lee, J. S., Park, P. S., Yun, S.H., Kannan, K., Yoo, Y.W., Ha, J.Y., & Lee, S. W. (2010). Polybrominated diphenyl ethers and synthetic musks in umbilical cord serum, maternal serum, and breast milk from Seoul, South Korea. *Chemosphere*, 80(2), 116-122. <https://doi.org/10.1016/j.chemosphere.2010.04.009>
- Kannan, K., Reiner, J. L., Yun, S. H., Perrotta, E. E., Tao, L., Johnson-Restrepo, B., & Rodan, B. D. (2005). Polycyclic musk compounds in higher trophic level aquatic organisms and humans from the United States. *Chemosphere*, 61(5), 693-700. <https://doi.org/10.1016/j.chemosphere.2005.03.041>
- Katuri, G. P., Fan, X., Siddique, S., Kubwabo, C., Kosarac, I., Harris, S. A., & Foster, W. G. (2020). A selective and sensitive gas chromatography-tandem mass spectrometry method for quantitation of synthetic musks in human serum. *J. AOAC Int.*, 103(6), 1461-1468. <https://doi.org/10.1093/jaoacint/qsaa051>.
- Kevekordes, S., Mersch-Sundermann, V., Diez, M., & Dunkelberg, H. (1997). In vitro genotoxicity of polycyclic musk fragrances in the micronucleus test. *Mutat. Res-Gen. Tox. En.*, 395(2-3), 145-150. [https://doi.org/10.1016/S1383-5718\(97\)00160-5](https://doi.org/10.1016/S1383-5718(97)00160-5)
- Klosterhaus, S. L., Grace, R., Hamilton, M. C., & Yee, D. (2013). Method validation and reconnaissance of pharmaceuticals, personal care products, and alkylphenols in surface waters, sediments, and mussels in an urban estuary. *Environ. Int.*, 54, 92-99. <https://doi.org/10.1016/j.envint.2013.01.009>
- Koleva, Y., & Georgieva, S. (2013). Environmental risk assessment of bisphenol A and its metabolites as endocrine disruptors. *Oxid. Commun.*, 36, 225-234. Assessed by (https://www.researchgate.net/publication/287549049_Environmental_risk_assessment_of_bisphenol_a_and_its_metabolites_as_endocrine_disruptors/stats)
- Kooijman, S. A. L. M. (1987). A safety factor for LC₅₀ values allowing for differences in sensitivity among species. *Water Res.* 21(3), 269-276. <https://doi.org/10.1016/0043->

- 1354(87)90205-3.
- Košnář, Z., Mercl, F., Chane, A. D., Pierdonà, L., Míchal, P., & Tlustoš, P. (2021). Occurrence of synthetic polycyclic and nitro musk compounds in sewage sludge from municipal wastewater treatment plants. *Sci. Total Environ.*, *801*, 149777. <https://doi.org/10.1016/j.scitotenv.2021.149777>
- Kraft, P., & Cadalbert, R. (2008). Cycloalkanecarboxylic acid derivatives as fragrances with musk characteristics: US. 7390779.
- Kraft, P., & Fráter, G. (2001). Enantioselectivity of the musk odor sensation. *Chirality*, *13*(8), 388-394. <https://doi.org/10.1002/chir.1050>
- Kraft, P., & Mueller, U., 2011. Odour compounds: WO. 2011029895
- Kronimus, A., Schwarzbauer, J., Dsikowitzky, L., Heim, S., & Littke, R. (2004). Anthropogenic organic contaminants in sediments of the Lippe river, Germany. *Water Res.*, *38*(16), 3473-3484. <https://doi.org/10.1016/j.watres.2004.04.054>
- Krzeminski, P., Schwermer, C., Wennberg, A., Langford, K., & Vogelsang, C. (2017). Occurrence of UV filters, fragrances and organophosphate flame retardants in municipal WWTP effluents and their removal during membrane post-treatment. *J. Hazard. Mater.*, *323*, 166-176. <https://doi.org/10.1016/j.jhazmat.2016.08.001>
- Kubinyi, H. (1997a). QSAR and 3D QSAR in drug design Part 1: methodology. *Drug Discov. Today*, *2*(11), 457-467. [https://doi.org/10.1016/S1359-6446\(97\)01079-9](https://doi.org/10.1016/S1359-6446(97)01079-9).
- Kubinyi, H. (1997b). QSAR and 3D QSAR in drug design Part 2: applications and problems. *Drug Discov. Today*, *2*(12), 538-546. [https://doi.org/10.1016/S1359-6446\(97\)01084-2](https://doi.org/10.1016/S1359-6446(97)01084-2).
- Kuhlich, P., Göstl, R., Teichert, P., Piechotta, C., & Nehls, I. (2011). Transformations of polycyclic musks AHTN and HHCB upon disinfection with hypochlorite: two new chlorinated disinfection by-products (CDBP) of AHTN and a possible source for HHCB-lactone. *Anal. Bioanal. Chem.*, *399*(10), 3579-3588. <https://doi.org/10.1007/s00216-011-4674-3>
- Kuz'min, V. E., Artemenko, A. G., Lozytska, R. N., Fedtchouk, A. S., Lozitsky, V. P., Muratov, E. N., & Mescheriakov, A. K. (2005). Investigation of anticancer activity of macrocyclic Schiff bases by means of 4D-QSAR based on simplex representation of molecular structure. *SAR QSAR Environ. Res.*, *16*(3), 219-230. <https://doi.org/10.1080/10659360500037206>
- La Farre, M., Pérez, S., Kantiani, L., & Barceló, D. (2008). Fate and toxicity of emerging pollutants, their metabolites and transformation products in the aquatic environment. *Trends Anal. Chem.*, *27*(11), 991-1007. <https://doi.org/10.1016/j.trac.2008.09.010>
- Lander, R. L., Hambidge, K. M., Westcott, J. E., Tejada, G., Diba, T. S., Mastiholi, S. C., Khan, U. S., Garcés, A., Figueroa, L., Tshefu, A., Lokangaka, A., Goudar, S. S., Somannavar, M. S., Ali, S. A., Saleem, S., McClure, E. M., Krebs, N. F., & Women First Preconception Nutrition Trial Group. (2019). Pregnant women in four low-middle income countries have a high prevalence of inadequate dietary intakes that are improved by dietary diversity. *Nutrients*, *11*(7), 1560. <https://doi.org/10.3390/nu11071560>.
- Lange, C., Kuch, B. & Metzger, J.W., 2015. Occurrence and fate of synthetic musk fragrances in a small German river. *J. Hazard. Mater.*, *282*, 34-40. <https://doi.org/10.1016/j.jhazmat.2014.06.027>
- Lee, C., Yang, W., & Parr, R. G. (1988). Development of the Colle-Salvetti correlation-energy formula into a functional of the electron density. *Phys. Rev. B*, *37*(2), 785. <https://doi.org/10.1103/PhysRevB.37.785>
- Lee, I. S., Lee, S. H., & Oh, J. E. (2010). Occurrence and fate of synthetic musk

- compounds in water environment. *Water Res.*, 44(1), 214-222.
<https://doi.org/10.1016/j.watres.2009.08.049>
- Lee, S., Kim, S., Park, J., Kim, H. J., Lee, J. J., Choi, G., Choi, S., Kim, S., Kim, S. Y., Choi, K., Kim, S., & Moon, H. B. (2015). Synthetic musk compounds and benzotriazole ultraviolet stabilizers in breast milk: Occurrence, time-course variation and infant health risk. *Environmental research*, 140, 466-473.
<https://doi.org/10.1016/j.envres.2015.04.017>
- Li, Q., Qiu, Y., & Li, Y. (2020b). Molecular design of environment-friendly PAE derivatives based on 3D-QSAR assisted with a comprehensive evaluation method combining toxicity and estrogen activities. *Water Air Soil Pollut.*, 231(5), 1-13.
<https://doi.org/10.1007/s11270-020-04574-2>
- Li, S., Zhu, F., Jiang, R., & Ouyang, G. (2016). Preparation and evaluation of amino modified graphene solid-phase microextraction fiber and its application to the determination of synthetic musks in water samples. *J. Chromatogra. A.*, 1429, 1-7.
<https://doi.org/10.1016/j.chroma.2015.11.025>
- Li, W., Nanaboina, V., Chen, F., & Korshin, G. V. (2016). Removal of polycyclic synthetic musks and antineoplastic drugs in ozonated wastewater: quantitation based on the data of differential spectroscopy. *J. Hazard. Mater.*, 304, 242-250.
<https://doi.org/10.1016/j.jhazmat.2015.10.035>
- Li, W., Nanaboina, V., Chen, F., & Korshin, G. V. (2016b). Removal of polycyclic synthetic musks and antineoplastic drugs in ozonated wastewater: quantitation based on the data of differential spectroscopy. *J. Hazard. Mater.*, 304, 242-250.
<https://doi.org/10.1016/j.jhazmat.2015.10.035>
- Li, X., Chu, Z., Yang, J., Li, M., Du, M., Zhao, X., Zhu, Z., & Li, Y. (2018). Synthetic Musks: A Class of Commercial Fragrance Additives in Personal Care Products (PCPs) Causing Concern as Emerging Contaminants. *Adv. Mar. Biol.*, 81, 213-280.
<https://doi.org/10.1016/bs.amb.2018.09.008>
- Li, X., Gu, W., Chen, B., Zhu, Z., & Zhang, B. (2021a). Functional modification of HHCB: Strategy for obtaining environmentally friendly derivatives. *J. Hazard. Mater.*, 126116. <https://doi.org/10.1016/j.jhazmat.2021.126116>.
- Li, X., Li, G., Chen, B., Lin, W., & Zhang, B. (2021b). 3D-QSAR-aided toxicity assessment of synthetic musks and their transformation by-products. *Environ. Sci. Pollut. Res.*, 1-13. <https://doi.org/10.1007/s11356-021-14672-1>.
- Li, X., Zhang, B., Huang, W., Cantwell, C., & Chen, B. (2020a) Integration of Fuzzy Matter-Element Method and 3D-QSAR Model for Generation of Environmentally Friendly Quinolone Derivatives. *Int. J. Environ. Res. Public Health*, 17, 3239.
<https://doi.org/10.3390/ijerph17093239>
- Li, X., Zhao, Y., Chen, B., Zhu, Z., Kang, Q., Husain, T., & Zhang, B. (2022). Inhalation and ingestion of Synthetic musks in pregnant women: In silico spontaneous abortion risk evaluation and control. *Environment International*, 158, 106911.
- Li, Z., & Jennings, A. (2017). Worldwide regulations of standard values of pesticides for human health risk control: A review. *Int. J. Environ. Res. Public Health*, 14(7), 826.
<https://doi.org/10.3390/ijerph14070826>
- Li, Z., Yin, N., Liu, Q., Wang, C., Wang, T., Wang, Y., Qu, G., Liu, J., Cai, Y., Zhou, Q., & Jiang, G. (2013). Effects of polycyclic musks HHCB and AHTN on steroidogenesis in H295R cells. *Chemosphere*, 90(3), 1227-1235.
<https://doi.org/10.1016/j.chemosphere.2012.09.056>
- Lim, M. K., Ku, C. W., Tan, T. C., Lee, Y. H. J., Allen, J. C., & Tan, N. S. (2020). Characterisation of serum progesterone and progesterone-induced blocking factor (PIBF) levels across trimesters in healthy pregnant women. *Sci. Rep.*, 10(1), 1-9.

- <https://doi.org/10.1038/s41598-020-59452-y>.
- Ling, Y., Liping, S., & Yongliang, Z. (2018). Preparation and identification of novel inhibitory angiotensin-I-converting enzyme peptides from tilapia skin gelatin hydrolysates: Inhibition kinetics and molecular docking. *Food Funct.*, 9(10), 5251-5259. 10.1039/C8FO00569A
- Liu S. Study on the relationship between molecular structure and odour of polycyclic musks [J]. *Flavour Fragrance Cosmetics*, 2004, 6: 24-29. (in Chinese)
- Liu, H., Huang, L., Chen, Y., Guo, L., Li, L., Zhou, H., & Luan, T. (2015a). Simultaneous determination of polycyclic musks in blood and urine by solid supported liquid–liquid extraction and gas chromatography–tandem mass spectrometry. *J. Chromatogr. B.*, 992, 96-102. <https://doi.org/10.1016/j.jchromb.2015.04.028>
- Liu, H., Sun, P., Liu, H., Yang, S., Wang, L., & Wang, Z. (2015b). Acute toxicity of benzophenone-type UV filters for *Photobacterium phosphoreum* and *Daphnia magna*: QSAR analysis, interspecies relationship and integrated assessment. *Chemosphere* 135, 182-188. <https://doi.org/10.1016/j.chemosphere.2015.04.036>.
- Liu, J., & Duan, G. (1998). Common structural characteristics of musk odorant molecules. *J. Mol. Struct-Theochem.*, 432(2), 97-103. [https://doi.org/10.1016/S0166-1280\(97\)00385-0](https://doi.org/10.1016/S0166-1280(97)00385-0)
- Liu, J., Zhou, D.J., Luo, Z.Q., & Yang, N.F., (2002). Synthesis of Decabromodiphenylethane Having Enhanced Whiteness [J]. *China Plastics Industry*, 30, 4-5.
- Liu, N., Shi, Y., Li, W., Xu, L., & Cai, Y. (2014). Concentrations and distribution of synthetic musks and siloxanes in sewage sludge of wastewater treatment plants in China. *Sci. Total Environ.*, 476, 65-72. <https://doi.org/10.1016/j.scitotenv.2013.12.124>
- Liu, X., Chen, Z., Wang, L., Wu, Y., & Garoma, T. (2012). Degradation of polycyclic musk HHCb in water by O₃, UV, and UV/O₃. *J. Photoch. Photobio. A.* 230, 1-9.
- Llompart, M., García-Jares, C., Salgado, C., Polo, M., & Cela, R. (2003). Determination of musk compounds in sewage treatment plant sludge samples by solid-phase microextraction. *J. Chromatogr. A.*, 999(1-2), 185-193. [https://doi.org/10.1016/S0021-9673\(03\)00449-7](https://doi.org/10.1016/S0021-9673(03)00449-7)
- López-Nogueroles, M., Chisvert, A., Salvador, A., & Carretero, A. (2011). Dispersive liquid–liquid microextraction followed by gas chromatography–mass spectrometry for the determination of nitro musks in surface water and wastewater samples. *Talanta*, 85(4), 1990-1995. <https://doi.org/10.1016/j.talanta.2011.07.048>
- López-Sánchez, L., Miralles, P., Salvador, A., Merino-Sanjuán, M., & Merino, V. (2021). In vitro skin penetration of bronidox, bronopol and formaldehyde from cosmetics. *Regul. Toxicol. Pharmacol.*, 122, 104888. <https://doi.org/10.1016/j.yrtph.2021.104888>
- Lou, Y. H., Wang, J., Wang, L., Shi, L., Yu, Y., & Zhang, M. Y. (2016). Determination of synthetic musks in sediments of Yellow River Delta Wetland, China. *Bull. Environ. Contam. Toxicol.*, 97(1), 78-83. <https://doi.org/10.1007/s00128-016-1814-7>
- Louie, J., Bielawski, C. W., & Grubbs, R. H. (2001). Tandem catalysis: The sequential mediation of olefin metathesis, hydrogenation, and hydrogen transfer with single-component Ru complexes. *J. Am. Chem. Soc.*, 123(45), 11312-11313. <https://doi.org/10.1021/ja016431e>
- Lourith, N., Kanlayavattanukul, M., Mongkonpaibool, K., Butsaratrakool, T., & Chinmuang, T. (2016). Rambutan seed as a new promising unconventional source of specialty fat for cosmetics. *Ind. Crops. Prod.*, 83, 149-154. <https://doi.org/10.1016/j.indcrop.2015.12.045>
- Lu, Y., Yuan, T., Wang, W., & Kannan, K. (2011a). Concentrations and assessment of

- exposure to siloxanes and synthetic musks in personal care products from China. *Environ. Pollut.*, 159(12), 3522-3528.
<https://doi.org/10.1016/j.envpol.2011.08.015>
- Lu, Y., Yuan, T., Yun, S. H., Wang, W., & Kannan, K. (2011b). Occurrence of synthetic musks in indoor dust from China and implications for human exposure. *Arch. Environ. Contam. Toxicol.*, 60(1), 182-189. <https://doi.org/10.1007/s00244-010-9595-1>
- Luckenbach, T., Corsi, I., & Epel, D. (2004). Fatal attraction: synthetic musk fragrances compromise multitaxenobiotic defense systems in mussels. *Mar. Environ. Res.*, 58(2-5), 215-219. <https://doi.org/10.1016/j.marenvres.2004.03.017>
- Lv, X., Jiang, Y., Wang, X., Dou, G., Wang, J., Yang, W., Xie H., Wang H. & Li, Z. (2021). Computational Study on Novel Natural Inhibitors Targeting BCL2. *Medical Oncology*, DOI: 10.21203/rs.3.rs-185749/v1.
- Lv, Y., Yuan, T., Hu, J., & Wang, W. (2009). Simultaneous determination of trace polycyclic and nitro musks in water samples using optimized solid-phase extraction by gas chromatography and mass spectrometry. *Anal. Sci.*, 25(9), 1125-1130. <https://doi.org/10.2116/analsci.25.1125>
- Ma, X., & Zhou, L. (2007). QSAR study of substituted 1-(2-naphthyl)-1H-pyrazole-5-carboxylamide factor Xa (fXa) inhibitors. *Mol. Simula.*, 33(15), 1213-1222. <https://doi.org/10.1080/08927020701730351>
- Maekawa, A., Matsushima, Y., Onodera, H., Shibutani, M., Ogasawara, H., Kodama, Y., ... & Hayashi, Y. (1990). Long-term toxicity/carcinogenicity of musk xylol in B6C3F1 mice. *Food Chem. Toxicol.*, 28(8), 581-586. [https://doi.org/10.1016/0278-6915\(90\)90159-K](https://doi.org/10.1016/0278-6915(90)90159-K)
- Marques, C., Tarek, R., Sara, M., & Brar, S. K. (2016). Sorbitol production from biomass and its global market. In *Platform Chemical Biorefinery* (pp. 217-227). <https://doi.org/10.1016/B978-0-12-802980-0.00012-2>
- Martin, Y. C. (1998). 3D QSAR: current state, scope, and limitations. In *3D QSAR in drug design* (pp. 3-23). Springer, Dordrecht. https://doi.org/10.1007/0-306-46858-1_1
- Martin, C., Moeder, M., Daniel, X., Krauss, G., & Schlosser, D. (2007). Biotransformation of the polycyclic musks HHCB and AHTN and metabolite formation by fungi occurring in freshwater environments. *Environ. Sci. Technol.*, 41(15), 5395-5402. <https://doi.org/10.1021/es0711462>
- McCall, S. L., Platzman, P. M., & Wolff, P. A. (1980). Surface enhanced Raman scattering. *Physics Letters A*, 77(5), 381-383. [https://doi.org/10.1016/0375-9601\(80\)90726-4](https://doi.org/10.1016/0375-9601(80)90726-4)
- McDonough, C. A., Helm, P. A., Muir, D., Puggioni, G., & Lohmann, R. (2016). Polycyclic musks in the air and water of the lower Great Lakes: Spatial distribution and volatilization from surface waters. *Environ. Sci. Technol.*, 50(21), 11575-11583. <https://doi.org/10.1021/acs.est.6b03657>
- Meng, X., Cui, L., Song, F., Luan, M., Ji, J., Si, H., Duan, Y., & Zhai, H. (2020). 3D-QSAR and molecular docking studies on design anti-prostate cancer curcumin analogues. *Curr. Comput.-Aided Drug Des.*, 16(3), 245-256. <https://doi.org/10.2174/1573409914666181029123746>
- Mensah, R.A., Kirton, S.B., Cook, M.T., Styliari, I.D., Hutter, V. & Chau, D.Y.S. (2019). Optimising poly (lactic-co-glycolic acid) microparticle fabrication using a Taguchi orthogonal array design-of-experiment approach. *PLoS One*, 14(9), p.e0222858. <https://doi.org/10.1371/journal.pone.0222858>
- Mersch-Sundermann, V., Emig, M., & Reinhardt, A. (1996). Nitro musks are cogenotoxicants by inducing toxifying enzymes in the rat. *Mutat. Res. - Fundam. Mol.*

- Mech. Mutagen.*, 356(2), 237-245. [https://doi.org/10.1016/0027-5107\(96\)00065-6](https://doi.org/10.1016/0027-5107(96)00065-6)
- Mersch-Sundermann, V., Kevekordes, S., & Jenter, C. (1998). Lack of mutagenicity of polycyclic musk fragrances in *Salmonella typhimurium*. *Toxicol. In Vitro* 12(4), 389-393. [https://doi.org/10.1016/S0887-2333\(98\)00007-1](https://doi.org/10.1016/S0887-2333(98)00007-1).
- Ming, L., Xiaoyu, Y., Hao, C., Huan, W., Lei, S., Wenjing, D., Baoquan, Z., Yongli, Y., Wu, D., & Jingfeng, Y. (2020). Effect of Galaxolide on Thyroid Hormones in Zebrafish Embryos. *Asian Journal of Ecotoxicol.*, (3), 81-89. 10.7524/AJE.1673-5897.20200220001
- Minocha, R., Damian, D. L., & Halliday, G. M. (2018). Melanoma and nonmelanoma skin cancer chemoprevention: A role for nicotinamide? *Photodermatol. Photoimmunolo. Photomed.*, 34(1), 5-12. <https://doi.org/10.1111/phpp.12328>
- Moldovan, Z., Chira, R., & Alder, A. C. (2009). Environmental exposure of pharmaceuticals and musk fragrances in the Somes River before and after upgrading the municipal wastewater treatment plant Cluj-Napoca, Romania. *Environ. Sci. Pollut. Res.*, 16(1), 46-54. <https://doi.org/10.1007/s11356-008-0047-7>
- Mombelli, E., & Devillers, J. (2010). Evaluation of the OECD (Q) SAR Application Toolbox and Toxtree for predicting and profiling the carcinogenic potential of chemicals. *SAR QSAR Environ. Res.*, 21(7-8), 731-752. <https://doi.org/10.1080/1062936X.2010.528598>
- Montesdeoca-Esponda, S., Checchini, L., Del Bubba, M., Sosa-Ferrera, Z., & Santana-Rodríguez, J. J. (2018). Analytical approaches for the determination of personal care products and evaluation of their occurrence in marine organisms. *Sci. Total Environ.*, 633, 405-425. <https://doi.org/10.1016/j.scitotenv.2018.03.182>
- Montesdeoca-Esponda, S., Vega-Morales, T., Sosa-Ferrera, Z., & Santana-Rodríguez, J. J. (2013). Extraction and determination methodologies for benzotriazole UV stabilizers in personal-care products in environmental and biological samples. *TrAC-Trends Anal. Chem.*, 51, 23-32. <https://doi.org/10.1016/j.trac.2013.05.012>
- Moon, H. B., Lee, D. H., Lee, Y. S., & Kannan, K. (2012). Occurrence and accumulation patterns of polycyclic aromatic hydrocarbons and synthetic musk compounds in adipose tissues of Korean females. *Chemosphere*, 86(5), 485-490. <https://doi.org/10.1016/j.chemosphere.2011.10.008>
- Morris, G. M., & Lim-Wilby, M. (2008). Molecular docking. In *Molecular modeling of proteins* (pp. 365-382). Humana Press. https://doi.org/10.1007/978-1-59745-177-2_19
- Mota, M. D., Costa, R. Y. S., e Silva, L. C. R. C., & Chinalia, F. A. (2019). Guava-fruit extract can improve the UV-protection efficiency of synthetic filters in sun cream formulations. *J. Photochem. Photobiol. B: Biol.*, 201, 111639. <https://doi.org/10.1016/j.jphotobiol.2019.111639>
- Mujtaba, S. F., Srivastav, A. K., Agnihotry, S., Negi, S., Upadhyay, J., & Ray, R. S. (2018). Role of Personal Care Products and Phototoxicity. In *Photocarcinogenesis & Photoprotection.*, 109-128. https://doi.org/10.1007/978-981-10-5493-8_11
- Mukherjee, R. K., Kumar, V., & Roy, K. (2022). Chemometric modeling of plant protection products (PPPs) for the prediction of acute contact toxicity against honey bees (*A. mellifera*): A 2D-QSAR approach. *J. Hazard. Mater.*, 423, 127230. <https://doi.org/10.1016/j.jhazmat.2021.127230>
- Müller, R. H., Petersen, R. D., Hommos, A., & Pardeike, J. (2007). Nanostructured lipid carriers (NLC) in cosmetic dermal products. *Adv. Drug Deliv. Rev.*, 59(6), 522-530. <https://doi.org/10.1016/j.addr.2007.04.012>
- Müller, S., Schmid, P., & Schlatter, C. (1996). Occurrence of nitro and non-nitro benzenoid musk compounds in human adipose tissue. *Chemosphere*, 33(1), 17-28. [https://doi.org/10.1016/0045-6535\(96\)00160-9](https://doi.org/10.1016/0045-6535(96)00160-9)

- Nagendrappa, G. (2014). Johann Friedrich Wilhelm Adolf von Baeyer. *Resonance*, 19(6), 489-522. <https://doi.org/10.1007/s12045-014-0055-5>
- Nakata, H., Hinosaka, M., & Yanagimoto, H. (2015). Macrocyclic-, polycyclic-, and nitro musks in cosmetics, household commodities and indoor dusts collected from Japan: implications for their human exposure. *Ecotox. Environ. Safe.*, 111, 248-255. <https://doi.org/10.1016/j.ecoenv.2014.09.032>
- Nakata, H., Sasaki, H., Takemura, A., Yoshioka, M., Tanabe, S., & Kannan, K. (2007). Bioaccumulation, temporal trend, and geographical distribution of synthetic musks in the marine environment. *Environ. Sci. Technol.*, 41(7), 2216-2222. <https://doi.org/10.1021/es0623818>
- Nakata, H., Shinohara, R. I., Nakazawa, Y., Isobe, T., Sudaryanto, A., Subramanian, A., Tanabe, S., Zakaria, M. P., Zheng, G., Lam, P., Kim, E. Y., Min, B. Y., We, S. U., Viet, P. H., Tana, T. S., Prudente, M., Frank, D., Lauenstein, G., & Kannan, K. (2012). Asia-Pacific mussel watch for emerging pollutants: distribution of synthetic musks and benzotriazole UV stabilizers in Asian and US coastal waters. *Mar. Pollut. Bull.* 64(10), 2211-2218. <https://doi.org/10.1016/j.marpolbul.2012.07.049>
- National Research Council. (2001). *A risk-management strategy for PCB-contaminated sediments*. National Academies Press.
- Nayyar, A., Malde, A., Coutinho, E., & Jain, R. (2006). Synthesis, anti-tuberculosis activity, and 3D-QSAR study of ring-substituted-2/4-quinolinecarbaldehyde derivatives. *Bioorg. Med. Chem.*, 14(21), 7302-7310. <https://doi.org/10.1016/j.bmc.2006.06.049>
- Nezzal, A., Aerts, L., Verspaille, M., Henderickx, G., & Redl, A. (2009). Polymorphism of sorbitol. *J. Cryst. Growth*, 311(15), 3863-3870. <https://doi.org/10.1016/j.jcrysgr.2009.06.003>
- Ngan, T. T. K., T. T. Hien, N. T. C. Quyen, P. N. Q. Anh, L. T. H. Nhan, M. H. Cang, D. D. Nhat, N. D. Phuc, & Bach, L.G. (2020). Application of coconut oil from Ben Tre Province (Vietnam) as the main detergent for body wash products. In IOP Conference Series: *Materials Science and Engineering*, 959, 012025. 10.1088/1757-899X/959/1/012025
- Ngo, N. T., Linares-Pastén, J. A., Grey, C., & Adlercreutz, P. (2021). Synthesis of novel oligomeric anionic alkyl glycosides using laccase/TEMPO oxidation and cyclodextrin glucanotransferase (CGTase)-catalyzed transglycosylation. *Biotechnol. Bioeng.*, 118, 2548–2558. <https://doi.org/10.1002/bit.27770>
- Ni, N., Wang, F., Song, Y., Bian, Y., Shi, R., Yang, X., Gu, C., & Jiang, X. (2018). Mechanisms of biochar reducing the bioaccumulation of PAHs in rice from soil: degradation stimulation vs immobilization. *Chemosphere*, 196, 288-296. <https://doi.org/10.1016/j.chemosphere.2017.12.192>
- Nnadi, C. O., Althaus, J. B., Nwodo, N. J., & Schmidt, T. J. (2018). A 3D-QSAR study on the antitrypanosomal and cytotoxic activities of steroid alkaloids by comparative molecular field analysis. *Molecules*, 23(5), 1113. <https://doi.org/10.3390/molecules23051113>
- NORMAN Available from: (<https://www.norman-network.net/?q=node/81>) (accessed 12 April 2021).
- O'Toole, S., & Metcalfe, C. (2006). Synthetic musks in fish from urbanized areas of the lower Great Lakes, Canada. *J. Great Lakes Res.*, 32(2), 361-369. [https://doi.org/10.3394/0380-1330\(2006\)32\[361:SMIFFU\]2.0.CO;2](https://doi.org/10.3394/0380-1330(2006)32[361:SMIFFU]2.0.CO;2)
- Oberdorf, C., Schmidt, T. J., & Wunsch, B. (2010). 5D-QSAR for spirocyclic σ_1 receptor ligands by Quasar receptor surface modeling. *Eu. J. Med. Chem.*, 45(7), 3116-3124. <https://doi.org/10.1016/j.ejmech.2010.03.048>

- Onoda, H., Yamaguchi, T., & Takenaka, A. (2012). Synthesis and pigmental properties of titanium phosphates with the addition of urea. *Int. J. Cosmet. Sci.*, *34*(1), 86-90. <https://doi.org/10.1111/j.1468-2494.2011.00685.x>
- Osemwengie, L. I. (2006). Determination of synthetic musk compounds in sewage biosolids by gas chromatography/mass spectrometry. *J. Environ. Monit.*, *8*(9), 897-903. DOI <https://doi.org/10.1039/B603113G>
- Ozkoc, H. B., Bakan, G., & Ariman, S. (2007). Distribution and bioaccumulation of organochlorine pesticides along the Black Sea coast. *Environ. Geochem. Health*, *29*(1), 59-68. DOI [10.1007/s10653-006-9064-y](https://doi.org/10.1007/s10653-006-9064-y)
- Paasivirta, J., Sinkkonen, S., Rantalainen, A. L., Broman, D., & Zebühr, Y. (2002). Temperature dependent properties of environmentally important synthetic musks. *Environ. Sci. Pollut. Res.*, *9*(5), 345-355. <https://doi.org/10.1007/BF02987579>
- Parolini, M., Magni, S., Traversi, I., Villa, S., Finizio, A., & Binelli, A. (2015). Environmentally relevant concentrations of galaxolide (HHCB) and tonalide (AHTN) induced oxidative and genetic damage in *Dreissena polymorpha*. *J. Hazard. Mater.*, *285*, 1-10. <https://doi.org/10.1016/j.jhazmat.2014.11.037>
- PDB Protein data bank: (<https://www.rcsb.org/structure/4Z>)
- Peck, A. M., & Hornbuckle, K. C. (2004). Synthetic musk fragrances in Lake Michigan. *Environ. Sci. Technol.*, *38*(2), 367-372. <https://doi.org/10.1021/es034769y>
- Peck, A. M., & Hornbuckle, K. C. (2006a). Synthetic musk fragrances in urban and rural air of Iowa and the Great Lakes. *Atmos. Environ.*, *40*(32), 6101-6111. <https://doi.org/10.1016/j.atmosenv.2006.05.058>
- Peck, A. M., Linebaugh, E. K., & Hornbuckle, K. C. (2006b). Synthetic musk fragrances in Lake Erie and Lake Ontario sediment cores. *Environ. Sci. Technol.*, *40*(18), 5629-5635. <https://doi.org/10.1021/es060134y>
- Pedersen, J. A., Soliman, M., & Suffet, I. H. (2005). Human pharmaceuticals, hormones, and personal care product ingredients in runoff from agricultural fields irrigated with treated wastewater. *J. Agr. Food Chem.*, *53*(5), 1625-1632. <https://doi.org/10.1021/jf049228m>
- Pedersen, S., Selck, H., Salvito, D., & Forbes, V. (2009). Effects of the polycyclic musk HHCB on individual-and population-level endpoints in *Potamopyrgus antipodarum*. *Ecotoxicol. Environ. Saf.*, *72*(4), 1190-1199. <https://doi.org/10.1016/j.ecoenv.2008.10.012>
- Peng, F. J., Hu, L. X., Pan, C. G., Ying, G. G., & Van den Brink, P. J. (2019). Insights into the sediment toxicity of personal care products to freshwater oligochaete worms using Fourier transform infrared spectroscopy. *Ecotoxicol. Environ. Saf.*, *172*, 296-302. <https://doi.org/10.1016/j.ecoenv.2019.01.098>
- Peng, F. J., Ying, G. G., Pan, C. G., Selck, H., Salvito, D., & Van den Brink, P. J. (2018). Bioaccumulation and biotransformation of triclosan and galaxolide in the freshwater oligochaete *Limnodrilus hoffmeisteri* in a water/sediment microcosm. *Environ. Sci. Technol.*, *52*(15), 8390-8398. <https://doi.org/10.1021/acs.est.8b02637>
- Polo, M., Garcia-Jares, C., Llompарт, M., & Cela, R. (2007). Optimization of a sensitive method for the determination of nitro musk fragrances in waters by solid-phase microextraction and gas chromatography with micro electron capture detection using factorial experimental design. *Anal. Bioanal. Chem.*, *388*(8), 1789-1798. <https://doi.org/10.1007/s00216-007-1359-z>
- Postigo, C., & Barceló, D. (2015). Synthetic organic compounds and their transformation products in groundwater: occurrence, fate and mitigation. *Sci. Total Environ.*, *503*, 32-47. <https://doi.org/10.1016/j.scitotenv.2014.06.019>
- Price, P. S., Conolly, R. B., Chaisson, C. F., Gross, E. A., Young, J. S., Mathis, E. T., &

- Tedder, D. R. (2003). Modeling interindividual variation in physiological factors used in PBPK models of humans. *Crit. Rev. Toxicol.*, 33(5), 469-503.
<https://doi.org/10.1080/10408440390242324>
- Qiu, Z., Qu, K., Luan, F., Liu, Y., Zhu, Y., Yuan, Y., Li, H., Zhang, H., Hai, Y., & Zhao, C. (2020). Binding specificities of estrogen receptor with perfluorinated compounds: A cross species comparison. *Environ. Int.*, 134, 105284.
<https://doi.org/10.1016/j.envint.2019.105284>
- Quednow, K., & Püttmann, W. (2008). Organophosphates and synthetic musk fragrances in freshwater streams in Hessen/Germany. *CLEAN–Soil, Air, Water*, 36(1), 70-77.
<https://doi.org/10.1002/clen.200700023>
- Raab, U., Preiss, U., Albrecht, M., Shahin, N., Parlar, H., & Fromme, H. (2008). Concentrations of polybrominated diphenyl ethers, organochlorine compounds and nitro musks in mother's milk from Germany (Bavaria). *Chemosphere*, 72(1), 87-94.
<https://doi.org/10.1016/j.chemosphere.2008.01.053>
- Rabideau, B. D., Soltani, M., Parker, R. A., Siu, B., Salter, E. A., Wierzbicki, A., West, K. N., & Davis, J. H. (2020). Tuning the melting point of selected ionic liquids through adjustment of the cation's dipole moment. *Phys. Chem. Chem. Phys.*, 22(21), 12301-12311. <https://doi.org/10.1039/D0CP01214A>
- Rainieri, S., Barranco, A., Primec, M., & Langerholc, T. (2017). Occurrence and toxicity of musks and UV filters in the marine environment. *Food. Chem. Toxicol.*, 104, 57-68.
<https://doi.org/10.1016/j.fct.2016.11.012>
- Rajuddin, R., Rizia, F., & Nainggolan, S. I. (2021). Role of C-Reactive Protein, Erythrocyte Sedimentation Rate, Progesterone and Estradiol Hormone Levels in First Trimester Threatened Abortion. *Indones. J. Soc. Obstet. Gynecol.*, 42-48.
<https://doi.org/10.32771/inajog.v9i1.1386>
- Rakibe, U., Tiwari, R., Mahajan, A., Rane, V., & Wakte, P. (2018). LC and LC–MS/MS studies for the identification and characterization of degradation products of acebutolol. *J. Pharm. Anal.*, 8(6), 357-365. <https://doi.org/10.1016/j.jpha.2018.03.001>
- Ramírez, N., Marcé, R. M., & Borrull, F. (2010). Development of a thermal desorption-gas chromatography–mass spectrometry method for determining personal care products in air. *J. Chromatogr. A*, 1217(26), 4430-4438.
<https://doi.org/10.1016/j.chroma.2010.04.049>
- Ramírez, N., Marcé, R. M., & Borrull, F. (2011). Development of a stir bar sorptive extraction and thermal desorption–gas chromatography–mass spectrometry method for determining synthetic musks in water samples. *J. Chromatogr. A*, 1218(1), 156-161. <https://doi.org/10.1016/j.chroma.2010.11.006>
- Raveh, L., Grunwald, J., Marcus, D., Papier, Y., Cohen, E., & Ashani, Y. (1993). Human butyrylcholinesterase as a general prophylactic antidote for nerve agent toxicity: in vitro and in vivo quantitative characterization. *Biochem. Pharmacol.*, 45(12), 2465-2474. [https://doi.org/10.1016/0006-2952\(93\)90228-O](https://doi.org/10.1016/0006-2952(93)90228-O)
- Rawlings, A. V., & Harding, C. R. (2004). Moisturization and skin barrier function. *Dermatol. Ther.*, 17, 43-48. <https://doi.org/10.1111/j.1396-0296.2004.04S1005.x>
- Regueiro, J., Garcia-Jares, C., Llompart, M., Lamas, J. P., & Cela, R. (2009). Development of a method based on sorbent trapping followed by solid-phase microextraction for the determination of synthetic musks in indoor air. *J. Chromatogr. A*, 1216(14), 2805-2815. <https://doi.org/10.1016/j.chroma.2008.09.062>
- Regueiro, J., Llompart, M., Garcia-Jares, C., & Cela, R. (2007). Development of a high-throughput method for the determination of organochlorinated compounds, nitromusks and pyrethroid insecticides in indoor dust. *J. Chromatogr. A*, 1174(1-2),

- 112-124. <https://doi.org/10.1016/j.chroma.2007.08.052>
- Reihaneh, S.S., & Jahan, G. (2013). Quasi 4D-QSAR and 3D-QSAR study of the pan class I phosphoinositide 3-kinase (PI3K) inhibitors. *Med. Chem. Res.* 22 (4),1587e1596. <https://doi.org/10.1007/s00044-012-0151-6>.
- Reiner, J. L., & Kannan, K. (2006). A survey of polycyclic musks in selected household commodities from the United States. *Chemosphere*, 62(6), 867-873. <https://doi.org/10.1016/j.chemosphere.2005.10.006>
- Reiner, J. L., & Kannan, K. (2011). Polycyclic musks in water, sediment, and fishes from the upper Hudson River, New York, USA. *Water Air Soil Poll.*, 214(1), 335-342. <https://doi.org/10.1007/s11270-010-0427-8>
- Reiner, J. L., Berset, J. D., & Kannan, K. (2007a). Mass flow of polycyclic musks in two wastewater treatment plants. *Arch. Environ. Contam. Toxicol.*, 52(4), 451-457. <https://doi.org/10.1007/s00244-006-0203-3>
- Reiner, J. L., Wong, C. M., Arcaro, K. F., & Kannan, K. (2007b). Synthetic musk fragrances in human milk from the United States. *Environ. Sci. Technol.*, 41(11), 3815-3820. <https://doi.org/10.1021/es063088a>
- Ren, S., Tan, F., Wang, Y., Zhao, H., Zhang, Y., Zhai, M., Chen, J., & Wang, X. (2020). In situ measurement of synthetic musks in wastewaters using diffusive gradients in thin film technique. *Water Res.*, 185, 116239. <https://doi.org/10.1016/j.watres.2020.116239>
- Ren, Z.X., Wang, S., Liu, D., Yu, J., Zhang, X.Y., Zhao, P.N., Sun, Y.X., & Han, S. (2021). Control strategies for the vertical gene transfer of quinolone ARGs in *Escherichia coli* through molecular modification and molecular dynamics. *J. Hazard. Mater.* 420, 126667. <https://doi.org/10.1016/j.jhazmat.2021.126667>.
- Ren, Z.X., Wang, Y.W., Xu, H.H., Li, Y.F., & Han, S. (2019). Fuzzy comprehensive evaluation assistant 3D-QSAR of environmentally friendly FQs to reduce ADRs. *Int. J. Environ. Res. Public Health*, 16, 3161-3181. <https://doi.org/10.3390/ijerph16173161>.
- Ribeiro, H., Ramos, S., Homem, V., & Santos, L. (2017). Can coastline plant species be used as biosamplers of emerging contaminants?-UV-filters and synthetic musks as case studies. *Chemosphere*, 184, 1134-1140. <https://doi.org/10.1016/j.chemosphere.2017.06.084>
- Ricking, M., Schwarzbauer, J., Hellou, J., Svenson, A., & Zitko, V. (2003). Polycyclic aromatic musk compounds in sewage treatment plant effluents of Canada and Sweden—first results. *Mar. Pollut. Bull.*, 46(4), 410-417. [https://doi.org/10.1016/S0025-326X\(02\)00480-0](https://doi.org/10.1016/S0025-326X(02)00480-0)
- Rico, A., de Oliveira, R., de Souza Nunes, G. S., Rizzi, C., Villa, S., López-Heras, I., Vighi, M., & Waichman, A. V. (2021). Pharmaceuticals and other urban contaminants threaten Amazonian freshwater ecosystems. *Environ. Int.*, 155, 106702. <https://doi.org/10.1016/j.envint.2021.106702>.
- Riedel, J., & Dekant, W. (1999). Biotransformation and toxicokinetics of musk xylene in humans. *Toxicol. Appl. Pharm.*, 157(2), 145-155. <https://doi.org/10.1006/taap.1999.8665>
- Rimkus, G. G. (1999). Polycyclic musk fragrances in the aquatic environment. *Toxicol. Lett.*, 111(1-2), 37-56. [https://doi.org/10.1016/S0378-4274\(99\)00191-5](https://doi.org/10.1016/S0378-4274(99)00191-5)
- Rimkus, G. G., Gatermann, R., & Hühnerfuss, H. (1999). Musk xylene and musk ketone amino metabolites in the aquatic environment. *Toxicol. Lett.* 111(1-2), 5-15. [https://doi.org/10.1016/S0378-4274\(99\)00190-3](https://doi.org/10.1016/S0378-4274(99)00190-3).
- Robinson, S. N., Zens, M. S., Perry, A. E., Spencer, S. K., Duell, E. J., & Karagas, M. R. (2013). Photosensitizing agents and the risk of non-melanoma skin cancer: a population-based case-control study. *J. Investig. Dermatol.*, 133(8), 1950-1955.

- <https://doi.org/10.1038/jid.2013.33>
- Roosens, L., Covaci, A., & Neels, H. (2007). Concentrations of synthetic musk compounds in personal care and sanitation products and human exposure profiles through dermal application. *Chemosphere*, 69(10), 1540-1547.
<https://doi.org/10.1016/j.chemosphere.2007.05.072>
- Rossiter, K. J. (1996). Structure– odor relationships. *Chemical reviews*, 96(8), 3201-3240.
<https://doi.org/10.1021/cr950068a>
- Ruiz, P., Mumtaz, M., & Gombar, V. (2011). Assessing the toxic effects of ethylene glycol ethers using Quantitative Structure Toxicity Relationship models. *Toxicol. Appl. Pharmacol.*, 254(2), 198-205. <https://doi.org/10.1016/j.taap.2010.10.024>
- Safavi-Sohi, R., & Ghasemi, J. B. (2013). Quasi 4D-QSAR and 3D-QSAR study of the pan class I phosphoinositide-3-kinase (PI3K) inhibitors. *Med. Chem. Res.*, 22(4), 1587-1596. <https://doi.org/10.1007/s00044-012-0151-6>
- Saillenfait, A. M., Sabate, J. P., & Gallissot, F. (2006). Developmental toxic effects of diisobutyl phthalate, the methyl-branched analogue of di-n-butyl phthalate, administered by gavage to rats. *Toxicol. Lett.* 165(1), 39-46.
<https://doi.org/10.1016/j.toxlet.2006.01.013>
- Salahinejad, M., & Ghasemi, J. B. (2014). 3D-QSAR studies on the toxicity of substituted benzenes to *Tetrahymena pyriformis*: CoMFA, CoMSIA and VolSurf approaches. *Ecotoxicol. Environ. Saf.*, 105, 128-134.
<https://doi.org/10.1016/j.ecoenv.2013.11.019>
- Sanchez-Prado, L., Lourido, M., Lores, M., Llompert, M., Garcia-Jares, C., & Cela, R. (2004). Study of the photoinduced degradation of polycyclic musk compounds by solid-phase microextraction and gas chromatography/mass spectrometry. *Rapid Commun. Mass Spectrom.*, 18(11), 1186-1192. <https://doi.org/10.1002/rcm.1459>
- Santiago-Morales, J., Gómez, M. J., Herrera, S., Fernández-Alba, A. R., García-Calvo, E., & Rosal, R. (2012). Oxidative and photochemical processes for the removal of galaxolide and tonalide from wastewater. *Water Res.* 46(14), 4435-4447.
<https://doi.org/10.1016/j.watres.2012.05.051>
- Sapozhnikova, Y., Liebert, D., Wirth, E., & Fulton, M. (2010). Polycyclic musk fragrances in sediments and shrimp tissues. *Polycycl. Aromat. Comp.*, 30(5), 298-308.
10.1080/10406638.2010.525160
- Saraiva, M., Cavalheiro, J., Lancelour, L., & Monperrus, M. (2016). Synthetic musk in seafood products from south Europe using a quick, easy, cheap, effective, rugged and safe extraction method. *Food. Chem.*, 200, 330-335.
<https://doi.org/10.1016/j.foodchem.2016.01.017>
- Schlichte, M. J., & Katta, R. (2014). Methylisothiazolinone: an emergent allergen in common pediatric skin care products. *Dermatol. Res. Pract.*, 2014.
<https://doi.org/10.1155/2014/132564>
- Schmid, P., Kohler, M., Gujer, E., Zennegg, M., & Lanfranchi, M. (2007). Persistent organic pollutants, brominated flame retardants and synthetic musks in fish from remote alpine lakes in Switzerland. *Chemosphere*, 67(9), S16-S21.
<https://doi.org/10.1016/j.chemosphere.2006.05.080>
- Schmitt, C., LaMoree, M., Leonards, P., Weiss, J. M., & de Deckere, E. (2013). In vivo effect confirmation of anti-androgenic compounds in sediment contact tests with *Potamopyrgus antipodarum*. *J. Environ. Sci. Health A., Part A*, 48(5), 475-480.
<https://doi.org/10.1080/10934529.2013.730387>
- Schnell, S., Martin-Skilton, R., Fernandes, D., & Porte, C. (2009). The interference of nitro- and polycyclic musks with endogenous and xenobiotic metabolizing enzymes in carp: an in vitro study. *Environ. Sci. Technol.*, 43(24), 9458-9464.

- <https://doi.org/10.1021/es902128x>
- Schreurs, R. H., Quaedackers, M. E., Seinen, W., & van der Burg, B. (2002). Transcriptional activation of estrogen receptor ER α and ER β by polycyclic musks is cell type dependent. *Toxicol. Appl. Pharm.*, *183*(1), 1-9.
<https://doi.org/10.1006/taap.2002.9458>
- Schwartz, S., Berding, V., & Matthies, M. (2000). Aquatic fate assessment of the polycyclic musk fragrance HHCB: Scenario and variability analysis in accordance with the EU risk assessment guidelines. *Chemosphere*, *41*(5), 671-679.
[https://doi.org/10.1016/S0045-6535\(99\)00510-X](https://doi.org/10.1016/S0045-6535(99)00510-X)
- Seyfried, M., Boschung, A., Miffon, F., Ohleyer, E., & Chaintreau, A. (2014). Elucidation of the upper pathway of alicyclic musk Romandolide[®] degradation in OECD screening tests with activated sludge. *Environ. Sci. Pollu. Res.*, *21*(16), 9487-9494.
<https://doi.org/10.1007/s11356-013-2347-9>
- Shek, W. M., Murphy, M. B., Lam, J. C., & Lam, P. K. (2008). Synthetic polycyclic musks in Hong Kong sewage sludge. *Chemosphere*, *71*(7), 1241-1250.
<https://doi.org/10.1016/j.chemosphere.2007.11.069>
- Siew, Y. Y., Rai, A., Pek, H. B., Ow, D. S. W., & Zhang, W. (2021). New and efficient purification process for recombinant human insulin produced in *Escherichia coli*. *Appl. Microbiol. Biotechnol.*, *105*, 9137–9151. <https://doi.org/10.1007/s00253-021-11697-x>
- Simonich, S. L., Federle, T. W., Eckhoff, W. S., Rottiers, A., Webb, S., Sabaliunas, D., & De Wolf, W. (2002). Removal of fragrance materials during US and European wastewater treatment. *Environ. Sci. Technol.*, *36*(13), 2839-2847.
<https://doi.org/10.1021/es025503e>
- Składanowski, A. C., Stepnowski, P., Kleszczyński, K., & Dmochowska, B. (2005). AMP deaminase in vitro inhibition by xenobiotics: A potential molecular method for risk assessment of synthetic nitro-and polycyclic musks, imidazolium ionic liquids and N-glucopyranosyl ammonium salts. *Environ. Toxicol. Phar.*, *19*(2), 291-296.
<https://doi.org/10.1016/j.etap.2004.08.005>
- Slanina, P. (2004). Risk evaluation of dietary and dermal exposure to musk fragrances. *Series Anthropogenic Compounds*. Springer, Berlin, Heidelberg, 281-310.
<https://doi.org/10.1007/b14124>
- Snyder, R. D., Pearl, G. S., Mandakas, G., Choy, W. N., Goodsaid, F., & Rosenblum, I. Y. (2004). Assessment of the sensitivity of the computational programs DEREK, TOPKAT, and MCASE in the prediction of the genotoxicity of pharmaceutical molecules. *Environ. Mol. Mutagen.*, *43*(3), 143-158. <https://doi.org/10.1002/em.20013>
- Sofuoglu, A., Kiyem, N., Kavcar, P., & Sofuoglu, S. C. (2010). Polycyclic and nitro musks in indoor air: A primary school classroom and a women's sport center. *Indoor Air*, *20*(6), 515-522. <https://doi.org/10.1111/j.1600-0668.2010.00674.x>
- Song, H., Zeng, X., Yu, Z., Zhang, D., Cao, S., Shao, W., Sheng, G., & Fu, J. (2015). Enantiomeric composition of polycyclic musks in sediments from the Pearl River and Suzhou Creek. *Environ. Sci. Pollut. Res.*, *22*(3), 1679-1686.
<https://doi.org/10.1007/s11356-014-3687-9>
- Sousa, S., Maia, M. L., Delerue-Matos, C., Calhau, C., & Domingues, V. F. (2021). The role of adipose tissue analysis on Environmental Pollutants Biomonitoring in women: The European scenario. *Sci. Total Environ.*, 150922.
<https://doi.org/10.1016/j.scitotenv.2021.150922>
- Sousa, S., Pestana, D., Faria, G., Vasconcelos, F., Delerue-Matos, C., Calhau, C., & Domingues, V. F. (2020). Method development for the determination of synthetic musks and organophosphorus pesticides in human adipose tissue. *J. Pharm. Biomed.*

- Anal.*, 191, 113598. <https://doi.org/10.1016/j.jpba.2020.113598>.
- Spencer, P. S., Bischoff-Fenton, M. C., Moreno, O. M., Opdyke, D. L., & Ford, R. A. (1984). Neurotoxic properties of musk ambrette. *Toxicol. Appl. Pharmacol.*, 75(3), 571-575. [https://doi.org/10.1016/0041-008X\(84\)90194-7](https://doi.org/10.1016/0041-008X(84)90194-7)
- Stockholm Convention on Persistent Organic Pollutants (2001) http://chm.pops.int/Portals/0/Repository/convention_text/UNEP-POPS-COP-CONVTEXT-FULL.English.PDF (accessed 12 April 2021).
- Subedi, B., Mottaleb, M. A., Chambliss, C. K., & Usenko, S. (2011). Simultaneous analysis of select pharmaceuticals and personal care products in fish tissue using pressurized liquid extraction combined with silica gel cleanup. *J. Chromatogr. A.*, 1218(37), 6278-6284. <https://doi.org/10.1016/j.chroma.2011.07.031>
- Subedi, B., Yun, S., Jayaraman, S., Bergen, B. J., & Kannan, K. (2014). Retrospective monitoring of persistent organic pollutants, including PCBs, PBDEs, and polycyclic musks in blue mussels (*Mytilus edulis*) and sediments from New Bedford Harbor, Massachusetts, USA: 1991–2005. *Environ. Monit. Assess.*, 186(8), 5273-5284. <https://doi.org/10.1007/s10661-014-3776-8>
- Sumner, N. R., Guitart, C., Fuentes, G., & Readman, J. W. (2010). Inputs and distributions of synthetic musk fragrances in an estuarine and coastal environment; a case study. *Environ. Pollut.*, 158(1), 215-222. <https://doi.org/10.1016/j.envpol.2009.07.018>
- Sun, P., Casteel, K., Dai, H., Wehmeyer, K. R., Kiel, B., & Federle, T. (2014). Distributions of polycyclic musk fragrance in wastewater treatment plant (WWTP) effluents and sludges in the United States. *Sci. Total Environ.*, 493, 1073-1078. <https://doi.org/10.1016/j.scitotenv.2014.04.038>
- Sununtasuk, C., & Fiedler, J. L. (2017). Can household-based food consumption surveys be used to make inferences about nutrient intakes and inadequacies? A Bangladesh case study. *Food Policy*, 72, 121-131. <https://doi.org/10.1016/j.foodpol.2017.08.018>.
- Svoboda, M. L., Yang, J. J., Falletta, P., & Lee, H. B. (2007). A Microwave-assisted Extraction Method for the Determination of Synthetic Musks in Sewage Sludge. *Water Qual. Res. J. Can.*, 42, 11-19.
- Tai, A., Bianchini, R., & Jachowicz, J. (2014). Texture analysis of cosmetic/pharmaceutical raw materials and formulations. *Int. J. Cosmet. Sci.*, 36(4), 291-304. <https://doi.org/10.1111/ics.12125>
- Tanabe, S. (2005). Synthetic musks-arising new environmental menace? *Mar. Pollut. Bull.*, 50(10), 1025-1026. [10.1016/j.marpolbul.2005.07.005](https://doi.org/10.1016/j.marpolbul.2005.07.005)
- Tanabe, Y., Misaki, T., Nagase, R., & Matsumoto, K. (2007). Process for producing muscone and its intermediate: US. 7268258.
- Tang, Z.H., Zhang, Z.H., Zhang, H., Wang, Y.H., Zhang, Y., Zhao, J.H., Yang, H.Q., & Wang, Z.C. (2019). Autophagy attenuation hampers progesterone synthesis during the development of pregnant corpus luteum. *Cells.*, 9(1), 71-80. <https://doi.org/10.3390/cells9010071>.
- Tasselli, S., & Guzzella, L. (2020). Polycyclic musk fragrances (PMFs) in wastewater and activated sludge: analytical protocol and application to a real case study. *Environ. Sci. Pollut. R.*, 1-10. <https://doi.org/10.1007/s11356-019-06767-7>.
- Tasselli, S., Valenti, E., & Guzzella, L. (2021). Polycyclic musk fragrance (PMF) removal, adsorption and biodegradation in a conventional activated sludge wastewater treatment plant in Northern Italy. *Environ. Sci. Pollut. R.*, 1-11. <https://doi.org/10.1007/s11356-021-13433-4>
- Taylor, K. M., Weisskopf, M., & Shine, J. (2014). Human exposure to nitro musks and the evaluation of their potential toxicity: an overview. *Environ. Health.*, 13(1), 1-7. <https://doi.org/10.1186/1476-069X-13-14>

- Ternes, T. A., Bonerz, M., Herrmann, N., Teiser, B., & Andersen, H. R. (2007). Irrigation of treated wastewater in Braunschweig, Germany: an option to remove pharmaceuticals and musk fragrances. *Chemosphere*, *66*(5), 894-904. <https://doi.org/10.1016/j.chemosphere.2006.06.035>
- Ternes, T. A., Stüber, J., Herrmann, N., McDowell, D., Ried, A., Kampmann, M., & Teiser, B. (2003). Ozonation: a tool for removal of pharmaceuticals, contrast media and musk fragrances from wastewater? *Water Res.*, *37*(8), 1976-1982. [https://doi.org/10.1016/S0043-1354\(02\)00570-5](https://doi.org/10.1016/S0043-1354(02)00570-5)
- Tian, Y. X., Wang, M. E., Chen, W. P., & Wang, Z. (2011). Analytical methods for synthetic musk in wastewater and sewage sludge. *Chin. J. Ecol.*, *30*(2), 395-400.
- Tolls, J., Berger, H., Klenk, A., Meyberg, M., Müller, R., Rettinger, K., & Steber, J. (2009). Environmental safety aspects of personal care products-a European perspective. *Environ. Toxicol. Chem.*, *28*(12), 2485.
- Tomazelli, L. C., de Assis Ramos, M. M., Sauce, R., Cândido, T. M., Sarruf, F. D., de Oliveira Pinto, C. A. S., de Oliveira, C. A., Rosado, C., Velasco, M. V. R., & Baby, A. R. (2018). SPF enhancement provided by rutin in a multifunctional sunscreen. *Int. J. Pharm.*, *552*(1-2), 401-406. <https://doi.org/10.1016/j.ijpharm.2018.10.015>
- Trabalón, L., Cano-Sancho, G., Pocurull, E., Nadal, M., Domingo, J. L., & Borrull, F. (2015). Exposure of the population of Catalonia (Spain) to musk fragrances through seafood consumption: risk assessment. *Environ. Res.*, *143*, 116-122. <https://doi.org/10.1016/j.envres.2015.04.007>
- Tracey, G. A., & Hansen, D. J. (1996). Use of biota-sediment accumulation factors to assess similarity of nonionic organic chemical exposure to benthically-coupled organisms of differing trophic mode. *Arch. Environ. Contam. Toxicol.*, *30*(4), 467-475. <https://doi.org/10.1007/BF00213397>
- Tseng, W. J., & Tsai, S. W. (2019). Assessment of dermal exposures for synthetic musks from personal care products in Taiwan. *Sci. Total Environ.* *669*, 160-167. <https://doi.org/10.1016/j.scitotenv.2019.03.046>.
- Tumová, J., Šauer, P., Golovko, O., Učun, O. K., Grabic, R., Máchová, J., & Kroupová, H. K. (2019). Effect of polycyclic musk compounds on aquatic organisms: A critical literature review supplemented by own data. *Sci. Total Environ.*, *651*, 2235-2246. <https://doi.org/10.1016/j.scitotenv.2018.10.028>
- United Nations. Globally harmonized system of classification and labelling of chemicals (GHS) [M]. 8th ed. New York: United Nations, 2019. Available from https://unece.org/fileadmin/DAM/trans/danger/publi/ghs/ghs_rev08/ST-SG-AC10-30-Rev8e.pdf (accessed 12 April 2021).
- USEPA, 2014. Available from <https://nepis.epa.gov/Exe/ZyPDF.cgi/P100N41I.PDF?Dockey=P100N41I.PDF> (accessed 12 April 2021).
- USEPA, 2014. TSCA Work Plan Chemical Risk Assessment HHCB 1,3,4,6,7,8-Hexahydro-4,6,6,7,8,8-hexamethylcyclopenta-g-2-benzopyran. https://www.epa.gov/sites/production/files/201509/documents/hhcb_wp_ra_final_08_27_14.pdf. (Accessed 6 March 2021)
- Vallecillos, L., Borrull, F., & Pocurull, E. (2012a). Determination of musk fragrances in sewage sludge by pressurized liquid extraction coupled to automated ionic liquid-based headspace single-drop microextraction followed by GC-MS/MS. *J. Sep. Sci.*, *35*(20), 2735-2742. <https://doi.org/10.1002/jssc.201200326>
- Vallecillos, L., Borrull, F., & Pocurull, E. (2013a). An automated headspace solid-phase microextraction followed by gas chromatography–mass spectrometry method to determine macrocyclic musk fragrances in wastewater samples. *Anal. Bioanal.*

- Chem.*, 405(29), 9547-9554. <https://doi.org/10.1007/s00216-013-7375-2>
- Vallecillos, L., Borrull, F., & Pocurull, E. (2014a). On-line coupling of solid-phase extraction to gas chromatography–mass spectrometry to determine musk fragrances in wastewater. *J. Chromatogr. A.*, 1364, 1-11. <https://doi.org/10.1016/j.chroma.2014.08.018>
- Vallecillos, L., Borrull, F., & Pocurull, E. (2015a). Recent approaches for the determination of synthetic musk fragrances in environmental samples. *TrAC-Trends Anal. Chem.*, 72, 80-92. <https://doi.org/10.1016/j.trac.2015.03.022>
- Vallecillos, L., Pedrouzo, M., Pocurull, E., & Borrull, F. (2014b). Headspace stir bar sorptive extraction followed by thermal desorption and gas chromatography with mass spectrometry to determine musk fragrances in sludge samples without sample pretreatment. *J. Sep. Sci.*, 37(11), 1322-1329. <https://doi.org/10.1002/jssc.201400048>
- Vallecillos, L., Pocurull, E., & Borrull, F. (2012b). Fully automated ionic liquid-based headspace single drop microextraction coupled to GC–MS/MS to determine musk fragrances in environmental water samples. *Talanta*, 99, 824-832. <https://doi.org/10.1016/j.talanta.2012.07.036>
- Vallecillos, L., Pocurull, E., & Borrull, F. (2012c). Fully automated determination of macrocyclic musk fragrances in wastewater by microextraction by packed sorbents and large volume injection gas chromatography–mass spectrometry. *J. Chromatogr. A.*, 1264, 87-94. <https://doi.org/10.1016/j.chroma.2012.09.049>
- Vallecillos, L., Pocurull, E., & Borrull, F. (2013b). A simple and automated method to determine macrocyclic musk fragrances in sewage sludge samples by headspace solid-phase microextraction and gas chromatography–mass spectrometry. *J. Chromatogr. A.*, 1314, 38-43. <https://doi.org/10.1016/j.chroma.2013.09.033>
- Vallecillos, L., Pocurull, E., & Borrull, F. (2015b). Influence of pre-treatment process on matrix effect for the determination of musk fragrances in fish and mussel. *Talanta*, 134, 690-698. <https://doi.org/10.1016/j.talanta.2014.12.010>
- Vallecillos, L., Sadeh, Y., Borrull, F., Pocurull, E., & Bester, K. (2017). Degradation of synthetic fragrances by laccase-mediated system. *J. Hazard. Mater.* 334, 233-243. <https://doi.org/10.1016/j.jhazmat.2017.04.003>.
- Vecchiato, M., Barbaro, E., Spolaor, A., Burgay, F., Barbante, C., Piazza, R., & Gambaro, A. (2018a). Fragrances and PAHs in snow and seawater of Ny-Ålesund (Svalbard): Local and long-range contamination. *Environ. Pollut.*, 242, 1740-1747. <https://doi.org/10.1016/j.envpol.2018.07.095>
- Vecchiato, M., Cremonese, S., Gregoris, E., Barbaro, E., Gambaro, A., & Barbante, C. (2016). Fragrances as new contaminants in the Venice lagoon. *Sci. Total Environ.*, 566, 1362-1367. <https://doi.org/10.1016/j.scitotenv.2016.05.198>
- Vecchiato, M., Gregoris, E., Barbaro, E., Barbante, C., Piazza, R., & Gambaro, A. (2017). Fragrances in the seawater of Terra Nova Bay, Antarctica. *Sci. Total Environ.*, 593, 375-379. <https://doi.org/10.1016/j.scitotenv.2017.03.197>
- Vecchiato, M., Turetta, C., Patti, B., Barbante, C., Piazza, R., Bonato, T., & Gambaro, A. (2018b). Distribution of fragrances and PAHs in the surface seawater of the Sicily Channel, Central Mediterranean. *Sci. Total Environ.*, 634, 983-989. <https://doi.org/10.1016/j.scitotenv.2018.04.080>
- Verma, J., Khedkar, V. M., & Coutinho, E. C. (2010). 3D-QSAR in drug design-a review. *Curr. Top. Med. Chem.*, 10(1), 95-115. <https://doi.org/10.2174/156802610790232260>
- Vilar, S., Cozza, G., & Moro, S. (2008). Medicinal chemistry and the molecular operating environment (MOE): application of QSAR and molecular docking to drug discovery. *Curr. Top. Med. Chem.*, 8(18), 1555-1572. <https://doi.org/10.2174/156802608786786624>

- Villa, S., Vighi, M., & Finizio, A. (2014). Theoretical and experimental evidences of medium range atmospheric transport processes of polycyclic musk fragrances. *Sci. Total Environ.*, 481, 27-34. <https://doi.org/10.1016/j.scitotenv.2014.02.017>
- Villaverde, J. J., Santín-Montanyá, I., Sevilla-Morán, B., Alonso-Prados, J. L., & Sandín-España, P. (2018). Assessing the effects of alloxidim phototransformation products by QSAR models and a phytotoxicity study. *Molecules*, 23(5), 993. <https://doi.org/10.3390/molecules23050993>
- Vimalkumar, K., Nikhil, N. P., Arun, E., Mayilsamy, M., & Babu-Rajendran, R. (2021). Synthetic musks in surface water and fish from the rivers in India: Seasonal distribution and toxicological risk assessment. *J. Hazard. Mater.*, 414, 125558. <https://doi.org/10.1016/j.jhazmat.2021.125558>
- Wan, Y., Wei, Q., Hu, J., Jin, X., Zhang, Z., Zhen, H., & Liu, J. (2007). Levels, tissue distribution, and age-related accumulation of synthetic musk fragrances in Chinese sturgeon (*Acipenser sinensis*): Comparison to organochlorines. *Environ. Sci. Technol.*, 41(2), 424-430. <https://doi.org/10.1021/es061771r>
- Wang, H., Xiao, Y., Zhang, L., & Gao, Q. (2018). Maternal early pregnancy vitamin D status in relation to low birth weight and small-for-gestational-age offspring. *J. Steroid Biochem. Mol. Biol.*, 175, 146-150. <https://doi.org/10.1016/j.jsbmb.2017.09.010>
- Wang, L., & Liu, X. (2019). Degradation of aqueous polycyclic musk tonalide by ultraviolet-activated free chlorine. *Processes* 7(2), 95. <https://doi.org/10.3390/pr7020095>
- Wang, M., Peng, C., Chen, W., & Markert, B. (2013). Ecological risks of polycyclic musk in soils irrigated with reclaimed municipal wastewater. *Ecotox. Environ. Safe.*, 97, 242-247. <https://doi.org/10.1016/j.ecoenv.2013.07.032>
- Wang, R., Lu, Y., & Wang, S. (2003). Comparative evaluation of 11 scoring functions for molecular docking. *J. Med. Chem.*, 46(12), 2287-2303. <https://doi.org/10.1021/jm0203783>
- Wang, R., Zhang, L., Chen, Y., Zhang, S., Zhuang, T., Wang, L., Xu, M., Zhang, N., & Liu, S. (2020). Elevated non-essential metals and the disordered metabolism of essential metals are associated to abnormal pregnancy with spontaneous abortion. *Environ. Int.*, 144, 106061. <https://doi.org/10.1016/j.envint.2020.106061>
- Wang, W., Li, H., Hou, X., Zhang, Q., & Tian, S. (2021). Multi-criteria evaluation of distributed energy system based on order relation-anti-entropy weight method. *Energies*, 14(1), 246. <https://doi.org/10.3390/en14010246>
- Wang, X., Chu, Z., Yang, J., & Li, Y. (2017a). Pentachlorophenol molecule design with lower bioconcentration through 3D-QSAR associated with molecule docking. *Environ. Sci. Pollu. R. Int.*, 24(32), 25114-25125. <https://doi.org/10.1007/s11356-017-0129-5>
- Wang, X., Gu, W., Guo, E., Cui, C., & Li, Y. (2017b). Assessment of long-range transport potential of polychlorinated Naphthalenes based on three-dimensional QSAR models. *Environ. Sc. Pollut. R.*, 24(17), 14802-14818. <https://doi.org/10.1007/s11356-017-8967-8>
- Wang, X., Li, Q., Li, M., & Li, Y. (2018). Interference adsorption mechanisms of dimethoate, metalaxyl, atrazine, malathion and prometryn in a sediment system containing coexisting pesticides/heavy metals based on fractional factor design (resolution v) assisted by 2d-qsar. *Chem. Res. Chin. Univ.*, 34(3), 397-407. <https://doi.org/10.1007/s40242-018-7253-8>
- Wang, X., Meng, H., Chen, P., Yang, N., Lu, X., Wang, Z. M., Gao, W., Zhou, N., Zhang, M., Xu, Z., Chen, B., Tao, Z., Wang, L., Yang, Z., & Zhu, T. (2014). Beneficial effects

- of muscone on cardiac remodeling in a mouse model of myocardial infarction. *Int. J. Mol. Med.*, 34(1), 103-111. <https://doi.org/10.3892/ijmm.2014.1766>
- Wang, Y.N., Chen, J., Li, X., Wang, B., Cai, X. & Huang, L. (2009). Predicting rate constants of hydroxyl radical reactions with organic pollutants: algorithm, validation, applicability domain, and mechanistic interpretation. *Atmos. Environ.*, 43(5), pp.1131-1135. <https://doi.org/10.1016/j.atmosenv.2008.11.012>
- Ward, A., Greenberg, V., Valcarcel, B., Boelig, R.C., Al-Kouatly, H.B., & Berghella, V. (2020). Intramuscular progesterone in women with twins and a prior singleton spontaneous preterm birth. *A. J. O. G. MFM*, 2(3), 100124. <https://doi.org/10.1016/j.ajogmf.2020.100124>.
- Westermaier, Y., Ruiz-Carmona, S., Theret, I., Perron-Sierra, F., Poissonnet, G., Dacquet, C., Boutin, J.A., Ducrot, P., & Barril, X. (2017). Binding mode prediction and MD/MMPBSA-based free energy ranking for agonists of REV-ERB α /NCoR. *J. Comput. Aided Mol. Des.*, 31(8), 755-775. <https://doi.org/10.1007/s10822-017-0040-7>.
- Wezel, A. P. V., & Opperhuizen, A. (1995). Narcosis due to environmental pollutants in aquatic organisms: residue-based toxicity, mechanisms, and membrane burdens. *Crit. Rev. Toxicol.*, 25(3), 255-279. <https://doi.org/10.3109/10408449509089890>
- Williams, A.S. (2000). Esters with musk odor and their use in perfumery: WO. 0014051.
- Winkler, D. A. (2018). Sparse QSAR modelling methods for therapeutic and regenerative medicine. *J. Comput. Aid. Mol. Des.* 32(4), 497-509. <https://doi.org/10.1007/s10822-018-0106-1>.
- Winkler, M., Kopf, G., Hauptvogel, C., & Neu, T. (1998). Fate of artificial musk fragrances associated with suspended particulate matter (SPM) from the River Elbe (Germany) in comparison to other organic contaminants. *Chemosphere*, 37(6), 1139-1156. [https://doi.org/10.1016/S0045-6535\(98\)00110-6](https://doi.org/10.1016/S0045-6535(98)00110-6)
- Witorsch, R. J., & Thomas, J. A. (2010). Personal care products and endocrine disruption: a critical review of the literature. *Crit. Rev. Toxicol.*, 40(sup3), 1-30. <https://doi.org/10.3109/10408444.2010.515563>
- Woker, G. (2002). The Relation between Structure and Smell in Organic Compounds. *J. Phys. Chem.*, 10(6), 455-473.
- Wolfgang, K.G.B., & Karl-Heinrich S.O. (1992). Esters and their use in perfumery: US. 5166412.
- Wollenberger, L., Breitholtz, M., Kusk, K. O., & Bengtsson, B. E. (2003). Inhibition of larval development of the marine copepod *Acartia tonsa* by four synthetic musk substances. *Sci. Total Environ.*, 305(1-3), 53-64. [https://doi.org/10.1016/S0048-9697\(02\)00471-0](https://doi.org/10.1016/S0048-9697(02)00471-0)
- Wu, C. Y., Bai, L., Gu, F., Wei, W., Guo, L. X., & Wen, D. M. (2018). Elimination of typical polycyclic musks in a full-scale membrane bioreactor combined with anaerobic–anoxic–oxic process in municipal wastewater treatment plant. *Water Sci. Technol.* 78(7), 1459-1465. <https://doi.org/10.2166/wst.2018.423>.
- Wu, Q., Li, H., Leng, Y., Deng, H., Cheng, H., & Shen, W. (2014). Determination of muscone in rats plasma following oral administration of artificial musk: using of combined headspace gas chromatography-mass spectrometry. *J. Spectro.*, 2014, 1-5. <https://doi.org/10.1155/2014/906928>
- Wu, S. F., Liu, L. L., & Ding, W. H. (2012). One-step microwave-assisted headspace solid-phase microextraction for the rapid determination of synthetic polycyclic musks in oyster by gas chromatography–mass spectrometry. *Food Chem.*, 133(2), 513-517. <https://doi.org/10.1016/j.foodchem.2012.01.017>
- Xie, Z., Ebinghaus, R., Temme, C., Heemken, O., & Ruck, W. (2007). Air– sea exchange

- fluxes of synthetic polycyclic musks in the North Sea and the Arctic. *Environ. Sci. Technol.*, *41*(16), 5654-5659. <https://doi.org/10.1021/es0704434>
- Xu, Z., Chen, Y., Qiu, Y., Gu, W., & Li, Y. (2016). Prediction of stability for polychlorinated biphenyls in transformer insulation oil through three-dimensional quantitative structure-activity relationship pharmacophore model and full factor experimental design. *Chem. Res. Chinese U.*, *32*(3), 348-356. <https://doi.org/10.1007/s40242-016-5461-7>
- Yamada, T., Habuka, A., & Hatta, I. (2021). Moisturizing mechanism of glycerol and diglycerol on human stratum corneum studied by synchrotron X-ray diffraction. *Int. J. Cosmet. Sci.*, *43*(1), 38-47. <https://doi.org/10.1111/ics.12664>
- Yamauchi, R., Ishibashi, H., Hirano, M., Mori, T., Kim, J. W., & Arizono, K. (2008). Effects of synthetic polycyclic musks on estrogen receptor, vitellogenin, pregnane X receptor, and cytochrome P450 3A gene expression in the livers of male medaka (*Oryzias latipes*). *Aquat. Toxicol.*, *90*(4), 261-268. <https://doi.org/10.1016/j.aquatox.2008.09.007>
- Yang, C. Y., & Ding, W. H. (2012). Determination of synthetic polycyclic musks in aqueous samples by ultrasound-assisted dispersive liquid-liquid microextraction and gas chromatography-mass spectrometry. *Anal. Bioanal. Chem.*, *402*(4), 1723-1730. <https://doi.org/10.1007/s00216-011-5573-3>
- Yang, H., Du, Z., Lv, W. J., Zhang, X. Y., & Zhai, H. L. (2019). In silico toxicity evaluation of dioxins using structure-activity relationship (SAR) and two-dimensional quantitative structure-activity relationship (2D-QSAR). *Arch. Toxicol.*, *93*(11), 3207-3218. <https://doi.org/10.1007/s00204-019-02580-w>
- Yang, J. J., & Metcalfe, C. D. (2006). Fate of synthetic musks in a domestic wastewater treatment plant and in an agricultural field amended with biosolids. *Sci. Total Environ.*, *363*(1-3), 149-165. <https://doi.org/10.1016/j.scitotenv.2005.06.022>
- Yang, L., Li, M., & Liu, M. (2021). Establishment of a CoMFA model based on the combined activity of bioconcentration, long-Range transport, and highest infrared signal intensity and molecular design of environmentally friendly PBB derivatives. *Polymers*, *13*(3), 356. <https://doi.org/10.3390/polym13030356>
- Yang, X., Flowers, R. C., Weinberg, H. S., & Singer, P. C. (2011). Occurrence and removal of pharmaceuticals and personal care products (PPCPs) in an advanced wastewater reclamation plant. *Water Res.*, *45*(16), 5218-5228. <https://doi.org/10.1016/j.watres.2011.07.026>
- Yang, Y., Ok, Y. S., Kim, K. H., Kwon, E. E., & Tsang, Y. F. (2017). Occurrences and removal of pharmaceuticals and personal care products (PPCPs) in drinking water and water/sewage treatment plants: A review. *Sci. Total Environ.*, *596*, 303-320. <https://doi.org/10.1016/j.scitotenv.2017.04.102>
- Ye, J.X., & Sun, X.M. (2011). Asymmetric synthesis of chiral Muscone and other 3-methyl ketones: CN. 101982451.
- Yin, J., Wang, H., Li, J., Wu, Y., & Shao, B. (2016). Occurrence of synthetic musks in human breast milk samples from 12 provinces in China. *Food Addit. Contam. A.*, *33*(7), 1219-1227. <https://doi.org/10.1080/19440049.2016.1201219>
- Yin, J., Wang, H., Li, J., Wu, Y., & Shao, B. (2016). Occurrence of synthetic musks in human breast milk samples from 12 provinces in China. *Food Addit. Contam.: Part A*, *33*(7), 1219-1227. <https://doi.org/10.1080/19440049.2016.1201219>
- Yin, J., Wang, H., Zhang, J., Zhou, N., Gao, F., Wu, Y., Xiang, J. & Shao, B. (2012). The occurrence of synthetic musks in human breast milk in Sichuan, China. *Chemosphere*, *87*(9), 1018-1023. <https://doi.org/10.1016/j.chemosphere.2011.11.068>

- Youli, Q., Long, J., & Yu, L. (2018). Theoretical support for the enhancement of infrared spectrum signals by derivatization of phthalic acid esters using a pharmacophore model. *Spectrosc. Lett.*, *51*(3), 155-162.
<https://doi.org/10.1080/00387010.2018.1442353>
- Yu, B., Ning, C. L., & Li, B. (2017). Probabilistic durability assessment of concrete structures in marine environments: Reliability and sensitivity analysis. *China Ocean Engineering*, *31*(1): 63-73. 10.1007/s13344-017-0008-3
- Yunlong, W., Kai, L., Guan, G., Yanyun, Y., & Fei, L. (2019). Evaluation method for Green jack-up drilling platform design scheme based on improved grey correlation analysis. *Applied Ocean Research*, *85*, 119-127.
- Zachary, M., & Greenway, G. M. (2009). Comparative PBT screening using (Q) SAR tools within REACH legislation. *SAR QSAR Environ. Res.*, *20*(1-2), 145-157.
<https://doi.org/10.1080/10629360902724143>
- Zarzo, M. (2007). The sense of smell: molecular basis of odorant recognition. *Biol. Rev.*, *82*(3), 455-479. <https://doi.org/10.1111/j.1469-185X.2007.00019.x>
- Zeng, X., Mai, B., Sheng, G., Luo, X., Shao, W., An, T., & Fu, J. (2008). Distribution of polycyclic musks in surface sediments from the Pearl River Delta and Macao coastal region, South China. *Environ. Toxicol. Chem.*, *27*(1), 18-23.
<https://doi.org/10.1897/07-106.1>
- Zeng, X., Sheng, G., Xiong, Y., & Fu, J. (2005). Determination of polycyclic musks in sewage sludge from Guangdong, China using GC–EI-MS. *Chemosphere*, *60*(6), 817-823. <https://doi.org/10.1016/j.chemosphere.2005.04.026>
- Zeng, X., Xu, L., Liu, J., Wu, Y., & Yu, Z. (2018). Occurrence and distribution of organophosphorus flame retardants/plasticizers and synthetic musks in sediments from source water in the Pearl River Delta, China. *Environ. Toxicol. Chem.* *37*(4), 975-982. <https://doi.org/10.1002/etc.4040>.
- Zhang, W., Gu, W., Sun, R., Zhou, M., Han, Z., & Li, Y. (2021). An adjusted 3D-QSAR model for the combined activity of fluoroquinolones photodegradation and microbial degradation assisted by dynamic simulation and its application in molecular modification. *Ecotoxicol. Environ. Saf.*, *212*, 111973.
<https://doi.org/10.1016/j.ecoenv.2021.111973>
- Zhang, C., Guo, T., Huang, Q., Wang, L., Ban, C., & Shen, G. (2020b). Solubility and thermodynamic properties of L-Pyroglutamic acid in pure and binary solvents. *J. Mol. Liq.*, *320*, 114361. <https://doi.org/10.1016/j.molliq.2020.114361>
- Zhang, H., Bayen, S., & Kelly, B. C. (2015a). Co-extraction and simultaneous determination of multi-class hydrophobic organic contaminants in marine sediments and biota using GC-EI-MS/MS and LC-ESI-MS/MS. *Talanta*, *143*, 7-18.
<https://doi.org/10.1016/j.talanta.2015.04.084>
- Zhang, H., Bayen, S., & Kelly, B. C. (2015b). Multi-residue analysis of legacy POPs and emerging organic contaminants in Singapore's coastal waters using gas chromatography–triple quadrupole tandem mass spectrometry. *Sci. Total Environ.*, *523*, 219-232. <https://doi.org/10.1016/j.scitotenv.2015.04.012>
- Zhang, H., Bu, Q., Wu, D., & Yu, G. (2020a). Polycyclic musks in surface water and sediments from an urban catchment in the megacity Beijing, China. *Environ. Pollut.*, *263*, 114548. <https://doi.org/10.1016/j.envpol.2020.114548>
- Zhang, L., Mao, H., Liu, L., Du, J., & Gani, R. (2018c). A machine learning based computer-aided molecular design/screening methodology for fragrance molecules. *Comput. Chem. Eng.*, *115*, 295-308.
<https://doi.org/10.1016/j.compchemeng.2018.04.018>
- Zhang, S., Yang, Q., Li, Z., Wang, W., Zang, X., Wang, C., & Wang, Z. (2018b). Solid

- phase microextraction of phthalic acid esters from vegetable oils using iron (III)-based metal-organic framework/graphene oxide coating. *Food Chem.* 263, 258-264. <https://doi.org/10.1016/j.foodchem.2018.04.132>.
- Zhang, W., Sun, R., Hou, Y., Qiu, Y., & Li, Y. (2020c). Investigation of the potential environmental risks of phthalate derivatives designed to be environmentally friendly. *Environ. Toxicol. Chem.*, 39(6), 1138-1148. <https://doi.org/10.1002/etc.4710>
- Zhang, W., Sun, R., Zhao, X., & Li, Y. (2020d). Environmental Conversion Path Inference of New Designed Fluoroquinolones and Their Potential Environmental Risk. *Arch. Environ. Con. Tox.* 78(2), 310-328. <https://doi.org/10.1007/s00244-019-00672-3>.
- Zhang, W., Wei, Z., Lin, C., Wang, Z., Zheng, Z., & Li, S. (2019). 3D-QSAR study of the phenylsulfamic acid derivatives as HPTP β inhibitors. *Journal of Molecular Structure*, 1186, 11-22. <https://doi.org/10.1016/j.molstruc.2019.02.107>
- Zhang, X., Jing, Y., Ma, L., Zhou, J., Fang, X., Zhang, X., & Yu, Y. (2015c). Occurrence and transport of synthetic musks in paired maternal blood, umbilical cord blood, and breast milk. *Int. J. Hyg. Envir. Heal.*, 218(1), 99-106. <https://doi.org/10.1016/j.ijheh.2014.08.005>
- Zhang, X., Liang, G., Zeng, X., Zhou, J., Sheng, G., & Fu, J. (2011). Levels of synthetic musk fragrances in human milk from three cities in the Yangtze River Delta in Eastern China. *Res. J. Environ. Sci.*, 23(6), 983-990. [https://doi.org/10.1016/S1001-0742\(10\)60506-2](https://doi.org/10.1016/S1001-0742(10)60506-2)
- Zhang, X., Xu, Q., Man, S., Zeng, X., Yu, Y., Pang, Y., Sheng, G., & Fu, J. (2013). Tissue concentrations, bioaccumulation, and biomagnification of synthetic musks in freshwater fish from Taihu Lake, China. *Environ. Sci. Pollut. Res.*, 20(1), 311-322. <https://doi.org/10.1007/s11356-012-1095-6>
- Zhang, X., Yao, Y., Zeng, X., Qian, G., Guo, Y., Wu, M., Sheng, G., & Fu, J. (2008). Synthetic musks in the aquatic environment and personal care products in Shanghai, China. *Chemosphere*, 72(10), 1553-1558. <https://doi.org/10.1016/j.chemosphere.2008.04.039>
- Zhang, X., Yu, Y., Gu, Y., Li, X., Zhang, X., & Yu, Y. (2017a). In vitro determination of transdermal permeation of synthetic musks and estimated dermal uptake through usage of personal care products. *Chemosphere*, 173, 417-424. <https://doi.org/10.1016/j.chemosphere.2017.01.001>
- Zhang, X., Zheng, M., Wang, L., Lou, Y., Shi, L., & Jiang, S. (2018a). Sorption of three synthetic musks by microplastics. *Mar. Pollut. Bull.*, 126, 606-609. <https://doi.org/10.1016/j.marpolbul.2017.09.025>
- Zhang, Y., & Zhang, X. (2007). Grey correlation analysis between strength of slag cement and particle fractions of slag powder. *Cement and Concrete Composites*, 29(6), 498-504.
- Zhang, Y., Huang, L., Zhao, Y., & Hu, T. (2017b). Musk xylene induces malignant transformation of human liver cell line L02 via repressing the TGF- β signaling pathway. *Chemosphere*, 168, 1506-1514. <https://doi.org/10.1016/j.chemosphere.2016.12.001>
- Zhang, Z., Zhu, Q., Huang, C., Yang, M., Li, J., Chen, Y., Yang, B., & Zhao, X. (2020). Comparative cytotoxicity of halogenated aromatic DBPs and implications of the corresponding developed QSAR model to toxicity mechanisms of those DBPs: Binding interactions between aromatic DBPs and catalase play an important role. *Water Res.*, 170, 115283. <https://doi.org/10.1016/j.watres.2019.115283>
- Zhao, W., Xing, J., Chen, D., Jin, D., & Shen, J. (2016). Electrochemical degradation of Musk ketone in aqueous solutions using a novel porous Ti/SnO₂-Sb₂O₃/PbO₂ electrodes. *J. Electroanal. Chem.* 775, 179-188.

- <https://doi.org/10.1016/j.jelechem.2016.05.050>.
- Zhao, X. H., Wang, X. L., & Li, Y. (2018b). Relationship between the binding free energy and PCBs' migration, persistence, toxicity and bio-accumulation using a combination of the molecular docking method and 3D-QSAR. *Chem. Cent. J.*, 12(1), 1-12. <https://doi.org/10.1186/s13065-018-0389-2>
- Zhao, X., & Schwack, W. (1999). Photochemical behavior of musk ambrette. *Chemosphere*, 39(1), 11-21. [https://doi.org/10.1016/S0045-6535\(98\)00584-0](https://doi.org/10.1016/S0045-6535(98)00584-0)
- Zhao, Y., & Li, Y. (2018a). Modified neonicotinoid insecticide with bi-directional selective toxicity and drug resistance. *Ecotox. Environ. Safe.* 164, 467-473. <https://doi.org/10.1016/j.ecoenv.2018.08.055>.
- Zhao, Y., Gu, W., & Li, Y. (2018c). Molecular design of 1, 3, 5, 7-TetraCN derivatives with reduced bioconcentration using 3D-QSAR modeling, full factorial design, and molecular docking. *J. Mol. Graph. Model.*, 84, 197-214. <https://doi.org/10.1016/j.jmglm.2018.07.006>
- Zhao, Y.Y., Hou, Y.L., & Li, Y. (2020). Multi-directional selective toxicity effects on farmland ecosystems: A novel design of green substitutes for neonicotinoid insecticides. *J. Clean. Prod.*, 272, 122715. <https://doi.org/10.1016/j.jclepro.2020.122715>.
- Zhou, H., Huang, X., Gao, M., Wang, X., & Wen, X. (2009). Distribution and elimination of polycyclic musks in three sewage treatment plants of Beijing, China. *J. Environ. Sci. (China)*, 21(5), 561-567. [10.1016/s1001-0742\(08\)62308-6](https://doi.org/10.1016/s1001-0742(08)62308-6)
- Zhou, J. (2016). Synthetic musk in daily chemicals. *China Surfactant Detergent & Cosmetics*. 46(9), 530-538 (in Chinese).
- Zhou, J., Zeng, X., Zheng, K., Zhu, X., Ma, L., Xu, Q., Zhang, X., Yu, Y., Sheng, G., & Fu, J. (2012). Musks and organochlorine pesticides in breast milk from Shanghai, China: levels, temporal trends and exposure assessment. *Ecotox. Environ. Safe.* 84, 325-333. <https://doi.org/10.1016/j.ecoenv.2012.08.011>
- Zhu, T., Wu, J., He, C., Fu, D., & Wu, J. (2018). Development and evaluation of MTLSER and QSAR models for predicting polyethylene-water partition coefficients. *J. Environ. Manage.* 223, 600-606. <https://doi.org/10.1016/j.jenvman.2018.06.039>.
- Zou S., Xu W., Zhang R., Tang, J., Chen, Y., & Zhang, G. (2011). Occurrence and distribution of antibiotics in coastal water of the Bohai Bay, China: impacts of river discharge and aquaculture activities. *Environ. Pollut.* 159(10), 2913-2920. <https://doi.org/10.1016/j.envpol.2011.04.037>